

Backward Erosion Piping Initiation and Progression



Vera M. van Beek

BACKWARD EROSION PIPING

INITIATION AND PROGRESSION

BACKWARD EROSION PIPING INITIATION AND PROGRESSION

Proefschrift

ter verkrijging van de graad van doctor
aan de Technische Universiteit Delft,
op gezag van de Rector Magnificus prof. ir. K. C. A. M. Luyben,
voorzitter van het College voor Promoties,
in het openbaar te verdedigen op donderdag 26 november 2015 om 10:00 uur

door

Vera Maria VAN BEEK

Ingenieur Technische Aardwetenschappen

Technische Universiteit Delft

geboren te Alkemade, Nederland

Dit proefschrift is goedgekeurd door de promotoren:

Prof. dr. M.A. Hicks en Prof. dr. ir. A. Bezuijen

Samenstelling promotiecommissie:

Rector Magnificus	voorzitter
Prof. dr. M.A. Hicks	Technische Universiteit Delft, promotor
Prof. dr. ir. A. Bezuijen	Universiteit Gent, promotor

Onafhankelijke leden:

Prof. dr. C. Jommi	Technische Universiteit Delft
Prof. dr. ir. W.S.J. Uijttewaai	Technische Universiteit Delft
Prof. dr.-ing. K.J. Witt	Bauhaus-Universität Weimar
Dr. M.K. Sharp	USACE Engineer Research and Development Center
Em. prof. ir. A.F. van Tol	Technische Universiteit Delft (reservelid)

Overige leden:

Dr. ir. J.B. Sellmeijer	Deltares (gepensioneerd)
-------------------------	--------------------------

Em. prof. dr. ir. F.B.J. Barends heeft als promotor in de eerste jaren van het onderzoek in belangrijke mate bijgedragen aan de totstandkoming van het proefschrift.

Key words: Backward erosion piping, internal erosion, seepage, sand boil, initiation, progression, Sellmeijer model, physical modelling, ground water flow, heave, viscous flow, incipient motion, primary erosion, secondary erosion.

Printed by: Ipskamp drukkers

Cover illustration: Artist impression by Ineke Verdel

Copyright © 2015 by Vera M. van Beek

ISBN 978-94-6259-940-6

An electronic version of this dissertation is available at

<http://repository.tudelft.nl/>.

ACKNOWLEDGEMENTS

Back in 2009, immediately after I had given a presentation on the small-scale backward erosion experiments at Deltares, Frans Barends asked me whether I would like to start a doctorate study to address the fundamental questions arising from those experiments. I agreed, because I was interested in the physical aspects of the piping phenomenon and I had always intended to engage in a doctorate at some time in my career.

The conversations I had with Frans during the early years of the doctorate were always interesting. Frans believed that personal development was an important part of a doctorate and we often talked about life in general rather than piping. He left the actual research to me, guiding me in the right direction when I asked. The approach worked very well for us. His attitude towards supervising students can be summed up in his comment: 'Now and then, there is an opportunity to give a push to the swing, after which I hope students will swing higher themselves'. Unfortunately, Frans was unable to supervise me through to the completion of my doctorate due to illness. I am very grateful for the lessons I learned from him and for the supervision in the early years, and I wish him all the best.

As a supervisor and reviewer of piping research since 2009, Adam Bezuijen was willing to take over the doctorate supervision, at first temporarily and later officially. I have very much enjoyed our discussions about piping, which always generated more ideas for research and experiments than could possibly be accommodated by the available budget. Through Adam, I have learned a great deal about physical modelling and experiment analysis and I have tried to adopt his idea of always using experiments as a basis for the elaboration of theory. Even more importantly, I have got to know Adam as a very kind person. I have very much appreciated his day-to-day supervision.

Michael Hicks was already involved at the beginning of the doctorate when we submitted a research proposal for the physical and numerical modelling of piping. When I asked him to be one of my supervisors, the completion of my doctorate was already in sight. Nevertheless, he agreed to act as the promotor from Delft University of Technology. His fresh approach to reviewing my work, as someone who was not fully immersed in the topic, was very useful indeed.

I would also like to express my gratitude to the many colleagues who have helped me during my research. The experimental part of the research would have been impossible without the help of my colleagues in the Deltares laboratory and most specifically Ferry Schenkeveld. His expertise guaranteed high-quality physical models that were the basis for successful analysis and interpretation. Not only that, I have also very much enjoyed conducting the experiments with him. Hans Sellmeijer helped me to derive the analytical equations for groundwater flow and was always patient in our discussions of the piping models. During the course of the research, I have been privileged to work

with Ulrich Förster, Harry van Essen, John van Esch, André Koelewijn and many others. Suzanne van Eekelen, apart from being my coach, paved the way during every step of her doctorate and provided me with useful advice.

The team that conducted the IJkdijk experiments (who included Huub de Bruijn, Han Knoeff, André Koelewijn, Goaitske de Vries, Bernard van der Kolk, Dennis Peters, Enno van Waardenberg and Lambert Smidt) and the organisations that made the experiments possible (Deltares, TNO ICT, NV NOM, STOWA, Rijkswaterstaat, SNN and the European Regional Development Fund) also deserve mention here. It has been a unique opportunity to be part of the team conducting these experiments and to be able to use the data for my doctoral research.

I was very lucky that I could conduct a large part of my doctorate as part of the 'Research and development of flood defence assessment tools WTI2017' programme funded by Rijkswaterstaat. I am also grateful to Deltares for giving me the opportunity to pursue and finish my research, and for their trust and support.

In recent years, I have worked with several international researchers involved in piping. I have found that conducting experiments together contributes significantly to knowledge exchange and to the development of new ideas. I would therefore like to thank Qiuling Yao, Kristine Vandenboer and, more recently, Bryant Robbins for our enjoyable discussions and collaboration.

I would also like to express my appreciation to the committee members, who have taken the time to review and discuss the dissertation.

Linguist Pete Thomas deserves mention for his pleasant and thorough approach to correcting the journal papers and the dissertation.

Last but not least I would like to thank my family for their support throughout the years. The combination of young children and a doctorate was challenging, but I could always rely on Tino, my parents and Tino's mother and father[†]. James and Noah have unknowingly contributed to the completion of this endeavour by bringing joy and diversion.

ABSTRACT

Backward erosion piping is an internal erosion mechanism during which shallow pipes are formed in the direction opposite to the flow underneath water-retaining structures as a result of the gradual removal of sandy material by the action of water. It is an important failure mechanism in both dikes and dams where sandy layers are covered by a cohesive layer. Sand boils can indicate that backward erosion is present and they are observed regularly during high water and floods. Although failure resulting from backward erosion piping is not common, several dike failures in the US, China and the Netherlands have been attributed to this mechanism.

Given the impact that climate change is expected to have, prediction models for backward erosion piping are becoming increasingly important in flood-risk assessment. The prediction models available until now, such as Bligh's rule and the Sellmeijer model, were validated in the research programme 'Strength and loads on flood defence structures' (*SBW: Sterkte en Belastingen Waterkeringen*) in the period 2008-2010 using small-, medium- and large-scale experiments. These experiments showed that an empirical adjustment of the Sellmeijer model was required to take the effect of the sand type into account and that validation was not possible for loose sand types because the erosion mode is different in those conditions.

However, the absence of a theoretical basis makes this proposed empirical adjustment unsatisfactory because it lacks robustness. The main question addressed by this dissertation is how to explain and predict the pipe-forming erosion processes in uniform sands.

A review of the literature, in conjunction with additional experiments, showed that the critical head in pipe formation leading to dike failure depends on either pipe initiation or pipe progression. In some experiments, the critical head for pipe initiation exceeds that of pipe progression and equilibrium is therefore prevented.

The experiments in which no equilibrium was observed allowed for the development of a model for pipe initiation. It was possible to relate the observed differences in critical gradient caused by scale, sand type and configuration to the fluidisation of sand very close to the exit, where the local gradients are high.

In the field, pipe progression is likely to determine the critical gradient. The Sellmeijer model predicts the progression of the pipe on the basis of the equilibrium of particles on the bottom of the pipe. The literature, and an analysis of the pipe width, depth, gradient and erosion process in experiments, indicate that pipe progression relies on two processes: primary erosion, which causes the removal of particles at the pipe tip, and secondary erosion, which causes the erosion of the pipe walls and bottom. Although the Sellmeijer model does not include primary erosion, it does function well for sand layers

with a 2D exit configuration in which there is no variation in the grain size along the pipe path. The adaptation of the Sellmeijer model that was found necessary to account for the effect of sand type can be replaced by using the original model in combination with a variable bedding angle based on incipient motion experiments from the literature.

The Sellmeijer model does not predict the critical gradient well for 3D configurations such as flow towards a single point, or for heterogeneous soils. Variations in the grain size in the pipe path were found to result in significantly higher critical gradients than expected, whereas a strong concentration of the flow towards the exit led to a fall in the critical gradient. 3D numerical calculations and the inclusion of primary erosion in the Sellmeijer model are needed to predict piping under these conditions.

SAMENVATTING

Piping, ofwel terugschrijdende erosie, is een vorm van interne erosie, waarbij ondiepe holle ruimtes worden gevormd onder een dijk, tegen de richting van de grondwaterstroming in, ten gevolge van het geleidelijk afvoeren van zandkorrels. Het is een belangrijk faalmechanisme voor dammen en dijken met een zandige ondergrond afgedekt is door een cohesieve ondoorlatende laag. Zandmeevoerende wellen, vaak waargenomen tijdens hoogwater, geven een aanwijzing dat er mogelijk sprake is van terugschrijdende erosie. Het bezwijken van een dijk ten gevolge van piping komt gelukkig zelden voor, maar er zijn gevallen bekend in de Verenigde Staten, China en Nederland waarvoor piping als hoofdoorzaak is aangewezen.

Met de verwachte invloed van klimaatverandering worden rekenmodellen voor piping steeds belangrijker. De beschikbare predictie modellen, zoals de regel van Bligh en het model van Sellmeijer, zijn daarom in de periode 2008-2010 gevalideerd met kleine-, medium- en grote-schaal experimenten als onderdeel van het onderzoeksprogramma Sterkte, Belastingen en Waterkeringen. Op basis van deze experimenten is een empirische aanpassing van het Sellmeijer model voorgesteld, om te invloed van het zandtype op het kritiek verval goed te kunnen voorspellen. Daarnaast kon op dat moment geen validatie van het model voor losgepakte zanden worden uitgevoerd, omdat er een ander erosiemechanisme waargenomen werd voor deze zanden.

Door het ontbreken van een theoretische basis van de aanpassing in het Sellmeijer model is de aanpassing onbevredigend en weinig robuust. In dit proefschrift wordt daarom ingegaan op de vraag hoe we de erosieprocessen in uniform zand kunnen verklaren en voorspellen.

Literatuuronderzoek en experimenten lieten zien dat het kritiek verval voor piping bepaald kan worden door pipe initiatie of door pipe progressie. In sommige experimenten is het kritiek verval voor pipe initiatie groter dan voor pipe progressie, wat betekent dat de pipe na initiatie bij gelijkblijvend verval niet in evenwicht komt maar direct doorgroeit.

De experimenten waarin geen evenwicht is waargenomen gaven aanleiding tot de ontwikkeling van een predictie model voor pipe initiatie. Hierbij werd gevonden dat de waargenomen verschillen in kritieke gradiënt ten gevolge van schaal, vorm of zandtype verklaard konden worden door het fluïdiseren van zand dichtbij het uittreepunt, waar de lokale gradiënt hoog is.

In het veld zal door de grotere schaal over het algemeen evenwicht waargenomen worden en is de progressie van de pipe maatgevend voor het kritiek verval. Het Sellmeijer model is een model dat de progressie van de pipe voorspelt, gebaseerd op evenwicht van korrels op de bodem van de pipe. Uit literatuuronderzoek en analyse van

experimenten (pipe diepte en breedte, pipe gradiënt, erosiemechanisme) kon worden geconcludeerd dat pipe progressie van twee mechanismen afhangt: primaire erosie, waarbij korrels aan de kop van de pipe in transport worden gebracht en secundaire erosie, wat erosie van de bodem en wanden van de pipe veroorzaakt.

Hoewel primaire erosie niet in het Sellmeijer model is meegenomen, functioneert het model toch goed voor 2D zandlagen met weinig variatie in de korrelgrootte in de baan van de pipe. Het gebruik van een variabele rolweerstandshoek (gebaseerd op experimenten uit de literatuur waarin het begin van bewegen is bestudeerd in laminaire stroming) in het originele rekenmodel, blijkt vergelijkbare resultaten te geven als het aangepaste model met constante rolweerstandshoek.

Voor situaties waarbij de stroming sterk convergeert naar het uittreepunt (3D configuratie) en voor heterogene zanden (met variatie van korrelgrootte in de baan van de pipe), blijkt het Sellmeijer model niet goed te functioneren. Variatie in korrelgrootte in de baan van de pipe blijkt tot een relatief hoge kritieke gradiënt te leiden, terwijl de concentratie van stroming naar het uittreepunt de kritieke gradiënt juist doet afnemen. Het berekenen van de stroming in 3D en het implementeren van een criterium voor primaire erosie zijn noodzakelijke stappen om in deze condities piping te voorspellen.

CONTENTS

Acknowledgements.....	vii
Abstract	ix
Samenvatting	xi
Contents.....	xiii
1. Introduction	1
1.1. Flood risk and the failure of dike systems	1
1.2. Backward erosion piping	2
1.3. Research outline	6
1.3.1. Problem statement	6
1.3.2. Research question	6
1.3.3. Method.....	7
1.3.4. Contribution.....	7
1.3.5. Context.....	8
1.4. Dissertation structure.....	8
2. Literature.....	11
2.1. Introduction.....	11
2.2. Experiments.....	12
2.2.1. Overview.....	12
2.2.2. Set-up	13
2.2.3. Experiments at the University of Berlin.....	15
2.2.4. Experiments at the University of Florida.....	19
2.2.5. Experiments for C.O.W.: De Wit (1984).....	20
2.2.6. Delta flume experiments: Silvis (1991)	23
2.2.7. Lateral heterogeneity experiments and SBW experiments	24
2.2.8. IWHR experiments	30
2.2.9. Experiments containing separate engineering structures or with partly vertical seepage paths	30
2.3. Prediction models.....	31
2.3.1. Early models (1900-1970)	31

2.3.2. Explanation of scale effects by De Wit (1984)	33
2.3.3. Experiment simulation by Hanses (1985)	35
2.3.4. Sellmeijer's model	37
2.3.5. Piping by heave	40
2.3.6. Schmertmann (2000)	41
2.3.7. Ojha and Singh (2003)	41
2.3.8. Discrete element modelling (El Shamy and Aydin, 2008)	42
2.4. Summary	43
3. Processes	45
3.1. Introduction	45
3.2. Sequence of processes leading to failure	45
3.2.1. Seepage	45
3.2.2. Backward erosion – initiation and progression	46
3.2.3. Widening	48
3.2.4. Failure	48
3.3. Backward erosion	49
3.3.1. Transport of single grains	50
3.3.2. Sand boiling phase	50
3.3.3. Regressive or equilibrium phase	51
3.3.4. Progressive phase	53
3.3.5. Which process will occur when?	53
3.4. Summary	56
4. Experimental work	57
4.1. Introduction	57
4.2. General description of set-up	58
4.3. Sample preparation and sand types	61
4.4. Test procedure and example results	64
4.4.1. Test procedure	64
4.4.2. Examples of sand boils and pipe formation	64
4.4.3. Example test data	66
4.5. Assessing the relevance of forward erosion	68
4.5.1. Objectives	68
4.5.2. Set-up and experimental programme	70
4.5.3. The electrical density method	72
4.5.4. Results	74
4.5.5. Summary	80

4.6. Backward erosion process.....	80
4.6.1. Objectives.....	80
4.6.2. Set-up and experimental programme	81
4.6.3. Results	81
4.7. initiation: Effect of soil type.....	83
4.7.1. Objectives.....	83
4.7.2. Set-up and experimental programme	83
4.7.3. Results	83
4.8. Progression: small-scale experiments	84
4.8.1. Objectives.....	84
4.8.2. Set-up and experimental programme	84
4.8.3. Results	85
4.8.4. Summary	89
4.9. Progression: medium-scale experiments.....	90
4.9.1. Objectives.....	90
4.9.2. Set-up and experimental programme	90
4.9.3. Results	91
4.9.4. Summary	95
4.10. Progression: visualisation experiments.....	95
4.10.1. Objectives	95
4.10.2. Set-up and experimental programme.....	96
4.10.3. Results.....	97
4.10.4. Summary.....	100
4.11. Progression: experiments for pipe dimensions.....	100
4.11.1. Objectives	100
4.11.2. Set-up and experimental programme.....	101
4.11.3. Results.....	101
4.11.4. Summary.....	107
4.12. Summary of laboratory experiments.....	107
5. Pipe initiation	109
5.1. Introduction.....	109
5.2. Past initiation experiments	110
5.3. Initiation head analysis	112
5.3.1. Effect of exit configuration on initiation gradient	112
5.3.2. Effect of scale on initiation gradient	113
5.3.3. Effect of sand layer shape on initiation gradient	114

5.3.4. Effect of sand characteristics on initiation gradient	115
5.3.5. Relationship between H_b and H_c	117
5.4. Model development	117
5.4.1. Theory of pipe initiation	117
5.4.2. Exit gradient analysis	118
5.4.3. Experiment analysis.....	122
5.5. Discussion	131
5.6. Summary	133
6. Pipe progression	135
6.1. Introduction.....	135
6.2. Available progression experiments.....	136
6.3. Critical head analysis.....	138
6.3.1. Effect of exit configuration on critical gradient	138
6.3.2. Effect of grain size on critical gradient	138
6.3.3. Effect of uniformity coefficient on critical gradient.....	139
6.3.4. Effect of relative density on critical gradient.....	139
6.3.5. Effect of scale on critical gradient	139
6.3.6. Effect of sand layer shape on critical gradient	141
6.3.7. Conclusions	141
6.4. Validation of Sellmeijer model.....	142
6.4.1. Validation for 2D configuration.....	142
6.4.2. Validation for 3D configuration.....	143
6.4.3. Conclusions	147
6.5. Empirical pipe characteristics	147
6.5.1. Pipe width.....	147
6.5.2. Pipe depth	153
6.5.3. Width-to-depth ratio	154
6.5.4. Pipe gradient	156
6.5.5. Particle and flow velocity	159
6.5.6. Conclusions	162
6.6. Pipe flow	162
6.6.1. Effect of pipe shape	162
6.6.2. Hydraulic regime.....	165
6.6.3. Flow development	168
6.6.4. Conclusions	168
6.7. Erosion processes	168

6.8. Modelling primary erosion.....	169
6.9. Modelling secondary erosion.....	173
6.9.1. Forces on the particles.....	174
6.9.2. The Shields diagram.....	176
6.9.3. Incipient motion in laminar flow.....	177
6.9.4. Effect of outward gradient on incipient motion.....	184
6.9.5. Effect of slope angle on incipient motion.....	184
6.9.6. Conclusions.....	186
6.10. Synthesis: Validation and extrapolation.....	187
6.10.1. Basic assumptions.....	187
6.10.2. Validation of limit-state equilibrium - pipe depth.....	188
6.10.3. Validation of limit-state equilibrium - pipe shape.....	190
6.10.4. Validation of limit-state equilibrium - critical head.....	192
6.10.5. Validation of hydraulic regime in the pipe.....	194
6.10.6. Discussion and conclusions.....	196
6.11. Discussion.....	197
6.11.1. Primary and secondary erosion.....	197
6.11.2. Modelling primary and secondary erosion.....	197
6.11.3. Effect of sand type on primary and secondary erosion.....	198
6.11.4. Effect of scale on primary and secondary erosion.....	200
6.12. Conclusions.....	201
7. Conclusions.....	203
7.1. Main findings.....	203
7.2. Practical implications.....	205
7.3. Recommendations.....	206
References.....	207
A. Overview of piping experiments.....	215
A.1. Area-type experiments.....	215
A.2. Ditch-type experiments.....	218
A.3. Hole-type experiments.....	219
A.4. Slope-type experiments.....	222
B. Sand characteristics.....	225
B.1. Overview of sand characteristics.....	225
B.2. Friction angles at low stresses.....	226
C. Filter resistance.....	229
C.1. Filter resistance.....	229

D. Pipe contours.....	233
D.1. Small-scale experiments.....	233
D.2. Medium-scale experiments.....	242
List of symbols.....	245
List of figures	249
List of tables	257
List of publications.....	259
Curriculum Vitae	263

1. INTRODUCTION

*'We are not to tell nature what she's got to be.
She's always got better imagination than we have.'*

Richard Feynman

1.1. FLOOD RISK AND THE FAILURE OF DIKE SYSTEMS

Flooding constitutes a major threat for much of the world's population. It may occur when water levels rise in seas, rivers or lakes as a result of storm surges, heavy rainfall or snow melt. Although the accumulation of rainwater in saturated ground can lead to flooding, the most severe floods occur when the rising water overflows or breaches a water-retaining structure.

History provides us with clear instances of the disastrous consequences of flooding, both economic and social. There are numerous recent examples: hurricane Katrina submerged New Orleans in 2005; the western coast of France was flooded by the storm Xynthia in 2010; river floods had a devastating impact on Bangkok in 2011; dikes on the Elbe and Danube in Germany were overtopped and breached in 2013; the South-East of England suffered severe flooding in 2014 and there was flooding recently (May, 2015) in Texas as a result of heavy rainfall.

In 1980-2008, 2887 flooding events were registered worldwide. They caused nearly 200,000 casualties and economic damage amounting to USD 400 billion and affected 2.8 billion people (Flood – Data and Statistics, n.d.). Climate change is expected to lead to more events and more damage unless action is taken. The frequency of flood events in Germany and central Europe has increased by a factor of two since 1980 (Munich Re, 2013).

The habitability of coastal areas and flood plains depends entirely on how water-retaining structures perform when water levels are high. These flood defence structures – generally dikes, storm-surge barriers or dunes – form closed systems to prevent the flooding of the hinterland.

Modern approaches to the assessment of flood defence systems are based on the identification of risk (defined as the probability of flooding multiplied by the impact)

and this, in turn, requires an estimate of the probability of failure in a flood defence system.

Although, worldwide, flooding mainly results from overtopping and the resulting damage to the dike inflicted by the water flowing over it, there are other mechanisms that may result in dike failure. Figure 1.1 gives an overview of failure mechanisms for dikes. All failure mechanisms must be considered in a safety assessment and a sound understanding of the processes involved is therefore needed so that we can predict each mechanism. This dissertation focuses on backward erosion piping, a failure mechanism in which the groundwater flow causes internal erosion that undermines a dike.

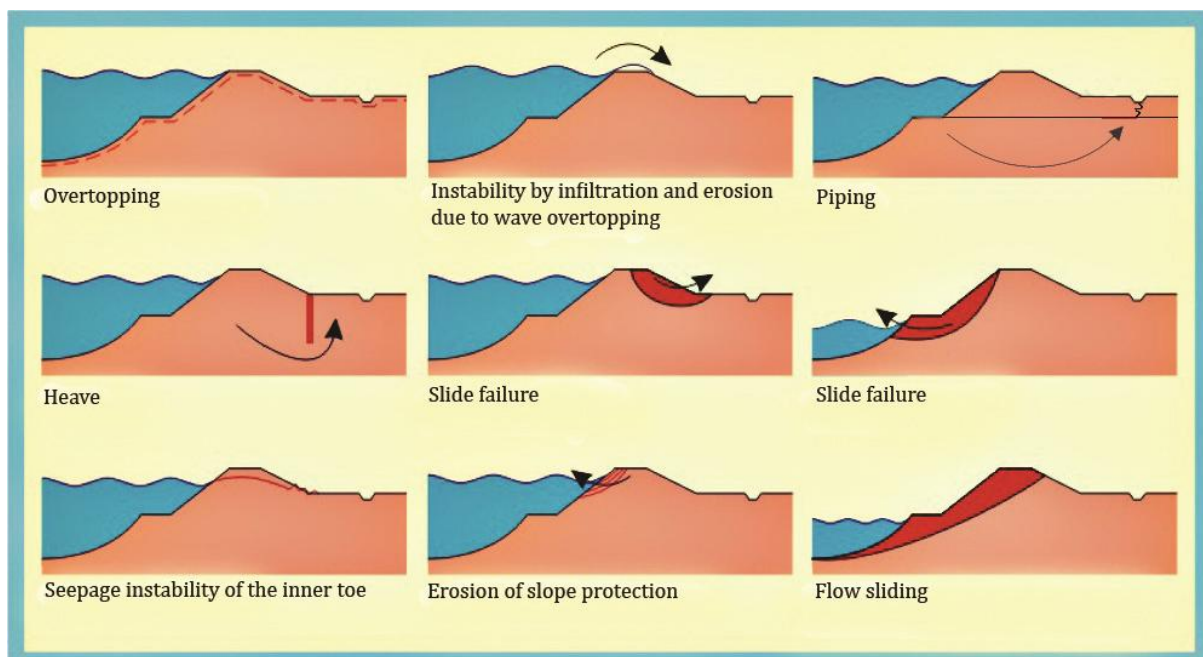


Figure 1.1 Overview of failure mechanisms (adapted after Ministerie van Verkeer en Waterstaat, 2007)

This chapter sets out the background to the dissertation and the reasons for the research, and gives an introduction to flood risk, dikes and backward erosion piping, followed by a presentation of the objectives, contribution and context of this study.

1.2. BACKWARD EROSION PIPING

Backward erosion piping is an internal erosion mechanism in which hollow spaces (pipes) are formed in or underneath water-retaining structures as a result of the removal of soil by the action of water. Seepage causes sand grains to be transported to the downstream side of the structure, leading to the development of shallow pipes that form in an upstream direction, while depositing eroded material on the downstream side of the structure. The pipes develop at the interface of the aquifer and an impermeable cohesive layer since the latter forms the roof above the pipes. One pipe or a pattern of pipes will form in the upstream direction and, when a pipe reaches the upstream side, the continuous flow may cause the pipe to widen and deepen to such an extent that the water-retaining structure becomes unstable.

Several conditions make a water-retaining structure susceptible to backward erosion piping. The hydraulic head has to be high enough to drive pipe formation. However, even when the head is high enough, the process can only occur if a cohesive roof with low permeability is present above the pipes. The impermeable cohesive roof is necessary to prevent the collapse of the pipe and to cause a concentration of flow lines near the outflow area. An open and unfiltered exit is the final pre-condition required for the process to begin. When there is a cohesive top layer, this process can only start after heave or hydraulic fracturing: the uplifting or cracking of the top layer as a result of high water pressure. Cracks may also form over time due to shrinking. In some cases, an open exit will already be present. Seepage erosion – the washing away of the particles – then begins.

The different phases leading to a breach as a result of backward erosion piping are shown in Figure 1.2, showing how the process of backward erosion itself is only one phase in the entire process leading to the breach of the water-retaining structure.

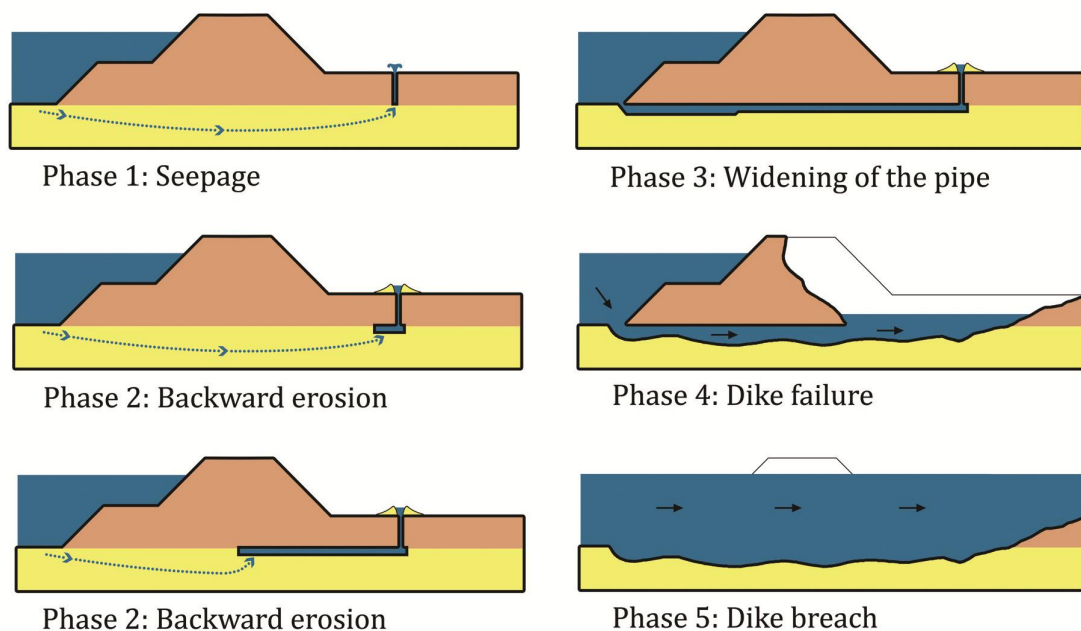


Figure 1.2 Backward erosion leading to dike failure and breach

The Dutch literature often refers to this mechanism as piping. However, in the international literature, 'backward erosion' or 'backward erosion piping' are the preferred terms because piping may refer to other internal erosion phenomena. This dissertation uses the terms 'backward erosion' and 'piping': 'backward erosion' specifically for the process of pipe formation in uniform granular materials in the opposite direction to the water flow, and 'piping' as a more general term for the formation of pipes.

Backward erosion is a form of internal erosion. In many dike systems it is also the only internal erosion failure mode that is considered. However, the other internal erosion mechanisms may also be relevant, especially for other water-retaining structures, such as dams, which can be situated in different geological conditions.

Internal erosion occurs when soil particles in an embankment dam or its foundations are carried downstream by seepage flow. There are four types of internal erosion: concentrated leak erosion, backward erosion, suffusion and soil contact erosion. Suffusion occurs in graded and gap-graded soils and involves the erosion of finer particles from a matrix of coarser particles, removing the finer particles through the pores of the larger particles by seepage flow, leaving behind a soil skeleton consisting of the coarser particles. Contact erosion is a form of internal erosion in which the flow passing through a relatively coarse layer removes fine particles from an adjacent fine-grained layer. Concentrated leak erosion assumes the presence of an opening such as a crack in clay. The walls of the opening are eroded by water flowing through the opening (ICOLD, 2013).

In coastal and delta areas where uniform sands predominate, backward erosion is essentially the only possible type of internal erosion. These conditions are often found in river dikes, such as those on the main rivers in the Netherlands, the Mississippi in the US, and the Yangtze and Nenjiang Rivers in China. In these river systems, backward erosion is known to have led to sand boils and dike failures during floods.

The typical geology near rivers is dominated by alluvial deposits overlying older strata. The shallow subsurface of river systems is therefore highly heterogeneous, with alternating deposits of clay, sand or silt intersected by old river channels. The dikes usually consist of local impermeable material. In the Western part of the Netherlands, the alluvial Holocene layers intersect with (and generally cover) a Pleistocene sandy layer that extends to a considerable depth. In coastal areas and the eastern part of the country, man-made dikes are built directly on sand layers. The situation in which there is a cohesive top layer overlying a sandy aquifer, or a cohesive clay dike located directly on a sandy aquifer, is therefore common in the case of river dikes.

Sand boils are often observed in these river systems. In 1993 and 1995 in the Netherlands, the water in the rivers rose to 0.50-1.50 m below the design level. Approximately 120 and 180 sand-transporting sand boils were observed respectively in those years on the Rhine, Waal, IJssel and Meuse rivers, indicating the susceptibility of Dutch dikes to this mechanism. Although the dikes did not fail, several failures in the past have been attributed to backward erosion piping, examples being the failures near Zalk, Nieuwkuijk and Tholen (Vrijling et al., 2010).

In China, there were several dike breaches on the Yangtze River and Nenjiang River in 1998, at least three of which were caused by backward erosion piping (Yao et al., 2009). Historically, dike failures caused by backward erosion piping have accounted for 90% of the total number of failures in China (Cao, 1994).

On the Mississippi, the St. Louis District authorities documented excessive underseepage (seepage through the aquifer in the foundation of the levee) and the formation of sand boils during the flood events of 1973, 1993, and 1995. Despite continued investigations, analyses, and the addition of control measures since the 1950s, excessive underseepage and the formation of sand boils are still observed. During the flood of 1993, the level of the Mississippi River equalled or exceeded the design level and serious underseepage was encountered in 5% of the reaches (without relief wells) on average, as evidenced by sand boils or piping (districts Alton to Gale, Mansur et al., 2000). The 1995 flood was a lower intensity event. Nevertheless, piping incidents in the Prairie Du Rocher and Fort Chartres Levee District were found to be more numerous

during this flood than during the larger floods of 1993 and 1973 (Glynn and Kuszmaul, 2004). One of the failures in the levee system of New Orleans (2005) was most likely caused by backward erosion, even though the water level had been high for only a couple of hours (Vrijling et al., 2010). Of the sixty major breaches along the Lower Mississippi River in the period between 1890 and 1927, at least six were attributed to piping (USACE, 1956).

Several methods are available to predict the critical head at which backward erosion leads to dike failure: Bligh's empirical rule (Bligh, 1910, Bligh, 1915) and Sellmeijer's model (Sellmeijer, 1988) are the best known in the Netherlands. Bligh (1910) established an empirical relation based on failure and survival observations of embankments. His empirical rule links the critical head H_c to the seepage length L (defined as the pipe path between the upstream level and the downstream level) and soil properties. The Sellmeijer model (1988) is a more advanced approach that adopts the equilibrium of particles in the pipes as a criterion for pipe progression. The critical head is determined by linking the flow towards and in the pipe to this criterion.

The Sellmeijer model is used for safety assessments in the Netherlands. The model was used to predict backward erosion piping for the first time along entire dike rings in the project 'Flood Risk in the Netherlands' (Veiligheid Nederland in Kaart: VNK). This long-term project, for which the final report was delivered in 2014 (VNK, 2014), investigated flood risk and the consequences of flooding in the Netherlands, with the aim of designing measures for cost-effective flood protection. Unexpectedly high failure probabilities were found for the mechanism of piping (early results reported by Vrijling et al., 2010, final results in VNK, 2014), raising questions about the validity of the Sellmeijer model and its application.

This led to a renewed effort to validate the Sellmeijer model for backward erosion in the research programme 'Strength and loads on flood defence structures' (*SBW: Sterkte en Belastingen Waterkeringen*, since 2012 combined with WTI: *Wettelijk toetsinstrumentarium*, which translates as the Statutory Assessment Instrument). The Sellmeijer model (1988) predicts the critical gradient above which the process of piping leads to failure. SBW compared the results of model calculations with the results of small-, medium- and full-scale experiments. It soon became apparent that the model worked well for fine sands, but poorly for medium-grained sands. Validation also proved impossible for loosely-packed sands since the erosion mechanism was found to be different (Van Beek et al., 2009a).

On the basis of multivariate regression using the results of the small- and medium-scale experiments, an empirical change was therefore made to account for the influence of grain size, uniformity coefficient and relative density (Sellmeijer et al., 2011), but a theoretical explanation remained forthcoming. The major implications of the empirical adaptation underlined the need for a more detailed investigation of the backward erosion mechanism.

The results of the SBW research did not indicate that the Sellmeijer model was too conservative (this would have explained the high failure probabilities for piping found in the VNK safety assessment). On the contrary, the failure probabilities increased due to both the adaptation of the Sellmeijer model and the inclusion of the length effect.

In addition, Vrijling et al. (2010) concluded that substantial changes in the outcomes of the VNK study were unlikely using schematisation refinements and that the VNK study

probably presents a realistic picture of dike safety. The conclusion is therefore that piping continues to be the most important potential failure mechanism in the dike rings considered and that the fundamental questions raised by the SBW research require further examination.

The purpose of this study is to examine the backward process in more detail, to establish a theoretical explanation for the outcomes of the empirically adapted Sellmeijer model of 2011 in coarser sands and to devise a validated prediction model. The relevance of the new erosion mechanism for loose sand will be investigated. The present study focuses mainly on backward erosion in homogeneous sands. In the field, the heterogeneity of the subsoil will affect both parameter selection and the process of backward erosion, as will be discussed later. Kanning (2012) has investigated the effect of the spatial variability of soil characteristics and the corresponding parameter selection. Recent research by Schweckendiek (2014) shows that investment in uncertainty reduction measures such as monitoring or site investigation can be very cost-effective. For a proper understanding of the backward erosion mechanism, a study in homogeneous sands is an essential first step. The application of the model to the field has proven to be a second, but no less important, step.

1.3. RESEARCH OUTLINE

1.3.1. PROBLEM STATEMENT

Dike safety assessment requires a way of predicting the occurrence of backward erosion. At present, the Sellmeijer model (Sellmeijer, 1988) is the most advanced method in use in the Netherlands. Recent laboratory experiments (Van Beek et al., 2011) suggest that the Sellmeijer model is unsuitable for the prediction of backward erosion in medium-grained sands or loose sands. An empirical adaptation has been proposed in line with those findings (Sellmeijer et al., 2011). However, due to the lack of a theoretical basis, this proposed empirical adjustment is unsatisfactory and lacks robustness. Furthermore, in experiments with loosely packed sands, a different erosion mechanism has been observed in which the pipes form in the direction of the flow rather than in the opposite direction. The practical implications of this newly observed mechanism are unclear.

1.3.2. RESEARCH QUESTION

On the basis of the problem statement, the research question is:

How can we explain and predict the pipe-forming erosion processes in uniform sands?

The following sub-questions have been defined:

- What are the processes that determine pipe formation and progression?
- Which mechanisms are observed in experiments that are not described by Sellmeijer's model (1988), or not adequately described?
- How can we improve the model to remedy any shortcomings?
- What are the practical implications of the mechanism in loose sand in which the pipe develops in the direction of flow?

1.3.3. METHOD

The method adopted to establish answers to the research questions was primarily experimental. The experiments were used to analyse the different phenomena involved.

To explain the discrepancies observed between the model calculations and the results of backward erosion experiments, and to investigate the mechanism of forward erosion, the erosion processes were investigated in greater detail. The available experiments (from both the SBW programme and the literature) were analysed to describe the piping process from the first signs of erosion to failure. Additional experiments were performed to elucidate some aspects of this process. In addition, experiments were performed to test the relevance of the mechanism of forward erosion in loose sands.

In some experiments, equilibrium in pipe formation was seen; in others, the pipe developed in the upstream direction without the hydraulic head being increased. The resulting analysis and development of the prediction models was therefore subdivided into two areas: pipe initiation and pipe progression.

Experiments conducted in the past were used as the principal basis for modelling pipe initiation. Additional experiments were performed to clarify the individual effects of grain size and uniformity coefficient. The modelling of pipe initiation was based on an analytical description of groundwater flow.

Since there have only been small numbers of experiments in the past in which the progression phase dominated, many additional experiments were performed to clarify and model the pipe-progression phase. These additional experiments served to determine the critical head and to study the erosion mechanism, pipe hydraulics and pipe dimensions. Physical equations for pipe flow were used to understand these components better.

1.3.4. CONTRIBUTION

The study contributes to our understanding of the piping process. The main contribution is the distinction between pipe initiation and pipe progression as separate processes and the determination of how they affect the critical head. Understanding the interaction between initiation and progression is fundamental to any experimental research looking at piping, but it also produces relevant information for practice, where the assessment of sand boils in relation to the groundwater flow configuration can be useful in determining dike stability.

In the case of both initiation and progression, the critical head is sensitive to the type of exit. A 3D exit causes the flow to concentrate, resulting in a lower critical head than in an equivalent situation with a 2D exit.

Pipe initiation will prove to be predominantly relevant in small-scale experiments with a large exit area. Predicting pipe progression will therefore remain the main instrument for predicting piping in the field. The future numerical modelling of pipe progression requires an examination – and this is the main focus of this dissertation – of the erosion process, pipe hydraulics, pressure distribution in the pipe and pipe dimensions. The proposed beneficial effects of heterogeneity on critical head can be calculated once the relevant models have been elaborated further on these lines.

1.3.5. CONTEXT

Before this research began, the Sellmeijer model was validated in the SBW programme, as summarised in Van Beek et al. (2011) and Sellmeijer et al. (2011). Several fundamental questions arising from the SBW programme will be addressed in this dissertation. Large parts of the research described here were conducted within the framework of the 'Research and Development of Flood Defence Assessment Tools WTI2017', a programme funded by Rijkswaterstaat (Centre for Water Management) on behalf of the Dutch Ministry of Infrastructure and the Environment.

1.4. DISSERTATION STRUCTURE

Backward erosion has already been investigated extensively by other researchers. This dissertation therefore starts in Chapter 2 with a description of the literature and a review of the available experiments and prediction models, showing that, depending on the soil characteristics and set-up, a range of processes have been observed in experiments in which a sand bed is subjected to a hydraulic head. The type of process (observed equilibrium and progression-dominated or no equilibrium and initiation-dominated) has been neglected so far in the calibration and derivation of prediction models, which effectively link all the critical heads obtained from experiments to the prediction model at hand. In Chapter 3, the observations of the available backward erosion experiments in uniform soils are analysed to establish a description of the backward erosion piping processes, with the experiments being subdivided into those dominated by either pipe 'initiation' or pipe 'progression'.

In experiments where pipe initiation predominates (when no equilibrium in pipe formation is observed), a different prediction method is required than in experiments where pipe progression is the dominant factor (when equilibrium is observed in pipe formation). When initiation predominates, the local gradients near the exit determine the critical head; when progression predominates, the hydraulic conditions in and around the pipe play a role. This dissertation analyses both processes in greater detail.

Chapter 4 reports on the experimental work conducted in order to address the research questions. Some of the experimental work was conducted to address questions related to the process, such as the assessment of the relevance of the 'forward piping' observed in loose sands, or the assessment of the relationship between configuration and the type of process. Another part of the experimental work was performed to quantify the backward erosion process, such as those experiments that add to the database of pipe initiation experiments, or the investigation of the influence of sand type on the critical head for pipe progression. Some experiments served both purposes, such as the small-scale experiments in which the depth and width of the pipe were measured using a laser.

The experiments – both the experiments from the literature and the new experiments – were used to investigate the prediction of pipe initiation and pipe progression. No model was yet available for pipe initiation and so a new model was developed based on the fluidisation of sand near the exit of an experiment. This model is described in Chapter 5.

Chapter 6 describes a detailed study of the mechanisms relating to the progression of the pipe. The experiments confirm the findings of Hanses (1985) that the progression of the pipe results from two erosion processes with different physical origins: primary

erosion, which governs erosion at the pipe tip and results in lengthening, and secondary erosion, which governs erosion at the pipe walls and the pipe bottom, broadening and deepening the pipe. Both processes have been analysed, providing a better understanding of the backward erosion mechanism and establishing a basis for improvements to the Sellmeijer model.

The dissertation ends with a chapter containing conclusions and recommendations.

2. LITERATURE

'Most likely everyone who has studied the piping problem realizes its complexity and difficulty.'

John H. Schmertmann

2.1. INTRODUCTION

This chapter describes the experimental work conducted in the past, as well as the models and calculation rules developed for backward erosion piping.

Failure involving piping is not a common event and specific cases are often poorly documented. Sand boils are observed when water levels are high, but the mechanism takes place below the surface and so the process itself is difficult to study in the field. Experiments are therefore indispensable to understand and predict piping. They allow for the detailed investigation of the mechanism and for the investigation of critical head in controlled conditions so that models can be developed, calibrated or validated. As described in this chapter, the critical heads obtained in the experiments, and to a lesser extent the processes by which erosion occurs, depend on many variables. Scale, shape, inlet and exit configuration, sand type and relative density are variables that affect the critical head and critical gradient. As a result, critical heads in different set-ups cannot be compared directly. The experiments in the literature can be grouped on the basis of the research centres or institutes that use the same set-up, allowing for the direct comparison of critical heads. The experiments presented here have therefore been grouped by research institute, after an overview and a general description of the differences in set-up.

Various models are available for predicting the critical head (the head at which the pipe reaches the upstream side). Most of them are based on experiments or case histories, and some on theoretical descriptions of the phenomena involved, such as groundwater flow and sand transport, that have been subsequently validated in experiments. These models are described in section 2.3.

2.2. EXPERIMENTS

This section summarises the experiments that have been conducted in the past, providing a general description of the variations in set-up and the main results. The overview (2.2.1) and the descriptions of the set-ups (2.2.2) have been taken from Van Beek et al. (2013). The relevant detailed data and more specific set-up schematics can be found in Appendix A. The focus is on experiments with a horizontal seepage path. However, for the sake of completeness, this chapter also provides summaries of experiments involving distinct engineering structures requiring a vertical piping path.

2.2.1. OVERVIEW

Several authors have studied the process of backward erosion piping in a variety of laboratory set-ups. The goal of experimental work on backward erosion piping is mainly to investigate the erosion mechanism, or to develop or validate safety assessment criteria for dikes and dams. All the experiments subject a sand sample to a horizontal hydraulic gradient. The exit is such that sand grains are free to be transported at the downstream side of the sand sample. A horizontal cover consisting of a cohesive and impermeable material is placed on top of the sand sample to confine the sand layer and to act as a stable roof for the pipes. The main differences in set-up relate to the type of inlet, the exit, the scale, the preparation method, the cover type and the parameters measured. The experiments have been subdivided into the categories small-scale (<1 m of seepage length), medium-scale (1-5 m of seepage length) and large-scale (>5 m seepage length).

Table 2.1 shows an overview of the experimental studies of the phenomenon of backward erosion piping in the foundations of dikes containing no engineering structures (horizontal seepage path). Table 2.2 gives an overview of experiments that do contain separate structures or in which some parts of the seepage path are vertical.

Table 2.1 Overview of research on backward erosion piping (horizontal piping path)

Source	Goal of research
Miesel (1978)	Erosion mechanism and effect of size of exit diameter.
Müller-Kirchenbauer (1978)	Erosion mechanism in sand samples with multiple layers.
Pietrus (1981)	Effect of artificially created pipe length and radius on critical head.
Hanses (1985)	Erosion mechanism, pressure development in pipe and effect of scale on the critical head.
De Wit (1984)	Effect of scale, type of exit point and sand properties on the critical head.
Townsend et al. (1988)	Effect of sand characteristics on the critical head.
Silvis (1991)	Investigation of scale effects.
Van Beek et al. (2008)	Lateral heterogeneity.
Yao et al. (2007)	Investigation of effect of configuration on piping process and critical head.
Ding et al. (2007)	Investigation of piping in sand samples with multiple layers.
Van Beek et al. (2011)	Effect of scale and sand properties on the critical head.

Table 2.2. Overview of experiments containing a separate engineering structure or a partly vertical seepage path

Source	Goal of research
Achmus and Mansour (2006)	Effect of relative depth and location of multiple cut-off walls.
Okajima and Tanaka (2008)	Validation of prediction models for the failure of embedded structures with different widths.
Ding et al. (2008)	Effect of relative depth and location of cut-off wall on critical head.
Van Den Ham (2009)	Investigation of process and critical head.
Okajima et al. (2010)	Validation of prediction models for the failure of an embedded structure or structure with cut-off at different locations.

2.2.2. SET-UP

A variety of experimental set-ups have been used in the past, each of which have specific advantages and disadvantages. All the backward erosion piping set-ups prepare a sand sample in a box in such a way that it can be covered by a cohesive material. An inlet and outlet are present and a constant hydraulic head difference can be applied to the sand sample. The main differences are found in the type of outlet and inlet, the cover type and the method adopted for sample preparation. There is no optimal set-up for every situation. The benefits and drawbacks of each aspect of the set-up should be carefully considered in backward erosion piping tests.

The types of inlet and outlet are important since both have a major impact on the flow pattern in the sand. Figure 2.1 provides an overview of the different types of inlets and outlets. The inlet is usually a vertical filter (type I). Some set-ups have used a horizontal inflow area (type II) (Silvis, 1991, large-scale experiments by Van Beek et al., 2011). The type II inlet has also been often used in experiments containing distinct engineering structures (Achmus and Mansour, 2006; Okajima and Tanaka, 2008; Okajima et al., 2010), and in this case no filter is needed to retain the sand.

The type of exit can be divided into four main categories: plane (type A), ditch (type B), hole (type C) and slope (type D). Several researchers have specifically investigated the impact of exit type on process and critical head. De Wit (1984) used the plane-type exit (A) in most experiments but also performed a few experiments using a ditch-type (B) and hole-type (C) exit to investigate the role played by exit configuration. Yao et al. (2007) investigated the plane type and the hole type. Miesel (1978) varied the diameter of the exit hole (type C) to investigate the differences in the erosion process and critical head.

Few experimental series have varied the exit type. The hole-type exit has been used by many researchers (Miesel, 1978; Müller-Kirchenbauer, 1978; Hanses, 1985; Ding et al., 2007; Yao et al., 2007). In most experiments the thickness of the cohesive blanket layer, d in Figure 2.1, is explicitly taken into account by placing a vertical tube, as shown in Figure 2.4, on the hole-shaped outlet (type C). The sand needs to be transported through the tube before it can be deposited. An additional head drop is required to overcome this considerable vertical distance.

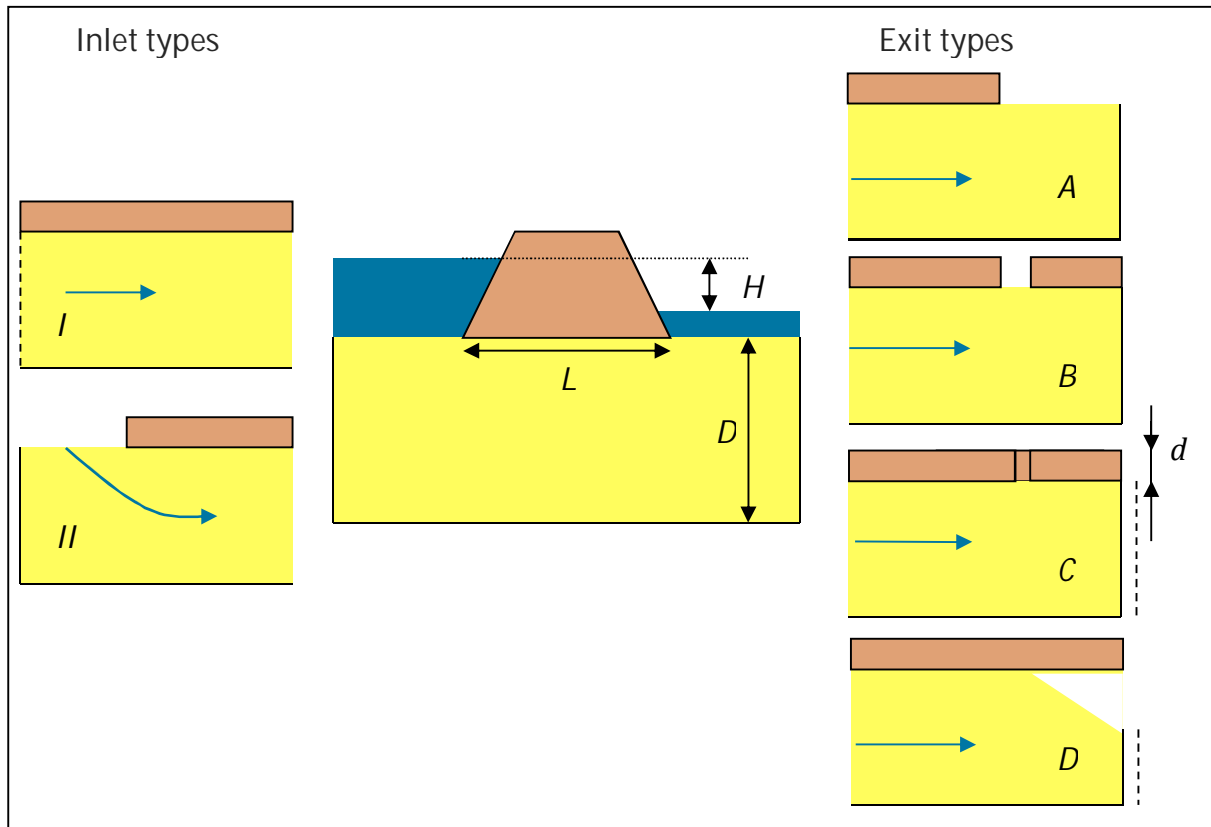


Figure 2.1. Different inlet types (vertical filter (I) and horizontal inlet (II)) and exit types (plane- (A), ditch- (B), hole- (C) and slope-type (D) exit); the slope- and hole-type exits can have either a filter or closed boundary at the downstream end.

Plane-type exits were most widely used in experiments involving a distinct engineering structure (Achmus and Mansour, 2006; Okajima and Tanaka, 2008; Okajima et al., 2010), in the full-scale experiments described by Van Beek et al. (2011), and in the small- and medium-scale experiments conducted by De Wit (1984). Silvis (1991) described large-scale experiments with a ditch-type exit (type B). Experiments by Townsend et al. (1988) and Pietrus (1981) and the small- and medium-scale experiments of Van den Ham (2009) and Van Beek et al. (2011) used the fourth exit type: a slope (type D).

All the types of inlets and outlets may correspond to particular field conditions. In some cases, the river is deep and cuts through the cohesive blanket layer and the sand. The set-up with a vertical filter (type A) is the best approximation of the flow in this situation. In other cases, the river does not cut through the sand layer and the inflow is mainly in the vertical direction (in some cases covered by a semi-permeable layer). In that case, a set-up with a horizontal sand bed is more appropriate (type B). The degree to which the downstream part of the sandy layer is covered by a cohesive layer determines the kind of exit that is most suitable. Figure 2.2 shows three exit types: plane (a), ditch (c) and hole (b). The slope exit type is not very common in the field.

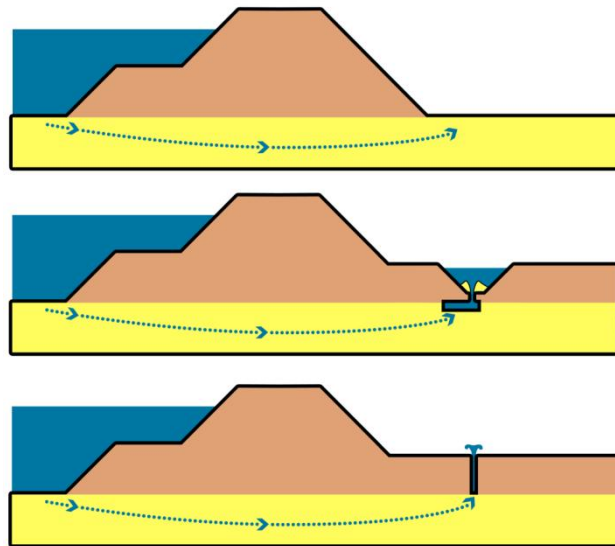


Figure 2.2. Three exit types: plane (a), ditch (b) and hole (c)

Several types of configuration can be used to investigate the presence of backward erosion in the presence of separate engineering structures with a vertical section like a cut-off. Embedded structures have often been used (Okajima and Tanaka, 2008; Okajima et al., 2010; Achmus and Mansour, 2006) in combination with one or more cut-off walls at various locations. Other experiments have used only cut-off walls at different locations beneath the simulated dike (Van den Ham et al., 2009; Ding et al., 2008).

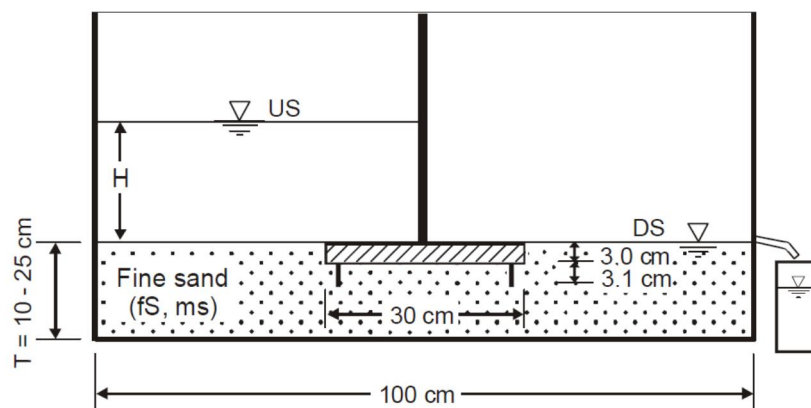


Figure 2.3. Example of an embedded structure in combination with cut-offs (set-up used by Achmus and Mansour, 2006)

2.2.3. EXPERIMENTS AT THE UNIVERSITY OF BERLIN

A major research programme was conducted at the University of Berlin to investigate the mechanism of backward erosion piping. The experiments were described in Miesel (1978), Müller-Kirchenbauer (1978), Hanses (1985) and Müller-Kirchenbauer et al. (1993).

Miesel (1978) investigated the piping process in two experimental set-ups. The first was a scaled version of a zoned dam on a sand layer (seepage length 1.36 m, width 0.32 m, thickness ~ 0.10 m), with a thin blanket layer downstream of the dam. For reasons of convenience a more practical set-up was developed later (Figure 2.4) consisting of an acrylate box with a vertical filter inlet and a hole-type outlet containing a sand bed measuring $0.77 \times 0.168 \times 0.168$ m (seepage length 0.71 m). The downstream blanket layer was simulated using a vertical tube. The diameter of the exit hole was varied to investigate its effect on the erosion process and critical head. All experiments were performed with Sand F, about which no details were given.

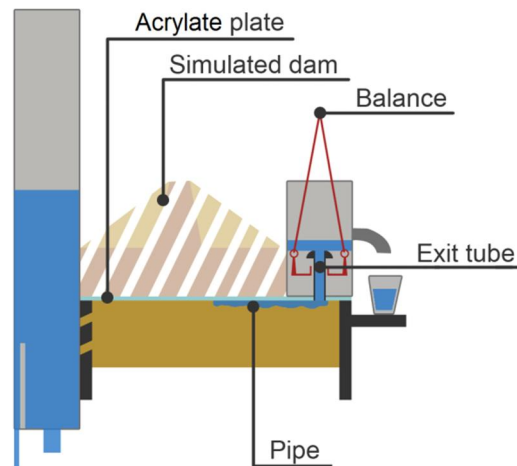


Figure 2.4. Schematic of the set-up used at the University of Berlin

On the basis of the experiment with the simulated dam, the following observations were made with respect to the sequence of processes:

1. Stationary flow, no fluidisation.
2. Fluidisation: sand is loosened in the exit hole, grain sorting in the sand suspension, but no sand ejection.
3. Ejection of all grain fractions (fine followed by coarse fractions) and pipe formation.
4. Pipe formation to the upstream side.

It was noted that the pipe formation in phase 3 did not continue unless a critical head was reached, marking the transition to phase 4.

The experimental results for the different exit diameters can be found in Figure 2.5. At a very small diameter, fluidisation did not take place at all due to bridging; a minimum diameter of 2.65 mm was necessary for sand grains to pass through the hole, which was approximately 4 times d_{95} . When the exit diameter was small, fluidisation occurred at a relatively low head. A head increase led to the gradual filling of the vertical section at the outlet with a sand suspension, indicating the transport of sand from the sample. After several increases in the head, the tube filled up and the sand was ejected, after which pipe development stopped repeatedly, starting again when the head increased, at which point the pipe developed in the upstream direction. Once a given head drop was reached, pipe development did not stop until the pipe reached the upstream side. At

larger exit diameters ($>13\text{mm}$), fluidisation occurred at a relatively high head and several head increases were needed before the tube filled up and the sand was ejected from the tube. Once the tube was full and sand was ejected, the pipes developed in the upstream direction without any further head increase being required.

Müller-Kirchenbauer (1978) used a similar set-up to that developed by Miesel (1978) to investigate how multiple layers affect the process and critical head. The dimensions of the sand sample in this set-up were $0.79 \times 0.24 \times 0.24\text{ m}$, with a seepage length of 0.73 m , an exit-hole diameter of 6 mm and a vertical exit length of 0.184 m . In these experiments a relatively fine sand layer ($d_{60}/d_{10}=2$ and $d_{10}=0.15\text{ mm}$) was located on top of a coarser sand layer ($d_{60}/d_{10}=2$ and $d_{10}=0.15\text{ mm}$), and the ratio of the thicknesses of the two layers was varied. Although the process was not affected by the configuration, the critical head was found to fall in line with the ratio between fine and coarse layer thicknesses.

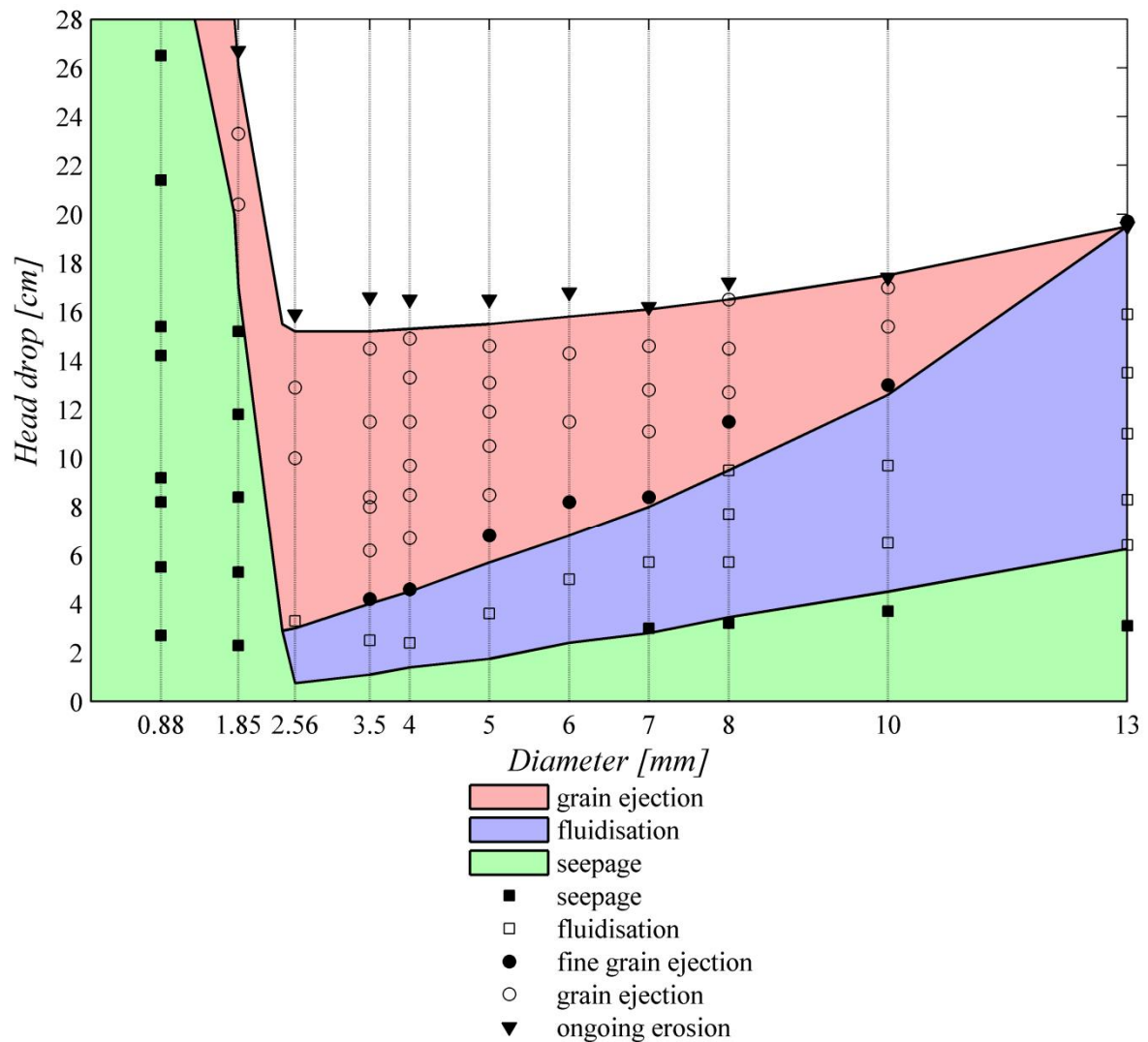


Figure 2.5. Effect of exit diameter on piping process (based on figure in Miesel (1978))

Hanses (1985) investigated the effect of geometric variations in the sand sample on the pipe formation in both homogeneous sand layers and multiple layers. Four configurations were used – M0, M1 and M3 – which varied both in scale ($M1/M3=3$) and D/L ratio:

- M0: 0.96x0.24x0.24 m, seepage length 0.72 m
- M1: 0.90x0.083x0.165 m, seepage length 0.66 m
- M3: 3.52x0.33x0.66 m, seepage length 2.64 m

M0-2 was identical to M0, but with a filter layer underneath the fine sand layer. The experiments for configurations M0, M1 and M3 were performed using a hole-type exit with a diameter of 6 mm and those for configuration M0-2 used a diameter of 8 mm. The critical gradient was found to depend on the configuration and to decrease with scale.

Hanses (1985) distinguished between two types of erosion: primary erosion, which is the erosion of grains from the soil matrix at the tip of the pipe, and secondary erosion, which is the widening and deepening of the pipe. According to Hanses (1985), primary erosion occurs when the hydraulic gradient at the head of the pipe reached a critical value such that fluidisation of sand took place, allowing the sand to be transported. The flow velocity in the pipe as determined by the inflow of water from the sand matrix may reach a critical value that leads to secondary erosion. It was noted that the sand transport at the tip of the pipe was intermittent: groups of sand grains went into suspension and formed 'clouds' of particles that were transported through the pipe. The pipe shape was determined by making a plaster cast of the pipe and the pipe depth was found to be approximately 1-2 mm (5 times the mean grain diameter) near the pipe tip, where there was only a small increase in the pipe width of 15-20 mm. Further from the tip, and with increasing length, the pipe widened and deepened. In the case of long erosion pipes (>0.25 - 0.30 m), scour led to changes in the lateral position of the pipe.

Given the finding that the pipe-tip dimensions remained similar when the set-up dimensions varied, Hanses (1985) concluded that the hydraulic conditions near the pipe head had to be the same in each of the experiments, indicating the importance of primary erosion for the development of the pipe.

The hydraulic heads in the pipe at the critical head were obtained by extrapolating the hydraulic head distribution at the subcritical head. The head loss along the length of the pipe was found to be approximately linear. The average pipe gradients varied for the different configurations. The experimental results – critical heads and pipe gradients – are listed in Appendix A and in Chapter 6.

The pipe volumes were determined on the basis of the weight of the ejected sand volume. In the homogeneous sand experiments, there was a linear relationship between the pipe length and pipe volume. The volumes of the pipes in M0 and M3 were more or less the same for comparable pipe lengths, but the volume was much smaller in M1, a finding that was explained by the smaller erosion lens. No relationship was established between pipe depth and pipe length, due to the interference from the erosion lens.

Given the pipe contours and eroded volumes in some of the experiments performed in their research programme in Berlin, Müller-Kirchenbauer et al. (1993) calculated the pipe depth using the eroded volume of sand and assuming a triangular pipe. An important finding was that the pipes expanded laterally, while the average depth remained virtually constant, as the pipes lengthened.

2.2.4. EXPERIMENTS AT THE UNIVERSITY OF FLORIDA

A total of 37 piping experiments were performed at the University of Florida from 1981 to 1995. The experiments have been described in Pietrus (1981), Wong (1981), Townsend et al. (1988) and Schmertmann (1995), and summarised by Schmertmann (2000). Most of the tests were performed by Pietrus (1981) and Townsend et al. (1988).

The set-up used for these experiments included a vertical filter inlet and a slope-type exit (Figure 2.6). The sand bed contained in the flume measured 1.88x0.305x0.305 m and the seepage length was 1.524 m. A pressure bladder was used to simulate overburden. An artificial pipe was created before the start of all experiments.

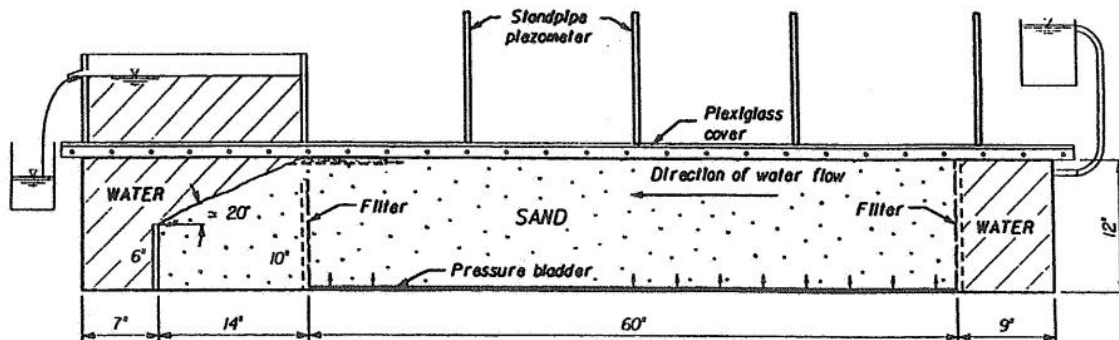


Figure 2.6. Schematic of UF flume (Schmertmann, 2000)

Pietrus (1981) varied the dimensions of this artificial pipe to investigate its effect on the critical head and the process in one sand type (Reid Bedford: $d_{60}/d_{10}=1.5$ and $d_{50}=0.20$ mm). The artificial pipe was created by inserting a semi-circular dowel with a radius of 3.2-15.2 mm and a length that was 10% to 50% of the total seepage length. In all experiments, the effective stresses in the sand were increased by pressurising the bladder. In most experiments, the bladder pressure was 34.5 kPa; the pressure was doubled in two experiments to investigate the impact on the critical head and it was concluded that bladder pressure does not significantly affect the test results.

The pipe dimensions affected both the process and the head at which pipe initiation and pipe progression occurred. The test results indicated lower initiation gradients at smaller pipe diameters and longer pipe penetrations. However, the final gradient required for the pipe to progress fell as pipe penetration and diameter increased (Figure 2.7). Equilibrium in pipe formation was not always seen in these experiments. In some experiments the eroded sand was deposited in the pipe and blocked it.

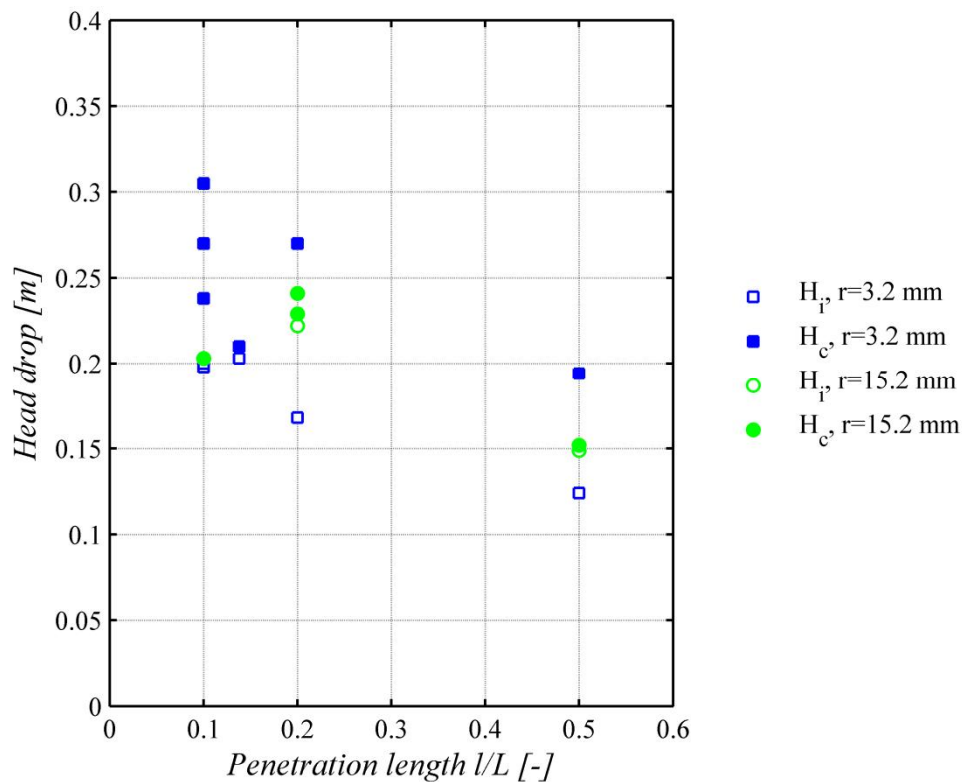


Figure 2.7. Initiation and critical heads from the experiments by Pietrus (1981) using dowels with different penetration lengths and radii

Townsend et al. (1988) used the same configuration to investigate the role of soil type, including uniform, graded and gap-graded sands. Artificial semi-circular pipes were created with a radius of 3.2 mm and different penetration lengths (15-50%). The graded and gap-graded soils did not undergo pipe formation but 'sheet flow', in which a large part of the surface fluidised at once. By contrast, in the non-uniform sand types ($d_{60}/d_{10} > 5$), there was no failure at all in the range of the gradient used in the set-up (the maximum gradient was 1.2). The uniform sands investigated were Reid Bedford, 20/30 ($d_{60}/d_{10} = 1.6$ and $d_{50} = 0.93 \text{ mm}$) and 8/30 ($d_{60}/d_{10} = 2.1$ and $d_{50} = 1.6 \text{ mm}$). Townsend et al. concluded that a higher gradient is required to induce piping in a well-graded cohesion-less soil than in a uniform cohesion-less soil. The initiation gradient increased with grain diameter in uniform sands. In some experiments, equilibrium was observed, requiring an increase in the head for the pipe to progress whereas, in other experiments, the pipe developed in the upstream direction without any further increase in the head.

2.2.5. EXPERIMENTS FOR C.O.W.: DE WIT (1984)

The Laboratory for Soil Mechanics in Delft conducted a large research programme for C.O.W. (Centrum Onderzoek Waterkeringen, the Water Defences Research Centre) to investigate the mechanism of piping with the intention of producing recommendations for dike design. The results of this research programme were summarised in De Wit

(1984). The programme studied the effects of geometry, soil type, relative density and exit configuration on the piping process and critical head.

The experiments were performed in small- and medium-scale set-ups consisting of a box in which the sand sample could be prepared and covered by a clay layer. The clay layer was loaded with weights. Most experiments were performed in models I and II, as shown in Figure 2.8, with a vertical filter inlet and plane-type outlet. Models III and IV were identical to model II except for the clay covers, which were 4.5 m and 1.2 m long respectively. The medium-scale set-up was also used to perform experiments with a hole-type exit. In these experiments, the entire sand bed was covered by clay, with circular holes (diameter 0.04 m and 0.10 m) at a distance of 2.4 m and 4.5 m (model VI). The ditch-type exit was investigated in the small- and medium-scale set-up, in which the seepage lengths were 0.90 m and 2.70 m and the ditch width was 0.05 m (models V and VII).

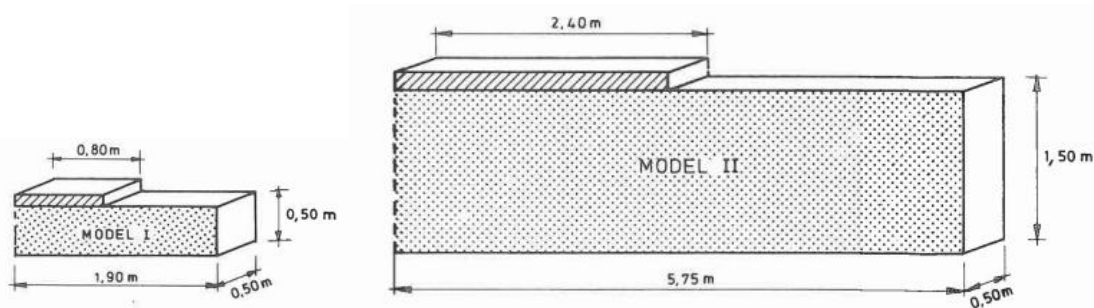


Figure 2.8. Plane-type exit models Model I and II (De Wit, 1984)

The sand types tested were Dune sand ($d_{60}/d_{10}=1.48$, $d_{50}=0.190$ mm), Beach sand ($d_{60}/d_{10}=1.33$, $d_{50}=0.200$ mm), River sand 1 ($d_{60}/d_{10}=2.30$, $d_{50}=0.400$ mm), Sieved River sand 1A ($d_{60}/d_{10}=2.10$, $d_{50}=0.365$ mm) and Coarse sand ($d_{60}/d_{10}=3.85$, $d_{50}=0.750$ mm).

The observations during the experiments were comparable for most sand types and configurations, although some differences are noteworthy. The clay cover meant that observations were limited to the processes at the toe of the dike:

1. Expansion of the sand bed: at the toe of the clay layer the sand started to expand, creating an elevated area 1 mm high and 15 to 20 mm wide (clearly observable in fine sands, not very evident in medium-grained sands and not visible in coarse sand).
2. Small holes due to the local wash-out of grains near the toe of the dike.
3. When the head was increased, small sand boils that lifted and deposited sand were seen. There was no sand transport.
4. When the head was increased further, more boiling of sand was seen in sand boils but there was generally no sand transport.
5. When the head was increased further again, a sand boil started to deposit sand and grow in size. A crater was formed. The process continued until breach.

In the experiments with a hole-type exit, observations 1-4 were similar. However, as soon as sand was transported, the hole was filled with a layer of sand. In a test with a relatively small exit diameter (0.04 m), sand transport stopped after a period of time. A further increase in the head drop caused the level of sand in the hole to rise. When the

sand reached the top of the clay layer and sand was deposited on top of the clay layer, the process continued without any further increase in the head. In the test with a 0.1 m diameter exit hole, sand transport did not stop once it had started. The hole was filled with sand and erosion continued until breach without any increase in the head. The observation that sand transport does not stop once it is transported on top of the clay layer concurs with Miesel's findings (1978, described in section 2.2.3), who also found this behaviour for a relatively large exit hole.

Most experiments measured both the head required for sand boiling and the critical head. The difference between these two heads was limited in some experiments (plane-type, fine sands) and considerable in others (ditch-type, coarse sands).

Figure 2.9 and Figure 2.10 show the critical gradients for the small- and medium-scale plane-type configurations. The critical head was affected by all the variables tested:

- Scale: the critical gradient decreased with increasing scale in all configurations.
- Soil type: the critical gradient increased with increasing grain diameter.
- Relative density: the critical gradient decreased slightly as porosity increased, although the relationship was not the same for all sand types.

Finally, the role of a pressure load that resulted in an increase in effective stress was tested in small-scale plane-type experiments on Beach sand. The load on the clay cover was increased threefold with respect to the load in 'standard' experiments so that a load ranging from 8.8 to 16.2 kPa was present from the downstream to the upstream side of the clay layer. The critical head in the more heavily loaded sample was comparable with critical heads found for the usual experiments (De Wit, 1977).

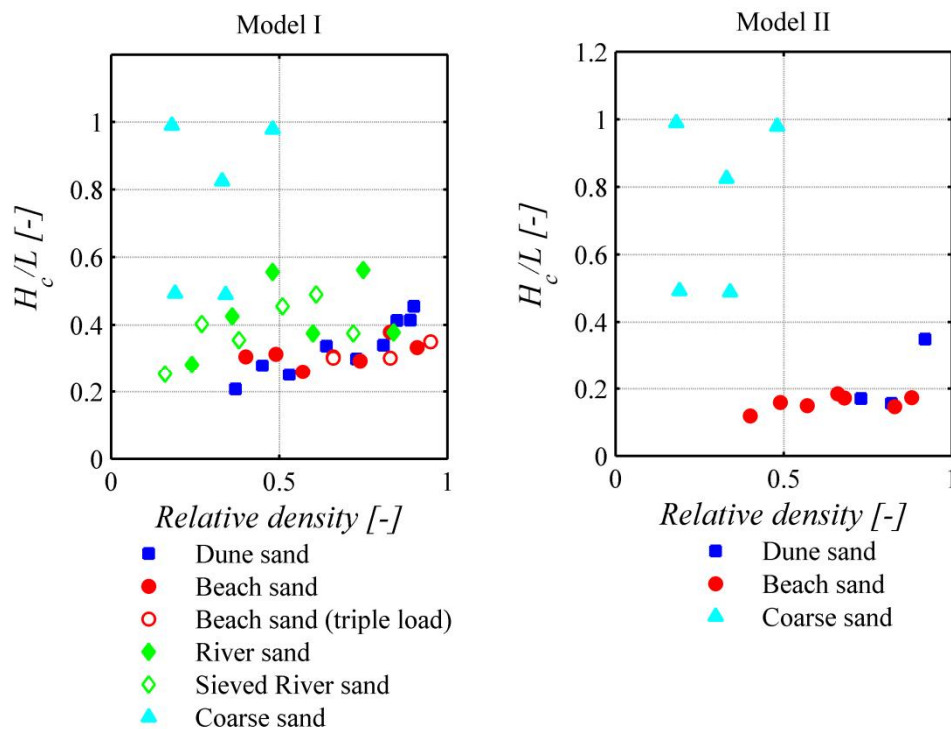


Figure 2.9. Critical gradients as a function of relative density for models I and II (plane-type exit)

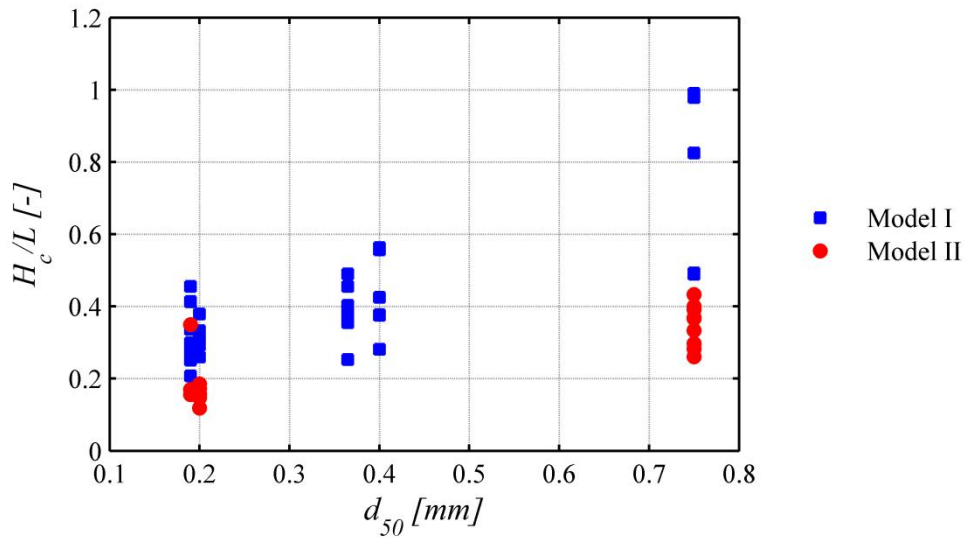


Figure 2.10. Critical gradients as a function of grain size for models I and II (plane-type exit)

2.2.6. DELTA FLUME EXPERIMENTS: SILVIS (1991)

Silvis (1991) described the large-scale experiments conducted in the Delta Flume to validate the original Sellmeijer model (Sellmeijer, 1988). In the first test, there were leaks between the different parts of the cover. After several adjustments had been made to the set-up, three successful experiments were conducted with different seepage lengths: 6, 9 and 12 m. A horizontal inlet was installed and the water exited via a ditch that was 0.5 m wide (Figure 2.11). The dimensions of the sand bed were 33.5x6x5 m, and the downstream length was 10.5 m. The tested sand type was Marsdiep sand ($d_{60}/d_{10}=1.6$, $d_{50}=0.211$ mm). The sand bed was covered by a plastic sheet and a steel plate. Part of the steel plate was replaced with acryliclate so that pipe formation could be observed.

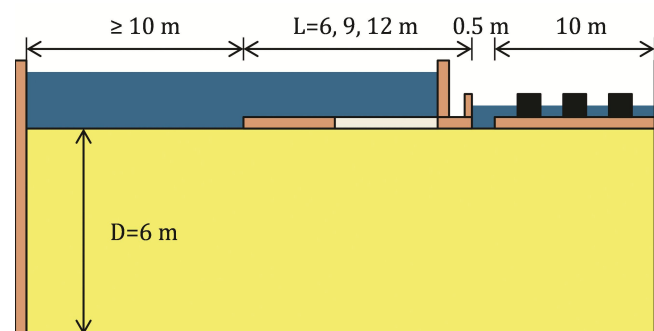


Figure 2.11. Schematic of the large-scale experiments (Silvis, 1991)

When the head was increased, the following observations were made:

1. Turbid water as a result of fine particles in suspension.
2. Sand boils: no sand transport.
3. Sand boils transporting sand: a crater was formed. The process stopped in time and continued when the head was increased.

4. With increasing head, the sand boils increased in size and the pipes increased in length. A pattern of pipes was formed (Figure 2.12). The experiments were stopped when the pipe reached half the seepage length.

In all experiments the critical gradient was approximately 0.18 irrespective of the seepage length. It is assumed here that the gradient at which the pipe reaches half of the seepage length is equal to the critical gradient.

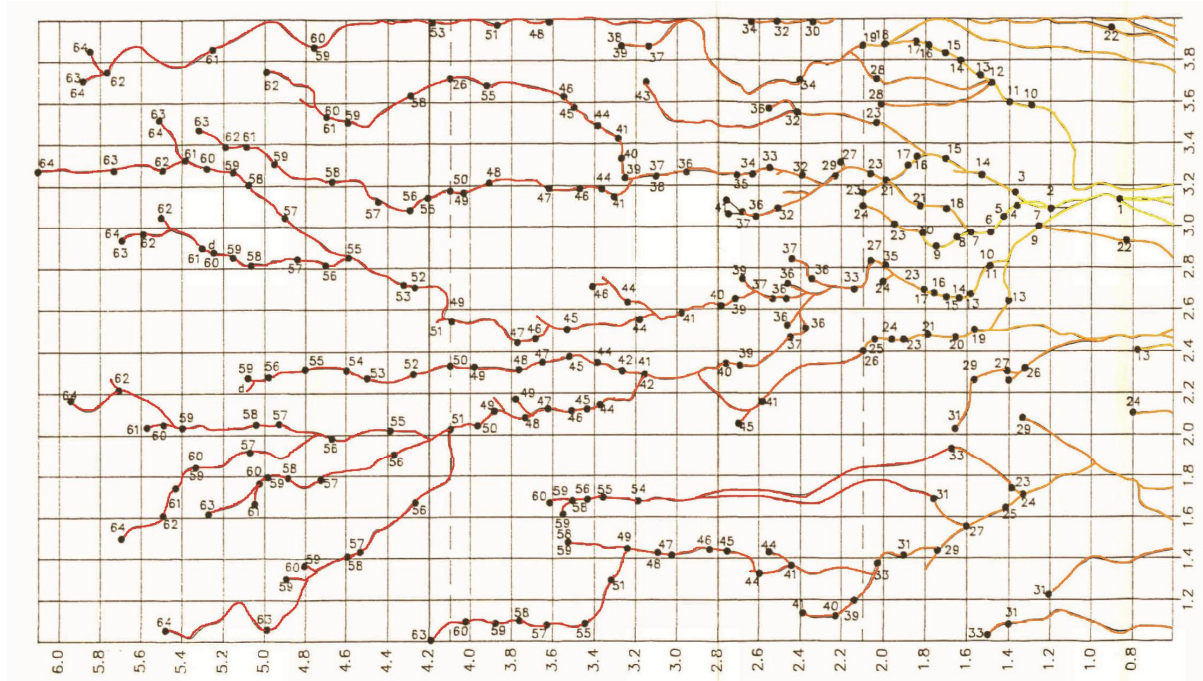


Figure 2.12. Final pipe pattern in experiment T3 ($L=12$ m) registered at different head drops

2.2.7. LATERAL HETEROGENEITY EXPERIMENTS AND SBW EXPERIMENTS

Small-scale experiments were performed in 2008 to investigate the effect of lateral heterogeneity on the piping process (Van Beek et al., 2008). After several trials to optimise the set-up, seven experiments were performed with various combinations of fine and coarse sand. The small-scale set-up developed for this purpose formed the basis for experiments in the SBW programme in the period 2006-2010. The fundamental questions raised subsequent to this part of the SBW programme led to this thesis. This section will describe both the heterogeneity experiments and the SBW experiments, starting with a description of the set-ups and followed by the results.

The SBW programme revalidated the Sellmeijer model in small-, medium- and large-scale experiments (Van Beek et al., 2011). The investigated parameters were sand type and relative density. The characteristics of the sand types are given in Appendix B. They were all uniform sands with a range of ($d_{60}/d_{10}=1.3\text{-}2.6$, $d_{50}=0.132\text{-}0.380$ mm). A total of 48 small-scale experiments, 14 medium-scale experiments and 4 large-scale experiments were conducted with a range of sand types and relative densities. Figure 2.13 shows photographs of these experiments.



Figure 2.13. Small-, medium- and full-scale experiments

The small-scale set-up used for both the heterogeneous experiments and the SBW experiments consisted of a PVC box with an acrylate cover. It was designed to have a vertical inlet and a slope-type exit. The sand bed measured $0.38 \times 0.10 \times 0.30$ m. A downstream filter with a height of 8 cm retained the sand to produce a natural slope. A cavity was created in the middle of the sand bed to reduce the seepage length in the middle of the set-up. This ensured that pipe formation occurred in the middle of the sample rather than along the wall and resulted in a seepage length of approximately 0.33 m. The upstream filter was partially closed at the sides of the filter, concentrating the flow through the middle.

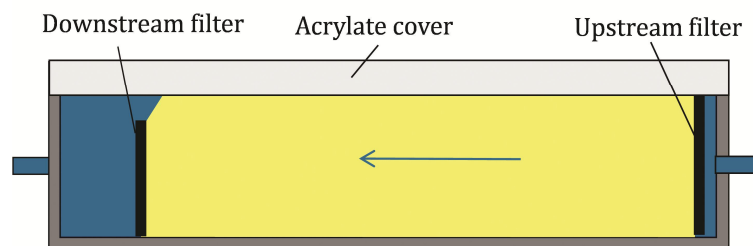


Figure 2.14. Schematic for small- and medium-scale experiments

The medium-scale experiments were a scaled version of the small-scale experiments, with dimensions exceeding those of the small-scale experiments by a factor of approximately 4. The sand bed measured $1.55 \times 0.88 \times 0.40$ m. The height of the downstream filter was 0.38 m, resulting in a natural slope. As in the small-scale experiments, part of the sand was removed to create a cavity, resulting in an average seepage length of 1.4 m.

The large-scale experiments were performed at the IJkdijk location. This is a facility for testing monitoring technology in the North-East of the Netherlands. Controlled experiments were performed in two impermeable trapezoidal basins with base dimensions of 27×9 m and 1:1 slopes. The two basins were filled with a three-metre thick layer of sand. A clay dike with a height of 3.5 m and 1:2 slopes was built on top of the sand bed, as shown in Figure 2.15, to obtain a seepage length of 15 m.

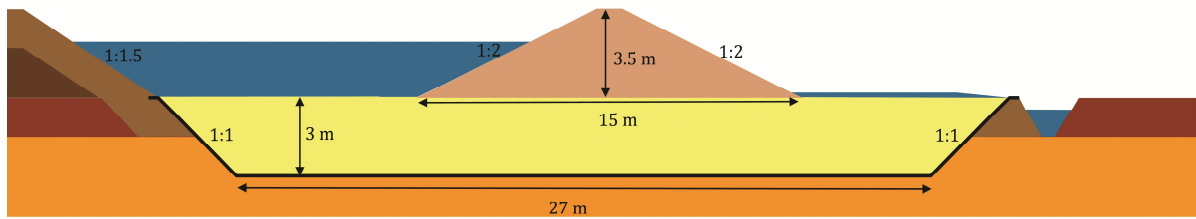


Figure 2.15. Schematic of full-scale experiments at the IJkdijk location

The paragraphs below contain a description of the results for each of the experimental series (lateral heterogeneous experiments, small-, medium- and IJkdijk experiments).

Lateral heterogeneous small-scale experiments (Van Beek et al., 2008)

The effect of lateral heterogeneity was tested by performing experiments in which the pipe path passes through different sand types in succession. Two sand types were selected (Playground sand and Masonry sand). They were first tested individually and then combinations of the two were tested (fine sand downstream, coarse sand upstream, fine sand with a band of coarse sand).



Figure 2.16. Pipe formation in laterally heterogeneous sands (fine downstream, coarse upstream)

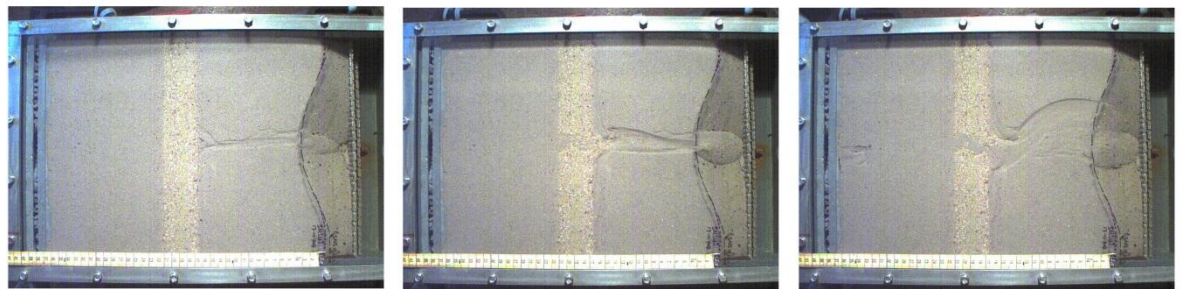


Figure 2.17. Pipe formation in laterally heterogeneous sands (fine sand with a band of coarse sand)

In the homogeneous samples the pipe developed in the upstream direction without any head increase: no equilibrium was achieved in pipe formation. In the heterogeneous samples a pipe formed in the downstream fine sand and stopped at the interface with the coarse sand. An increase in the head resulted in the deepening and widening of the channel in the fine sand, and elongation perpendicular to the flow direction along the interface between the fine and coarse sand. After the head was increased significantly

(to a level approximately 2-3 times higher than the critical head in a homogeneous fine sand sample), a pipe formed in the coarse sand, causing the failure of the sample.

The critical gradients for the individual sands appeared to be much lower than for the heterogeneous samples. The configuration with a band of coarse sand was found to be least amenable to pipe formation, due to the combination of the low permeability of the fine sand and large grain size of the coarse sand.

SBW small- and medium-scale experiments (Van Beek et al., 2011)

In the small-scale experiments for SBW, the impact of relative density on the piping process and critical head was investigated in two sand types. In the medium-dense to dense samples (relative density >50%), the erosion process was similar to that observed in previous slope-type experiments:

1. Small rearrangements of grains, movement of individual grains through the sand matrix, development of very small pipes (pipe length < 10 mm, pipe depth < 1 mm).
2. A head increase resulted in the development of larger (straight or branching), shallow (up to a few millimetres) pipes 5-50 mm wide which developed in the upstream direction. As soon as the pipe established a connection between the downstream and upstream sides, the erosion rate increased at the upstream side, mobilising a large quantity of sand and leading to the widening and deepening of the pipe. The widening phase took between a few seconds and a few minutes.

The same processes were observed in the medium-scale experiments as in the small-scale experiments. The backward erosion piping process appeared to result in pipes of similar dimensions, although multiple parallel pipes appeared in most medium-scale experiments and single pipes were often seen in the small-scale experiments. In some experiments, pipe formation did not start at the downstream side, but several centimetres upstream of the exit.

More time was required for backward pipe development in the medium-scale experiments than in the small-scale experiments. This was due to both the lower growth velocity and the larger seepage length in the medium-scale experiments. The lower growth velocity was related to the relatively low critical gradient in the medium-scale experiments, in which the widening process took about 15 minutes. The widened pipes appeared to be larger (approximately 0.1 m wide and several millimetres deep) than the widened pipes in the small-scale tests (which were approximately 0.05 m wide and several millimetres deep).

A different process was found in low-density experiments (relative density <50%) than in the dense sand samples (Van Beek et al., 2009). The piping process started at the upstream side and appeared to develop in the downstream direction as a result of local densification and the displacement of the sand sample (Figure 2.18). This process, which is called forward erosion, occurred at critical gradients that were relatively low by comparison with those in dense samples.

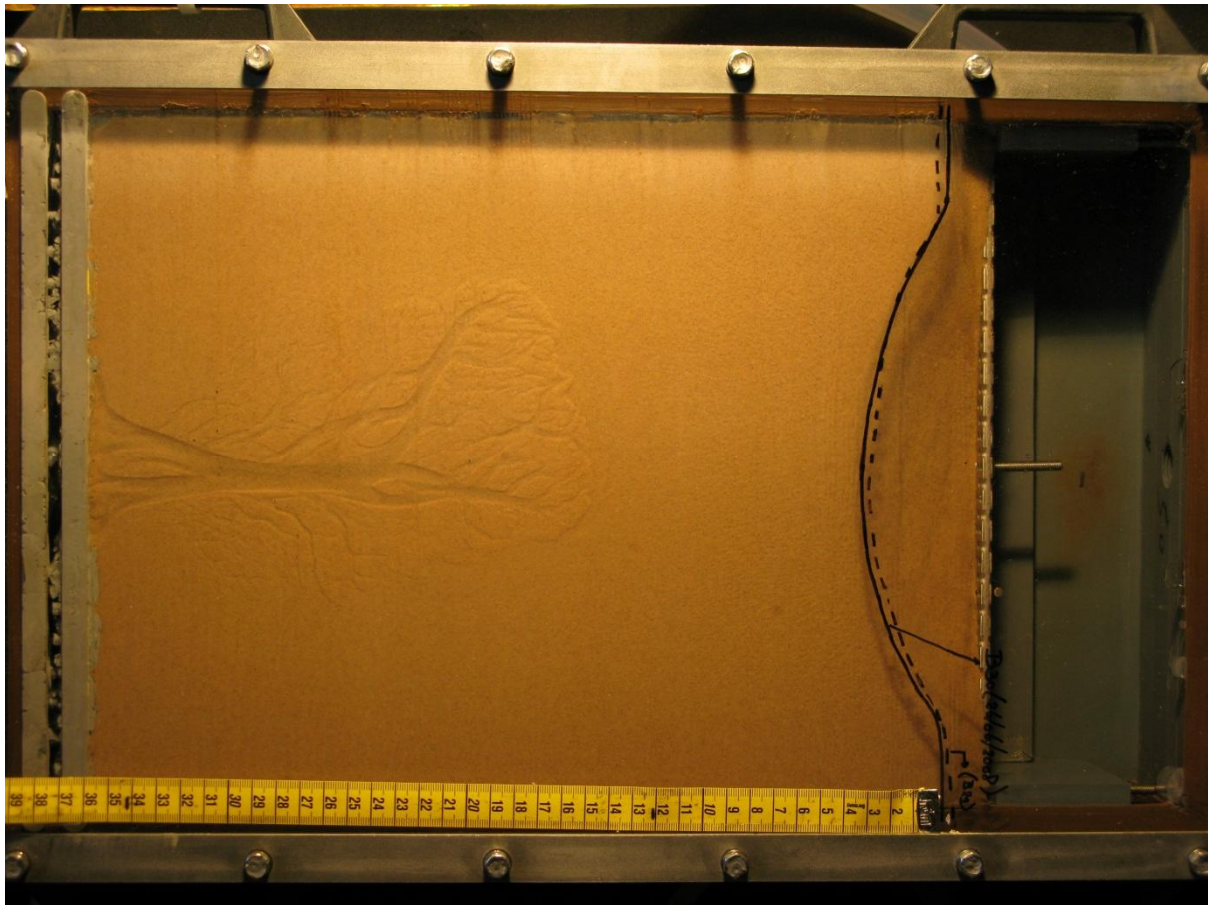


Figure 2.18. Forward erosion as observed in one of the small-scale experiments (B30)

After the series of small-scale experiments had been conducted, it was found that the permeability of the upstream filter was relatively low by comparison with the permeability of some of the sands (Van Beek et al., 2011). A correction for the critical head was applied accordingly on the basis of the flow rate through an empty box. This correction was also found to be necessary for the heterogeneous experiments. In the medium-scale experiments, the head loss caused by the filter was found to be negligible.

Analysis of the corrected critical gradients led to the conclusion that the critical gradient fell in line with increasing scale, decreasing relative density and increasing grain size. It should be noted here that the permeability of the sand sample also increased with grain size and porosity.

Large-scale experiments

The large-scale experiments were conducted to validate the findings of the small- and medium-scale experiments, and to visualise the process from sand boil to failure. Although the clay dike hid the pipes from view, pore pressure transducers at the interface of the clay and sand were used to monitor pipe progress. The scale of the experiment may have prevented the observation of all phenomena, an example being heave near the toe. The following observations were made:

1. Sand traces, small holes and sand boils. No visible sand transport and no pipe formation.

2. After an increase in the head, sand boils were seen to form a sand crater. The pore pressures indicated the presence of pipes under the dike. The size of the sand boils was limited (in the order of cubic centimetres).
3. After a further increase in the head, the sand boils started to transport sand continuously, indicating pipe development. The craters were removed regularly and the amount of sand removed was registered. Sand transport remained constant during pipe development and as the pipe subsequently widened. It increased sharply with the flow upon completion of the pipe widening phase.

The increase in the flow and sand transport after the widening phase resulted in the failure of the dike in the experiments with 'fine sand'. The sudden increase in sand transport was followed by the formation of a 'mud fountain' through which the sand and water were flushed violently out of the pipe (Figure 2.19). Cracks appeared in the dike, which then subsided. The toe of the clay dike eroded on the downstream side and the dike subsided on the upstream side.

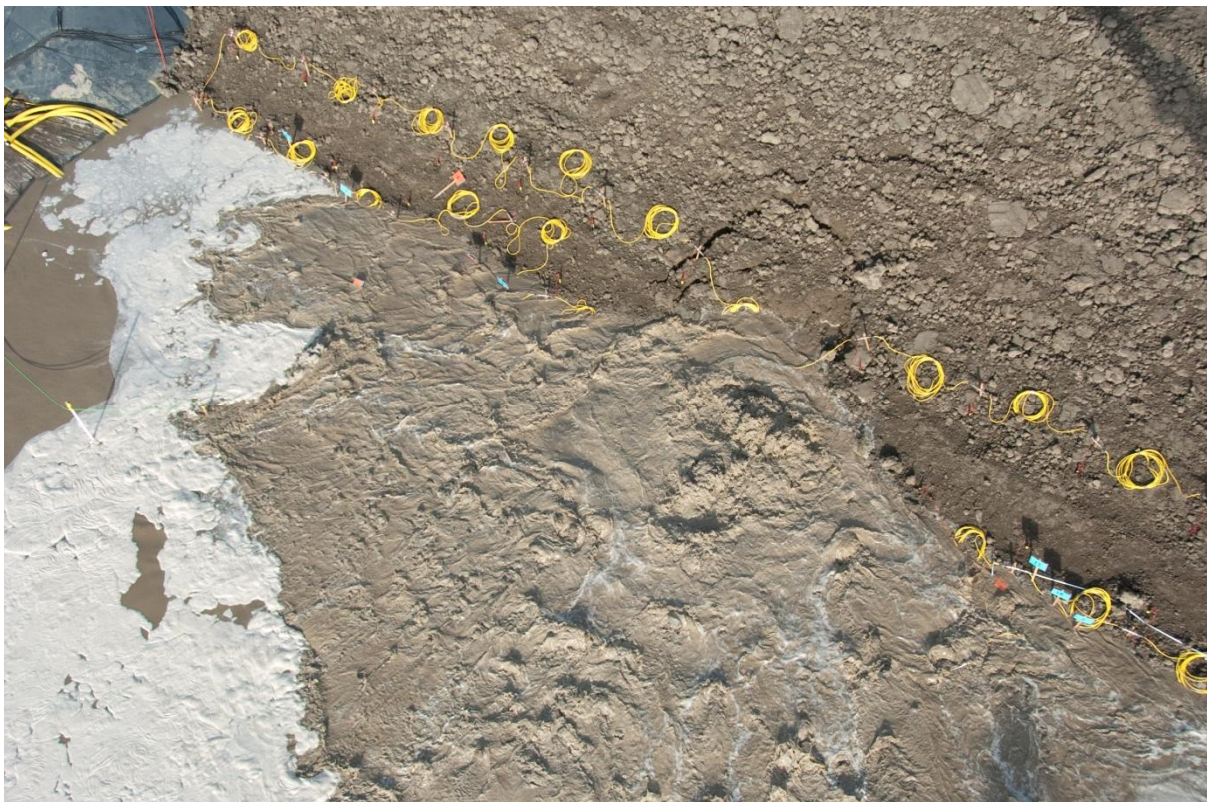


Figure 2.19. 'Mud fountain' after the completion of the widening phase in one of the large-scale experiments at the IJkdijk location

In the experiments with 'coarse sand' the increase in sand transport did not immediately result in failure. The clay dike settled, cracks appeared and sand transport and flow diminished. After some time, a new mud fountain formed, through which sand burst. At this stage, there were marked fluctuations in the readings from the pore pressure gauges and the flow rates. In the days that followed, sand burst out on several occasions. A few days after the first outburst of sand, the dike failed.

The critical gradients obtained with these experiments confirmed the effect of scale and sand type that was also found in the small- and medium-scale experiments: the critical gradient was lower in larger-scale aquifers and in coarser sand types.

2.2.8. IWHR EXPERIMENTS

Research performed at IWHR (Yao et al., 2007; Ding et al., 2007) focused on multi-layer structures and different exit configurations.

Yao et al. (2007) performed medium-scale experiments in a set-up containing a sand sample measuring 2.25x0.6x0.8 m (seepage length=1.40 m). The set-up had a vertical inlet and either a plane-type exit configuration or a hole-type exit (0.04 m in diameter, thickness of acrylate cover 15 mm). All experiments were performed with one sand type ($d_{60}/d_{10}=3.5$ and $d_{60}=0.28$ mm).

The observed process was similar for both exit types. Pipe development stopped unless the head drop was increased to a critical head, after which pipe development continued until breach. The critical gradient was considerably lower with a hole-type exit than with a plane-type exit (0.214 and 0.278 respectively).

Ding et al. (2007) performed experiments with multiple layers in the set-up with the hole-type exit. Different thickness ratios were tested between an upper layer with fine sand and a lower layer with gravel ($d_{60}/d_{10}=11.4$ and $d_{60}=19$ mm). In the experiments in which the top layer made up less than 10% of the total soil thickness, a different process was observed: 'deep-seated piping'. When the exit was exposed, an erosion lens was formed in which sand boils emerged. Increasing the head resulted in the formation of a deep and wide pipe. When the pipe approached the upstream filter, smaller and shallower pipes were formed as well.

The critical gradient was found to increase as the ratio of the fine layer thickness to total layer thickness increased.

2.2.9. EXPERIMENTS CONTAINING SEPARATE ENGINEERING STRUCTURES OR WITH PARTLY VERTICAL SEEPAGE PATHS

Achmus and Mansour (2006), Okajima and Tanaka (2008), Ding et al. (2008), Van den Ham (2009) and Okajima et al. (2010) have conducted experiments containing separate engineering structures. The variables investigated were sand layer depth and relative density (Achmus and Mansour, 2006), the type of vertical structure (embedded structure or cut-off wall) (Okajima et al., 2010), the location of the cut-off wall (Okajima et al., 2010; Ding et al., 2008), penetration depth (Van den Ham, 2009) and seepage length (Okajima and Tanaka, 2008).

The process described was the same in all these experiments. The structure formed a barrier to pipe progression and the fluidisation of sand downstream of the structure was required for pipe progression to continue. The observations by Ding et al. (2008) in experiments with a single cut-off and a hole-type exit can be considered exemplary:

1. Heaving and boiling in the piping hole. Some muddy water flowed out, but no sand was deposited.

2. Piping channels propagated towards the river side. During this process, the head was increased several times.
3. Piping channels propagated perpendicularly to the flow.
4. Piping channels passed the cut-off and caused a breach.

Equilibrium in pipe formation was observed in step 2 of the experiments by Ding et al. (2008) but not in the slope-type experiments by Van den Ham (2009).

With respect to the critical head, some general conclusions can be drawn from these experiments. The critical gradient is relatively large for:

- small seepage lengths
- large penetration depths
- cut-offs located near the downstream toe rather than near the upstream toe
- sand beds with high relative densities
- embedded structures as opposed to cut-off walls (assuming equal seepage lengths and penetration depths).

All of these trends could be fairly well explained by simulating the groundwater flow around the structure in a numerical model (Van Beek et al., 2013) using the method described in 2.3.5.

2.3. PREDICTION MODELS

Designing dams and dikes requires the development of prediction models for piping. The earliest models, which date back to early last century, were based on field cases. Current models rely on finite element model calculations and approaches involving discrete element models are being developed.

2.3.1. EARLY MODELS (1900-1970)

Since the turn of the last century the process of piping has been studied in the context of weir and dam design. At that time, no distinction was made between backward erosion and suffusion as piping mechanisms.

Clibborn (1902) was the first to establish a linear relationship between the length of seepage and the critical head across the structure ($L = CH$). Bligh (1910) embraced this idea and established coefficients of percolation (C) to predict safe values for hydraulic head on the basis of weirs in India. The maximum percolation factor, for very fine sands and silts, was found to be 18. Griffith (1913) (and subsequently in the discussion of Lane, 1935) also found values for the percolation factor which had been sufficient to ensure stability in what was then the United Provinces in India.

Lane (1935) stated some objections to these methods on the grounds that they do not consider the greater resistance to erosion of vertical sections by comparison with horizontal sections. He formulated a new empirical relationship on the basis of 278 cases. In this relationship, a weighting was assigned to the horizontal path of $1/3$ and the vertical path was included in full. In the discussion of this paper, there was appreciation for the number of cases presented but the weighting factor of $1/3$ was criticised (Burroughs, Streiff and Griffith in discussion of Lane, 1935). Another criticism was that the approach considered only the average gradient across the structure, even

though the local gradient is highly dependent on the type of structure. It has therefore been argued that an empirical approach is inappropriate (Casagrande, Harza in discussion of Lane, 1935). Chugaev (1965) adopted a similar approach to Bligh and Lane's to predict a safe gradient. On the basis of data for 175 barrages and weirs, allowable gradients were designed for a range of materials from fine sand to coarse gravel and clay (Davidenkoff (1970) after Chugaev).

Harza (1935) argued in favour of a more scientific approach than empirical modelling. Piping cannot occur if sand heave is impossible and so Harza calculated the uplift head near the toe for different situations using the electric analogy method. It was noted that, as the exit gradient approaches infinity near the toe for horizontal sand layers without cut-offs, the foundation of the soil should never be at the same level as the dam body. A depressed toe or cut-off is required.

Terzaghi and Peck (1967) described the mechanics of piping due to heave by assuming the fluidisation of a prism of sand downstream of a structure. Experiment results (Terzaghi, 1922) indicate that this prism has a depth of D and a width of $D/2$. For piping to occur, the excess hydrostatic pressure at the base of the structure must equal the weight of the overlying sand. Terzaghi and Peck suggested the use of flow nets to compute the hydraulic pressure around the structure.

The occurrence of seepage and sand boils during the 1937 flood along the Lower Mississippi Rivers resulted in a large study for the phenomenon of underseepage (USACE, 1956). On the basis of geological studies and field investigations at fifteen sites along the Lower Mississippi Rivers determining the subsurface geology and hydraulic gradient beneath and landward of the dikes, it was concluded that the severity of underseepage depends on the head on the dike, the source of seepage, the permeability of the substratum, and the characteristics of the landside top layer.

The observation of the severity of underseepage in combination with piezometer readings during the 1950 flood allowed for the development of a design tool that has become known as the blanket method. Figure 2.23 shows the observation of phenomena plotted against the upward gradient in the top-layer downstream of the dike. Sand boils were observed at upward gradients of 0.5 to 0.8.

The blanket method uses analytical equations to estimate the upward gradient in the confining layer which are described in detail in (USACE, 2000). On the basis of the observations of the 1950 flood a maximum upward gradient of 0.5 is allowed. The blanket method is still used in the US. It should be noted that the design tool is not a prediction tool for piping; rather it determines when it is likely that cracking of the confining top layer and subsequent sand boil formation can occur.

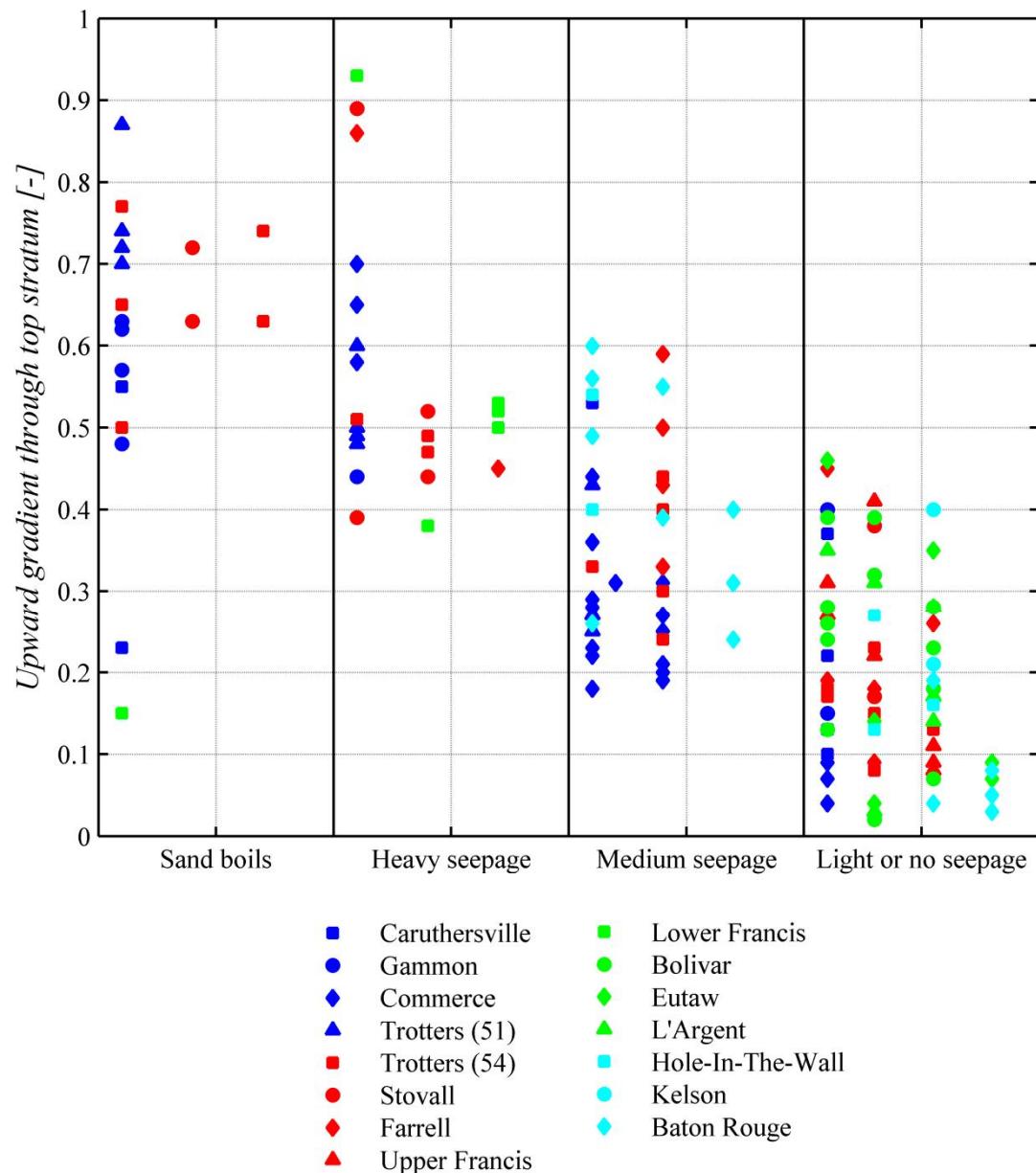


Figure 2.20. Observations from the 1950 flood in relation to the upward gradient through the confining layer at fifteen instrumented sites along the Lower Mississippi River (modified after USACE, 1956).

2.3.2. EXPLANATION OF SCALE EFFECTS BY DE WIT (1984)

On the basis of the experiments reported in De Wit (1984), which looked at the roles played by geometry, soil type and soil density, theoretical work was performed to explain the change in the critical gradient associated with those parameters.

No equilibrium in pipe formation was observed in most of the experiments by De Wit. As soon as sand transport took place, the pipe developed to the upstream side without any further head increase.

De Wit (1984) concluded that the critical head could be related to the hydraulic head distribution in the intact sand sample. To explain differences in the critical head linked

to scale, the head distribution in the top of the intact sand bed was studied in the plane-type configuration (models I and II). The calculations of head distribution showed that, when the local head distribution near the exit was equal at both scales, the overall gradient was not the same (Figure 2.21).

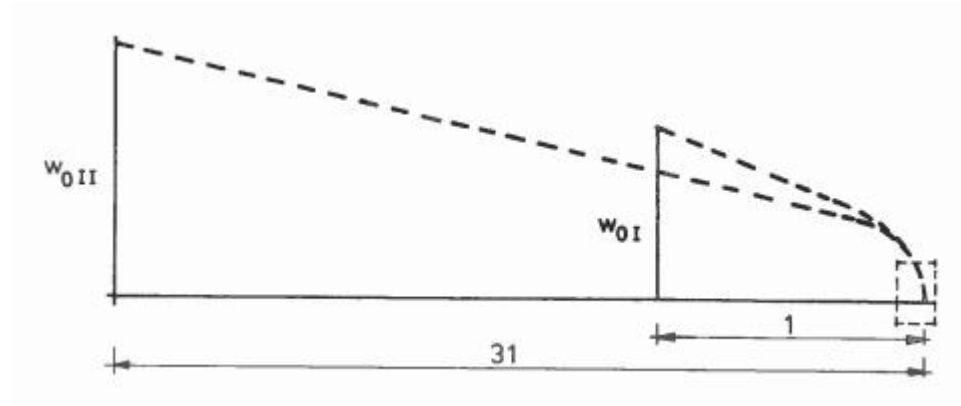


Figure 2.21. Head distribution for models I and II

On the basis of the comparison of head distributions for models I and II, the theoretical scale factor explained the change of critical head for these set-ups:

$$\lambda = \frac{H_{c,II}}{H_{c,I}} = \sqrt{\frac{D_{II}}{D_I}} = \sqrt{3} \quad 2.1$$

in which:

λ scale factor for critical head

D_I sand bed thickness in model I (0.5 m)

D_{II} sand bed thickness in model II (1.5 m)

The theoretical scale factor was compared with the experimental scale factor: the ratio between the critical heads in the experiments. After the critical heads obtained in the experiments were averaged, the ratios obtained experimentally were indeed close to 1.7, but it is worth noting that they were always slightly lower (Dune sand $\lambda=1.62$, Beach sand $\lambda=1.54$, Coarse sand $\lambda=1.37$).

In the same way, theoretical scale factors for experiments with other configurations can be determined and compared with scale factors determined on the basis of experiments. This has been done for experiments with constant thickness but different lengths (comparison of model II with III and IV), small- and medium-scale ditch experiments, and the hole-type experiments. Accordingly, analytical equations were derived for the distribution of potential along the top of the sand layer for these configurations. The theoretical scale factors for models II-III and III-IV are 1.69 and 0.60 respectively. The scale factors for the averaged critical gradients in the experiment were found to be 1.71 and 0.59 respectively, indicating a good match between experiments and theory.

Scale effects observed in the ditch-type experiments could not be fully explained by the head distribution. The theoretical scale factor is 1.18 and the experimental scale factor

was found to be 1.61. However, the experimental scale factor for sand boiling was close to the theoretical value (1.12).

The distribution of head in the top of the sand bed was also calculated for the experiments with a circular hole. The measured heads near the exit hole were found to be lower than the calculated heads, which is most likely due to the fact that some pipe formation had already taken place when the measurements were made. Nevertheless, when the comparison was made with the experiments, the experimental scale effects were found to be a reasonable match with the scale effects predicted by theory.

These results show that the scale effects observed in the experiments are caused by the relationship between the applied head and the local head near the exit. The head near the exit is constant for different scales. No explanations were found for the impact of configuration, sand type and relative density on the critical head.

2.3.3. EXPERIMENT SIMULATION BY HANSES (1985)

Hanses (1985) simulated the flow pattern in the experiments using sources and sinks, and imaging. To this end, the pipe was simplified as a rectangular shape with no physical depth. The effect of the pipe on the flow pattern was modelled using sources, with the pipe being broken down into 70 elements (Figure 2.22). The pipe was not simulated physically. The effect of the boundaries of the experiment (upstream filter, bottom, sides and rear) were included by mirroring. Using the equations obtained, it was possible to calculate the flow towards each source (Figure 2.22) after the input of the head difference across the structure and the average head loss in the pipe. Once the flow through the sources was known, the distribution of heads in the sample was calculated.

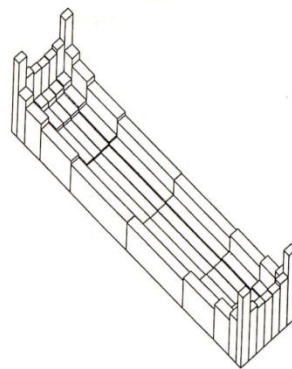


Figure 2.22. Pipe discretisation showing the calculated distribution of flux (Hanses, 1985)

In this way, the hydraulic head distribution near the tip of the pipe was calculated for each of the experiments. It was concluded that, at a distance of 20 mm upstream of the pipe tip, the hydraulic head was approximately 30 mm for all pipe lengths and experiments, indicating an average gradient of 1.5 (Figure 2.23). The exit gradients in the pipe bottom fell with distance from the pipe tip from ~4 to ~1.5 in the first 50 mm. It should be noted that pipe depth was omitted from the calculations, which may account in part for the high gradients (Figure 2.24). Arching at the tip of the pipe and at the side of the pipe was a second explanation for gradients exceeding the critical

gradient for the fluidisation of sand (~ 1). The finding that the gradient was comparable in each of the experiments is a strong indicator of the role played by primary erosion in the prediction of piping. The effect of secondary erosion was included by matching the pipe gradients measured in the experiments to those in the model.

Hanses (1985) concluded his work with a parametric study, but the experimental simulation was not used to make the step to a tool that can be used in practice.

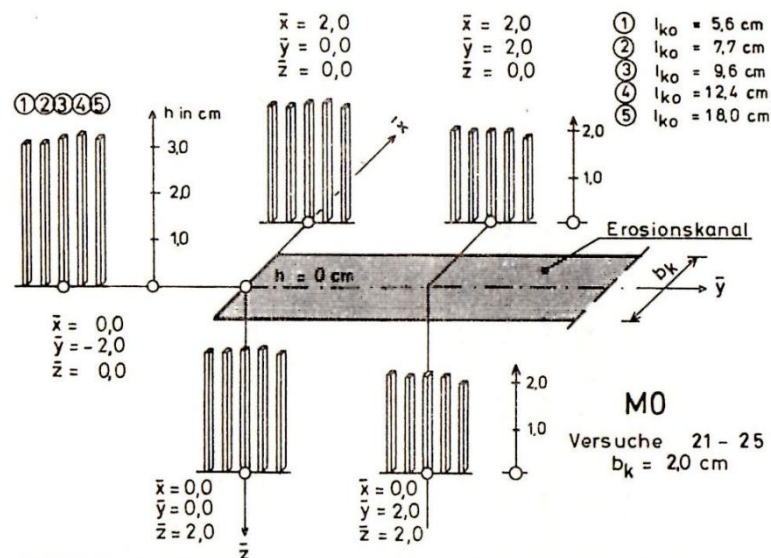


Figure 2.23. Potentials around the tip of the pipe for tests 21-25 with different pipe lengths (Hanses, 1985)

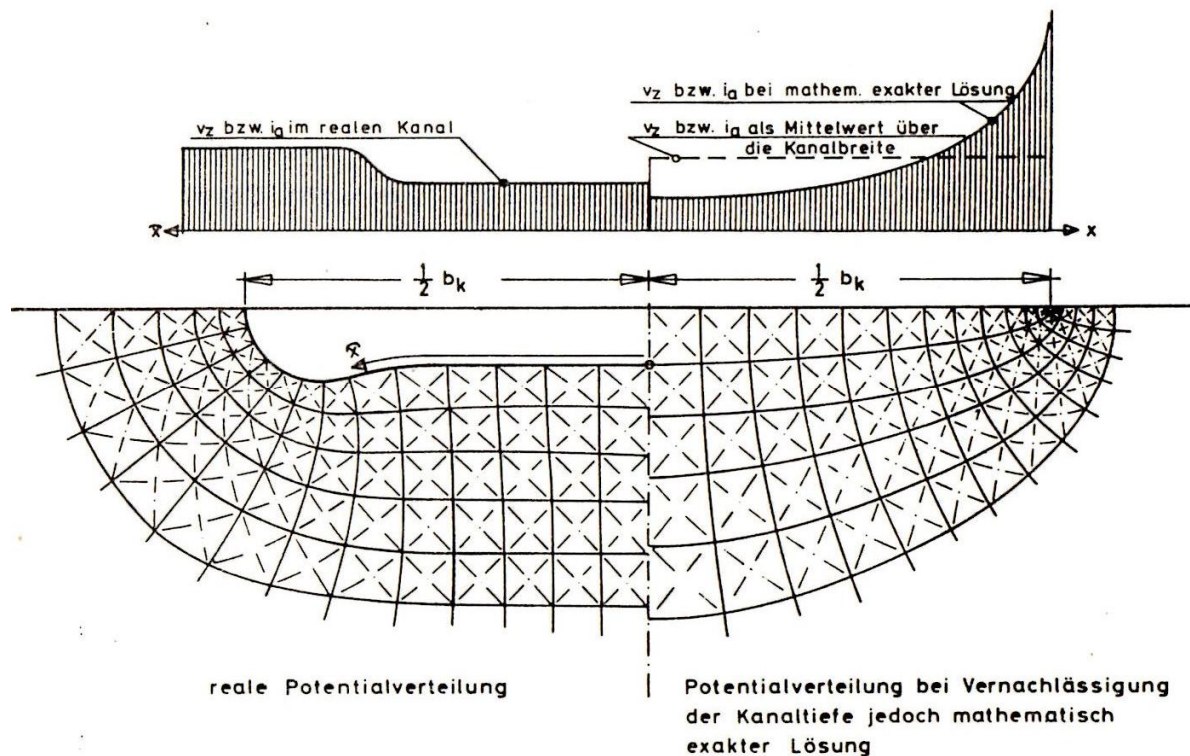


Figure 2.24. Comparison of real and simulated head distributions around the pipe and corresponding exit velocities in a cross-section of the pipe (b =pipe width) (Hanses, 1985)

2.3.4. SELLMEIJER'S MODEL

The experimental series performed for C.O.W. was followed by theoretical research to develop a model for pipe prediction. Assuming pipe equilibrium at some point in time, Sellmeijer (1988) developed a model for predicting the head difference across the dike at which the grains at the bottom of the pipe reach a limit-state equilibrium. Accordingly, the equilibrium of forces on the grains was considered, taking the flow in the pipe and the flow towards the pipe into consideration.

Sellmeijer calculated the equilibrium of forces on the grains on the basis of White's approach (1940), initially after including forces for vertical and horizontal gradients. This equilibrium resulted in a critical shear strength on the grains exerted by the water flowing through the pipe.

The pipe was modelled in 2D, as was the groundwater flow. To determine the laminar pipe flow, Sellmeijer (1988) solved the Navier-Stokes equations for laminar flow, obtaining the equation for Poiseuille flow between parallel plates. To determine the head difference across the dike that supplies the flow through the pipe for limit-state equilibrium, the Laplace equation was solved with a specific boundary condition for the pipe, using the Cauchy integral and the method of conformal mapping. A program was written to calculate the equilibrium head with increasing pipe length, and it was found that this head reached a maximum when the pipe length was approximately half the seepage length (Koenders en Sellmeijer, 1991). Below this maximum head level, which is termed the 'critical head', pipe formation does take place but it will reach equilibrium until the head is increased further. Once the critical head has been exceeded, no equilibrium is possible and the pipe will develop progressively and reach the river side of the dike. Using curve fitting, a relationship was found between clusters of parameters and the critical gradient (developed in 1989, published in Koenders en Sellmeijer, 1991):

$$\frac{H_c}{L} = c \frac{\gamma'_p}{\gamma_w} \tan \theta (1 - 0.65c^{0.42}) \quad 2.2$$

$$c = \frac{1}{4} \pi \eta^3 \sqrt{\frac{2d^3}{\kappa L}}$$

in which:

H_c	critical head [m]
L	seepage length [m]
γ'_p	submerged unit weight of grains [N/m ³]
γ_w	unit weight of water [N/m ³]
θ	bedding angle [°]
η	White's coefficient [-]
κ	intrinsic permeability [m ²]

Initially the situation was modelled as a dike on top of an infinitely deep sand layer. In practice the depth of the sand layer is limited. To account for this, Sellmeijer derived a

factor for the effect of the ratio of thickness to seepage length by curve fitting. A new formula was obtained in which a factor accounting for the shape of the sand sample was added to the design rule (Sellmeijer et al., 1989):

$$\begin{aligned} \frac{H_c}{L} &= \alpha c \frac{\gamma'_p}{\gamma_w} \tan \theta (0.68 - 0.1 \ln c) \\ c &= \eta \sqrt[3]{\frac{d^3}{\kappa L}} \\ \alpha &= \left(\frac{D}{L} \right) \left(\frac{D}{L} \right)^{\frac{0.28}{2.8} - 1} \end{aligned} \quad 2.3$$

in which:

D thickness of the sand bed [m]

Experiments in the Delta Flume allowed for the validation of the bedding angle, which had been selected on the basis of the literature and engineering judgement (Weijers and Sellmeijer, 1993). In their opinion, the pattern of pipes formed in this experiment justified the use of a 2D model. The rule as displayed in Equation 2.3 was prescribed for piping prediction in Dutch practice (TAW, 1999).

To make the model suitable for multi-layer systems, the piping criterion was implemented in the finite element groundwater modelling program MSEP. As it was thought that, in a heterogeneous mixture of sand grains, the bigger sand grains stick out and are therefore not affected by forces resulting from vertical seepage gradients, the particle model was refined as a 2-force equilibrium (Sellmeijer, 2006). This change meant that the predicted heads varied slightly in the different models. The combination of flow through the pipe and the limit state equilibrium of grains results in a boundary condition for the pipe that has to be fulfilled for each point along the pipe:

Pipe flow,

$$a^3 \frac{\partial \phi}{\partial x} = 12 \frac{\mu}{\gamma_w} Q \quad 2.4$$

and particle equilibrium,

$$\frac{a}{d} \frac{\partial \phi}{\partial x} = \frac{\pi}{3} \frac{\gamma'_p}{\gamma_w} \eta \tan \theta \quad 2.5$$

resulting in,

$$\left(\frac{\partial \phi}{\partial x} \right)^2 Q = \frac{\gamma_w}{12\mu} \left(\frac{\pi}{3} \frac{\gamma'_p}{\gamma_w} \eta \tan \theta d \right)^3 = c \quad 2.6$$

in which

$$Q = \int_{x=0}^{x=l} k \frac{\partial \phi}{\partial y} dx \quad 2.7$$

and

μ dynamic viscosity [Pa s]

k	permeability coefficient [m/s]
a	pipe depth [m]
l	pipe length [m]
φ	head [m]
x	horizontal coordinate [m]
y	vertical coordinate [m]

MSEEP calculations are relatively time-consuming by comparison with calculations using a rule. A neural network for a standard two-layer configuration was set up for more speed and ease of use (Sellmeijer and Koelewijn, 2007).

As already pointed out in the paper by Weijers and Sellmeijer (1993), the model does not predict critical gradients well for experiments on coarse sands when the bedding angle is kept constant at the calibrated value found for the Delta Flume experiments. The finding that the theoretical effect of the sand type does not concur with experiments was confirmed after validation in the SBW experiments (Sellmeijer et al., 2011). A multivariate analysis of the available small-scale experiments allowed for the assessment of the effect of parameters and the model was empirically adapted to account for the deviations (Sellmeijer et al., 2011). The formula was also rearranged in meaningful clusters, and the 2-force equilibrium was implemented in the formula:

$$\begin{aligned}
 \frac{H}{L} &= F_R F_S F_G \\
 F_R &= \eta \frac{\gamma'_p}{\gamma_w} \tan \theta \left(\frac{RD}{RD_m} \right)^{0.35} \left(\frac{U}{U_m} \right)^{0.13} \left(\frac{KAS}{KAS_m} \right)^{-0.02} \\
 F_S &= \frac{d_{70}}{\sqrt[3]{\kappa L}} \left(\frac{d_{70,m}}{d_{70}} \right)^{0.6} \\
 F_G &= 0.91 \left(\frac{D}{L} \right)^{\frac{0.28}{\left(\frac{D}{L} \right)^{2.8} - 1} + 0.04}
 \end{aligned} \tag{2.8}$$

in which:

RD	relative density [-]
U	uniformity coefficient d_{60}/d_{10} [-]
KAS	measure for the angularity of grains ranging from 0 (very round) to 100 (very angular) [-]
m	mean value from selected small-scale experiments
$d_{70,m}$	0.208 mm
RD_m	72.5 %

U_m 1.81
 KAS_m 49.8%

The critical gradient in this equation is determined by three components, F_R , F_S and F_G , resistance, scale and geometry respectively. The resistance factor is a function of the equilibrium of forces, the scale factor a function of the ratio of grain size to seepage length, and the geometry factor a function of the effect of aquifer shape on the groundwater flow. The geometry factor was obtained from a curve fit of a collection of FEM groundwater flow computations for different geometries. A curve fit of this kind matches the computed range as accurately as possible. It has recently been found that, well outside that range, an undesirable singularity is introduced using the geometry factor in equation 2.8. A slight adaptation was therefore introduced which has hardly any effect on the original computations but does eliminate the singularity (Van Beek et al., 2013):

$$F_G = 0.91 \left(\frac{D}{L} \right)^{\frac{0.24}{\left(\frac{D}{L} \right)^{2.8} - 1}} \quad 2.9$$

The uniformity coefficient and grain angularity proved to have a negligible effect on the critical gradient in the tested range, but they have been included in the formula for the sake of completeness. The empirically adapted model shown in Equation 2.8 and 2.9 was validated in medium-scale and large-scale experiments (Sellmeijer et al., 2011) that demonstrated the need for an adaptation of this kind, because the original model described in Equation 2.3 significantly overpredicted the critical head for the medium-coarse sands in these experiments.

2.3.5. PIPING BY HEAVE

Sellmeijer (1995) reported a method for calculating the critical head in dikes containing a separate engineering structure: the fragments method. As in the approach by Terzaghi, the method assumes that the pipe will progress under the structure when the vertical average gradient downstream of the structure equals the heave criterion. A conservative value of 0.5 was selected as the critical vertical gradient. To calculate the distribution of hydraulic pressure, the sand layer was divided into fragments (Figure 2.25) and vertical equipotential lines between the fragments were assumed. This assumption is valid for structures that extend to relatively large depths in the sand layer ($d > 0.2D$). The distribution of potentials in the fragments was calculated using analytical solutions for groundwater flow.

It should be noted that the distribution of potentials can also be calculated easily with finite element models. The method has been tested in various experiments described in the literature (see section 2.2.9) and there was a good match (Van Beek et al., 2013) using a critical heave gradient of approximately 1.

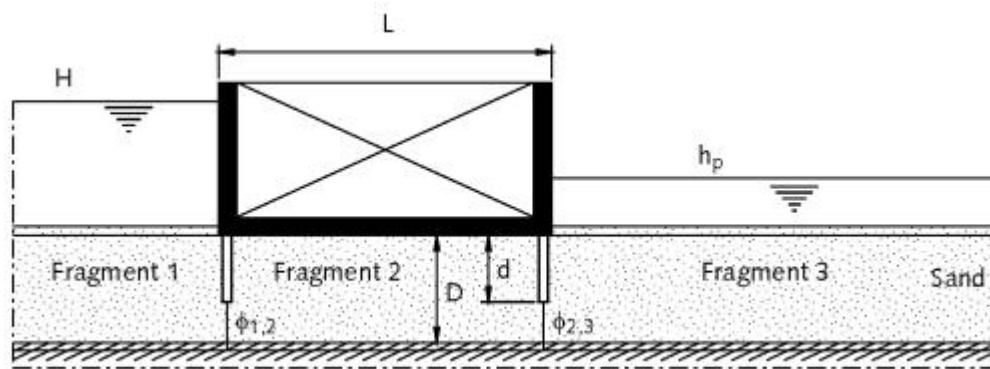


Figure 2.25. Dividing the sand layer into fragments (TAW, 1999)

2.3.6. SCHMERTMANN (2000)

Schmertmann (2000) developed a model that relies mainly on the variations in critical gradient observed in experiments with horizontal flow. The experiments performed in the UF Flume, the tests performed by De Wit (1984) and the large-scale experiments described by Silvis (1991) were analysed to determine the role of geometry parameters and sand characteristics.

Schmertmann (2000) drew on the concept that the vertical seepage gradient below the pipe (in other words, the local gradient) determines its advance and that the pre-pipe gradients along the seepage path have an important effect on the critical gradient, and therefore on the safety factor. Flow nets (without a pipe) were therefore used to determine a geometry factor that determined the relationship between the overall and local vertical gradients along the pipe path.

The model includes a factor for the effect of the ratio of depth to length, the ratio of the overall to the local test gradient (obtained with flow nets), the curvature of the dam, seepage length, grain size (d_{10}), anisotropy in permeability, high-permeability sub-layers, density and pipe inclination. A factor was added to the formula for each of the variables. Some factors relied on the theory of Sellmeijer (section 2.3.4) although empirical modifications were generally preferred.

The Schmertmann model emphasises the uniformity coefficient as one of the most influential factors for the critical gradient. It should be noted here that the number of experiments with higher uniformity coefficients is limited and often other phenomena such as sheet flow have often been observed in these experiments (see section 2.2.4). Interestingly, Schmertmann suggests that the influence of grain size should be smaller than was suggested in the original Sellmeijer model.

The requirement of the flow net complicates the use of the model. The simplified method offered by Schmertmann, for which no flow net is required, reduces its accuracy significantly.

2.3.7. OJHA AND SINGH (2003)

Ojha and Singh (2003) proposed two new models to calculate the critical head. In the first model, the head loss in the sand bed was calculated using the Carman-Kozeny head loss model. It was assumed that a critical shear stress on the particles had to be

exceeded for erosion to take place. The critical shear stress was assumed to be linearly related to d_{50} in a way that is similar to that proposed by Khilar et al. (1985), who established a relationship for the erosion of clay. The actual shear stress on the grains was calculated by representing the pores as parallel pipes with diameter d_{50} . Ojha and Singh (2003) indicated that the approach using tractive stress may not properly describe the onset of grain movement in a porous medium. They also neglected the geometry of the sand bed in their calculations of the head loss through the sand. Combining the formulae described above resulted in an equation similar to the relationship postulated by Bligh (1910).

In the second model, a critical velocity concept after Garde and Ranga Raju (1985) was considered to be the driving force for the initiation of particle motion. The role played by porosity was investigated by calibrating the model using some of De Wit's experiments (1984).

2.3.8. DISCRETE ELEMENT MODELLING (EL SHAMY AND AYDIN, 2008)

Shamy and Aydin (2008) simulated the piping process using a discrete element model (DEM). The fluid flow was modelled using the averaged Navier-Stokes continuity and momentum equations. To reduce the number of particles, a high- g -level concept was used. A gravitational field of 100 g was applied and viscosity was adjusted to compensate for the high g -level. It should be noted that the grains were not scaled. The simulated dike had a seepage length of 5 m on top of a 10-metre-deep granular layer. The hydraulic structure, which was positioned on the granular layer, was simulated in such a way that it behaved as a rigid body with an impermeable boundary condition. The translation and rotation of the hydraulic structure were allowed. Model runs produced the hydraulic gradient at failure and a process description.

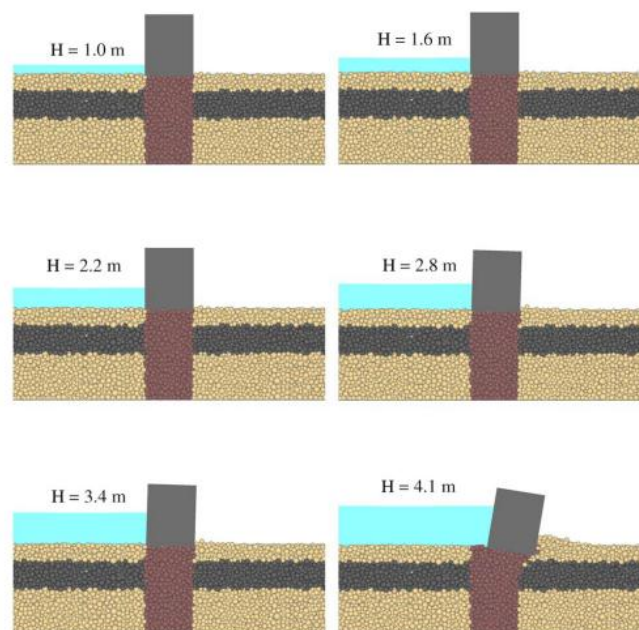


Figure 2.26. Simulation of particles under a dike at different water levels (El Shamy and Aydin, 2008)

Sand boiling was observed at an overall hydraulic gradient of about 0.42. As a result of the increase in the water level, a pipe started to form gradually underneath the hydraulic structure, causing the structure to tilt. A significant increase in porosity was observed near the toe of the hydraulic structure as piping began. This process of increasing local porosity continued under the structure.

It should be noted that the tilting of the structure is not very likely in the field, as the particles will be much smaller and the depth and width of the pipes will be limited. However, the discrete element model simulations provide an insight into the future possibilities of erosion modelling.

2.4. SUMMARY

The observations in experiments and the field make a general description of the piping process possible. However, the observations were not the same in each experimental series and the underlying process can sometimes even be different when there are variations in an experimental series.

The main variations in the experiments that lead to differences in the process are soil characteristics, type of exit and scale. In some experiments, the process observed was a completely different one to the formation of shallow pipes, as will be explained in the following paragraphs.

In small- and medium-scale experiments on loose sand samples by Van Beek et al. (2011) forward, rather than backward, erosion was observed. The relevance of this mechanism for practice still has to be investigated and it is one of the research questions in this thesis.

Ding et al. (2007) observed 'deep-seated piping' for experiments with a relatively thin fine-sand upper layer and a coarse granular sub-layer. Deep-seated piping appears to be linked to heave in the top layer, which can occur in multi-layer configurations with a highly permeable lower layer and a relatively thin, less permeable, top layer. This process has not been investigated in greater detail in this research since permeability contrasts in the foundations of Dutch dikes are generally not very large (personal communication Jan Blinde, 2014).

Townsend et al. (1988) tested non-uniform soils and found no piping at all or 'sheet flow'. The present study looks briefly at the role of the grading of the sand.

The presence of piping in a sand bed containing a separate engineering structure is linked to the fluidisation of sand downstream of the structure, a process that is fairly well understood (Van Beek et al., 2013) and does not require further investigation.

Difference processes have also been observed in experiments with backward shallow pipe formation. In some experiments 'equilibrium' occurred after pipe formation: the lengthening of the pipe stopped until the head was increased (Müller-Kirchenbauer et al., 1993; Hanses, 1985; Miesel, 1978; Silvis, 1991; some of the experiments by Townsend et al., 1988; Pietrus, 1981; Van Beek et al., 2011). It can therefore be concluded that the presence of the pipe affects the continuation of pipe development. In other experiments, no equilibrium was observed: the pipe developed continuously in the upstream direction at the head at which pipe formation started (small-scale experiments by Van Beek et al. (2011), most experiments by De Wit (1984) and some of

the experiments by Townsend et al. (1988) and Pietrus (1981)). Essentially, in the second type of experiment, the critical gradient (H_c/L) is determined by the initiation, rather than by the progression, of the pipe. As there was no equilibrium during pipe development, it must be concluded that, in these experiments, the initiation of the pipe required a larger head than the head required for the progression of the pipe.

The variety of the processes has implications for the critical head and for predicting piping. In the models that predict the critical gradient by including the presence of a pipe, such as the Sellmeijer model (1988), it is assumed that the lengthening of the pipe will cease after initiation, resulting in equilibrium. Accordingly, these models calculate the gradient at which the pipe will progress to the upstream side. The implicit assumption is that the onset of pipe development, or initiation, requires a lower head drop than the progression of the pipe. Experiments indicate that this assumption is not always true and not all experiments are therefore suitable for the calibration of progression-based models.

The final critical head, whether dominated by the initiation or progression of the pipe, will be affected by the characteristics of the sand bed and the configuration of the set-up. Regardless of the process, the critical gradient seems to increase with decreasing scale and with increasing relative density. The effect of grain size has not been determined unambiguously since the critical gradient in some experimental series rose at larger grain sizes, but fell in other experimental series.

To quantify and understand these effects, it is necessary to subdivide the experiments on the basis of the type of process ('initiation-dominated' or 'progression-dominated') and analyse them accordingly. A general description of the piping process helps to establish an understanding of the mechanisms involved.

No model is available for pipe initiation that links the average critical head to the presence of sand boiling and sand transport, although De Wit (1984) explains scale effects by calculating the potential distribution near the toe structure. The prediction of pipe initiation is not relevant for laboratory testing only. In the field, it will be relevant to know which process dominates and whether equilibrium in pipe formation can be expected. The Sellmeijer model (Sellmeijer et al., 2011) is the most advanced model for the prediction of pipe progression in field conditions, although it currently lacks a sound theoretical explanation of the role played by sand characteristics and it has been validated in 2D experiments only. Experiments by Yao (2014) and Vandenboer et al. (2014b) have shown that piping is essentially a 3D process. The theory described by Hanses (1985) could complement the Sellmeijer model with respect to the erosion process. Finally it should be noted that in all experiments described in this section, the critical gradient was found by gradual increasing of the hydraulic head, whereas the head drop may increase suddenly in the field. A sudden increase in the head may lead to other pipe patterns or pipe development velocities than observed in the experiments described in this section.

3. PROCESSES

'Ons omdraaiend, zagen wij een modderfontein van manshoogte op de plek van den waargenomen wel. Het bleek alras, dat hier geen voorziening zou baten en dus werd in allerijl de brandklok geluid en werden de menschen in het achterland door estafettes per rijwiel gewaarschuwd.'

A. van Linden – van den Heuvel, reporting on the dike failure in Zalk (1926)

3.1. INTRODUCTION

This chapter is concerned with the processes involved in pipe formation, and how they may ultimately lead to dike failure. Numerous researchers have studied the process of backward erosion piping. Observations from experiments conducted in the past and from the additional experiments conducted in the context of the present study have been adopted as the basis for a description of the mechanisms involved.

This chapter provides an introductory overview of the sequence of processes leading to failure and then discusses backward erosion in greater detail.

3.2. SEQUENCE OF PROCESSES LEADING TO FAILURE

The process leading to failure due to backward erosion piping can be divided into several phases: seepage, backward erosion, widening and failure (see section 1.2). Each of these phases is associated with different mechanisms. These processes are explained in this section using a simple 2D geometry for a homogeneous sand layer below a cohesive material. In reality, the geology is more complex, with variations in soil properties in all directions. To understand the basic principles of backward erosion, a simple configuration will suffice based on the typical geology found in river or coastal areas.

3.2.1. SEEPAGE

Seepage drives the processes leading to failure. It is governed by the difference in the water level across the water-retaining structure. The water flow through the sand layer can be described by Darcy's law. The assumption of laminar flow in this equation is valid for the typical range of fluid velocities in water flows through sandy aquifers beneath dikes.

As noted already in the introduction to this thesis, a downstream unfiltered open exit is required if seepage is to occur. In some cases, an open exit is present naturally, for

example when there is no blanket layer on the downstream side of the water-retaining structure (Figure 2.2a), or when a ditch cuts through a thin blanket layer (Figure 2.2c). In other cases, an exit point is created when the water pressures directly under the blanket layer exceed the weight of the blanket layer, causing the layer to crack locally (Figure 2.2b). In many areas, seepage becomes apparent because of the presence of saturated areas or even water on the surface to the downstream side of the structure. This is clear to see in Figure 3.1.



Figure 3.1. Saturated fields during the flood of 1993 in the Betuwe polder district; picture taken from a river dike (www.beeldbank.rws.nl, Rijkswaterstaat)

3.2.2. BACKWARD EROSION – INITIATION AND PROGRESSION

Once there is seepage and an open exit, the hydraulic gradient near the exit determines whether erosion will begin. The initiation of backward erosion requires the fluidisation of sand near the exit point, which occurs when the seepage pressures in the sand match the submerged weight of the sand, resulting in the expansion of the sand, which then turns into a fluid sand-water mixture.

Clearly the exit velocity is highly dependent on the type of exit. In a crack in a soft soil layer (Figure 2.2b) the exit velocity will certainly be higher than the exit velocities found downstream of a structure where no cohesive blanket layer is present (Figure 2.2a). However, in the case of all exits shown in Figure 2.2, there is a concentration of flow lines near the exit point and therefore the local gradient near the exit point will be higher than the average gradient below the dike. Backward erosion piping can therefore start at relatively low average gradients: typically 0.05 to 0.1 in the field. This concept also explains the relevance of the presence of a roof to the pipe, as discussed in section 1.2. When the permeability of this roof is lower than the permeability of the sand (which is normally the case) there will be a concentration of flow lines near the exit point, leading to local higher water flow velocities and therefore making backward erosion piping more likely.

Pressure gradients that are high enough to cause fluidisation do not always cause sand transport and therefore pipe formation. Sand ‘boiling’ without sand transport - sand when it looks like a boiling fluid (Figure 3.2a) - is often observed in experiments and field situations. It should be noted that boiling does not always occur since the fluid flow can also be in equilibrium with the weight of the fluidised soil mass.

The equilibrium situation described above can be disturbed when the fluid flow is sufficient to carry soil particles outside the fluidised zone and deposit these particles in a ring outside the sand boil centre. This ring of deposited sand is known as a ‘sand volcano’. With each surge of fluidisation, sand is deposited and the volcano grows. These volcanoes are often observed in the field during high-water periods (Figure 3.3) and are also referred to as ‘sand boils’. They will occur only when the water velocity in the vertical part of the pipe (the ‘crater’) is higher than the falling velocity of the grains in the sand-water mixture.

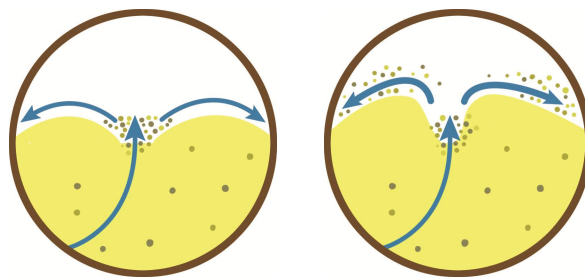


Figure 3.2. Sand boil, (left) without sand deposition, (right) with continuous sand deposition



Figure 3.3. Sand boil during high water period of 2011 (Herwijnen, Netherlands)

The sand deposited on the surface is transported from the aquifer. In this aquifer, shallow pipes (a few millimetres thick) are formed in the sand at the interface of the cohesive layer and the sand layer. The cohesive layer forms a roof to the pipe and allows the pipe to remain intact.

Sand deposition often stops in the field. This means that the development of the pipe can cease after some time. Apparently, there is a critical value for the head drop that needs to be exceeded before the pipe can progress in the upstream direction and connect the upstream and downstream sides.

3.2.3. WIDENING

As soon as the pipe has progressed across the entire base of the water-retaining structure, connecting the upstream and downstream sides, the flow in the pipe increases significantly since the flow resistance of the sand disappears. The resulting flow surge causes a large quantity of sand to be eroded near the upstream inlet of the pipe. Although a pattern of pipes is generally formed, the limited thickness (a few millimetres) and width (several centimetres) of a single pipe limits the transport capacity and the eroded material partly blocks the pipe further downstream. The sand in the blocked pipes is then removed during a new process of backward erosion. In this way, the widened upstream pipe becomes progressively longer, moving towards the downstream side of the dike (Van Beek et al., 2011).

When the pipe is widened over its full length from the upstream side to the downstream side, sand transport and flow increase significantly. The widened pipe has a large flow capacity that leads to increased scour in the pipe. The sudden transition from calm sand boiling and sand transport to the mud fountain observed in the large-scale experiments is very similar to the process observed during the dike failure in Zalk in 1926 (Van Dam and Beijersbergen, 1981) that was described on the first page of this chapter:

'When we turned round, we saw a man-sized fountain of mud where the boil had been. It soon became clear that no steps would avail and so the fire bell was sounded in all haste and bicycle relays were dispatched to warn the populace in the hinterland.'

The widening process takes considerable time, during which flow and sand transport rates are observed that are more or less comparable with those seen in the phase of backward erosion (Van Beek et al., 2011). Theoretically, a slight increase in flow and sand transport rates would be expected at the transition from backward erosion to widening and during the progress of the widening process, but this could not be concluded on the basis of the measurement data in large-scale experiments.

3.2.4. FAILURE

The failure of a dike due to backward erosion piping has been observed in full-scale experiments (Van Beek et al., 2011). It was found that, once the widening process had been completed, the increase of flow through the pipe led to further scour in the pipe, both in the sand and in the clay, resulting in the distortion and cracking of the dike. The scour in the sand is driven by water flow in a process similar to that seen during pipe formation, whereas the erosion of the cohesive base of the dike resembles concentrated leak erosion.

Two scenarios have been observed in experiments. The first scenario is the failure of the dike within 20 minutes after the first burst of water and sand transport as a result of the loss of stability in the dike body (sliding) (Figure 3.4). In the second scenario the dike settles and deforms in such a way that the widened pipes are closed off. The

connection between the upstream and downstream side then has to be re-established for sand transport and flow to increase again. There can be several phases of reconnection and deformation before the dike finally fails due to the loss of stability in the dike body. This scenario has been observed in the field in a dike near Greenville, Mississippi. During the high water of 1929, the removal of foundation material caused the dike to settle several feet. However, the dike did not fail here because the pipes were closed due to the settlement and there was no overtopping despite the settlement (USACE, 1956).



Figure 3.4. Failed dike in full-scale experiment (scenario 1)

3.3. BACKWARD EROSION

Although a dike will certainly not necessarily fail after the pipe has reached the upstream side, the phase of the development of the pipe over a critical distance is the most advanced way of predicting backward erosion failure. Once the critical head required for pipe development has been exceeded, it is only a matter of time before the dike fails unless the water level drops before failure. The focus of experiments in the laboratory is therefore generally the phase of backward erosion from the initiation of the pipe to progression in the upstream direction.

On the basis of observations in experiments (described in Chapter 2), the phase of backward erosion can be described as a sequence of events driven by increasing head. It emerges that the sequence of backward erosion processes and the corresponding critical hydraulic head depend on the geometry of the water outflow point (exit type) and the scale of the set-up. This sequence of events can be summarised as follows, bearing in mind that phase 3 is not always observed:

1. Single grain transport – development of preferential flow paths.
2. Boiling phase – sand boils without deposition of sand.
3. Regressive backward erosion phase. Sand is transported towards the exit and a pipe starts to form. Erosion will stop unless the head is increased.

4. Progressive backward erosion phase – the pipe develops in the upstream direction.

Each phase is described in greater detail here.

3.3.1. TRANSPORT OF SINGLE GRAINS

The first signs of erosion that can be observed are the ejection of single particles from the sand matrix. These are small grains that can be removed easily by a local concentrated water flow, possibly resulting in the formation of micro-scale holes, as seen in some experiments with a plane-type exit (De Wit, 1984; Van Beek et al., 2011). An example of these holes in a large-scale experiment is shown in Figure 3.5. In other experiments the washing out of small-sized grains results in turbid water (Silvis, 1991) or the formation of pipes at the pore scale (Van Beek et al., 2011). In all the experiments, this type of micro-scale erosion stabilises unless the head is increased.

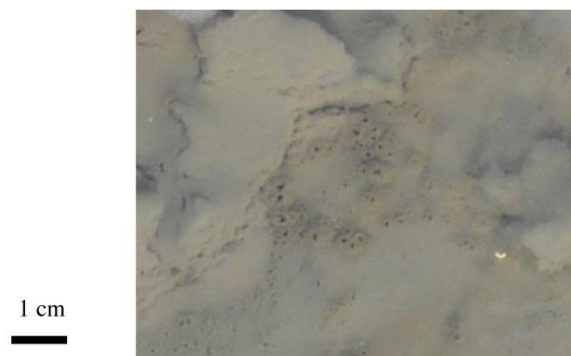


Figure 3.5. Small holes observed in a full-scale experiment (Van Beek et al., 2011)

3.3.2. SAND BOILING PHASE

As a result of increasing pore pressures near the exit, the bed expands and local fluidisation can be observed, resulting in the formation of sand boils. Bed expansion, the local uplift of the sand bed near the simulated dike toe due to increasing porosity, has been observed in experiments (De Wit, 1984). In the sand boil, the sand is lifted and dropped, but the water flow is insufficient to deposit sand outside the centre of the sand boil. This sand boiling phase has been observed in several experiments (De Wit, 1984; Silvis 1991; Van Beek et al., 2011). Miesel (1978) and Müller-Kirchenbauer (1978), in their discussion of their experiments with hole-type exit and a vertical tube (Figure 2.4), referred to this phase as 'fluidisation'. Fluidisation of the sand bed caused sand to be transported to the vertical tube so that the tube was gradually filled with a sand suspension. No clear distinction was made between fluidisation, which results in the expansion of the sand body, and the actual transport of particles from the sand body, which leads to pipe formation. Not surprisingly, given the fact that fluidised sand flows directly downwards along the slope, the sand boiling phase is not seen in slope-type experiments (Van Beek et al., 2011).

3.3.3. REGRESSIVE OR EQUILIBRIUM PHASE

As the head increases further, sand boiling will intensify and sand will be deposited near the exit point, resulting in the formation of hollow spaces in the sand body. At this point, the 'critical head' - the head required for the pipe to develop in the upstream direction (H_c) - will generally not have been exceeded yet and pipe formation will cease after some time, when equilibrium is reached in the pipe formation. This phase is therefore referred to as the regressive phase, or the equilibrium phase.

There are several possible causes of equilibrium in pipe formation. In the experiments by Miesel (1978) equilibrium occurred during the 'fluidisation phase'. In this phase sand was transported through the vertical section but not ejected from the tube. An increase in head was necessary to raise the level of fluidised sand in the tube. A similar process was observed in the experiments with a small hole-type exit (De Wit, 1984): the circular hole was gradually filled with sand, but the level of fluidised sand remained constant until the head was increased. After the head had been increased several times, the vertical tube was completely filled with sand and sand was ejected over the top of the tube and onto the cover layer in both experimental series. When the diameters were larger (0.04 m in De Wit's experiments and 0.013 m in Miesel's experiments), equilibrium was no longer observed at this stage: the pipe developed in the upstream direction without the head being increased further. It would appear that the presence of sand in the vertical section causes a pressure drop that hinders the ongoing development of the pipe.

In the case of exit holes with smaller diameters, equilibrium also occurred after sand was ejected. In Miesel's experiments, this was the case at diameters of less than 0.013 m. These experiments indicate that, in addition to the resistance in the vertical section, there is another reason for equilibrium. This was confirmed in the present study in experiments with a circular hole and a very small vertical section representing a thin blanket layer (see Chapter 4).

This equilibrium could be related to the decrease in the local hydraulic gradient when the pipe develops away from the exit hole, restricting the inflow towards the pipe and the gradient at the head of the pipe as the length of the pipe increases. This type of equilibrium can only occur relatively close to the exit; when the pipe extends over approximately half of the seepage length, the intact section of the seepage length becomes relevant, causing an increase in inflow and in the gradients around the pipe as the length of the pipe increases. This type of equilibrium has been frequently observed. The recurrence of equilibrium is clearly visible in large-scale tests (Silvis, 1991), in which pipe length as a function of head difference has been well documented. Figure 3.6 shows several pipes developing in line with increasing head in one of these large-scale experiments.

These two causes of regressive erosion - local gradients and exit loss - are not easily distinguishable in experiments simulating a considerable cohesive blanket layer. A third reason for equilibrium in pipe formation is the presence of a barrier in the path of the pipe such as a cut-off wall or a different soil type. Differences in soil characteristics such as grain size or permeability may cause additional resistance that needs to be overcome. After a developing pipe reaches the barrier, piping channels propagate parallel to the barrier until the head is large enough to take the pipes underneath the cut-off wall or through the other sand type (Van den Ham, 2009; Ding et al., 2008; Van Beek et al., 2008). Resistance in a vertical piping path is clearly much higher than in a horizontal

piping path (this concurs with the findings of Lane, 1935) as pipe continuation along the vertical path requires the fluidisation of the sand downstream of the structure (Terzaghi and Peck, 1967). However, a change in the soil type can also constitute a significant barrier, as observed in the experiments by Van Beek et al. (2008) and as will be seen in the medium-scale experiment Ims18 described in Chapter 4. It is therefore likely that in the field, where grain sizes in sandy layers vary in the lateral direction, resistance to piping is higher than found in model tests with a homogeneous sand sample.

In many other experiments, no equilibrium in pipe formation has been observed at all. Those experiments have been predominantly small-scale plane- and ditch-type experiments (De Wit, 1984), or slope-type exit experiments (Van Beek et al., 2011). In these experiments, the critical head for the progression of the pipe had already been exceeded when pipe formation started, since the head required for the fluidisation phase needed for pipe initiation exceeds the head required for the progression of the pipe (see section 3.3.5).

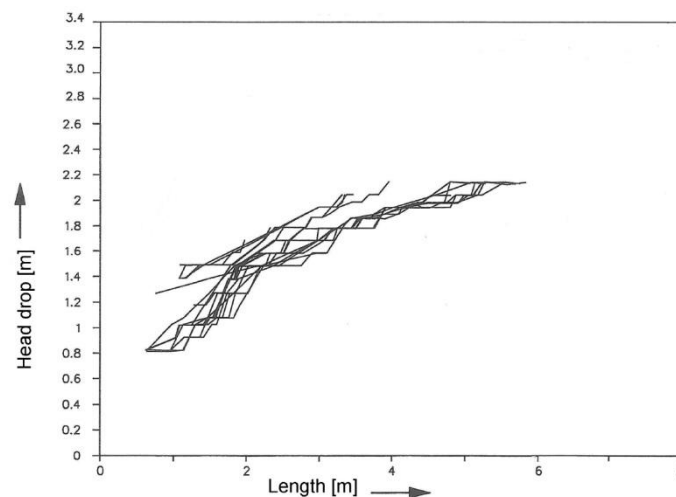


Figure 3.6. Pipe development (pipe length) and applied head in test T3 with a total seepage length of 12 m (Silvis, 1991)

Several researchers have conducted detailed studies of the erosion process in this phase of regressive erosion. Hanses (1985) studied backward pipe development at the micro-scale. Two types of erosion can be distinguished: primary erosion, which is the erosion of grains from the soil matrix at the head of the channel, and secondary erosion, which is the widening and deepening of the existing channel. Primary erosion occurs when the hydraulic gradient at the tip of the pipe reaches a critical value that leads to the fluidisation of the sand at the tip, after which the sand can be transported. The flow velocity in the pipe, which is determined by the inflow of water from the sand matrix, may reach a critical value that leads to secondary erosion. It should be noted that primary sand transport is intermittent: groups of sand grains go into suspension (sand clouds).

Townsend et al. (1988) have also studied the backward erosion piping process in detail and their observations were similar to those of Hanses (1985): particles slide into the pipe and, when the group of particles is washed away, several more new particles are

displaced in a retrogressive slide. Van der Zee (2011) has studied pipe formation at the micro-scale in a set-up with a very limited width in which the piping process could be observed from the side. He also observed an intermittent erosion process. Grain transport through the pipe caused secondary erosion and the sand bed appeared to be fluidised due to upward flow in the sand bed below the pipe. It should be noted that, due to the limited width, the applied gradient was much higher than in experiments with larger widths. In the visualisation experiment described in Chapter 3, erosion and the deposition of particles on the bottom of the pipe was observed but there was no net increase in the pipe depth.

Hanses (1985) also studied the shape of the pipe and observed that the size of the pipe at the tip remains the same during pipe development. At the tip, the depth of the pipe was found to be 3-5 times the average diameter of the grain. When the pipe increased in length, the pipe in the downstream area of the pipe widened and deepened (secondary erosion). The width of the pipe increased in the downstream direction (Figure 3.7).

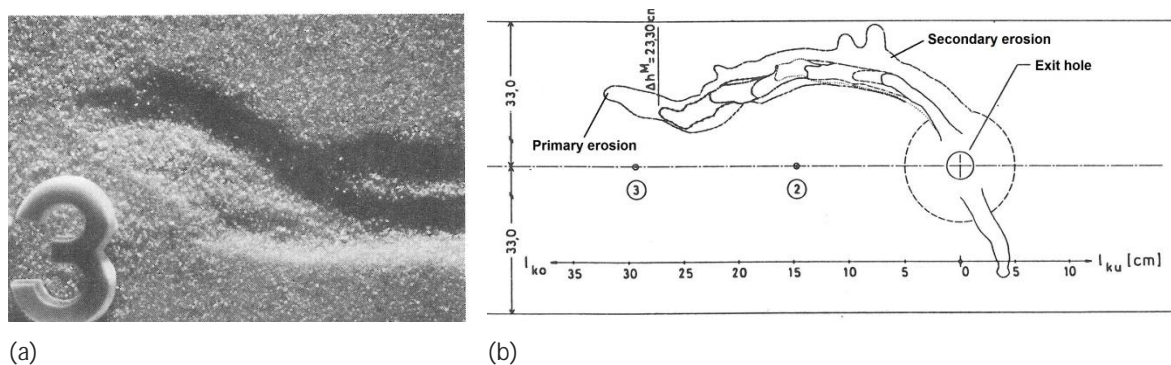


Figure 3.7. Photo of the tip of the pipe (a) and drawing showing pipe development over time in one of the tests (b) (modified after Hanses, 1985)

3.3.4. PROGRESSIVE PHASE

The progressive phase consists of ongoing erosion that results in pipe development to the upstream side of the sand body. This phase was finally reached in all experiments. Müller-Kirchenbauer et al. (1993) state that, in general, this phase is reached when the pipe has developed to between $1/3$ and $1/2$ of the seepage length. From this point onwards, the gradient and flow towards the pipe increase, and equilibrium is no longer possible. If a structure like a cut-off wall is present, the progressive phase is reached after the pipe has passed the structure.

3.3.5. WHICH PROCESS WILL OCCUR WHEN?

The variety of erosion processes makes it difficult to predict backward erosion. Why does equilibrium occur in some experiments but not in others? The answer can be found in the overall minimum hydraulic head required for each process. The transitions between the phases in each experiment will occur at different hydraulic heads:

- single grain transport to boiling phase (H_b);
- boiling to pipe initiation and regressive erosion (initiation head H_i);

- regressive erosion (pipe stops) to progressive erosion (pipe continues until breach) (progression head H_p).

The hydraulic head at which the pipe develops in the upstream direction – irrespective of the process that determines this hydraulic head – is generally referred to as the ‘critical head’ (H_c) in the literature.

In all experiments, pipe initiation must precede pipe progression. In some configurations, initiation, which is likely to correspond to the fluidisation of a group of particles such that sand deposition can take place, can occur at a relatively low overall head, as is the case for small hole-type exits. Here, the flow will concentrate at the small exit, resulting in a considerable¹ hydraulic gradient around the exit at a relative low overall hydraulic head. At this point, the hydraulic head required for the progression of the pipe (H_p) will not yet have been reached and equilibrium will occur. In other experiments, the flow lines are less concentrated and initiation occurs at a relatively high overall head (H_i), as in 2D slope- and plane-type experiments in which flow velocities are low near the exit. Once the pipe has been initiated, the progression head will already have been exceeded and no equilibrium will be observed. In this case, the formation of a pipe will result in a large change in the flow pattern: essentially a transition from 2D flow towards the exit to 3D flow towards the newly formed pipe tip. This will lead to the concentration of the flow. The gradients near the pipe tip are relatively high by comparison with the pre-pipe gradients at the 2D exit, and therefore a lower critical hydraulic head for pipe propagation is required once the pipe has formed.

Clearly, the backward erosion process is highly dependent on the exit geometry. This relationship was observed by Miesel (1978), who studied the erosion process as a function of circular exit diameter. The idea that the type of process is related to the exit configuration has been verified experimentally in the research for this dissertation (Chapter 4).

Scale represents another obstacle to predicting the course of the backward erosion process. It is known that the critical gradient for progression (H_p/L) is scale-dependent (Van Beek et al., 2011; Sellmeijer, 1988): the progression gradient falls with scale, generally expressed as seepage length, assuming a constant ratio of sand layer thickness and seepage length. When the scale effect of pipe initiation is different from that of progression, the processes observed can be different at different scales. Assuming no change in shape, the Sellmeijer model indicates that the critical gradient for pipe progression is inversely related to the cubic root of the seepage length ($H_p / L \propto 1/\sqrt[3]{L}$). However, Bezuijen and Steedman (2010) found that the critical gradient for pipe initiation in layers of infinite thickness is inversely related to the square root of the seepage length ($H_i / L \propto 1/\sqrt{L}$).

Figure 3.8 shows how the critical gradients could be related qualitatively in an arbitrary case. The figure shows that, in small-scale experiments, $H_i > H_p$, whereas $H_p > H_i$ in larger-scale experiments.

Figure 3.9 shows the available experiments (De Wit, 1984, Silvis, 1991, Hanses, 1985, Van Beek et al., 2011, Yao et al., 2007) grouped according to the type of process that

¹ Considerable means here a local gradient of around 1. This is approximately the vertical gradient necessary to fluidize a sand bed and slightly higher than the horizontal gradient required to move sand grains in horizontal direction.

dominates the critical head. The figure shows the dominant process for the critical head as a function of exit type and seepage length. The more concentrated the flow towards the exit point, the more likely it is that the critical head will be dominated by the head required for pipe progression. It should also be noted that Figure 3.9 indicates that ditch- and slope-type experiments at large scales are more likely to be dominated by regressive backward erosion than experiments at small scales. This confirms the theory described above.

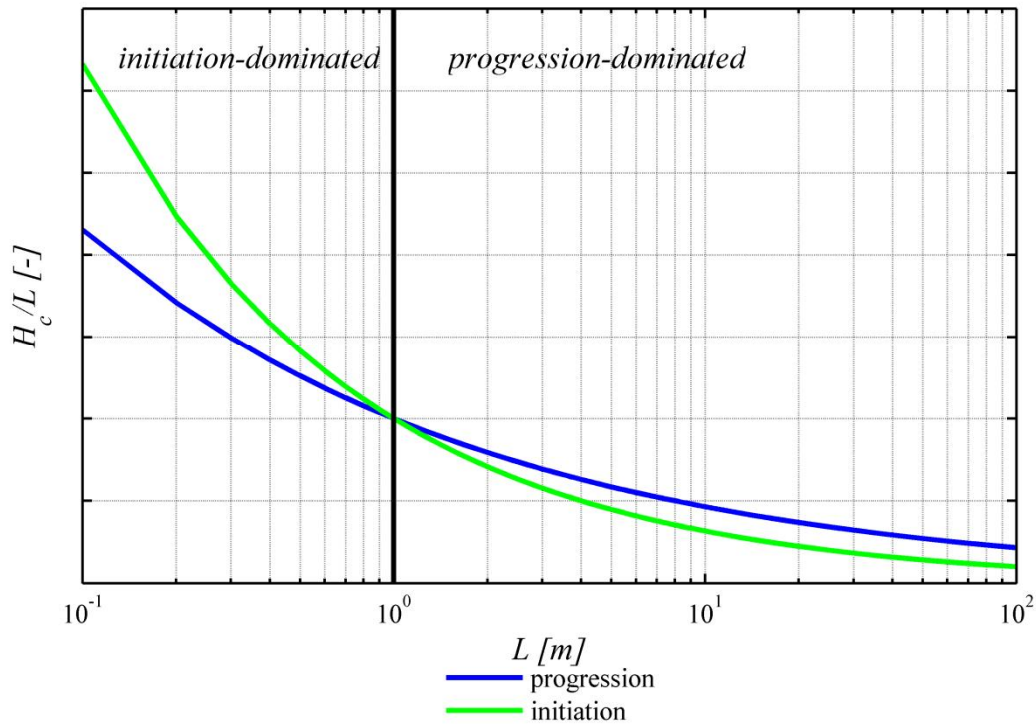


Figure 3.8. Qualitative interpretation of expected scale effects for pipe initiation and progression in an arbitrary case

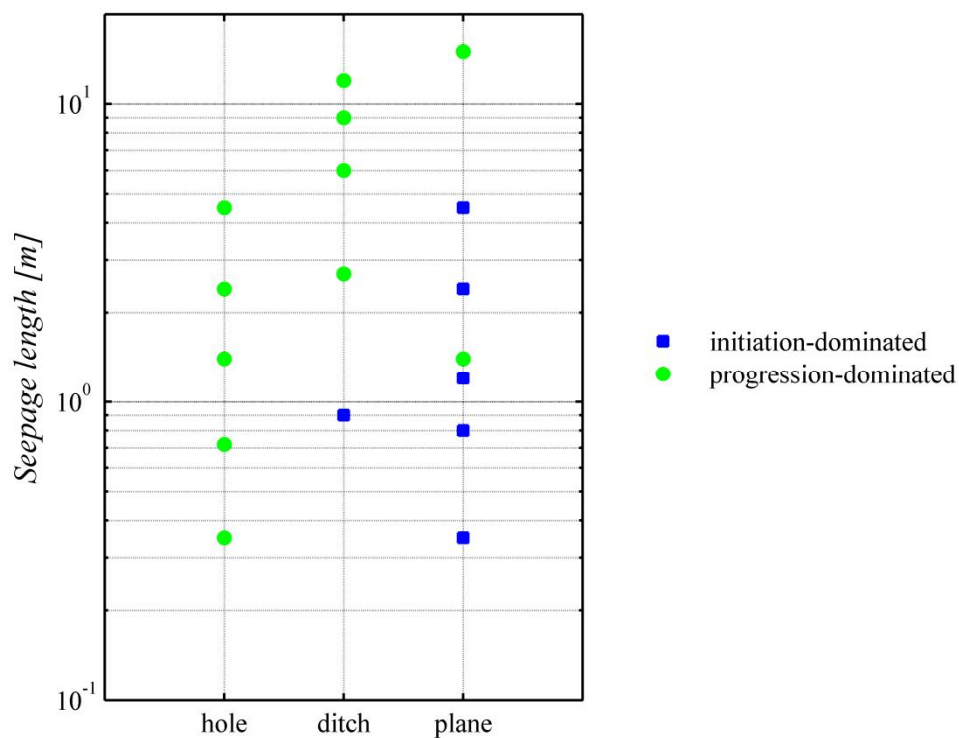


Figure 3.9. Relationship between the type of process, type of exit and seepage length

3.4. SUMMARY

The sequence of processes leading to failure is: seepage, backward erosion, widening and failure. This study focuses on the phase of backward erosion, which consists of single grain transport, sand boils, sand-transporting sand boils, regressive pipe formation (with equilibrium), and progressive pipe formation (critical head exceeded, no equilibrium).

Equilibrium in the pipe formation (or regressive pipe formation) is not always observed. In small-scale experiments and experiments with large outflow areas, the head required for pipe initiation may exceed the head required for pipe progression. This concept requires validation.

Pipe initiation is driven by the concentration of flow lines near the exit. Pipe progression is determined by the processes in and around the pipe. In the latter, Hanses (1985) distinguishes between primary and secondary erosion: erosion at the pipe tip and erosion that causes the pipe to widen and deepen. Equilibrium in pipe formation may occur due to a fall in gradients at larger distances from the exit or due to the presence of a barrier such as a cut-off wall or a sand layer with a different grain size.

4. EXPERIMENTAL WORK

'Physical simulation by means of tests and monitoring provides the means to check constitutive concepts, which form the fundamentals of prediction models'

Frans Barends

4.1. INTRODUCTION

The review of the literature and the analysis of the erosion processes led to a classification of experiments into those dominated by pipe initiation and those dominated by pipe progression. Nevertheless, several questions remained with respect to the processes leading to piping, such as the relevance of forward erosion for the field and the confirmation of whether the processes of initiation and progression are dependent on exit configuration.

The modelling of the processes of pipe initiation and pipe progression also required some quantitative answers. Although many experiments are available that can be used for the development of a model for pipe initiation, no relevant experiments have been performed using uniform sands with a relatively large grain size.

The roles of scale and sample shape on the critical head for pipe progression have been investigated but there are only a few experiments that look at the effect of soil type. When modelling pipe progression, comparing critical gradients with the Sellmeijer model does not explain the anomalous trend related to sand coarseness. This requires a closer investigation of the erosion mechanism and the pipe characteristics, such as the dimensions of the pipe and the hydraulic properties.

This chapter describes the laboratory experiments that were considered necessary to answer the research questions. The laboratory work consisted of six main experimental series designed to clarify the piping process and to improve and develop prediction models for piping. The different experimental series looked at the following areas:

- 1) The relevance of forward erosion.
- 2) Initiation and progression.
- 3) The effect of soil type on the initiation gradient.
- 4) The effect of soil type on progression gradients in small-scale experiments.
- 5) The effect of soil type and scale on progression gradients, and pipe hydraulics in medium-scale experiments.

- 6) Pipe hydraulics and erosion mechanisms in small-scale visualisation experiments.
- 7) Pipe dimensions in the equilibrium condition.

Figure 4.1 shows how the different experimental series are inter-related.

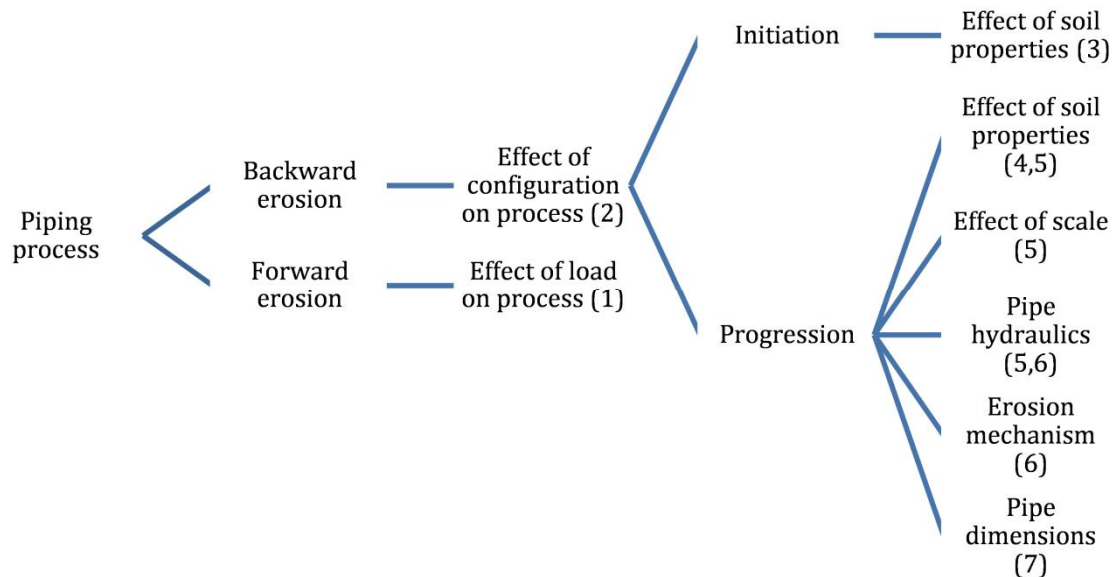


Figure 4.1. Schematic presentation of experimental work

In addition to the main experimental series, several supporting experiments were performed to analyse the friction angles at low effective pressures and to clarify the effect of the upstream filter in the small-scale slope experiments. These supporting experiments are described in Appendices B and C.

4.2. GENERAL DESCRIPTION OF SET-UP

Different types of set-up were used for the laboratory work. All the experiments subjected a confined sand sample to a head drop, simulating the flow of water through an aquifer beneath an impermeable water-retaining structure. Furthermore, all the experiments simulated the impermeable water-retaining structure using an acrylate plate that was roughened on the inside using silicone gel to resemble a clay layer. The dimensions and exit configurations in the set-ups varied. A general description is given here and details can be found in later sections.

The small-scale PVC box (described in Van Beek et al., 2011) with an acrylate cover and inner dimensions of 0.5x0.3x0.1 m was used for most of the experiments. Three types of exit configuration were used in this box: slope-type, area-type and hole-type exits (Figure 4.2). The experiments with an exit hole simulate the conditions in which a confining upper layer is punctured locally so that the flow from the aquifer converges to a small circular area. The experiments with an area-type exit simulate aquifers, which

are not covered by a cohesive blanket layer on the downstream side of the dike. The seepage length in these experiments is more or less the same (0.30-0.35 m for slope-type experiments, 0.344 m for hole-type experiments and 0.332 m for area-type experiments). An exit hole of 6 mm was used in the hole-type experiments. The exit-hole diameter was increased to 12 mm in selected experiments to investigate the effect of the hole diameter on the critical gradient. A cylinder filled with water was mounted on the plate and connected to the outlet to allow for the deposition of sand around the hole (Figure 4.2c).

In the medium-scale set-up, the sand bed was approximately four times larger in all dimensions (1.913x0.881x0.403 m). Experiments were performed with a hole-type exit. The exit hole was scaled so that the exit flow velocity was similar to the velocity with the 6 mm exit-hole diameter in the small-scale experiments. The scaling factor was calculated by comparing the expected flow towards the hole through the sand bed in both configurations. The cross-section of the medium-scale piping box was 11.7 times larger than the cross-section of the small-scale box. To obtain a similar flow velocity in the exit for both configurations, the area of the exit hole had to be 11.7 times larger for the medium-scale set-up, resulting in an exit-hole diameter of 20.5 mm. Pore pressure gauges and riser tubes were placed in the cover and bottom of the box to obtain information about the hydraulic conditions in and around the pipe.

The visualisation experiment developed to observe the pipe path in cross-section was designed as a small-scale experiment that was, as it were, cut in half along its centre axis so that the exit hole was on the wall of the box. It measured 0.48x0.15x0.10 m and the seepage length was 0.343 m. To observe the pipe path in cross-section, the side walls in this set-up were transparent. In the visualisation experiment, the exit hole was a semi-circle with a diameter of 6 mm.

In all hole-type experiments the height of the exit hole was sized so that it was small with respect to the size of the box: 10 and 20 mm respectively in the small- and medium-scale experiments (5-10% of the sand sample depth) in order to keep exit head losses as low as possible. This contrasts with the height of the exit in the experiments by Hanses (1985), which were approximately the same as the sand sample depth and which resulted in considerable exit losses in some experiments.

The crater formed below the water level in all experiments. In the field, a sand boil can form either below or above the water level. As particles are transported more easily when submerged, crater formation and the corresponding exit loss may differ in these two situations.

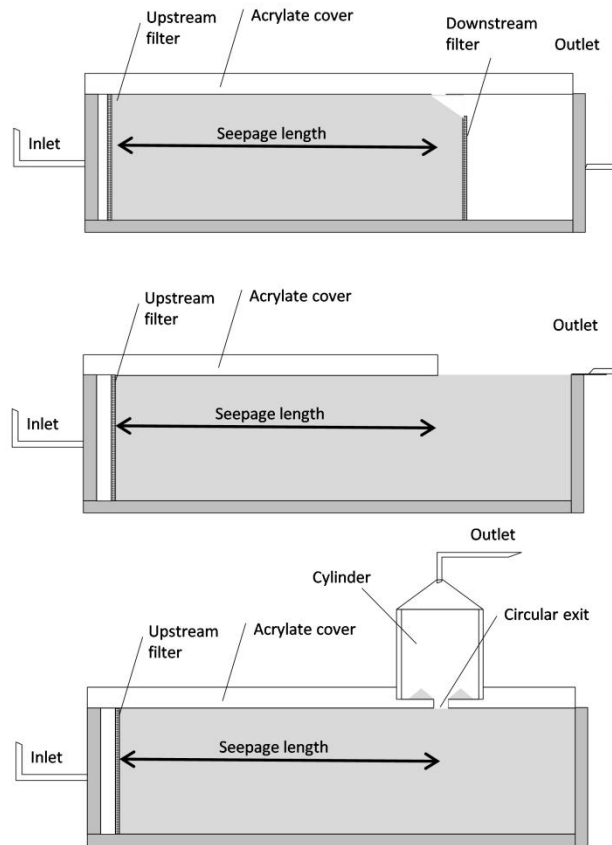


Figure 4.2. Schematics showing experimental set-ups with slope-type (top), area-type (middle) and hole-type (bottom) exits

The piping box was connected to an upstream water reservoir to maintain a constant head. The downstream set was connected to an overflow tube, the height of which could be adjusted. The water level in the upstream reservoir was maintained using a pump and an overflow (Figure 4.3). It should be noted that, for practical reasons, the head was increased on the upstream side and the head was kept constant on the downstream side in the medium-scale experiments and the area-type experiments. Riser tubes and/or pore pressure transducers were used in all experiments to monitor the head. The hydraulic heads in the sand sample in all experiments were measured using riser tubes or pore pressure transducers placed in various locations on the sides and bottom of the set-up. These measurements made it possible to estimate permeability and upstream filter resistance. In the visualisation and medium-scale experiments, additional riser tubes and pore pressure gauges were installed in the cover to analyse the pipe hydraulics. The accuracy of the readings of the riser tubes was within 0.5 mm. The accuracy of the pore pressure transducers varied but it was generally less than that of the manual riser tubes.

The flow was measured manually at regular time intervals during the experiment. One or more cameras were used to record the process of pipe formation.

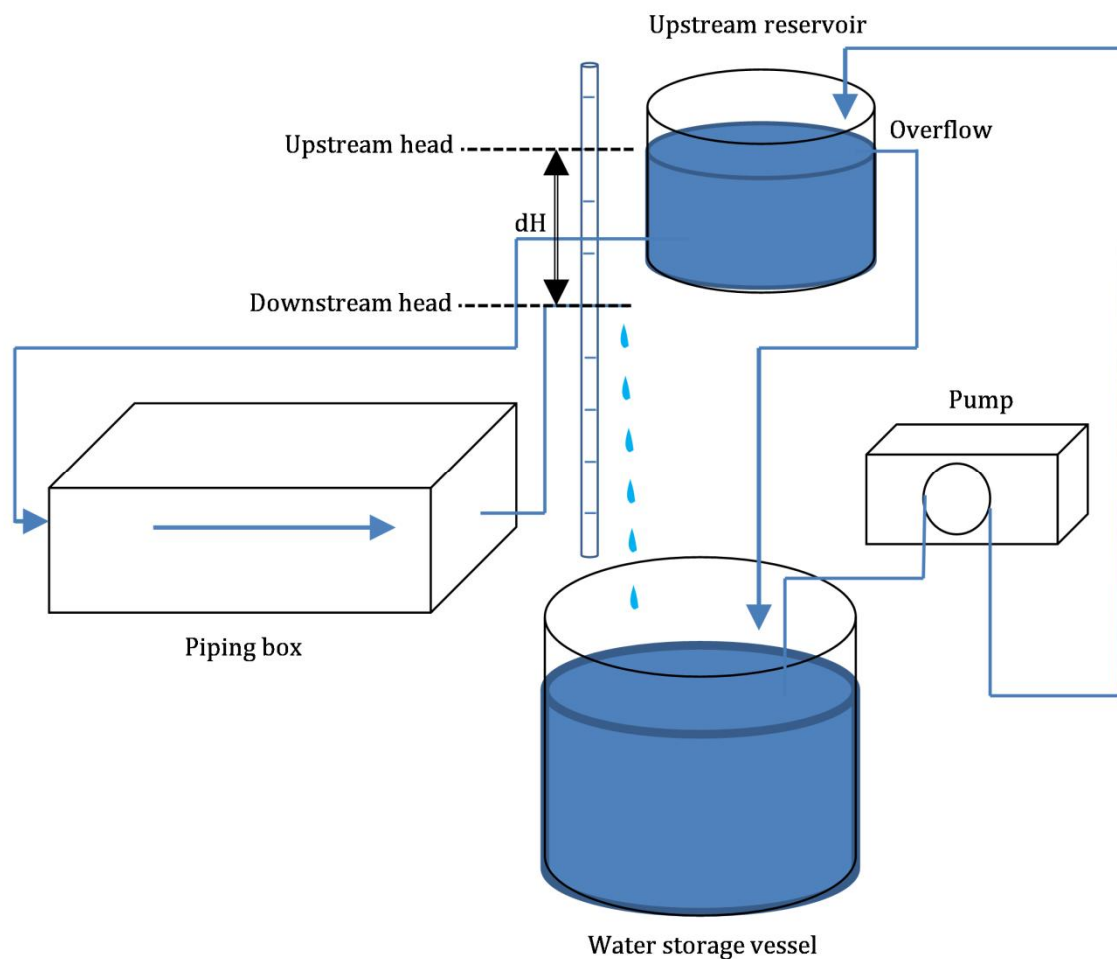


Figure 4.3. Schematisation of the water flow through the total set-up

4.3. SAMPLE PREPARATION AND SAND TYPES

The method used for sample preparation was more or less the same in all experiments. After the box was filled with de-aired water, the dry sand was sprinkled into the box while the box was in an upright position (with the closed flow inlet facing downward). Dense samples (relative density >85%) were prepared by sprinkling dry sand into de-aired water during continuous tamping. Loose to medium-dense samples were prepared by sprinkling dry sand into de-aired water to obtain a loose sample that was compacted to the required density by applying pulses. After filling, the lid was closed and the sample was placed back in the horizontal position (acrylate cover facing upward). The preparation method works well for less uniform samples as well providing that tamping is continuous and the water depth in the box during sprinkling is limited. The gradual sprinkling into de-aired water ensured that the sample was fully saturated. The saturation level was confirmed during the experiments: no air was released when a pipe formed in the sample.

In the area-type experiments, the acrylate cover consisted of two parts that could be connected seamlessly. After sample preparation, the sand box was placed in the horizontal position. The water level was lowered to the top of the sand layer in such a

way that the pores were still filled by water as a result of capillary forces. The lower half of the top plate was then removed to obtain a horizontal outflow area. The outflow area was surrounded by rubber strips to stop the water flowing in all directions. The water level at the upstream side was gradually increased until water flowed over the edge towards a PVC pipe where the outflow water was collected.

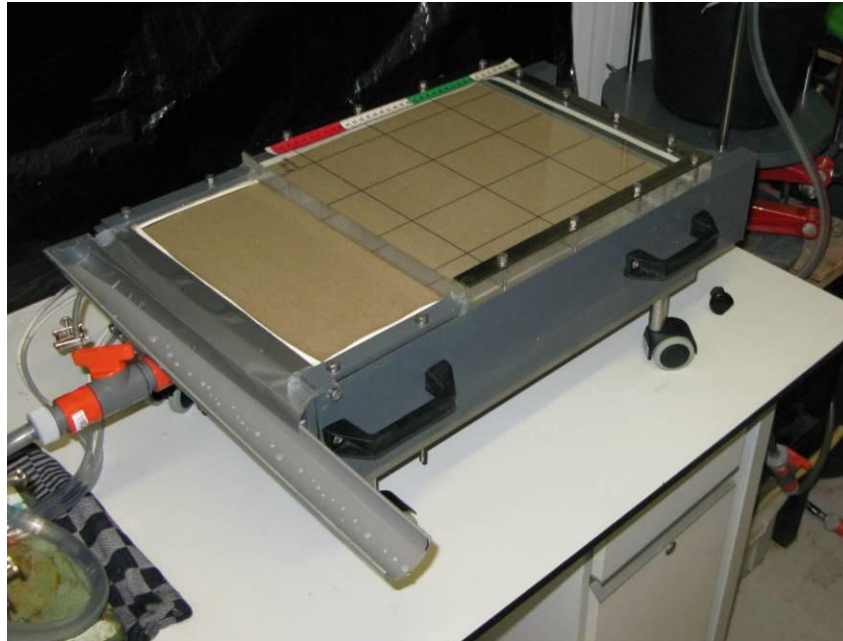


Figure 4.4. Set-up with prepared sand bed area

In the hole-type experiments, the hole was closed with a cork during preparation. After the sample had been placed in a horizontal position, the cork was removed and water was allowed to enter the sand sample in order to ensure that under-pressures did not disturb the sand sample around the hole.

In one of the medium-scale experiments (Ims18) the preparation method did not result in an entirely homogeneous sample: layering due to segregation during sample preparation was observed and this significantly affected pipe formation (Figure 4.28). The pipe developed perpendicularly to the direction of flow when it encountered a coarser layer. When the head was subsequently increased, the pipe then crossed the coarser layer. In the second experiment with this type of sand, more continuous tamping and sand sprinkling prevented the layering.

Baskarp sand was used in most of the experiments. Different sand types were used in the experiments investigating the soil type. The grain size distributions of all the sand types used are shown in Figure 4.5. Baskarp and Itterbeck sands are sieved fractions obtained from natural sands. Enschede sand, Waalre sand, Oostelijke rivierenzand and Sterksel sand are natural sands that represent deposits that are common in the Dutch subsurface. Mix 1 and Mix 2 consisted mainly of Itterbeck 125-250 μm sand mixed with different amounts of fine sand to obtain a more graded sample.

The main characteristics of the sand types can be found in Table 4.1.

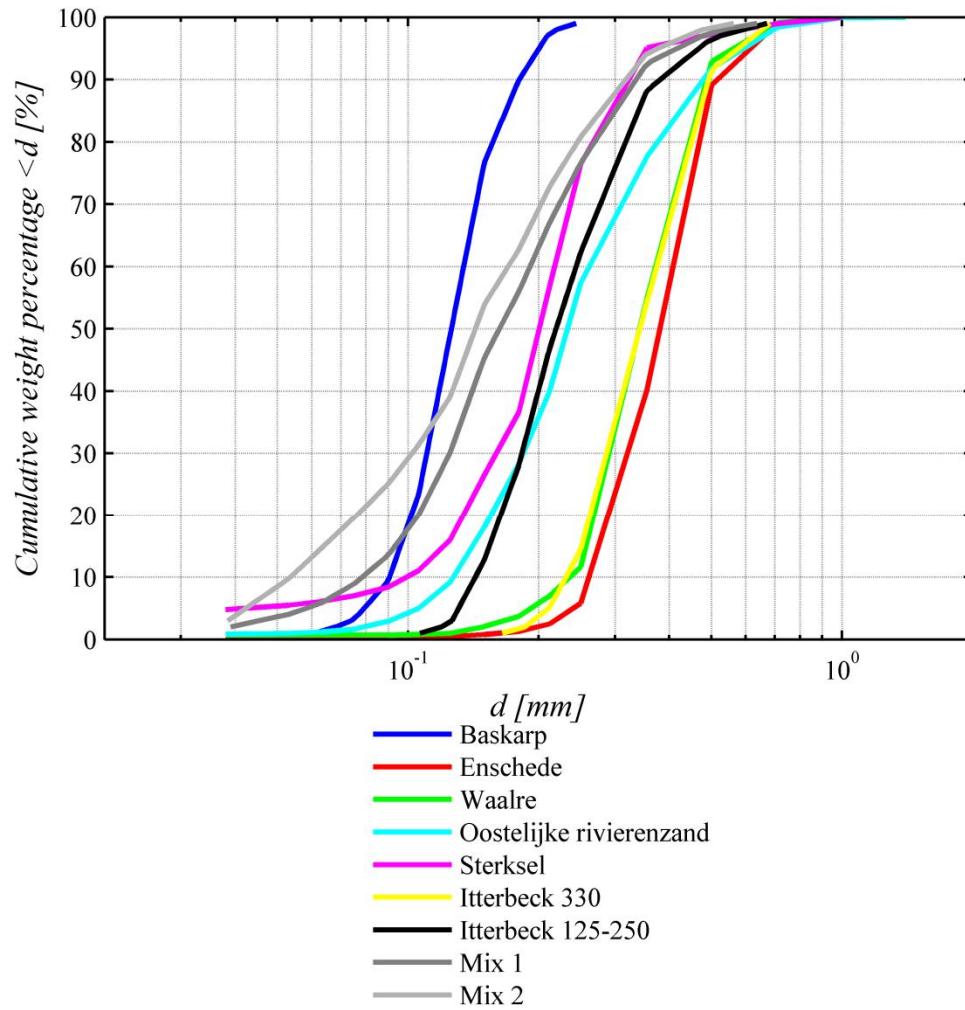


Figure 4.5. Grain size distributions of the sands used in the experiments

Table 4.1. Sand characteristics

Sand type	d_{50} [mm]	d_{70} [mm]	d_{60}/d_{10} [-]	min wet porosity [-]*	max wet porosity [-]*
Baskarp 1	0.132	0.154	1.54	0.340	0.469
Baskarp 2	0.132	0.152	1.50	0.367	0.477
Enschede sand	0.380	0.431	1.60	0.320	0.411
Hoherstall Waalre	0.341	0.400	1.58	0.350	0.450
Oostelijke rivierenzand	0.233	0.307	2.06	0.322	0.423
Itterbeck fraction 330 μm	0.342	0.410	1.60	0.337	0.434
Itterbeck 125-250 μm	0.219	0.278	1.71	0.345	0.465
Itterbeck mixture 1*	0.162	0.223	2.43	0.333	0.450
Itterbeck mixture 2**	0.143	0.203	3.17	0.319	0.440
Sterksel	0.228	0.300	2.25	0.357	0.474

*Minimum and maximum porosities were obtained with the same preparation method described in this section, but in a small column. Continuous tamping was used to achieve the minimum porosity. Results obtained with this method will differ slightly from the results obtained using the standard method, but these values are assumed to be more representative for wet sand.

4.4. TEST PROCEDURE AND EXAMPLE RESULTS

4.4.1. TEST PROCEDURE

The tests were performed by raising the hydraulic head in steps until erosion took place. The size of the step depended on the type of experiment: in the small-scale experiments the step size was 0.5 or 1 cm. In the medium-scale experiments, steps of 1 cm were used unless the course and duration of the experiment required larger steps. When sand transport was observed, the hydraulic head was not increased until the erosion process stopped, in other words when no sand was being transported in or near the pipes, and when the flow and heads observed in the riser tubes were constant. In the experiments investigating the influence of the configuration on the process (2) and in the visualisation experiments (6), the hydraulic head was reduced to zero after pipe formation and at various pipe lengths before being raised again in steps until erosion continued.

This manner of conducting tests is suitable for finding the critical gradient and the corresponding pipe development. It should be noted that a sudden increase in the head may lead to other pipe patterns or pipe development velocities than those observed when using the head application method described here.

The experimental programme consisted of slope-type experiments, area-type experiments and hole-type experiments. The typical course of these experiments and the corresponding output from the experiments are presented in the following sections.

4.4.2. EXAMPLES OF SAND BOILS AND PIPE FORMATION

In the hole-type experiments, the increase of head led to fluidisation in the exit hole, sand transport and sand boil formation (Figure 4.6). Equilibrium was observed and an increase of head was required for the pipe to progress in the upstream direction. Equilibrium was not observed in the slope-type and area-type experiments: in these experiments, the pipe developed immediately in the upstream direction once it had initiated. In the slope-type experiments, sand boils did not develop since the eroded sand flowed downward along the slope.



Figure 4.6. Example of sand crater and sand in transport

Figure 4.7 shows different examples of pipe formation in various experiments. The pipe can be quite straight, meandering or branching. Different pipe patterns are described in Van Beek et al. (2011). In hole-type experiments, pipes generally form in all directions initially due to the radial flow but they re-align in the upstream direction quite quickly. Clearly, the pipe develops in the upstream direction immediately in area-type experiments and slope-type experiments.

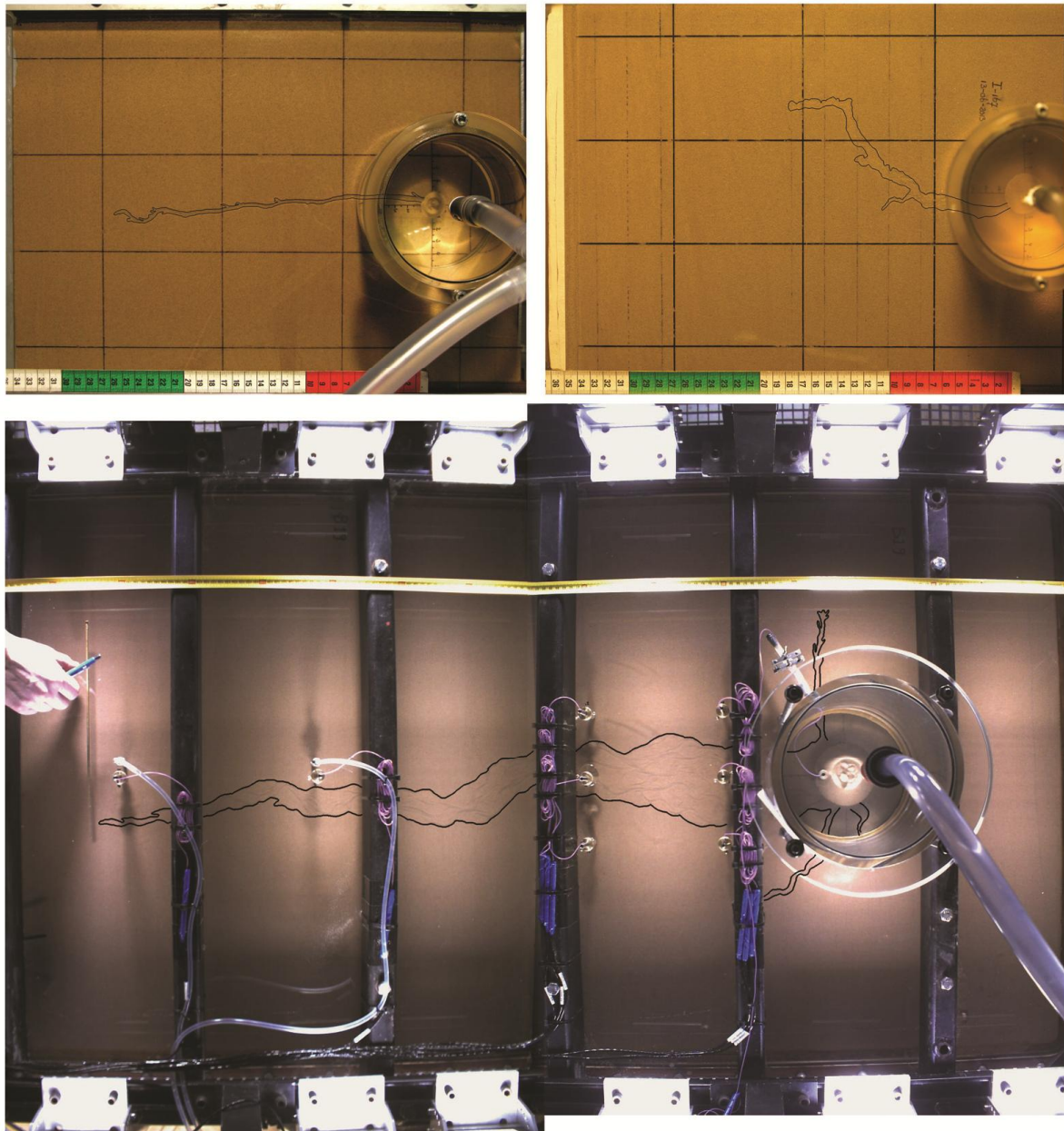


Figure 4.7. Examples of pipe formation in two small-scale experiments (left: B118, right: I167), and in one of the medium-scale experiments (Bms19)

4.4.3. EXAMPLE TEST DATA

Test B133 has been selected as a typical example of a test with a hole-type exit.

Figure 4.8 shows the application of head difference over time and the corresponding pipe development in one of the hole-type experiments. The right-hand figure shows pipe equilibrium (at 3 and 9 cm in this example) and the consequent increase of head.

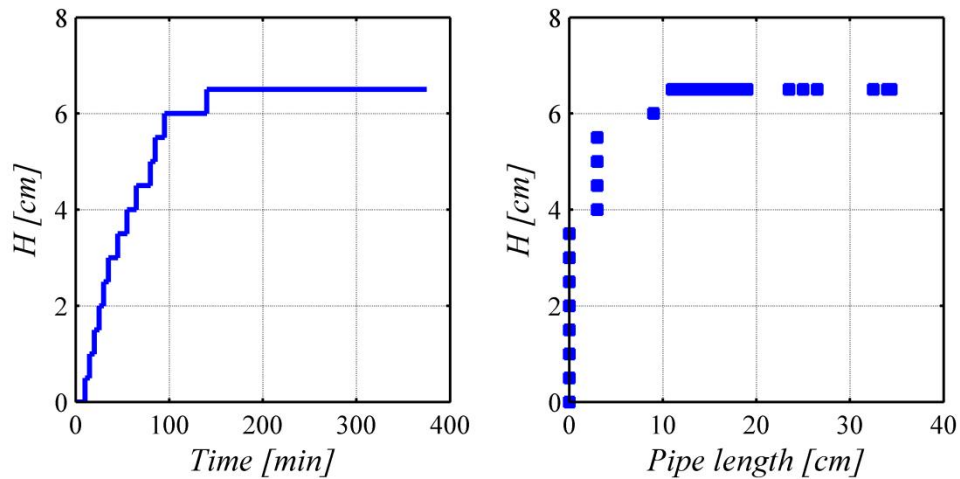


Figure 4.8. Applied head difference in time and as a function of pipe length

The measured flow initially increased linearly with the increase of applied head in agreement with Darcy's law. After pipe formation, the flow also increased in line with pipe length. The left-hand graph in Figure 4.9 initially shows that flow increases linearly as a result of the increase in the head. After 140 minutes, the head stayed constant (see Figure 4.8) and the subsequent increase in the flow was linked to pipe formation. Normalising the flow with the head made clear the increase in bulk permeability that occurred as a result of pipe development (Figure 4.9). As soon as the pipe reached the upstream side, the flow increased rapidly. The experiment was stopped at this point.

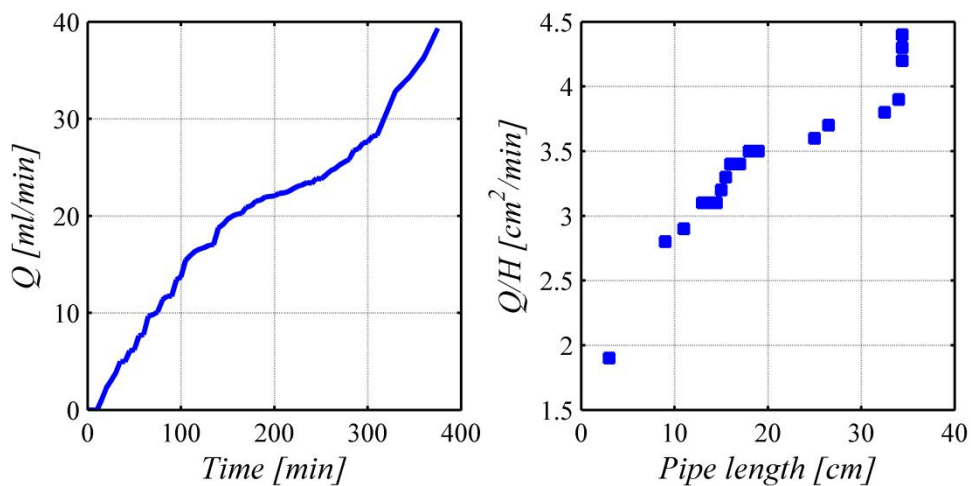


Figure 4.9. Measured flow as a function of time and measured flow normalised by the applied head as a function of pipe length (B133)

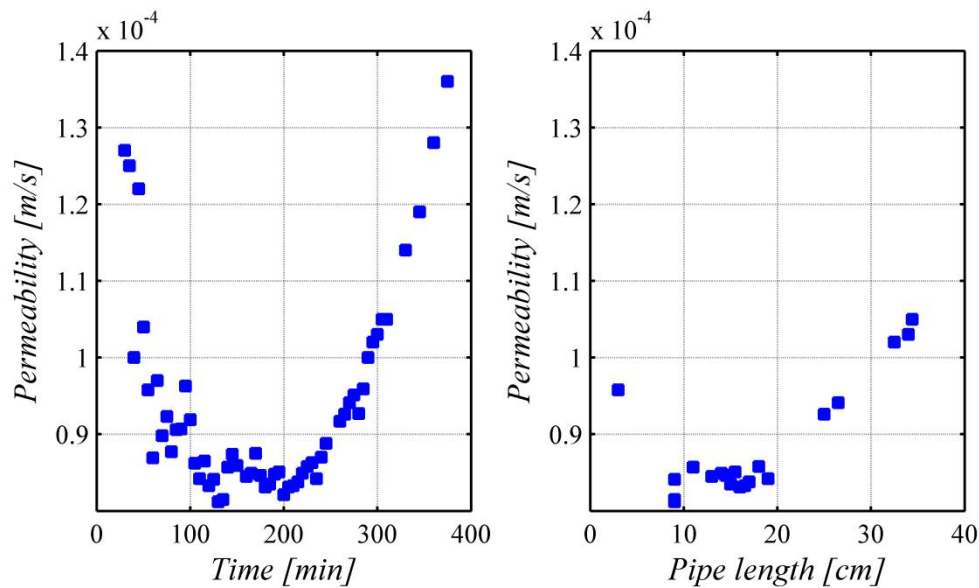


Figure 4.10. Permeability calculated using riser tubes h1 and h3 as a function of time and pipe length (B133)

The riser tubes installed in the bottom of the set-up were used to calculate the permeability of the sand bed. Figure 4.10 shows an example of permeability as a function of time and pipe length calculated using the riser tubes h1 and h3 located at 1 and 19 cm from the upstream filter at the bottom of the sand sample (for those pipe measurements that included the pipe length). Generally, the values for permeability are inaccurate at the beginning of the test because of the lack of accuracy of the measurements from the riser tubes and of the flow measurements. The increase in bulk permeability as a result of pipe development is generally not severe – it ranged from $0.8\text{E-}4$ to $1.4\text{E-}4$ m/s here, but it is clearly visible in the example shown (Figure 4.10).

The changes in flow and permeability were similar in all the experiment types.

4.5. ASSESSING THE RELEVANCE OF FORWARD EROSION

4.5.1. OBJECTIVES

The SBW research programme included experiments on sands with different relative densities (Van Beek et al., 2009a). In the small- and medium-scale experiments with loose sands (relative density $<50\%$), it was found that the process was different from that seen in the dense sand samples. The piping process started at the upstream side and appeared to develop towards the downstream side by means of local densification and the displacement of the sand sample (Figure 2.18). The process took place at critical gradients that were relatively low by comparison with those measured in dense samples.

At the time, doubts were raised about the relevance of this phenomenon for real dams and dikes. It was suggested that there may have been a gap between the sand and the cover that made forward erosion possible. To determine whether a gap was indeed present, a water-based colour was injected into the sample at different times during the

tests. The thinking was that, if a gap was present, the paint would pass the surface of the sand bed faster than it would pass through the bed. Figure 4.11 shows photographs of one of the experiments in which colour was injected at two different times during the test (top and bottom). The paint appears to pass through the sand bed and the top of the sand bed at the same speed for both phases of pipe formation, as can be seen in the images on the far right of Figure 4.11. Given this visual observation, it was concluded that there was no gap.

This dissertation investigates the practical relevance of the forward piping mechanism observed in the experiments reported by Van Beek et al. (2009a). Parts of the text in section 4.5 have been taken from Van Beek et al. (2012a).

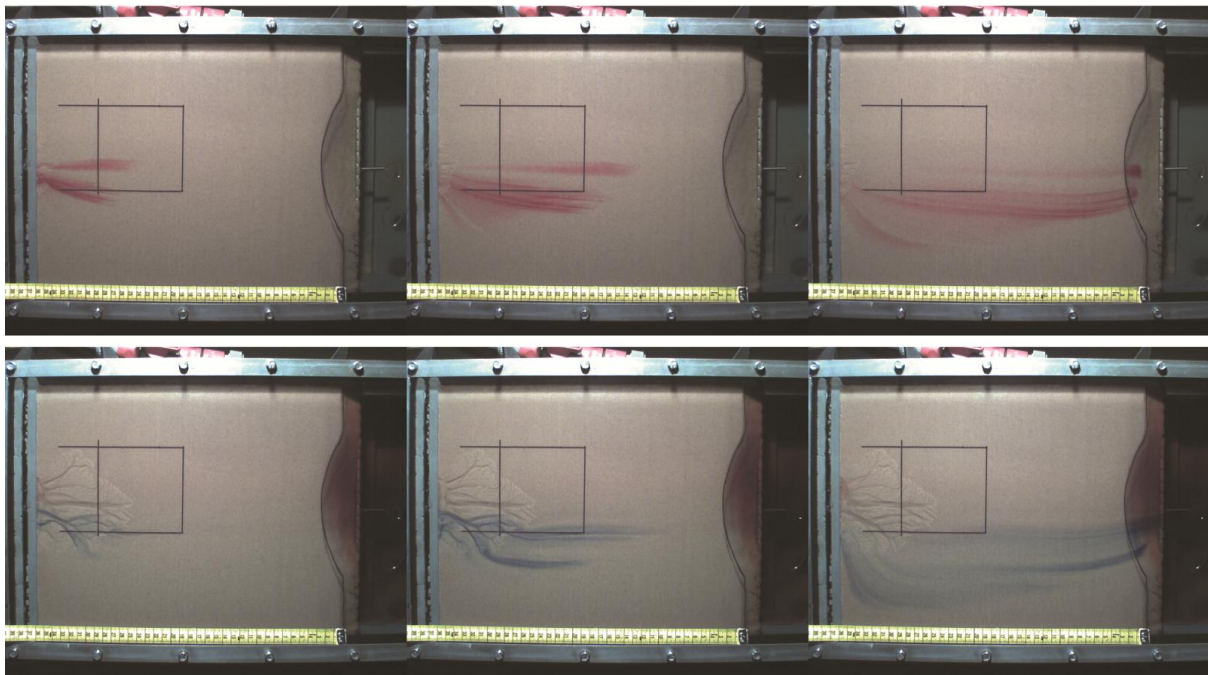


Figure 4.11. Colour injected to indicate preferential paths (photos from experiments presented in Van Beek et al., 2009)

Water flow through very loose granular samples has been described by several researchers. Similar forward-oriented processes were observed by Chevalier et al. (2009) (Figure 4.12), who studied the injection of water into granular suspensions in a Hele-Shaw cell (consisting of parallel flat plates), and by Johnsen et al. (2008), who studied the injection of air into a dry granular sample and silicone gel into a dense suspension. Johnsen et al. (2008) observed, in both cases, an initial hydrodynamically-driven decompaction process that controls the unjamming and prepares the final displacement process, which is characterised by finger-like patterns without grains.

All of the samples studied in both the SBW experiments and the experiments in the Hele-Shaw cell were unloaded. In reality, the sand bed is usually loaded since there will be a cohesive layer with a certain weight on top of the sand bed. Several researchers have described the effect of vertical loading on the backward erosion piping process: Schmertmann (2000) used different bladder pressures to ensure a proper contact between the cover plate and the sand and De Wit (1984) varied the load on the sand by

placing extra weights on the clay cover on top of the sand bed. Neither study found any difference in the piping process or the critical gradient. From a theoretical point of view, it can be argued that piping is governed by the conditions close to the pipe head, or in the pipe where the effective stresses are zero or close to zero. However, the effect of load on forward erosion has not yet been investigated and it may be a factor determining the occurrence of this mechanism. The load may fix grains in place and stop them being moved easily.

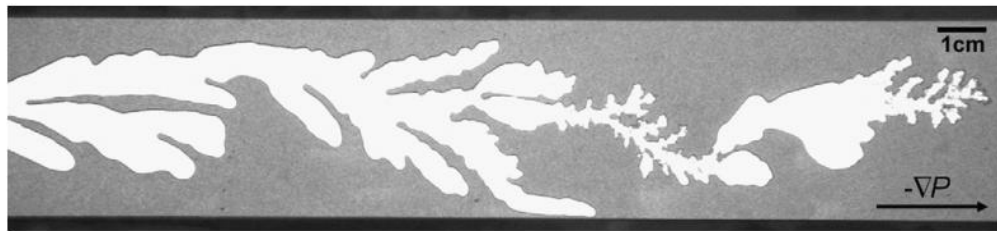


Figure 4.12. Pattern observed in Hele-Shaw cell for a grain fraction of 54% (Chevalier et al., 2009)

The first step in the assessment of the relevance of the process investigated in this dissertation is therefore to determine the effect of load on the process. It should be noted here that the loading process in the model tests differs from what is seen in practice and that it may cause the densification of the top of the sample. By contrast, in the field, there will be gradual loading as a result of the deposition of sediment, leaving the sand bed undisturbed.

The second step in this experimental series was therefore to determine the effect of the contact between the sand bed and cover (which causes the geometrical fixation of grains) on the piping process. Electrical density measurements, pore and total stress sensors were used to monitor the loading and piping processes in order to determine whether the loading process causes the densification of the top layer, to assess the contact between the sand and the cover, and therefore to determine the probability of displacement piping in loaded conditions.

4.5.2. SET-UP AND EXPERIMENTAL PROGRAMME

The experimental programme consisted of three parts. In the first test series, the loose sand samples were loaded to investigate the erosion process under loaded conditions. The next series of tests were performed with electrical resistance measurements. The second series was performed to determine the change of porosity in the top of the sample and in the depth of the sample as a result of loading. After the sample had been loaded, it was unloaded again before a hydraulic gradient was applied. The aim here was to distinguish between the possible effects of the alteration of the density of the sand sample and the loading itself. A third series of tests was conducted to determine whether a pipe that has formed upstream can continue to develop in a loaded sand sample. Table 4.2 gives an overview of the tests.

Table 4.2. Experimental programme

Test series	Test no.	Test objective
1.	B101, B103, B104	Influence of loading on pipe initiation process
2.	B121, B122	Influence of loading on porosity and influence of loading-unloading on pipe initiation
3.	B123	Influence of loading on pipe progression

The set-up with a slope-type exit (Figure 4.2a), the same as in earlier small-scale experiments (described in Van Beek et al., 2011), was used in these three experimental series. The small-scale PVC box was used (Figure 4.2) with an acrylate cover and inner dimensions of 0.5x0.3x0.1 m. The box was filled with sand, which was retained by two filters, resulting in a seepage length of approximately 0.30-0.35 m.

A compressible strip was placed between the cover and the box. The compressible strip allowed for the sand sample to be loaded after preparation by tightening down the cover on the box. Two total stress sensors and two pore pressure sensors in the acrylate cover (both at a distance of 125 and 250 mm from the upstream filter, Figure 4.13) were used to determine the vertical effective stresses in the sand. The total stresses measured were corrected for the pore pressures that had been determined at the same distance from the upstream filter (125 or 250 mm).

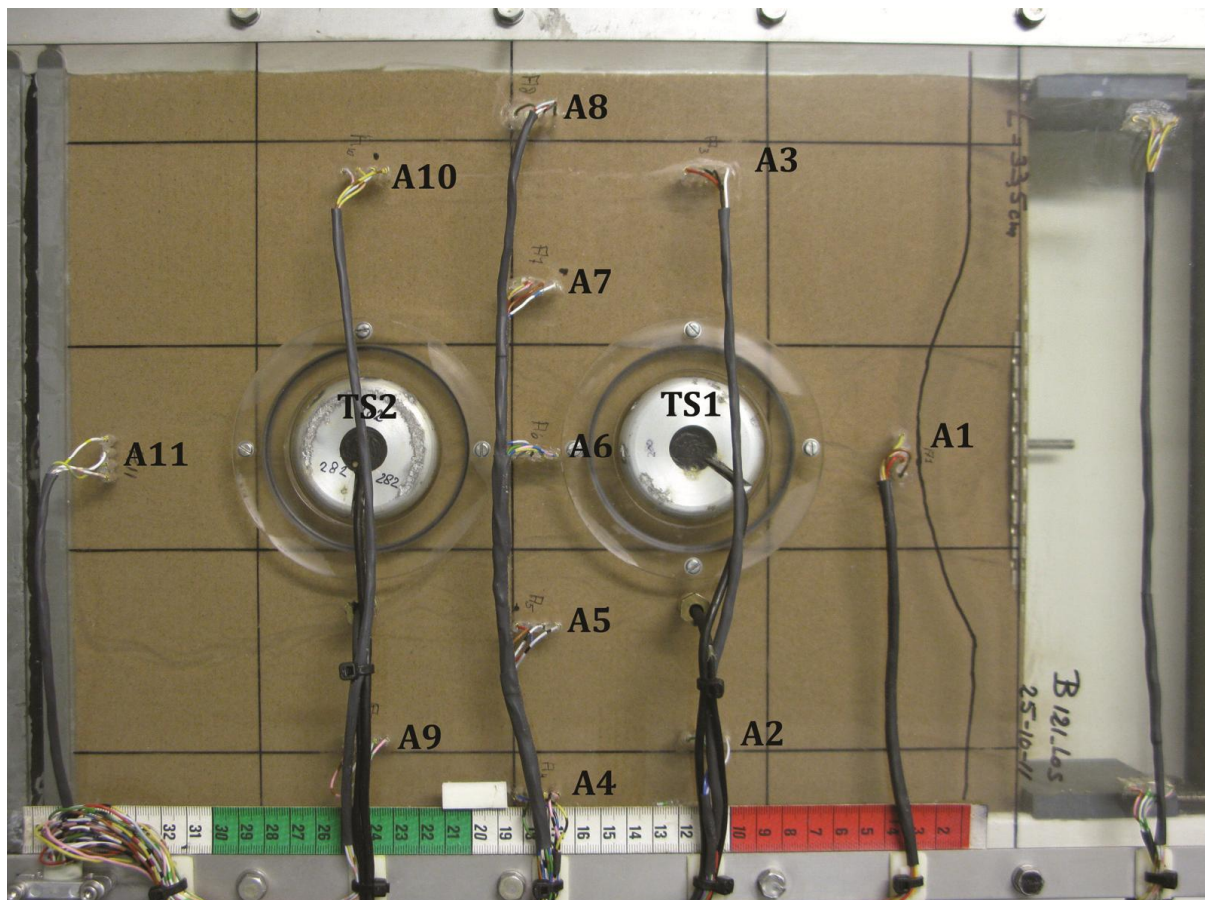


Figure 4.13 Measurement of electrical resistance using eleven rows of 4 needles and measurement of total stress using two stress sensors TS1 and TS2

In the second and third parts of this experimental series, rows of copper needles were glued in at 11 locations in the cover and 8 locations in the side of the box to measure electrical resistance both in the cover (Figure 4.13) and at the side of the box. The needles were inserted in such a way that only the rounded tops of the needles protruded 1mm from the inside of the cover. There were four needles in each location at intervals of 5 mm. An alternating current of 10 Hz was applied to the outer needles of each row and the electrical resistance was measured between the inner needles.

Baskarp sand was used in all the experiments. The relationship between porosity and electrical density for Baskarp sand saturated with de-aired water was calibrated in a column experiment (described in section 4.5.3).

4.5.3. THE ELECTRICAL DENSITY METHOD

To determine the porosity in the top of the sample, electrical resistance was measured using the four-point method. This involves applying an electrical current between two outer electrodes and measuring the resistance between two inner electrodes. Porosity n is related to the specific electrical resistance of the sand by the following equation (Vlasblom, 1977):

$$n = a + b(\rho_w / \rho_g) \quad 4.1$$

in which a and b are constants related to the type of soil that have to be determined empirically, and ρ_w and ρ_g are the specific electrical resistances of the pore water and the soil respectively. The specific electrical resistance of the soil can be obtained by measuring the electrical resistance (R) of the soil, which can be converted to the specific electrical resistance using calibration. For a specific soil type, temperature and water type, parameters a and b can be determined for each row of needles. A column experiment with three measurement locations in the sand sample (Figure 4.14) during which the relative density was gradually increased showed that the relationship between ρ_w/ρ_g and n is indeed approximately linear in the area of interest (Figure 4.15).

Once the relationship between electrical density and porosity had been established for Baskarp sand, the electrodes in the piping box were calibrated by measuring the resistance in the water and in the soil in both a dense sample and a loose sample.



Figure 4.14. Column experiment to investigate the relationship between porosity and electrical resistance. The figure shows the locations of the copper needles.

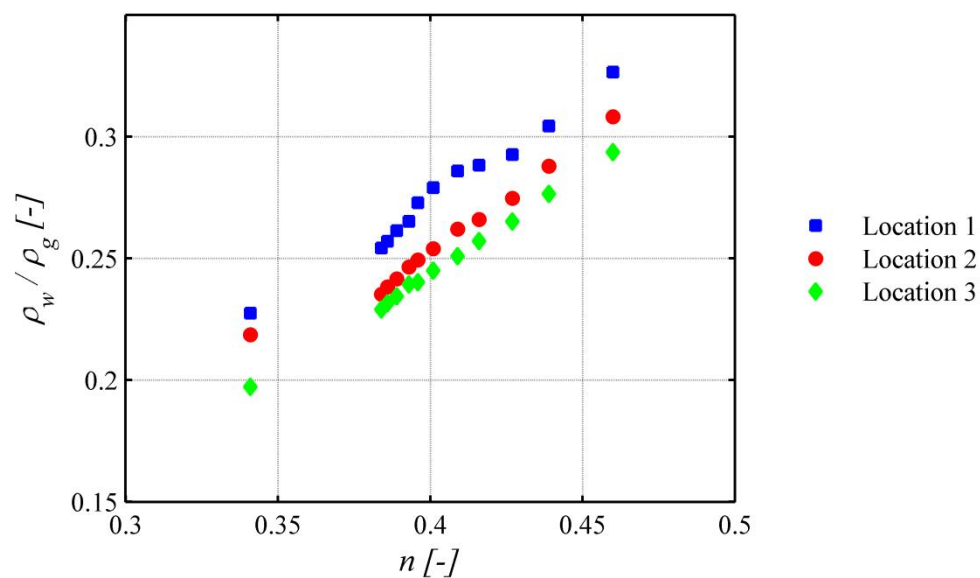


Figure 4.15. Relationship between calculated electrical density and porosity in column experiment for locations 1, 2 and 3

4.5.4. RESULTS

In the first test series, the sand sample was loaded to investigate the effect of vertical load on the initiation of the piping process. After the preparation of the sand sample, the cover was tightened down on the sand box to exert a load on the sand sample. The degree of compression was registered by measuring the distance between the cover and the sand box. It emerged that the strip required compression of a few millimetres before any effective stresses were generated (Figure 4.17).

Tightening down the cover on the box reduces the internal volume of the box and, because several millimetres of compression were needed, the loading appeared to cause the deformation and densification of the sand sample. Since bulk relative density had to remain below 50% (forward erosion has not been observed in samples with relative density higher than 50%), the level of loading was therefore restricted. The effective stresses derived from the stress sensors are given in Table 4.3 for three different tests. It should be noted that there were no effective stresses on the downstream slope because of the open outflow area; the stresses reached the maximum value at the upstream side, where the sand is contained by the filter.

The initial bulk relative density was determined after preparation by measuring the amount of sand in the box. After the loading of the sand, the number of millimetres of compression was used to correct the bulk relative density. The bulk relative density remained below 50% in all tests. In the first test, the initial relative density was relatively high and, after compression, the bulk density approached 50%. In the second and third tests, the initial relative density was lower and the final relative density remained well below 50%. In all tests, backward erosion was observed at a critical head of 8 cm.

Table 4.3. Test characteristics in first part (Experiments B101, B103 and B104)

Parameter	B101	B103	B104
Initial bulk relative density [%] (porosity [-])	31 (0.429)	9 (0.457)	9 (0.457)
Bulk relative density after loading [%](porosity [-])	47 (0.408)	24 (0.438)	24 (0.438)
Effective stress location 1 [kPa]	5.9	1.2	1.0
Effective stress location 2 [kPa]	12.7	3.7	4.2
Critical head [m]	0.08	0.08	0.08

The effective stresses in the area around the pipe were expected to be very low, and absent at the location of the pipe. This was confirmed by the measurement with the stress sensors: the derived effective stresses drop as soon as the pipe develops past the specific stress sensor (Figure 4.16). In Figure 4.16 it can be seen that the pipe first passes the stress sensors located downstream (blue line, transducer TS1) and then the stress sensors located upstream (red line, transducer TS2) a little later.

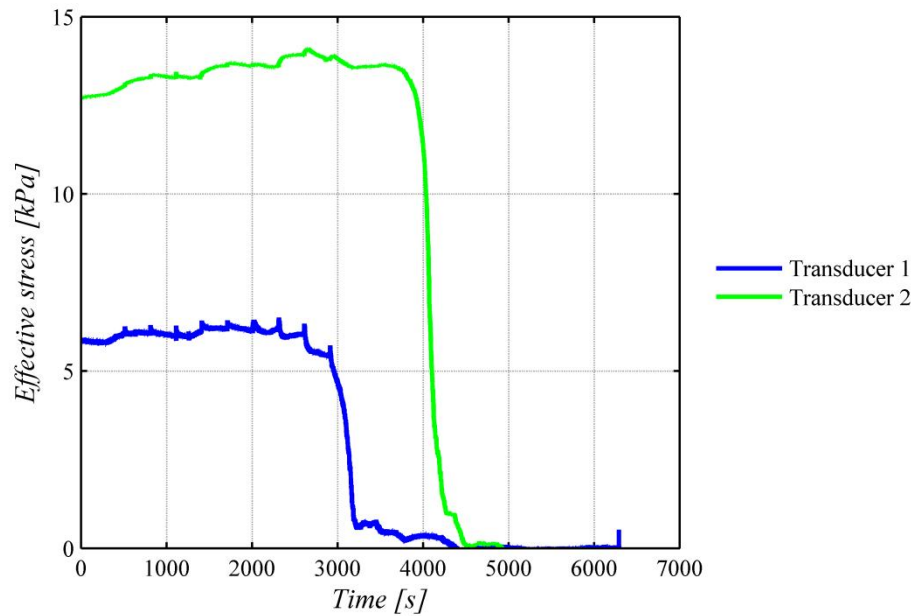


Figure 4.16. Effective stresses derived from stress sensors in test B101. The effective stress drops to 0 kPa when the pipe passes the stress sensors.

In the first test series, the compression of the sand bed did not result in a bulk relative density higher than 50%, but it may also have caused a local change in the relative density of the sand sample. If this change is predominantly confined to the upper centimetres of the sand bed, the upper layer can no longer be classified as loose and so the outcome of the experiment will be affected.

In the second series of tests, the effect of the loading process on relative density was therefore investigated using the electric density method. Two piping tests were performed. In both tests, the electrical resistance measurements in the cover showed that the initial porosity (before loading the sample) was exceptionally high (around 0.70) (Figure 4.18). The porosities obtained with the electrical density measurements at the side of the box were only slightly higher than the bulk porosity as determined on the basis of the weight of the sand in the box (Table 4.4). The small difference was most likely attributable to the minor variation in temperature between the calibration test and the piping tests.

In this same test series, visual observations showed that there was some space between the cover and the sand sample before loading. When the cover was tightened down on the sand box, the porosities in the top of the sample calculated on the basis of the electrical resistance measurements gradually declined to values that were a better match with the initial bulk porosity, whereas the values at the side of the sample remained constant. It was observed that the contact between the cover and the sand bed improved as a result of the applied pressure. At a given point, the values for porosity, as measured in the cover, remained more or less constant. This corresponded to the point where stress was built up in the sand sample (Figure 4.17 and Figure 4.18).

After the sample had been loaded, the load was reduced by gently releasing the cover so that the contact between the sand and the cover was maintained. This was confirmed by measuring electrical resistance, which did not change during the process of unloading.

As no gap apparently formed during unloading, it is reasonable to assume that the sand surface rebounded. Subsequently, the hydraulic head was gradually applied until a pipe formed. Backward erosion occurred in both tests.

Table 4.4. Test characteristics in second part (experiments B121 and B122)

	B121	B122
Initial bulk relative density based on weight [%] (porosity [-])	13 (0.452)	12 (0.454)
Average initial porosity at cover based on electrical resistance [-]	0.741	0.705
Average initial porosity at side of box based on elec. resistance [-]	0.501	0.484
Bulk relative density after loading based on mm compression [%] (porosity [-])	30 (0.430)	33 (0.426)
Average porosity after loading based on electrical resistance, in cover [-]	0.472	0.476
Average porosity after loading, based on elec. resistance, at side of box [-]	0.488	0.482
Effective stress location 1 at start of piping test [kPa]	0	0
Effective stress location 2 at start of piping test[kPa]	1.5	1.5
Critical head [m]	0.09	0.08

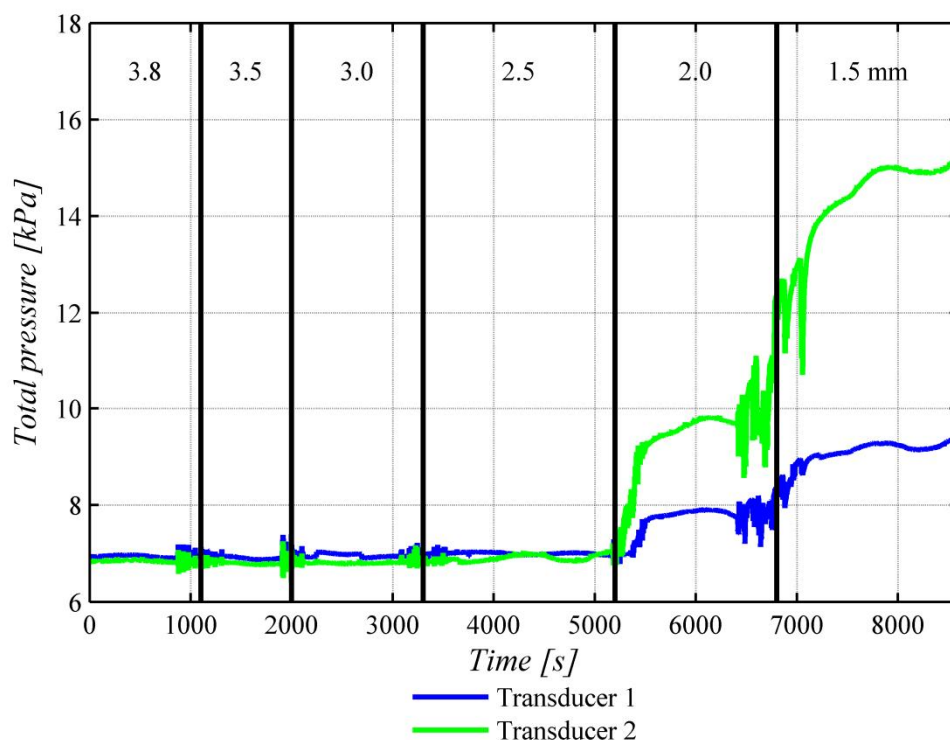


Figure 4.17. Total pressure development in time as a result of the compression of the strip between the cover and the sand box (the degree of compression is indicated as the distance in mm between the cover and the sand box)

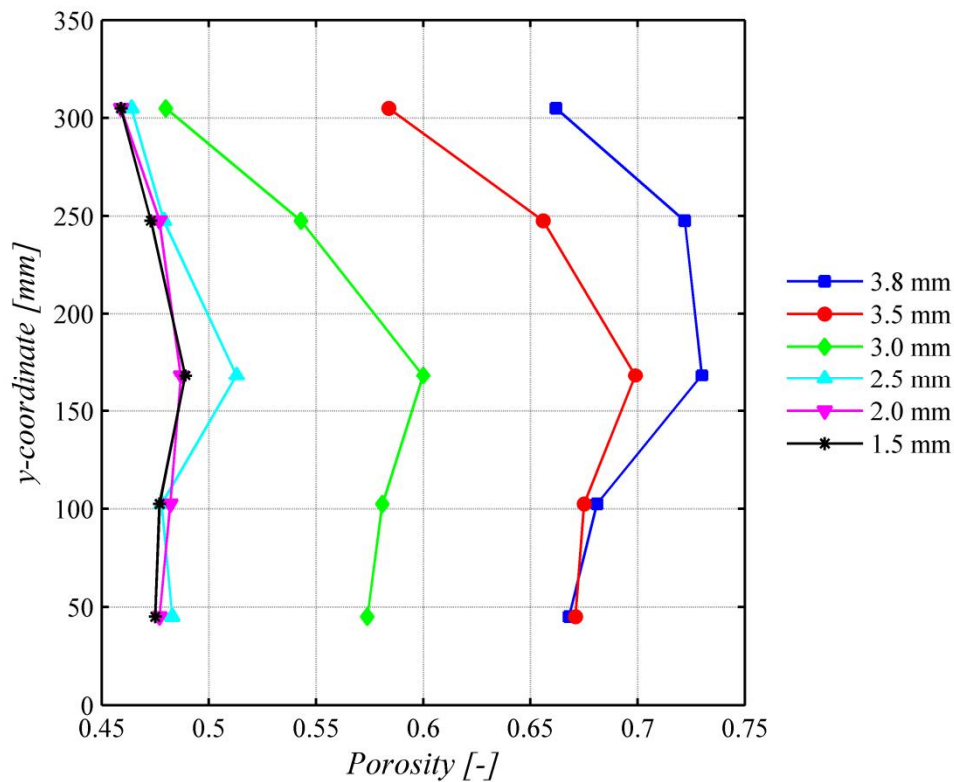


Figure 4.18. Porosity derived from electrical resistance measurements in the cover of the set-up in test B122 (location A4-A8) at different steps of the compression of the strip between cover and sand box (legend indicates the distance in mm between the cover and the sand box)

It was concluded that the contact between the cover and the sand sample was not optimal at the start of the loading phase, resulting in higher porosity values than would be normally expected in a porous medium. Tightening down the cover on the sand box resulted in a better contact between the sand sample and the cover so that effective stresses could be built up in the sand. The static pressure build-up did not cause a large fall in porosity, indicating that the top layer was still well below a relative density of 50%. The fact that backward erosion occurred after the release of some of the load indicates that forward erosion is not only prevented by load but also that it cannot occur when grains are geometrically fixed by the cover.

This conclusion contradicts the findings in Van Beek et al. (2009a), where it was concluded that a gap was unlikely because visual observations indicated that the injected coloured water did not move preferentially along the top plate. An explanation could be that the gap was very small, resulting in a permeability that exceeded the permeability of the sand only slightly, a difference too small to attract much of the coloured water.

However, using Kozeny-Carman's equation (Verruijt, 1982), $k = cd^2n^3 / (1-n)^2$, the contrast in permeability can be calculated for the initial top layer and the porous medium below it. Using a top layer porosity value of 0.70 and a lower layer porosity of 0.48, and assuming that both the electric density method and the Kozeny-Carman equation also perform reasonably well outside the calibrated range, the difference in permeability should be approximately a factor of 10. The coloured water that has

reached the top layer should therefore be transported significantly faster than the water in the porous medium below.

Given this consideration, a second explanation emerges: the layer of coloured water in the top of the bed may have been too thin to be seen properly given that the top layer will not attract much of the coloured water because it is so shallow. In the light of the outcome of the measurements, this seems to be the most likely explanation.

The third part of the experimental series looked at the progression of the pipe under loaded conditions. Although the forward piping process cannot begin when the sand grains are fixed by shear resistance, the process might be able to continue once it has started since the stresses around an existing pipe are very low. An experiment was therefore performed in which the loading phase was not fully completed. The strip between the cover and sand box was compressed until it was seen that the sand was in good contact with the cover. The electrical resistance measurements showed that, at this point, the porosity was still quite high, indicating a limited space between the cover and sand bed (Table 4.5). A hydraulic head was then applied to the sand sample, causing the forward development of a pipe of several centimetres, after which the hydraulic head was brought back to zero. In order to monitor the progression of the pipe in a sand bed subjected to vertical loading, the strip between the cover and the sand box was compressed until effective stresses built up in the sand sample. During this loading process the larger pipes remained intact, whereas smaller pipes disappeared (Figure 4.19).

The subsequent gradual re-application of the hydraulic head did not result in a continuation of the forward piping process but in backward erosion starting on the downstream side of the set-up. The hydraulic head required to create backward erosion (13 cm) exceeded the critical head for the creation of forward erosion in the first stage of the experiment (8 cm).

In the first phase of the experiment, the electrical resistance measurements showed that, although the sand bed appeared to be in good contact with the cover, the contact between cover and sand bed can still be poor. The loading process in the second phase of the experiment fixed the grains firmly, preventing the continuation of the forward piping process.

Table 4.5. Test characteristics for test B123, first phase

	B123a
Initial bulk relative density based on weight [%] (porosity [-])	12 (0.454)
Average initial porosity at cover based on electrical resistance meas. [-]	0.677
Average initial porosity at side of the box based on electrical resistance meas. [-]	0.479
Bulk relative density after compression based on mm compression [%] (porosity [-])	18 (0.446)
Average porosity after compression based on electrical resistance meas. in cover [-]	0.577
Average porosity after compression based on electrical res. meas. side of the box [-]	0.483
Critical head [m] (forward erosion)	0.08

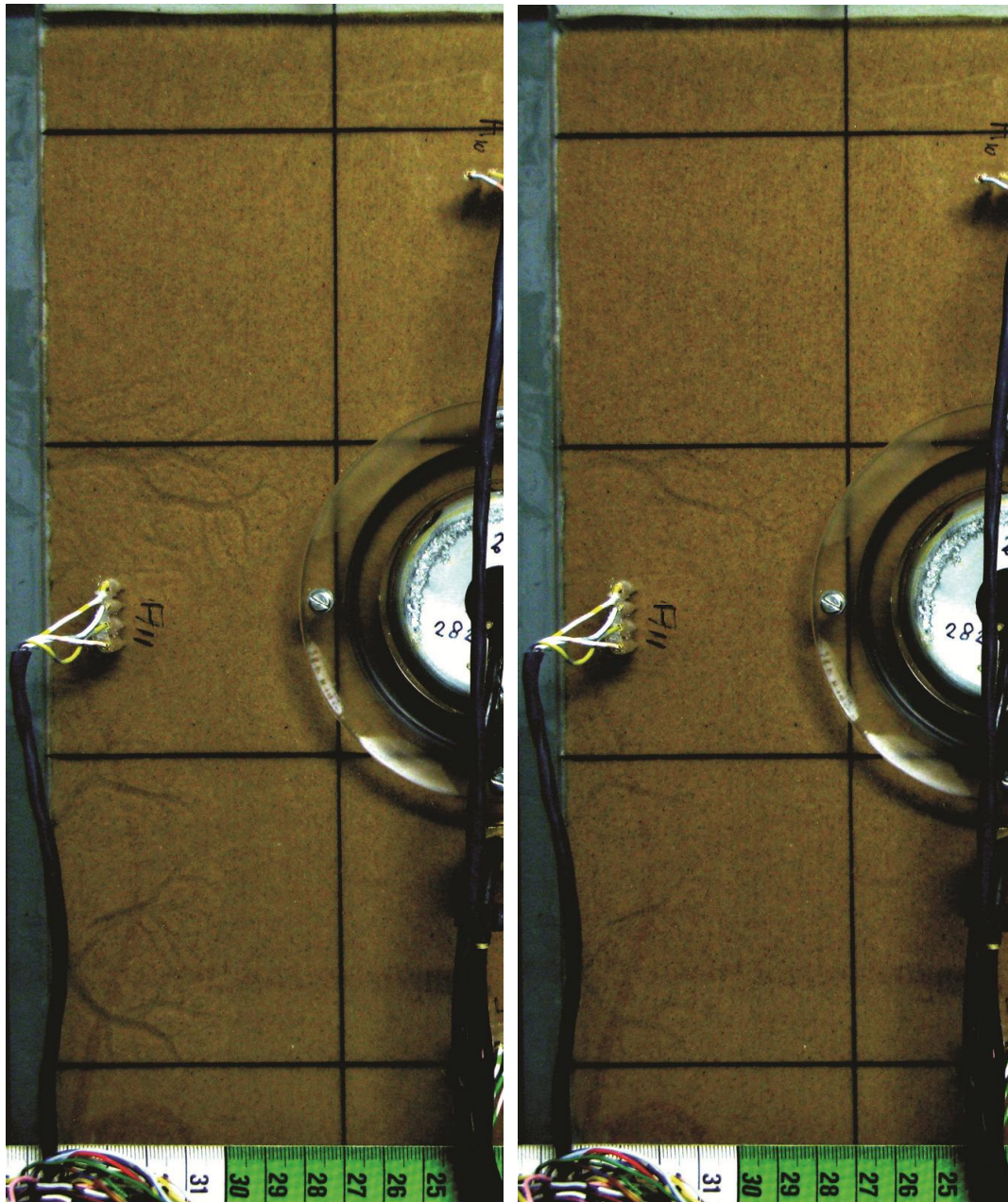


Figure 4.19. Pipes on the upstream side of the set-up, before (left) and after loading (right)

Table 4.6. Test characteristics for test B123, second phase

	B123b
Bulk relative density after loading based on mm compression [%] (porosity [-])	30 (0.430)
Average porosity after loading based on electrical resistance in cover [%]	*
Average porosity after loading based on electrical resistance side of the box [%]	*
Effective stress at location 1 [kPa]	1.0
Effective stress at location 2 [kPa]	5.8
Critical head [m] (continuation)	0.13

* Unreliable data due to change in temperature as a result of water flow in the previous phase

4.5.5. SUMMARY

Experiments were conducted with loose sand samples to assess the relevance of forward erosion in the field. It emerged that loading the sample prevented forward erosion. Additional experiments indicated that the loading process established a proper contact between the sand bed and the cover, fixing the grains in place. Forward erosion in loose sand beds as observed in the piping experiments described in Van Beek et al. (2009a) therefore seem to be related to the absence of shear stresses between the top sand grains and the cover.

Although several steps were taken in the experiments described in Van Beek et al. (2009a) to improve the contact between the sand bed and the cover, it is likely that there was some space between the cover and the sand bed. The measures included applying a silicone gel to the inside of the cover and applying limited pressure to the cover (effective stresses in the sand bed were not measured in these earlier experiments). Furthermore, colour injections and black lines on the inside of the cover were used to improve the visual assessment of the contact between the sand and the cover, but failed to detect the very small gap that was apparently present. It is therefore concluded that phenomena in loose sand beds must be investigated with caution and that it is advisable to measure the effective stresses in the soil to ensure that there is contact between the cover and the sand grains.

Apparently, the forward mechanism is possible, even when there is very limited space (<1 mm) between the cover and the sand bed. In the case of a soft or natural transition between the sand and the cover, as is the case in most dikes, the grains are geometrically fixed by a shear resistance between the cover and the sand grains, and the forward mechanism is unlikely. However, in the case of a rigid transition, which is not uncommon in artificial water-retaining structures, the grains may not be geometrically fixed and forward piping may cause instability problems. It should be stressed here that much smaller gradients than those commonly predicted for backward erosion can lead to the process of forward piping and it is therefore essential to fix the grains below rigid transitions to such an extent that forward erosion is prevented.

4.6. BACKWARD EROSION PROCESS

4.6.1. OBJECTIVES

The experiments in the literature vary remarkably in terms of the sequences of processes of backward erosion. In some of the experiments, equilibrium in pipe formation was seen, requiring an increase in the head for further development. In others, the pipe developed to the upstream side without stopping after the piping process had started.

In the latter case the critical head appears to be determined by the process of pipe initiation: once the pipe has initiated, equilibrium is not possible as the critical head required for progression has been exceeded. If this assumption is true, the exit type influences the process. In the case of a small exit, the flow towards the exit will be concentrated and the pipe will initiate at a relatively low head making it more likely that the head required for the progression of the pipe will not yet have been exceeded at this stage.

To validate the assumption that, depending on the exit size, the critical head is determined by initiation in some experiments and by progression in others, two experiments were performed with different exit types to determine the 'equilibrium heads'. The equilibrium head was defined as the head at which a pipe of certain length is in limit-state equilibrium. Theoretically, every pipe length has an equilibrium head. These experiments determined the equilibrium head for a few different pipe lengths. The comparison of equilibrium heads in set-ups with different exit types describes the relationship between the heads required for initiation and progression.

4.6.2. SET-UP AND EXPERIMENTAL PROGRAMME

Various small-scale experiments were performed: three with a slope-type exit (Figure 4.2a) and two with a hole-type exit (Figure 4.2c). All experiments were conducted with Baskarp sand (relative density >0.74).

The slope-type exit was used in the SBW experiments, where no equilibrium was found in pipe formation. To determine the equilibrium head, the head was gradually increased until a pipe formed. When the pipe was several centimetres long, the water supply was cut off and the head difference was brought back to zero. The head was then gradually reapplied until the pipe continued to progress. This process was repeated several times.

The set-up with the hole-type exit (with a diameter of 6 mm) was used to simulate a situation with concentrated flow lines near the exit. Due to the concentration of flow lines, a pipe should initiate at a head below the required head for pipe progression and equilibrium should occur.

4.6.3. RESULTS

A clear pipe formed in one of the slope-type experiments and it was possible to determine the equilibrium heads. In the other two experiments, the gradual increase of head resulted in 'cracquelé', a gradual process of pattern formation (described in Van Beek et al., 2011). These experiments were not suitable for assessing equilibrium heads. In experiment B105 a pipe formed at a head of 0.16 m (Figure 4.20). When the pipe was 0.11 m long, the water supply was cut off and the head was reduced and gradually reapplied. At a head difference of 0.11 m, the pipe continued to grow until the water supply was cut off again. The equilibrium heads were found to fall with increasing pipe length. In this experiment, the maximum (or critical) head is equal to the initiation head.

The two experiments with the hole-type exit produced similar results in terms of process and critical head. In both experiments, equilibrium was observed after pipe initiation, which was seen at a relatively low head of 0.06 m. An increase in the head was required before the pipe progressed to the upstream side at the critical head for pipe progression, which was 0.08 m. In this experiment, critical head was therefore determined by pipe progression.

Figure 4.20 shows the initiation and equilibrium heads for the slope-type experiment and the hole-type experiment. It should be noted that the equilibrium head for a given pipe length is stated here as the head at which the pipe starts to progress. The exact equilibrium heads cannot be determined in experiments and may be slightly lower than the values reported here because the head is applied in steps. The exact equilibrium head could be up to 5 mm lower than the reported value. The figure clearly illustrates

the difference in the head required for pipe initiation: 0.16 m in the slope-type experiment and 0.06 m in the hole-type experiment. It should also be noted that, in the slope-type experiment, the equilibrium head after pipe formation was much lower than the head required for initiation. By contrast, in the hole-type experiment, a head increase was required after pipe initiation.

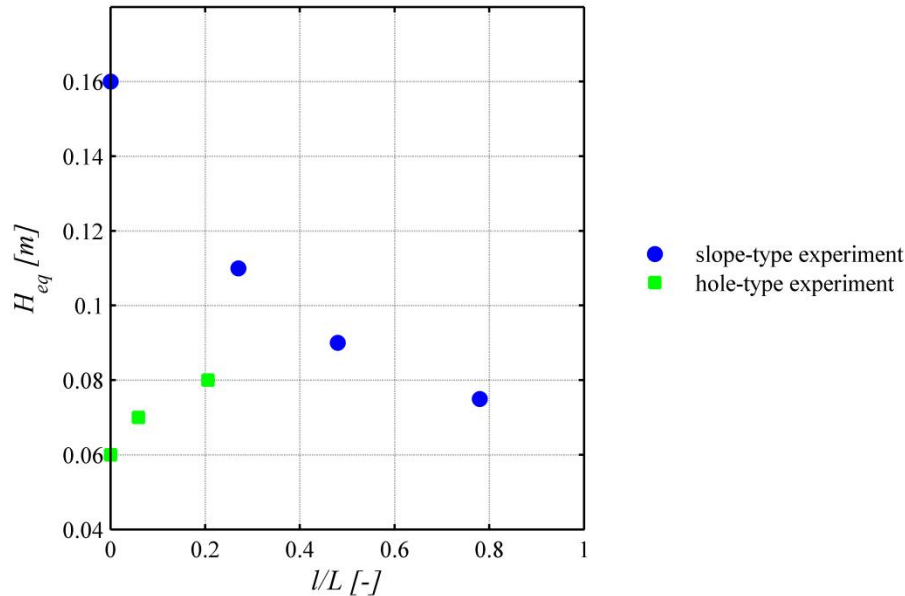


Figure 4.20. Equilibrium head as a function of normalised pipe length (pipe length divided by seepage length) for experiment B105 (slope-type experiment) and B118 (hole-type experiment)

The experiments demonstrate that the occurrence of equilibrium in experiments is related to the exit type and the corresponding head for pipe initiation. In experiments in which no equilibrium is observed, the critical head is dominated by pipe initiation; in experiments in which equilibrium is observed, the critical head is dominated by pipe progression. The observed critical head in the progression-dominated experiment was considerably lower than the observed critical head in the initiation-dominated experiment. This conclusion implies that only experiments in which equilibrium is observed are suitable for the validation and calibration of progression models such as the Sellmeijer model.

In the field, the presence of a small pipe can lead to significantly lower gradients than those observed in the laboratory experiments in which initiation dominated the critical head. The prediction of piping with models for pipe progression is therefore more reliable than with models for pipe initiation. Although experiments in which initiation dominated do not give the critical head for pipe progression, they do give an upper limit since the critical head for progression cannot exceed the critical head for initiation in experiments in which no equilibrium is observed.

4.7. INITIATION: EFFECT OF SOIL TYPE

4.7.1. OBJECTIVES

The availability of experiments in which no equilibrium was observed allows for the development of a model for pipe initiation. The experiments by De Wit (1984) with an area-type exit are suitable for this purpose since the exit conditions are clearly defined. Although different sand types were tested in this experimental programme, two variables were changed at a time: the uniformity coefficient increased with grain size for the sand types used. It was not therefore possible, in the analysis for pipe initiation, to distinguish between the effect of grain size and that of uniformity coefficient, and so additional experiments were conducted as part of the work for this dissertation on a uniform sand with relatively large grains.

4.7.2. SET-UP AND EXPERIMENTAL PROGRAMME

Three experiments were performed in the small-scale set-up with an area-type exit (Figure 4.2b). Two experiments were performed using Enschede sand and one using filter sand ($d_{50}=0.840$ mm, $d_{60}/d_{10}=1.2$). All the samples were prepared with a high relative density (~ 90 -100%).

4.7.3. RESULTS

The two experiments on Enschede sand were found to be similar in terms of process and critical head (0.28 m and 0.26 m for experiments E137 and E138 respectively). In both experiments, a pipe formed that developed to the upstream side immediately, indicating that the critical head was dominated by the process of initiation, as in the area-type experiments by De Wit (1984).

In the initiation experiment, the relatively wide pipe developed rapidly in the upstream direction (Figure 4.21).

The experiment on filter sand was unsuccessful. The permeability of the sand was relatively high by comparison with the permittivity of the upstream filter. The application of head therefore resulted in a large head loss at the filter and a limited head loss in the sand. It was therefore not possible to increase the head enough to initiate a pipe in this sand type.

The set-up was a lot smaller than those applied by De Wit (1984) and so the results are not directly comparable. The initiation heads obtained have been included in the analysis in Chapter 5.

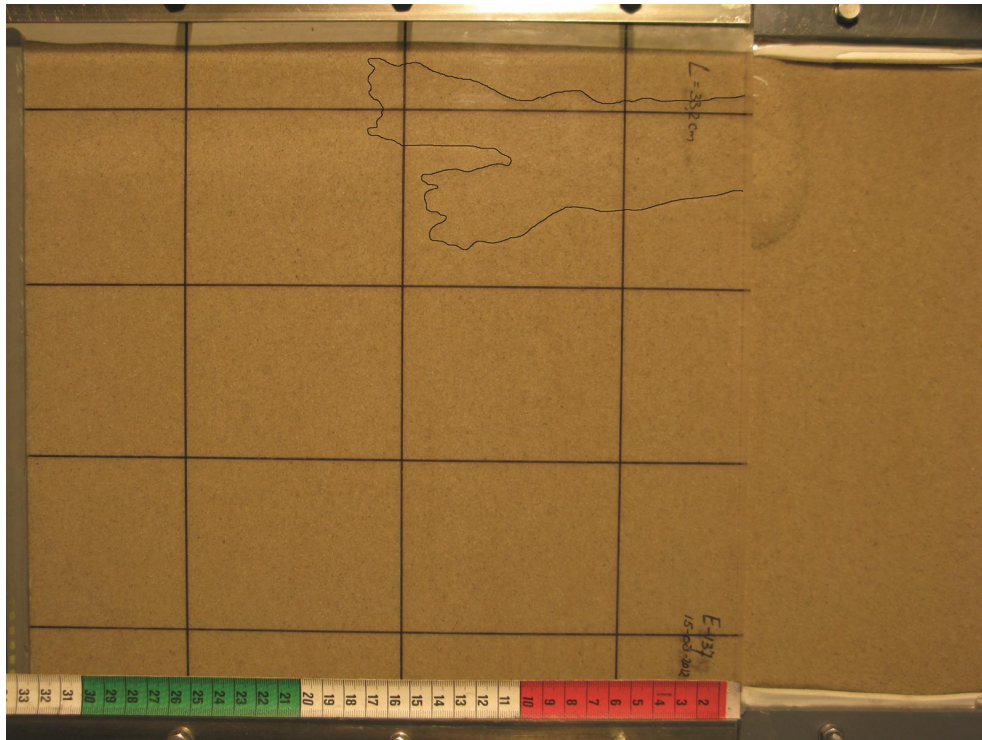


Figure 4.21. Pipe formation in experiment E137 (pipe contour drawn manually)

4.8. PROGRESSION: SMALL-SCALE EXPERIMENTS

4.8.1. OBJECTIVES

The finding that the critical heads in many of the available experiments were dominated by pipe initiation, and therefore not suitable for the validation of models in which the presence of a pipe is assumed, led to a considerable reduction in the number of experiments appropriate for the validation of these kinds of models. The appropriate experiments – those in which the process of pipe progression dominated the critical head – are mainly large-scale experiments (Delta Flume experiments and IJkdijk experiments) or experiments with relatively small exits (the hole-type experiments by Hanses (1985)). Equilibrium was also observed in some of the experiments by Townsend et al. (1988) and Pietrus (1981), but the use of an artificially created pipe makes these experiments less suitable for model validation. Only a few experiments are available that investigate the effect of sand type or relative density.

Additional small-scale experiments were therefore performed to study how sand type affects the critical gradient for pipe progression. The influence of hole diameter was also investigated.

4.8.2. SET-UP AND EXPERIMENTAL PROGRAMME

The experiments to determine the critical head for pipe progression were performed in the small-scale set-up with a hole-type exit (Figure 4.2c). It was known that the high flow velocity near the hole-type exit would ensure pipe initiation at a relatively low head drop, and this allowed for the investigation of the process of pipe progression. In

this set-up, the roles of relative density, sand type and exit-hole diameter on critical head were studied.

The sand types studied were Baskarp sand, Waalre sand, Oostelijke Rivierenzand, Enschede sand, Sterksel and Itterbeck 125-250. To investigate the role played by fines, Itterbeck 125-250 sand was mixed with finer fractions to obtain Mixture 1 and 2. The properties of all tested sand types can be found in Figure 4.5 and Table 4.1.

Baskarp sand was prepared at different densities: approximately 65% and 90%. The exit-hole diameter was also varied for this sand type. Experiments were performed with an exit-hole diameter of both 6 mm and 12 mm.

After the conclusion of one of the experiments (I167), the water level in the sand layer was lowered and the cover was removed. The pipe geometry was then measured using a laser.

4.8.3. RESULTS

The observations in the small-scale experiments were similar to the observations by Müller-Kirchenbauer (1978) and Miesel (1978) for a small exit diameter (described in Chapter 2). An important difference in the set-up was the vertical length of the hole-type exit, which was considerably smaller in these experiments than in the experiments in literature. Fluidisation of the sand bed occurred at a head drop of approximately 0.02-0.03 m in the small-scale experiments. The circular hole was gradually filled with sand, and sand was transported and deposited around the hole once the entire vertical section was full of sand at a head difference of approximately 0.03-0.06 m. In the small-scale experiments with a 12 mm exit-hole diameter, only part of the sand surface boiled.

Initially, pipes formed in all directions but, after a single head increase, one or two pipes developed in the upstream direction. The head had to be increased several times for the pipe to continue developing, indicating that the final critical head was dominated by the process of pipe progression.

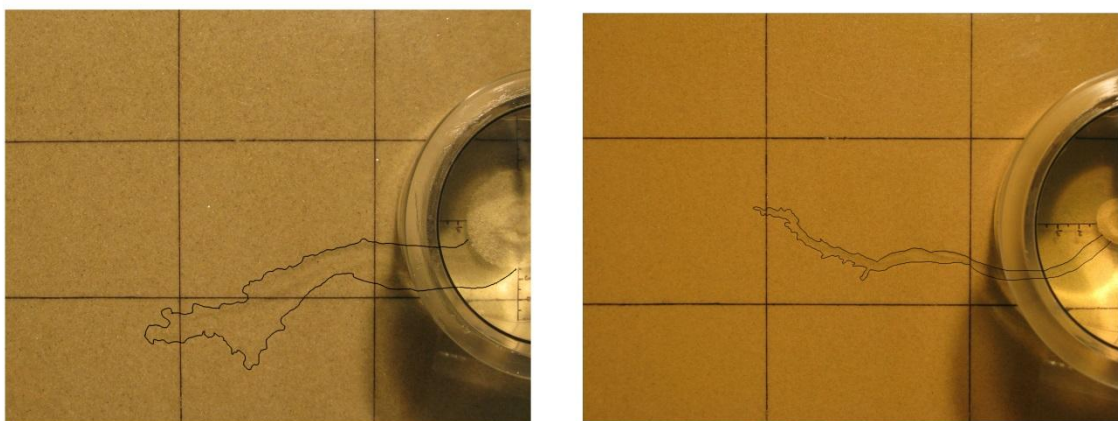


Figure 4.22. Pipe and crater development in small-scale experiments W131 with Waalre sand (left; $d_{50}=0.341$ mm) and experiment B142 with Baskarp sand (right; $d_{50}=0.132$ mm). The pipe length was approximately half the seepage length in both experiments.

The pipe proved to be wider in coarse sands than in fine sands. Pipe width is discussed in more detail in Chapter 6. As the pipe lengthened, secondary erosion caused the pipe to widen downstream of the tip. The resulting crater was found to be larger in coarser sand types than in finer sand types and this concurs with the conclusion about pipe width (Figure 4.22).

The small-scale experiments on Baskarp sand were performed with two exit-hole sizes, 6 and 12 mm, and two relative densities (65% and 90%). Figure 4.23 shows the critical gradients obtained in these experiments for two different relative densities. It was found that the critical gradient increased with an increase in relative density and also slightly with the exit-hole diameter, which confirms Miesel's findings (1978). It should be noted here that permeability was slightly lower in all experiments with a hole diameter of 12 mm than in the experiments with a hole diameter of 6 mm, and that this could also have contributed to the trend. If one takes these differences into account, the effect of the size of the exit hole on the progression gradient is even smaller. All in all, exit-hole diameter does not seem to have affected the results to a large extent.

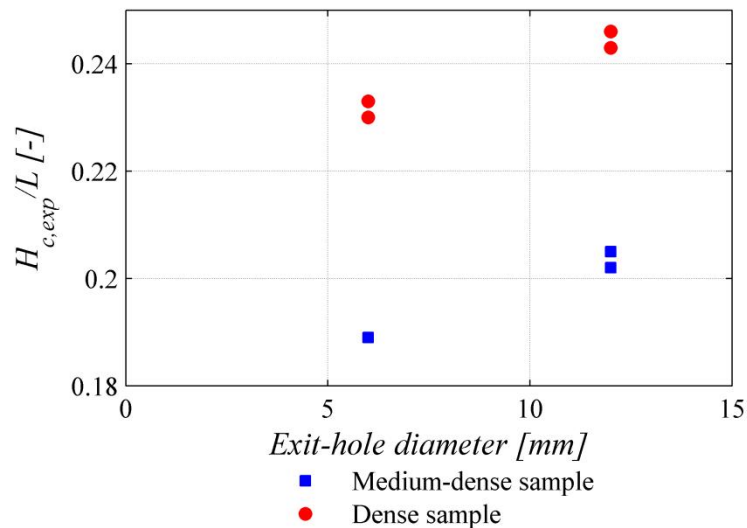


Figure 4.23. Influence of exit-hole diameter and relative density on critical gradient

Figure 4.24 (left) shows the effect of grain size in uniform sands ($\max d_{60}/d_{10} = 2.25$) for different relative densities. This figure shows that grain size has a limited effect on critical gradient. The critical gradients in two experiments were remarkably high. These were the experiments with the dense samples of Sterksel sand ($d_{50}=0.228$ mm) and Oostelijke rivierenzand ($d_{50}=0.233$ mm). In both experiments, a short pipe developed that stayed the same length for some time. There was then a sudden and rapid pipe formation after several head increases. The experiment on Sterksel sand may also have been affected by the migration of fines through the sand bed, since the exit cylinder appeared to be turbid and the results of the riser tubes indicated a fall in permeability towards the downstream exit.

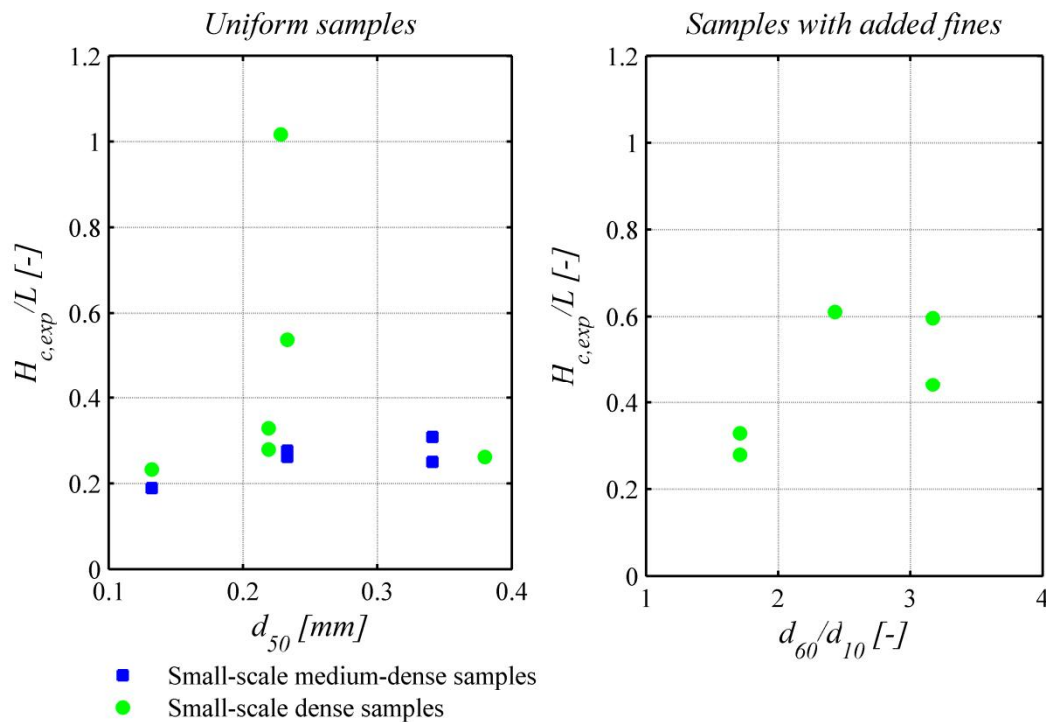


Figure 4.24. Influence of grain size in uniform sand types (left) and uniformity coefficient (right) on critical gradients for medium-dense and dense samples

In the other experiments on uniform sands, the critical gradient was not closely correlated to grain size. It can be concluded that the influence of grain size is limited, or compensated by other properties such as permeability. The influence of relative density was most clearly observed in Baskarp sand.

The effect of the uniformity coefficient was investigated by adding different amounts of fines to a sieved fraction of Itterbeck sand. Figure 4.24 shows the effect of the uniformity coefficient on critical gradient in these experiments: the addition of fines resulted in significantly stronger samples. It should be noted that permeability is also affected by the addition of fines. It should also be pointed out here that the addition of fines may have adversely affected the experiments. It is possible that experiments with sand samples involving larger fractions of fines require longer time intervals than those used in the series of experiments covered by this dissertation since, as pointed out by Moffat et al. (2011), the migration of fines can be time-consuming. The removal of fines from the sample is known to lead to a fall in the critical gradient (Richards and Reddy, 2012). It has been found that the samples containing fines were more permeable (by a factor of approximately 1.5) in the upstream area than in the downstream area. The lower permeability may be caused by particle bridging, a process that can occur in converging flows with high flow velocities (De Zwart, 2007). In this process fine particles moving through the pores of the sand collide as a result of the converging flow near the exit and form a bridge, resulting in a local decrease of permeability that the modelling does not account for.

The range of uniformity coefficients tested in this series was relatively small. Experiments using sand types with a higher uniformity coefficient are recommended,

although it should be realised that other processes, such as filtering of fines, may affect the critical gradient for these types of sands.

The pipe dimensions were analysed in one of the small-scale experiments (I167). After the pipe had reached the upstream level, the tap was closed and the cover was removed to expose the top of the sand bed. The pipe dimensions were recorded using laser equipment (the position of the sand surface was measured in a grid of 456×225 data points). Figure 4.25 shows the resulting pipe geometry.

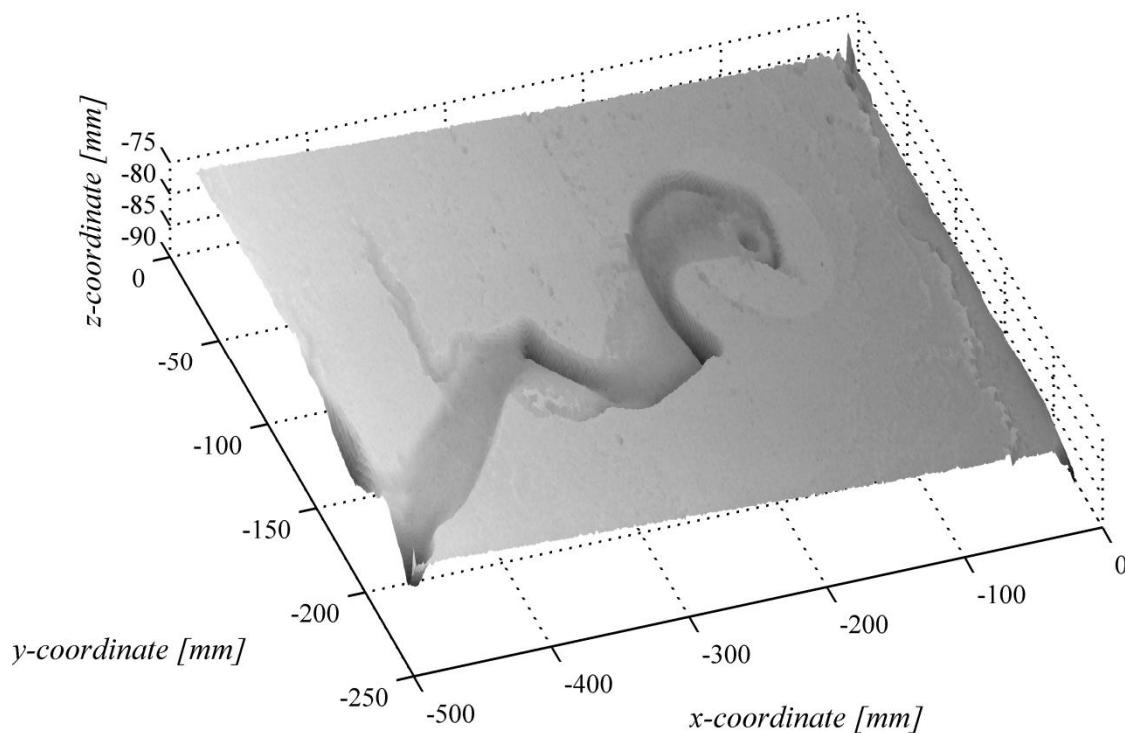


Figure 4.25. Pipe geometry in experiment I167.

Although the measurement was taken at the end of the test, an analysis of the pipe dimensions gave an indication of the depth of the pipe and its slope angles. Figure 4.26 shows the cross-section of the pipe at various distances from the upstream filter. This figure shows that the pipe depth varied over the width of the pipe, with larger depths in the eroding side of the bends of the pipe. The maximum depth observed in these cross-sections was 3.5 mm, which is 24 times the mean grain diameter. In most cross-sections the pipe was shallower: approximately 1-2 mm (7-14 times the grain diameter). No distinct depth increase was observed towards the pipe tail (near the exit hole).

The slopes of the side walls of the pipe were evaluated. In most cases, they were well below the slope corresponding to the expected friction angle. Only at one location, where the flow seems to create erosion in the corner (at $x=180$ mm in Figure 12), was the slope of the eroding side wall 40 degrees.

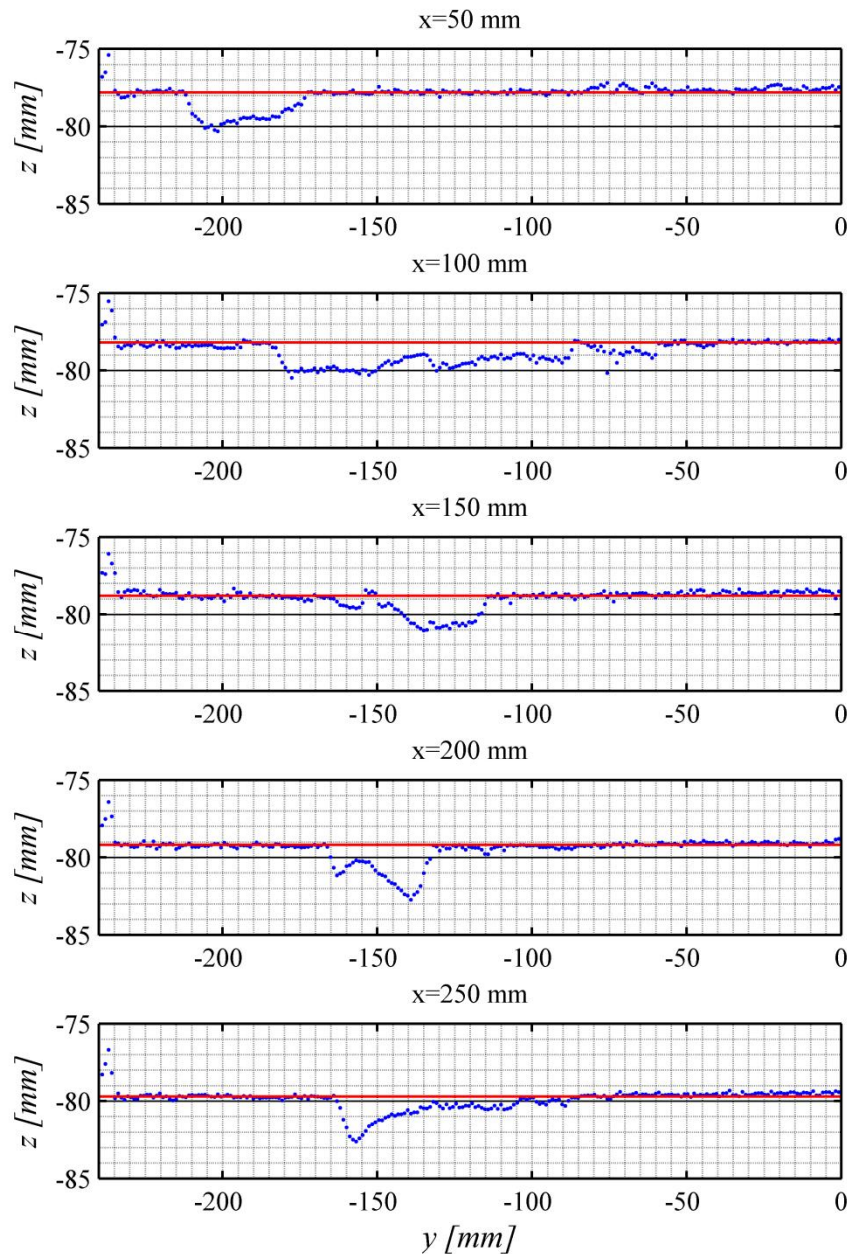


Figure 4.26. Cross-sections of the pipe at various distances from the upstream filter showing pipe width and depth

4.8.4. SUMMARY

Equilibrium was observed in all experiments. Pipe widths were found to be larger in coarser sands. Given the trends in critical gradients obtained from the experiments, it can be concluded that a higher relative density definitely results in higher critical gradients. The influence of relative density on critical gradient could be explained by the corresponding change of permeability and friction angle, or by the dilatancy of the sand. The exit size appeared to have a minor influence on critical gradient, as did the grain size of uniform sands. Permeability could account for the apparently minor role played by grain size in uniform sands since permeability increases with grain size: the load on larger grains will be higher due to the higher flow velocity. The addition of fines would

seem to result in higher critical gradients, although the experiments were not designed to take into account the migration of fines, which requires longer time intervals.

It is difficult to be conclusive about the effects of grain size, uniformity coefficient and relative density since these parameters cannot be varied independently. Using a model to compare measured critical gradients and predicted critical gradients could make matters clearer in this respect. This area will be discussed in Chapter 6.

4.9. PROGRESSION: MEDIUM-SCALE EXPERIMENTS

4.9.1. OBJECTIVES

Although progression-dominated experiments were available at different scales (experiments by Hanses (1985), Delta Flume and IJkdijk experiments), they cannot be directly linked to the small-scale experiments because more than one variable was changed. Medium-scale experiments were therefore conducted to assess the effect of scale on critical gradient in different sand types. However, looking at the critical gradient alone in experiments does not necessarily explain the causes of any differences found between models and experiments or why adjustments were found to be necessary in the Sellmeijer model (Sellmeijer et al., 2011). A possible explanation could be found in the pipe dimensions and hydraulics. The second objective in this series of experiments was therefore to investigate the head loss in the pipe and the dimensions of the pipe at longer pipe length.

4.9.2. SET-UP AND EXPERIMENTAL PROGRAMME

The experiments were performed in the medium-scale set-up with a hole-type exit (Figure 4.2c). The medium-scale set-up can contain a sand sample that is approximately four times larger than in the small-scale experiments. The exit diameter was scaled so that the flow conditions were similar to those in the small-scale experiments. On the basis of the available experiments and the expected scale effects (see Section 3.3.5), pipe progression was expected to occur at a higher head than pipe initiation in this configuration.

To measure the head in the pipe, pore pressure transducers were installed at several locations in the acrylic cover. Riser tubes were installed to allow for the measurement of the head distribution in the bottom of the sand sample.

Three experiments were performed on two sand types: Baskarp sand and Itterbeck 330 μm sand. As the reproducibility of Baskarp experiments was found to be good in the small-scale experiments, it was decided that a single experiment with Baskarp sand would suffice. The reproducibility of other sands is less certain and so two experiments were performed on Itterbeck 330 μm sand. It should be noted that the Itterbeck 330 μm sand used in the medium-scale experiments was comparable with the Enschede and Hoherstall Waalre sands used in the small-scale experiments. A different sand type was selected since the last two sand types were not available in large quantities. The properties of all the sand types tested are listed in Figure 4.5 and Table 4.1.

All the samples were prepared at a relative density of approximately 90%. In one of the medium-scale experiments (Ims18) the standard preparation method did not result in an entirely homogeneous sample: layering due to segregation during sample preparation was observed and this significantly affected pipe formation. In the second experiment on this type of sand (Ims20), more continuous tamping and sand sprinkling prevented the layering.

As in the other experiments, the hydraulic head was applied stepwise. However, due to time constraints associated with the gradual clogging of the upstream filter, the step size was increased in one of the experiments (Ims18). The critical gradient that was finally obtained was therefore determined less accurately.

4.9.3. RESULTS

The observations in the medium-scale experiments were similar to those obtained in the small-scale hole-type experiments. In all experiments, the erosion process started at a small head drop (<0.05 m). Fluidisation resulting from the concentrated flow near the exit caused the sand bed to expand and the first sand grains to be moved. Initially, pipe formation was in all directions. In all the experiments, pipes formed parallel to the flow direction. When the head drop was increased, the pipe lengthened but did not turn initially in the upstream direction. A further increase in head led to the formation of a new pipe pointing in the upstream direction. In time, erosion stopped and another increase of head was required to lengthen the pipe.

Differences in pipe width are not immediately apparent from the images but the pipe volume, which can be measured on the basis of the crater size, is significantly larger for Itterbeck sand (Figure 4.27). The degree of widening towards the downstream exit increases with increasing pipe length. The pipe also starts to meander and relocate when the pipes are longer.

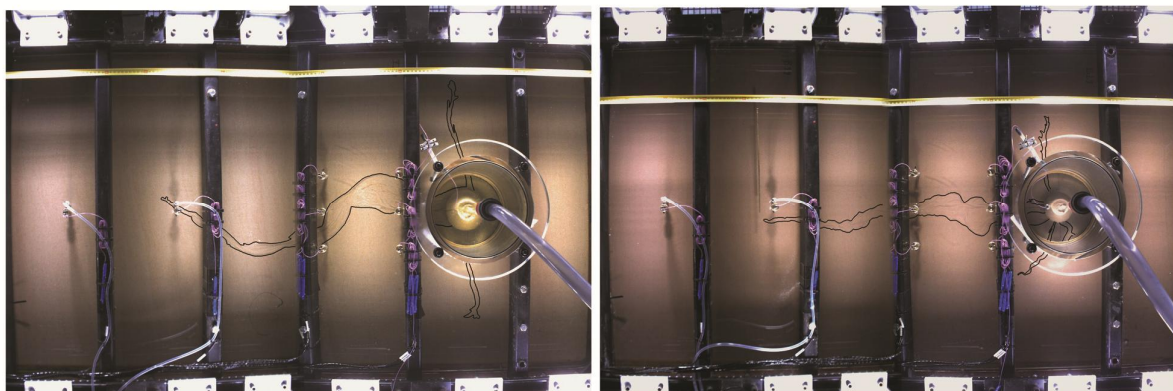


Figure 4.27. Pipe and crater formation in experiment Ims20 with Itterbeck 330 μm sand (left) and experiment Bms19 with Baskarp sand (right)

In the first of the two experiments with Itterbeck sand (Ims18), the stratification of the sand bed affected pipe formation. After lengthening, the pipe repeatedly developed in the direction perpendicular to the flow in a fine layer when reaching a relatively coarse layer. Figure 4.28 shows this stratification and the preferential path of the pipe. This

phenomenon was not observed in the second experiment on Itterbeck sand (Ims20), in which stratification was less pronounced.

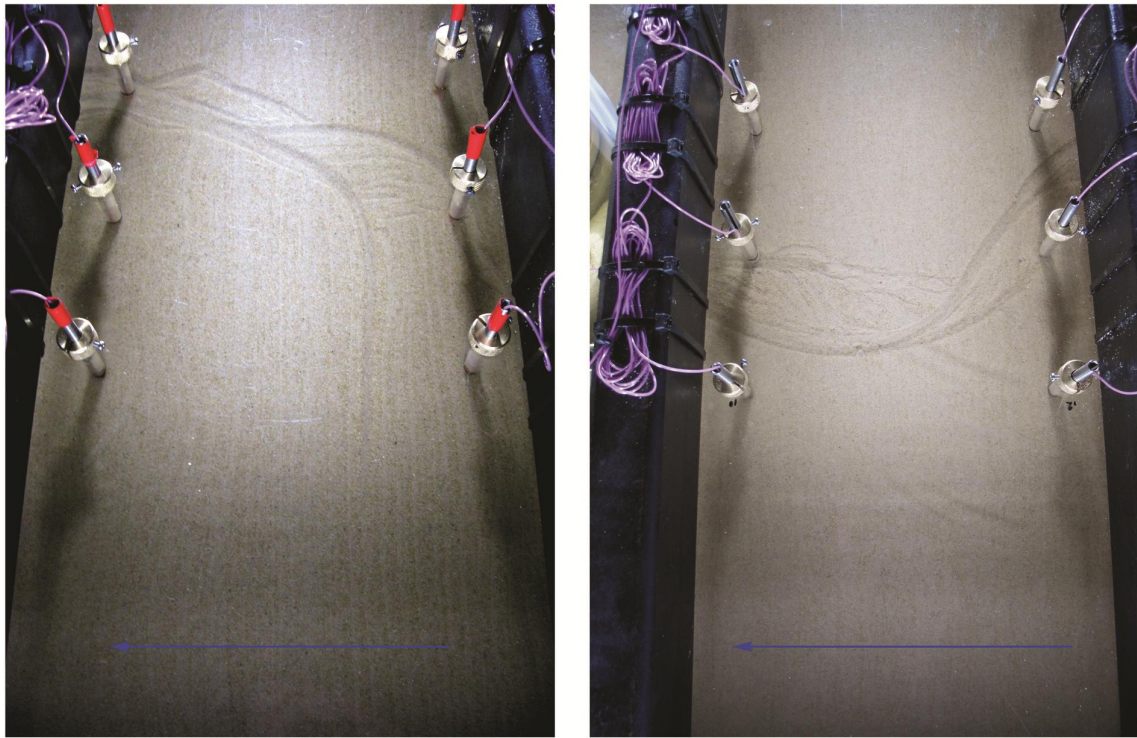


Figure 4.28. Photographs showing the pipe patterns in a section of the medium-scale set-up: the pipe develops parallel to the direction of the stratification in experiment Ims18 (left); there is no preferential pipe path in experiment Ims20 (right). The flow is in the direction of the arrows.

The difference in pipe formation led to a large difference in the critical head: the first experiment found a critical head of between 0.33 and 0.36 m ($H_c/L=0.238$ to 0.260) and the second experiment with Itterbeck 330 μm sand found a critical head of 0.194 m ($H_c/L=0.140$). The critical head in the Baskarp experiment was 0.21 m ($H_c/L=0.152$). This confirms the conclusion from the small-scale experiments that grain size has a small effect on the critical gradient in uniform sands. The critical gradients were significantly smaller than the critical gradients in the small-scale experiments, indicating the existence of a scale effect.

The pore pressure transducers in the acrylate cover made it possible to measure the pore pressure in the pipe. The pore pressures were analysed for experiments Bms19 and Ims20. A relatively straight pipe developed in these experiments underneath or very near to the pore pressure transducers along the centre line of the set-up. Figure 4.29 shows the location of the pipe in relation to the pressure transducers. In this figure, it can be seen that the pipe depth varied, with shallower zones and deeper preferential flow zones. The head may therefore have varied over the width of the pipe. This effect is not taken into account here.

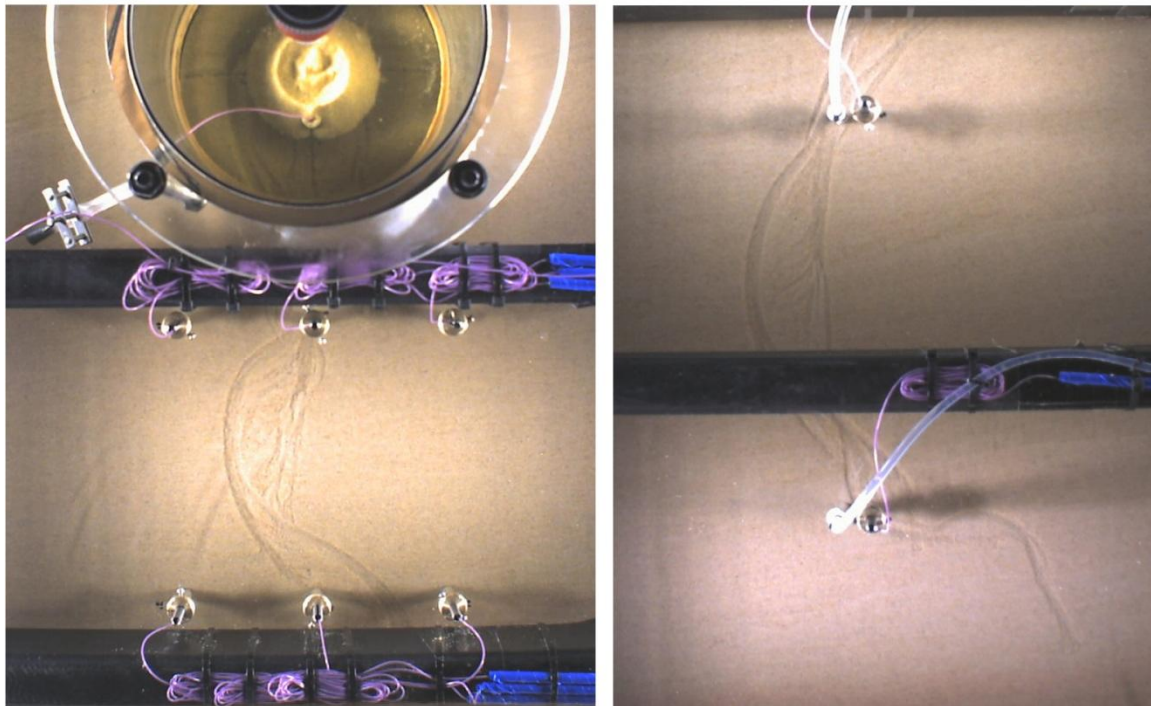


Figure 4.29. Pipe formation in relation to pore pressure transducers in experiment Ims20 at pipe lengths of 0.647 m (left, downstream transducers) and 1.197 m (right, upstream transducers).

Figure 4.30 shows the normalised hydraulic head as a function of the distance from the downstream hole, for various pipe lengths in equilibrium in experiments Bms19 (Baskarp sand) and Ims20 (Itterbeck 330 μm). The hydraulic head was divided by the overall applied head to compare the impact of the pipe on the groundwater flow at different pipe lengths. The pipe gradient proved to be higher in the experiment with Baskarp sand than in the experiment with Itterbeck sand. A comparison of average calculated gradients based on the linear interpolation of the pore pressures of those transducers which are located in, or very near to, the pipe, shows that the pipe gradient was indeed lower in the experiment with Itterbeck sand than in the experiment with Baskarp sand (Figure 4.31), whereas the overall gradients were comparable for both experiments. The pipe gradient did not increase significantly with increasing pipe length.

The exit losses (head loss in the sand boil, vertical section and at a distance of 30 mm around the hole) were considerably larger in the experiment with Itterbeck sand.

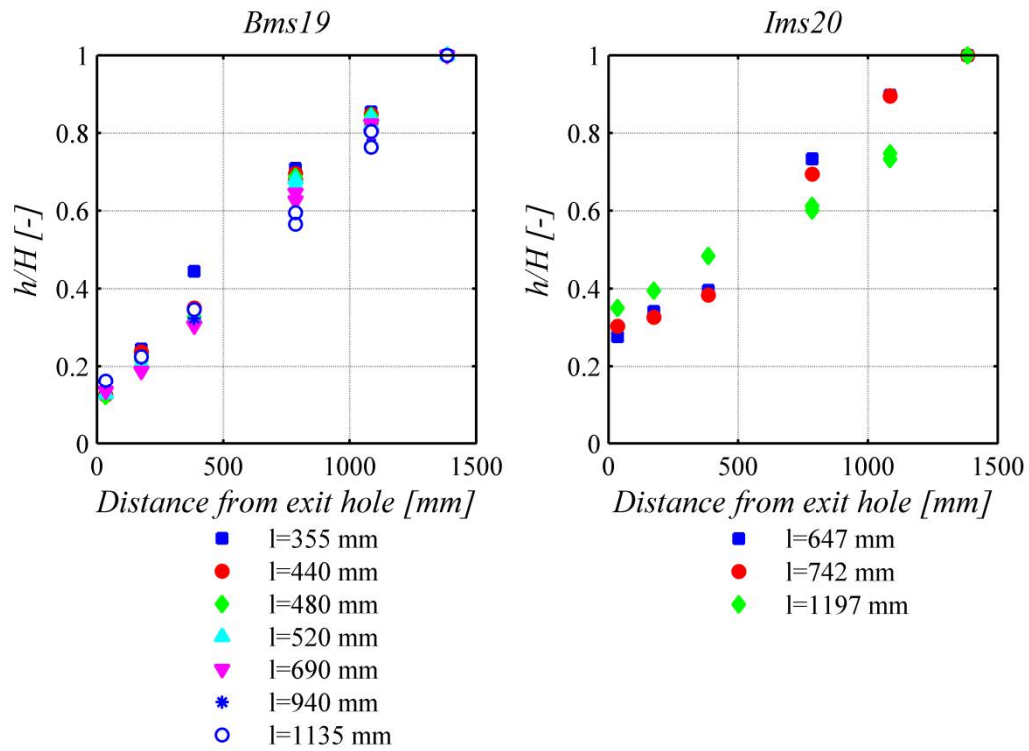


Figure 4.30. Normalised hydraulic head along the sand bed for different equilibrium pipe lengths in experiments Bms19 (left) and Ims20 (right).

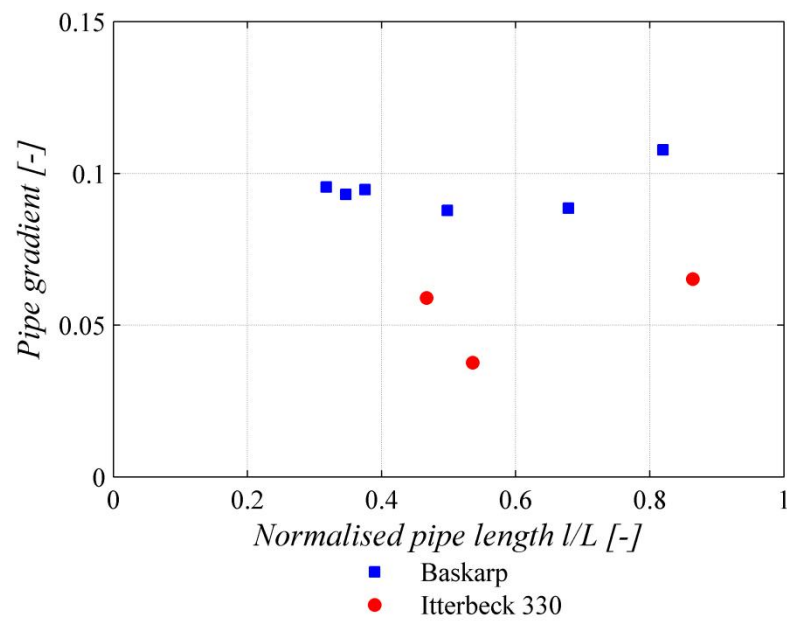


Figure 4.31. Average pipe gradient as a function of normalised pipe length in experiments Bms19 and Ims20

4.9.4. SUMMARY

In the medium-scale experiments with a hole-type exit, the process was similar to that seen in the small-scale hole-type experiments. The larger pipe length led to more pipe widening and meandering. An accidentally layered sample showed the effect of micro-heterogeneity: the pipe developed in the direction perpendicular to the flow when it encountered a relatively coarse layer. The pipe volume proved to be significantly larger in the experiment with relatively coarse sand (Itterbeck) than in the experiment with relatively fine sand (Baskarp). Accordingly, the pipe gradient was smaller in the experiment with Itterbeck sand than in the experiment with Baskarp sand.

The experiments confirm that the critical head is not significantly affected by the grain size of the uniform sand sample. The experiments also confirm the presence of a scale effect for pipe progression.

4.10. PROGRESSION: VISUALISATION EXPERIMENTS

4.10.1. OBJECTIVES

Many experiments have been performed to determine the critical head for piping. Since these experiments looked at the piping process from above, it was difficult to study the erosion processes at the micro-scale.

An attempt has been made to study the erosion process in more detail in a 2D set-up allowing for the observation of the erosion process in cross-section (Van der Zee, 2011). The 2D set-up, which is shown in Figure 4.32, comprised a piping box with the same dimensions as a traditional small-scale set-up, except that the sand sample was 1 cm wide.



Figure 4.32. 2D-set up (Van der Zee, 2011)

These experiments found that the gradient required for pipe initiation was much higher ($H_c/L \approx 1$) than in regular small-scale slope-type experiments. After initiation, the pipe developed very quickly to the upstream side. Not only was there no equilibrium during

pipe development due to the high gradients, the processes observed may not be representative of processes in the field. It should be noted that lower gradients have been found in a similar 2D set-up with finer sand (Vandenboer et al., 2014b).

During the test, different forms of sand movement were observed. They included bed erosion, head erosion, fluidisation of the bed and erosion caused by passing clouds of grains. It is not known whether all these processes play a role when the hydraulic head is smaller.

The high gradient was presumably related to the narrowness of the box. The type of configuration (slope) is the most likely cause of the absence of equilibrium (as observed earlier in these types of experiments). The objective for the visualisation experiments was therefore to investigate the erosion process at a more realistic gradient. A second objective was to analyse the pipe gradient and pipe depth.

4.10.2. SET-UP AND EXPERIMENTAL PROGRAMME

A piping box with a limited width and a hole-type exit configuration was used to reduce the hydraulic head but still allow for the visualisation of the erosion process (Figure 4.33). This box had the same dimensions as a traditional small-scale box but it was 15 cm wide and had transparent walls. The hole was located on the side of the box in order to stimulate pipe development along the wall of the set-up. The water head was measured in several places to determine the hydraulic conditions in the pipe. By contrast with the other experiments, the box was not coated with silicon on the inside.

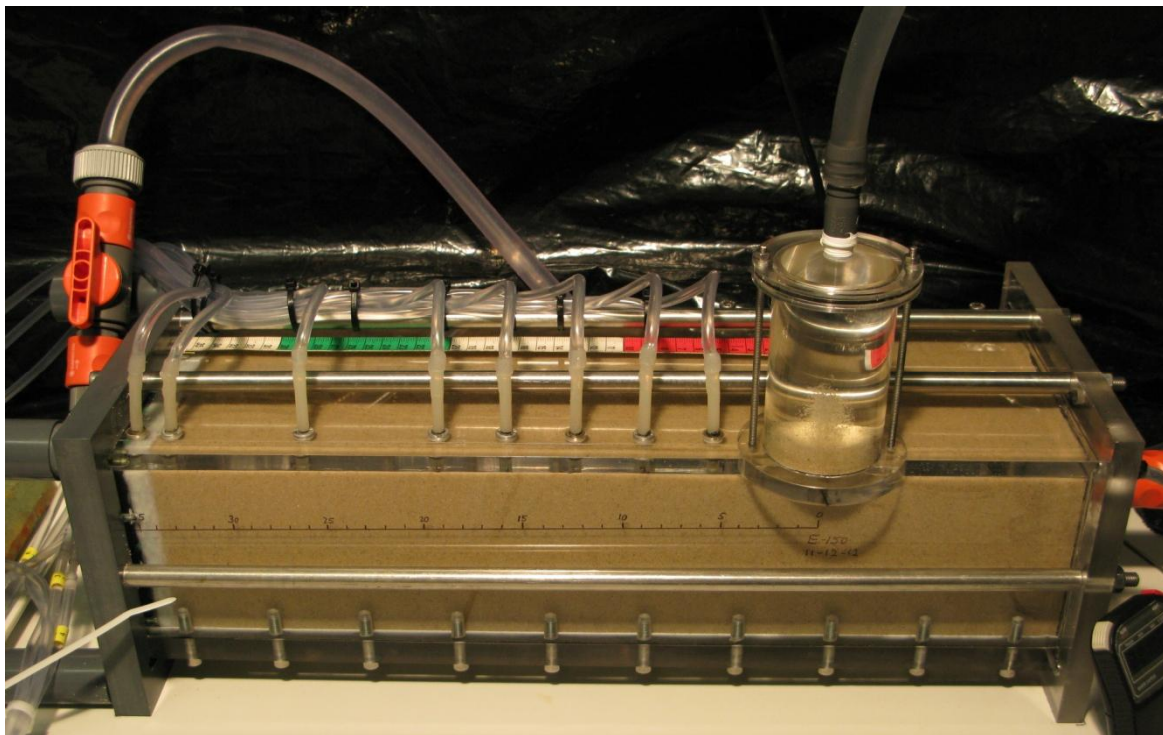


Figure 4.33. Visualisation set-up

A total of four experiments were conducted and it was found that pipe development in most experiments was not along the wall. Instead, the pipe tended to develop through the sand layer. In the first three experiments, which were performed with Baskarp sand, the pipe only touched the wall during the widening process. This was not expected because the pipe tended to progress along the wall in the first slope-type experiments.

In the fourth test (E150), in which Enschede sand was used, small sections of the pipe touched the wall during backward development. Although the process of erosion could not be fully observed, the test provided some insights into this process. This last test also provided the most accurate data for the hydraulic conditions in the pipe.

The experiments were performed by raising the hydraulic head in steps. When two pipe lengths were reached (175 mm and 235 mm), the tap was closed. The head was then brought back to 0 and then gradually reapplied to study the pipe hydraulics.

4.10.3. RESULTS

The observations in experiment E150 were similar to the observations in the other small-scale hole-type experiments. Although the pipe developed in part along the wall, erosion at the tip of the pipe could not be observed. The erosion in the pipe and the pipe depth were assessed at two intervals (at distances of 0-30 mm and 40-70 mm from the exit hole).

Observations of the erosion process showed that particles at the bottom of the pipe were eroded, but that others were deposited. Large differences in particle velocity were observed: some particles were rolling, sliding and saltating along the pipe bottom, whereas others were taken up in the flow and moved relatively fast. The particles seemed to originate from a location upstream of the visible pipe section.

Figure 4.34 shows the pipe section at a distance of -20 to 40 mm from the hole for pipe lengths of 60 mm and 97 mm and heads of 9 and 10 cm respectively. These images show that, although some of the particles were eroded, others were deposited and the net change in depth was negligible. Note, for example, the black particle in the top photograph (circled), which has been eroded in the bottom photograph of Figure 4.34. The maximum depth observed in this section, which was a few millimetres upstream of the exit hole, was 1.5 mm.

Figure 4.35 shows a pipe section at a distance of 30-80 mm from the exit hole at two points in time between which the pipe developed from 250 mm to 280 mm. The hydraulic head was constant during this interval and no depth increase was observed. The interval may have been too short for any difference to be seen. The increase in flow during this interval as a result of the lengthening of the pipe is expected to be limited. The maximum depth observed in this section was 2.5 mm.

The depth measurements were limited by the fact that some sections were not visible during the experiments. The difference in pipe depth observed between the two visible sections does not imply an increase in depth during pipe lengthening. The partial visibility and lateral variation in depth makes the quantitative interpretation of the pipe depth of 2D pipe sections difficult.

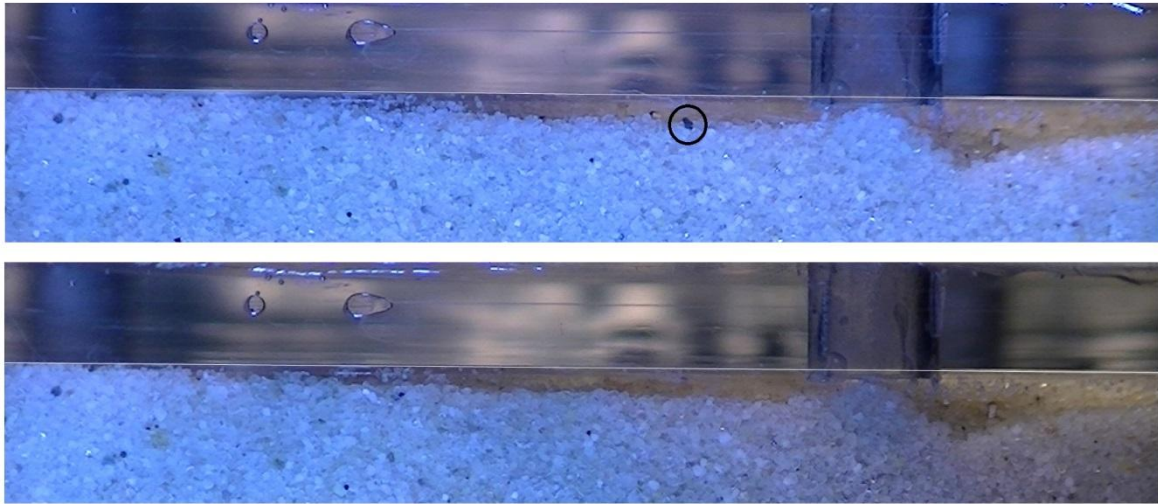


Figure 4.34. Pipe section at -2 to 4 cm from the exit hole when the pipe length was 60 mm (top photo, taken 135.5 minutes into the test, head drop 9 cm) and 97 mm (bottom photo, taken 200.67 minutes into the test, head drop 10 cm)

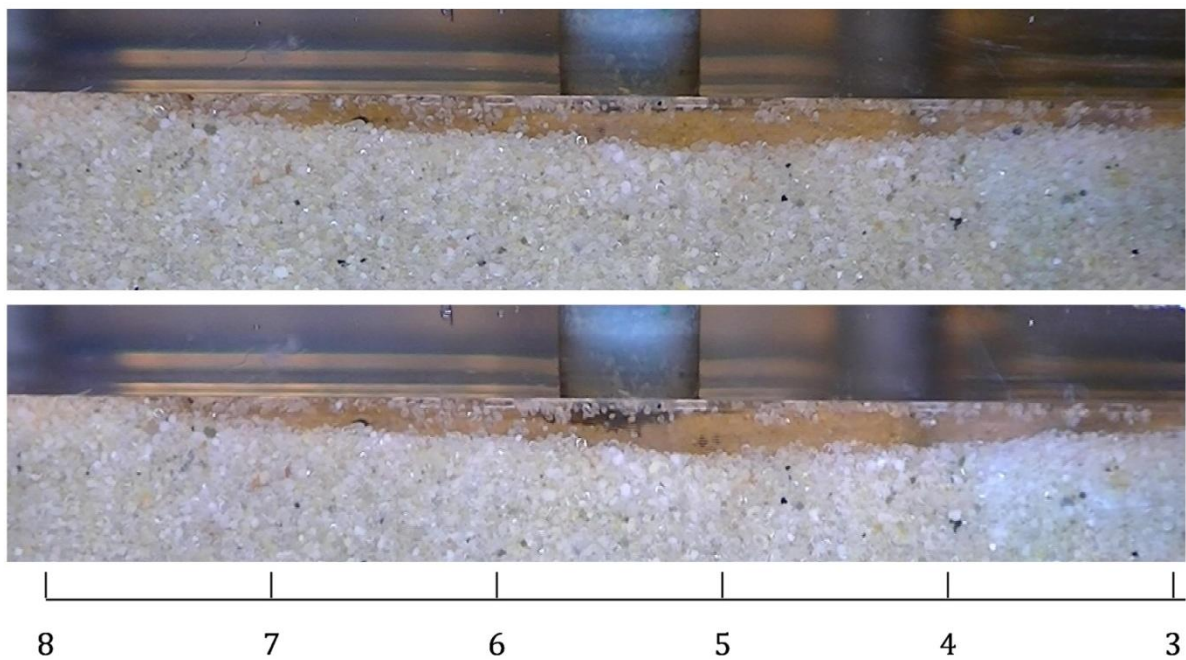


Figure 4.35. Pipe section at 3 to 8 cm from the exit hole when the pipe length was 250 mm (top photo, taken 373.45 minutes into the test, head drop 8 cm) and 280 mm (bottom photo, taken 375.58 minutes into the test, head drop 8 cm)

Figure 4.36 shows that the section 3-8 cm from the upstream hole is part of a scouring bend. The scouring action causes variation in depth, as can be seen in Figure 4.35. It therefore seems reasonable to expect that the maximum pipe depth will be larger in Figure 4.35 than in Figure 4.34.

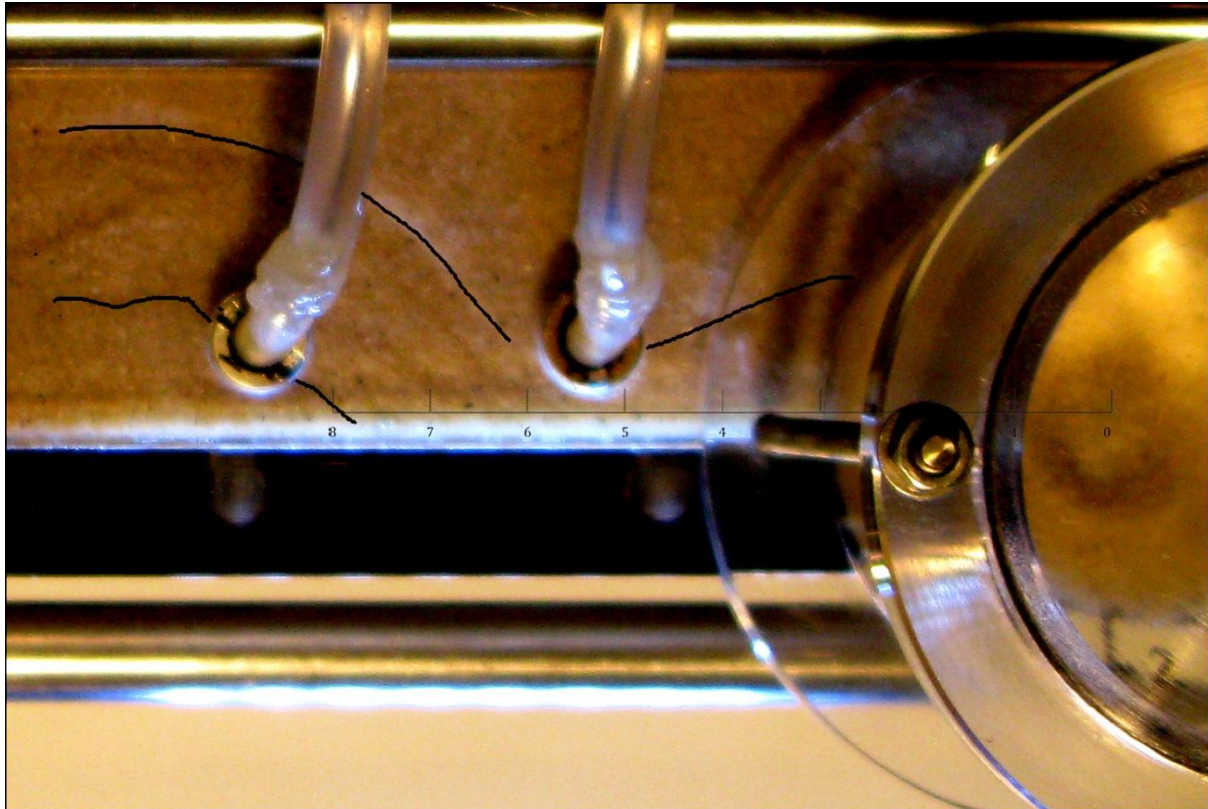


Figure 4.36. Downstream part of developed pipe viewed from above 373.45 minutes into the test

By coincidence, the pipe developed below the riser tubes, so that the measured heads could be used to determine the pipe gradient. It was possible to determine the particle velocity as an indication of the flow velocity in the pipe on the basis of the grain movement in the movies. When the length of the pipe reached 97 mm, natural equilibrium occurred. When the pipe lengths reached 175 and 235 mm, pipe development was stopped by cutting off the water supply.

Figure 4.37 shows the head distribution for the three pipe lengths. The head is normalised by dividing the head drops by the overall applied head. The impact of the pipe is clearly visible in this graph: the head decreases where the pipe is formed.

The pipe gradient was determined by the linear interpolation of the head drops measured with the riser tubes that were located in the pipe. The gradient was measured at various head drops for the pipe lengths of 175 and 235 mm until the pipes started to progress at the 'equilibrium head'. The 'critical pipe gradient' is defined here as the gradient in the pipe at which the applied head will lead to the progression of the pipe to the upstream side. The critical pipe gradient is obtained by multiplying the average of the normalised pipe gradients obtained at lower head drops by the head at which the pipe starts to progress. The resulting critical pipe gradients are listed in Table 4.7.

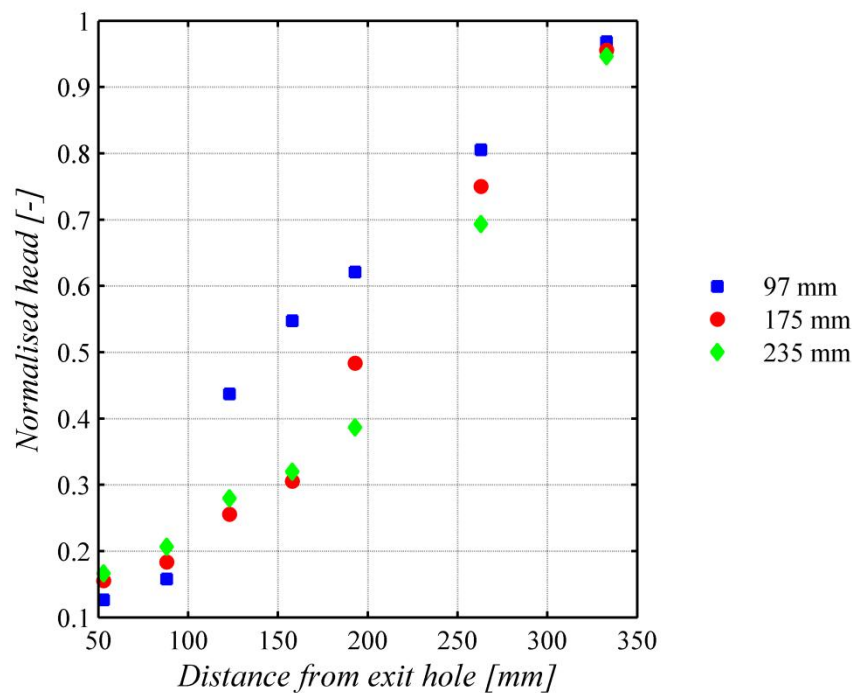


Figure 4.37. Normalised head distribution for different pipe lengths

Table 4.7. Critical pipe gradients at different pipe lengths

Pipe length [mm]	Progression head [m]	Critical pipe gradient [-]
97	0.010	0.090
175	0.093	0.131
235	0.079	0.119

4.10.4. SUMMARY

The experiment to visualise the piping process was successful in allowing for the observation of the piping process in the pipe. It was not possible to observe the process near the pipe tip since the pipe was only partially visible. The observations indicated that there was particle erosion on the bottom of the pipe but that this was followed by particle sedimentation and so the depth of the pipe remained unchanged in those sections of the pipe that could be observed. Measurements of the hydraulic head were used to determine the 'critical pipe gradient', which was defined as the gradient at which erosion leads to pipe progression.

4.11. PROGRESSION: EXPERIMENTS FOR PIPE DIMENSIONS

4.11.1. OBJECTIVES

The small-scale and visualisation experiments provided some information about the pipes that formed. The pipe width clearly increased and the pipe depth appeared to

remain unchanged in those sections that could be observed. However, only part of the pipe was visible in the visualisation experiments and the pipe depth could not be determined for the entire pipe. It therefore remained unclear how pipe depth develops in relation to pipe width.

This section describes experiments in which the pipe depth was measured using a laser after the removal of the top plate. This had already been done at the end of one of the experiments described in Section 4.8. However, at this point, the pipe had already widened and was no longer in equilibrium. When determining the pipe dimensions in order to model pipe progression, the pipe has to be considered in the critical equilibrium state.

4.11.2. SET-UP AND EXPERIMENTAL PROGRAMME

The experiments to determine the dimensions of the pipe were performed in the small-scale set-up with a hole-type exit (Figure 4.2c). The high flow velocity near the hole-type exit will ensure pipe initiation at a relatively low head drop and therefore several locations where the pipe is in equilibrium. Two tests were performed, one with Baskarp sand (B171) and one with Enschede sand (E172), to investigate of the effect of grain size on pipe dimensions. The properties of these sand types can be found in Figure 4.5 and Table 4.1. The sands were prepared with a relative density of approximately 90%.

The head drop was applied more gradually than in the other experiments in order to achieve the critical pipe length as accurately as possible. Initially, the head was raised by 0.5 cm every 5 minutes unless erosion took place. However, when the applied head approached the critical head, the head was increased in steps of 0.25 cm every 5 minutes or after longer time intervals when grain transport was still apparent.

When the final equilibrium state was reached, the water level was reduced so that capillary forces retained the water in the top of the sand bed. This allowed for the removal of the acrylate plate without much disturbance of the formed pipes. The pipe pattern was analysed with a laser.

4.11.3. RESULTS

The observations during the experiments were similar to the other small-scale experiments, except for the fact that the pipe formed in Baskarp sand appeared to be more sensitive to very local variations in the sand bed than in previous experiments. The pipe started to develop along a stratification layer, possibly because of the more gradual application of head in this experiment. The challenge in these experiments was to let the pipe develop to the maximum possible length, while reaching an equilibrium state without the need for a reduction in the head. This was achieved in both experiments. Figure 4.38 and Figure 4.39 show the pipes in equilibrium that were ultimately obtained. In both experiments, the critical head was comparable with the heads in other experiments with the same characteristics (Table 4.8). It should be noted that the pipe length was slightly shorter in experiment E172 than in experiment B171.

The pipe width and depth were analysed in cross-sections perpendicular to the pipe path at various distances along the pipe. Figure 4.40 shows the maximum depths obtained from these cross-sections in both experiments as a function of the position in the pipe measured from the exit hole.

Table 4.8. Comparison of similar experiments

Sand type	Experiment no.	Critical head [m]
Baskarp sand	B115	0.089
	B118	0.089
	B142	0.080
	B171	0.079
Enschede sand	E169	0.090
	E172	0.085

The figure shows that, despite the shorter length, the pipes in the experiment with Enschede sand were deeper. The figure also shows that the maximum pipe depth increased towards the exit in both experiments, confirming the findings from experiments performed at Ghent University (personal communication Kristine Vandenboer, 2014). Depth fell off abruptly near the pipe tip. This indicates that the pipe was formed with a certain depth (approximately 0.5 mm in Baskarp sand and 0.9 mm in Enschede sand), which increased as a result of secondary erosion. The increase seems to have been sharpest in the first 100 mm away from the tip. This initial pipe depth seems to be related to the grain size, but not linearly, as the initial depth was 3.8 times the mean grain diameter in Baskarp sand and only 2.4 times the mean grain diameter in Enschede sand.

It should be noted that the value for the maximum depth becomes less accurate close to the exit hole and near the pipe tip. Close to the exit hole, depth measurements will not be accurate because some of the sand in the crater formed during the experiment flows back into the hole once the hydraulic head is reduced. Near the tip, it was not possible to distinguish between the pipe and the observed variation in the sand bed. The observed variation in depth in the flat sand bed was approximately 0.1 mm in Baskarp sand and 0.2 mm in Enschede sand. This does not affect the main conclusions.

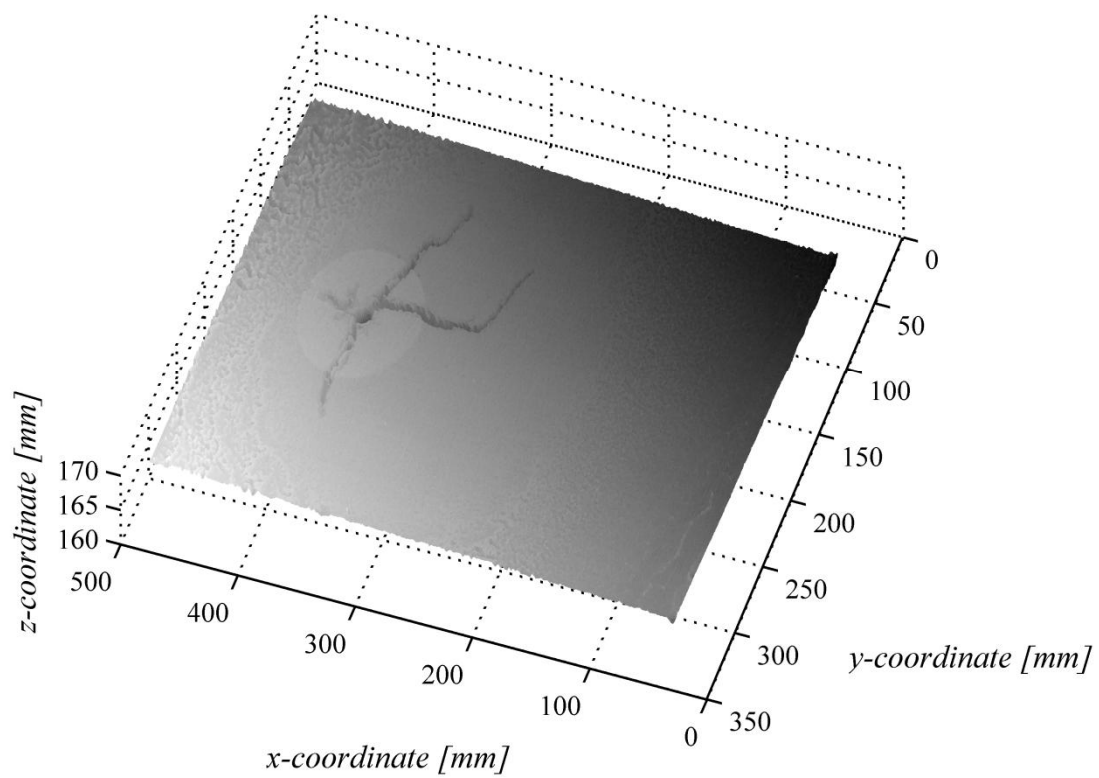


Figure 4.38. Laser data experiment B171

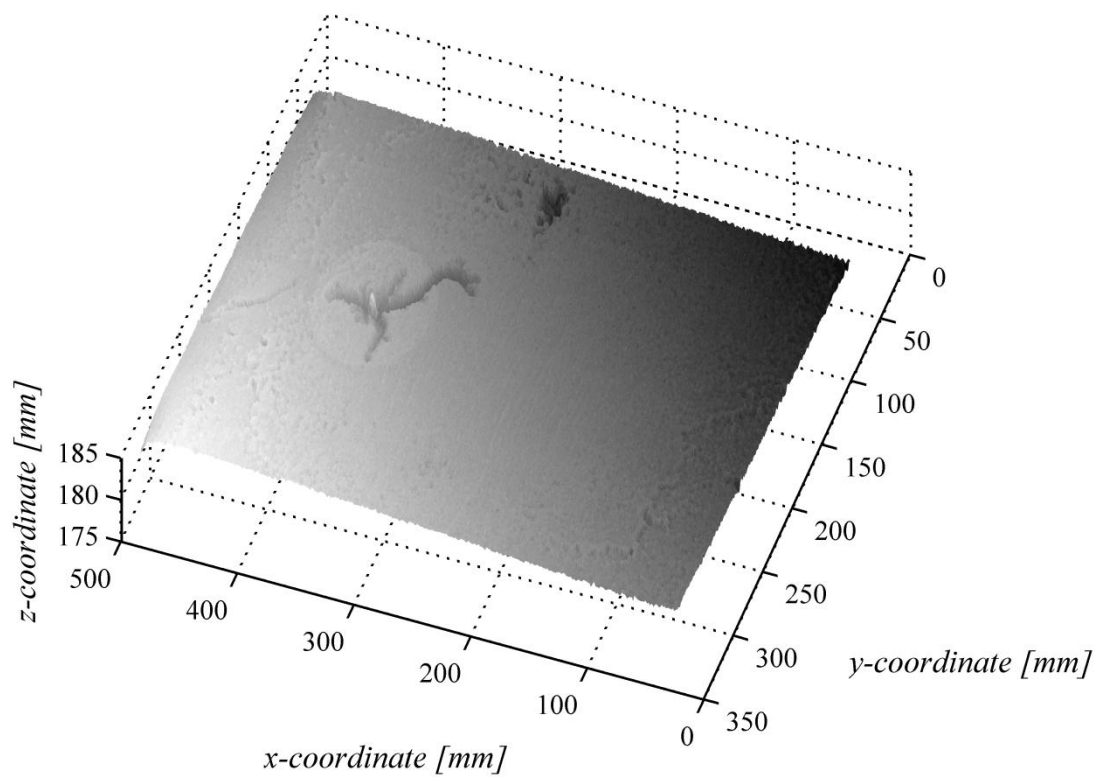


Figure 4.39. Laser data experiment E172

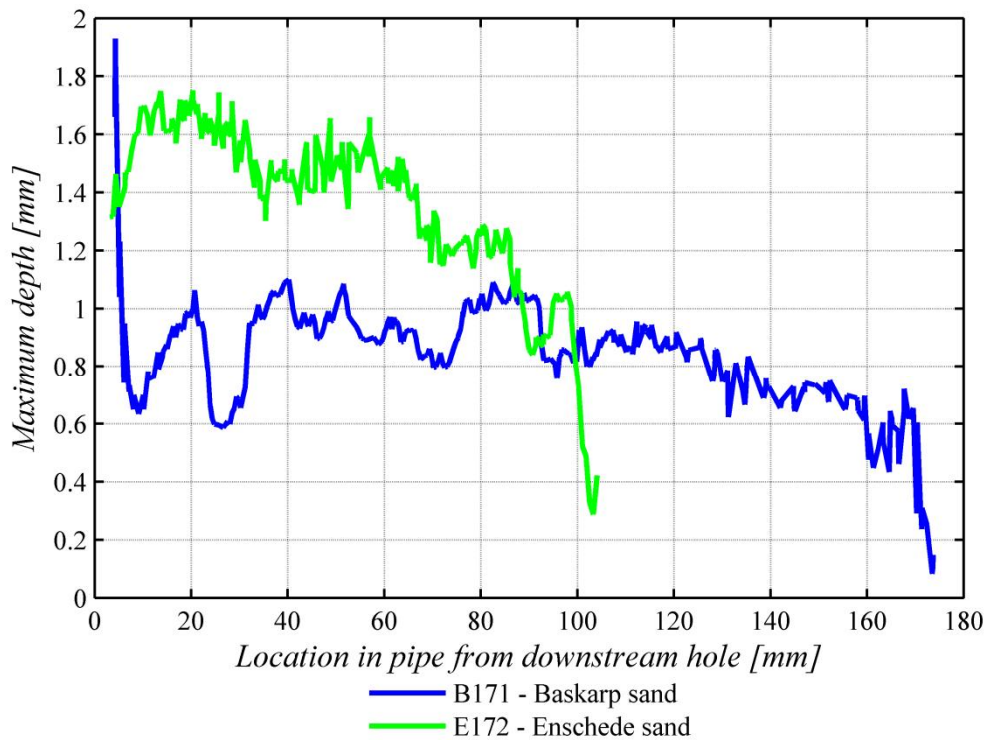


Figure 4.40. Maximum depth as a function of location in the pipe in the two experiments

The pipe width was measured by hand at the cross-sections, one of which is shown in Figure 4.41. The width was measured between the points where the extrapolated lines of the pipe walls cross the z -axis at the value of 0. In some cross-sections, the width was obvious and precise but, in others, the exact value was less clear, for example due to the merging of two pipes. The pipe widths obtained as a function of location in the pipe in the two experiments are shown in Figure 4.42. In general, an increase in width towards the exit was observed and the width was larger in Enschede sand than in Baskarp sand. The width fluctuated more sharply in Enschede sand than in Baskarp sand because of the presence of short branches at the side of the pipe. The width near the tip was approximately 4 mm in Baskarp sand, which is 30 times the mean grain diameter. The tip width in Enschede sand was more difficult to determine. Taking the scatter into account, a width of approximately 10 mm seemed a reasonable estimate. This was 26 times the mean grain diameter.

In experiment B171 the pipe developed perpendicularly to the direction of flow in a layering pattern. This is unusual as the sample was prepared as homogeneously as possible and Baskarp sand itself is a uniform sand. To determine the difference in particle size that can result in a deviation of the pipe path, the grain size distributions of the particles just upstream of the pipe and the layer of the pipe were analysed. Figure 4.43 shows the layering of the sand sample, which becomes more marked when the top layer is wet, but not fully saturated. The pipe developed in the dark layer and the layer upstream of the dark layer posed more resistance to pipe development.

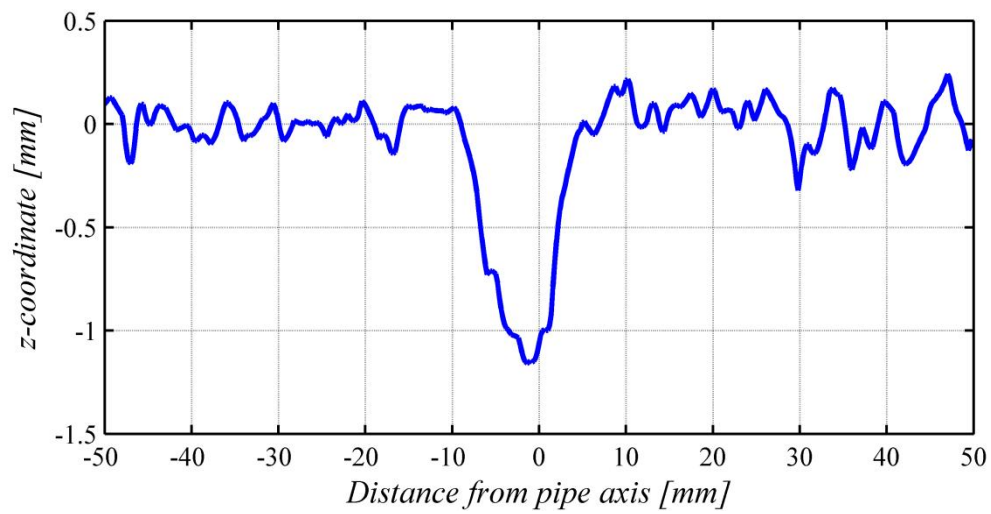


Figure 4.41. Example of a pipe cross-section

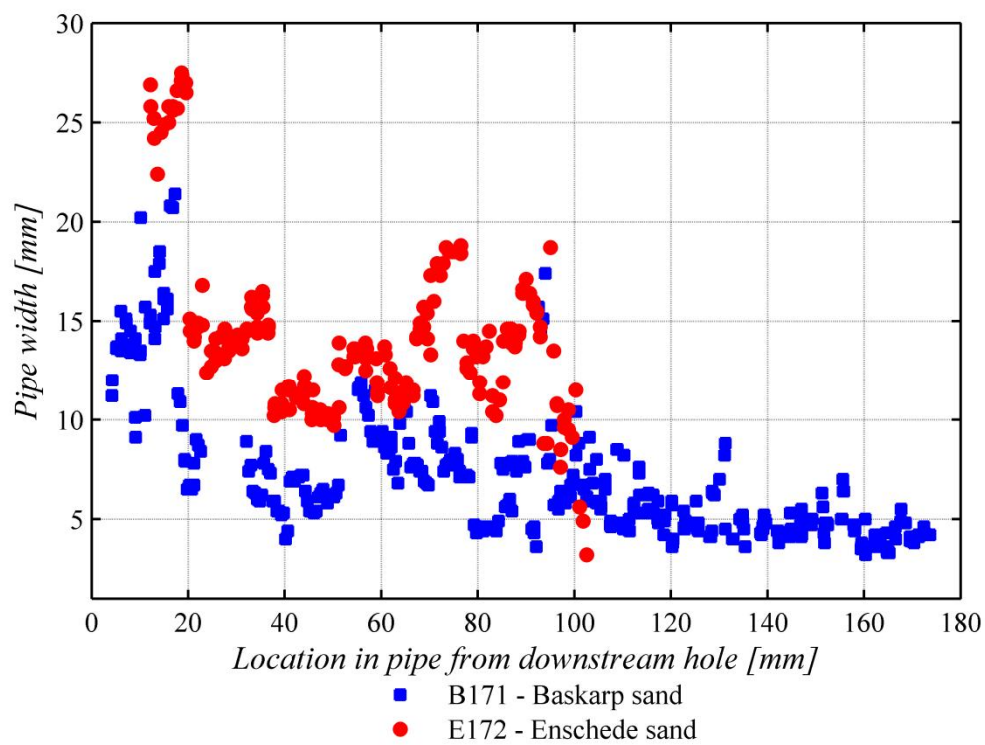


Figure 4.42. Pipe width as a function of location in the pipe in the two experiments

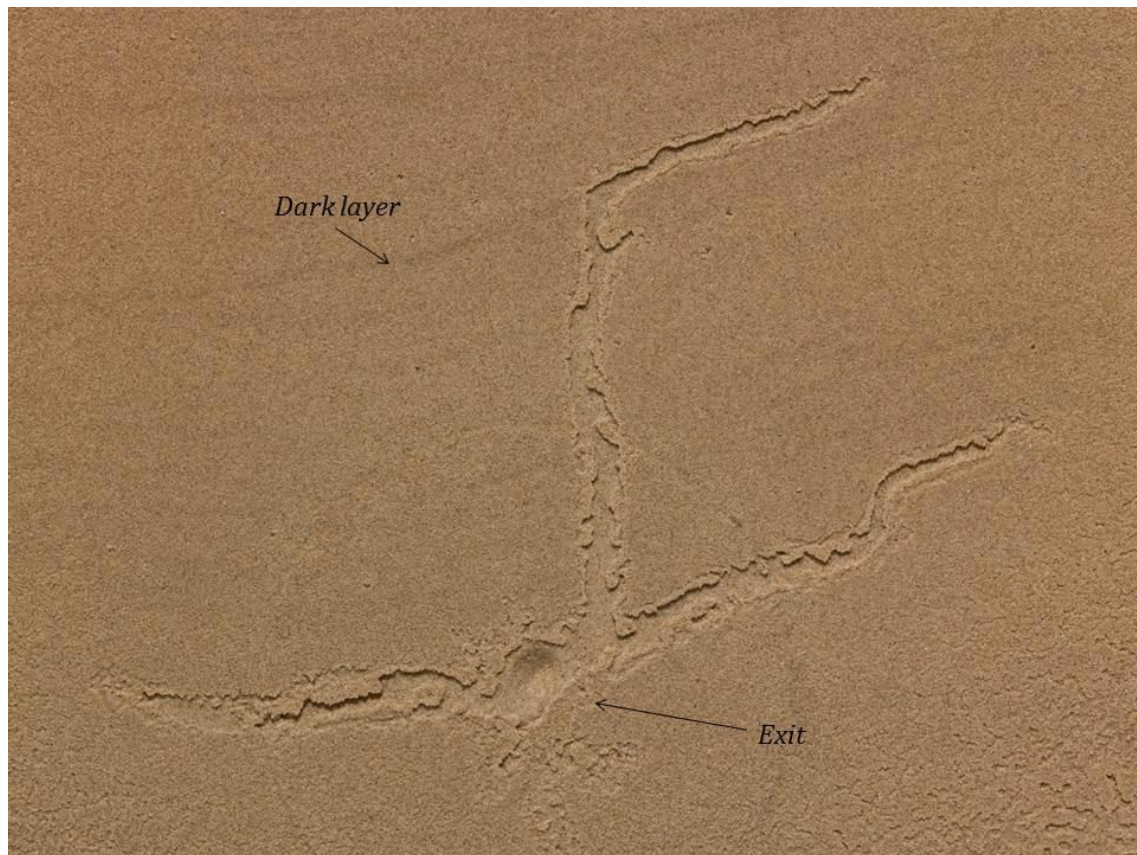


Figure 4.43. Pipe formation in experiment B171 (after test and removal of acrylate plate)

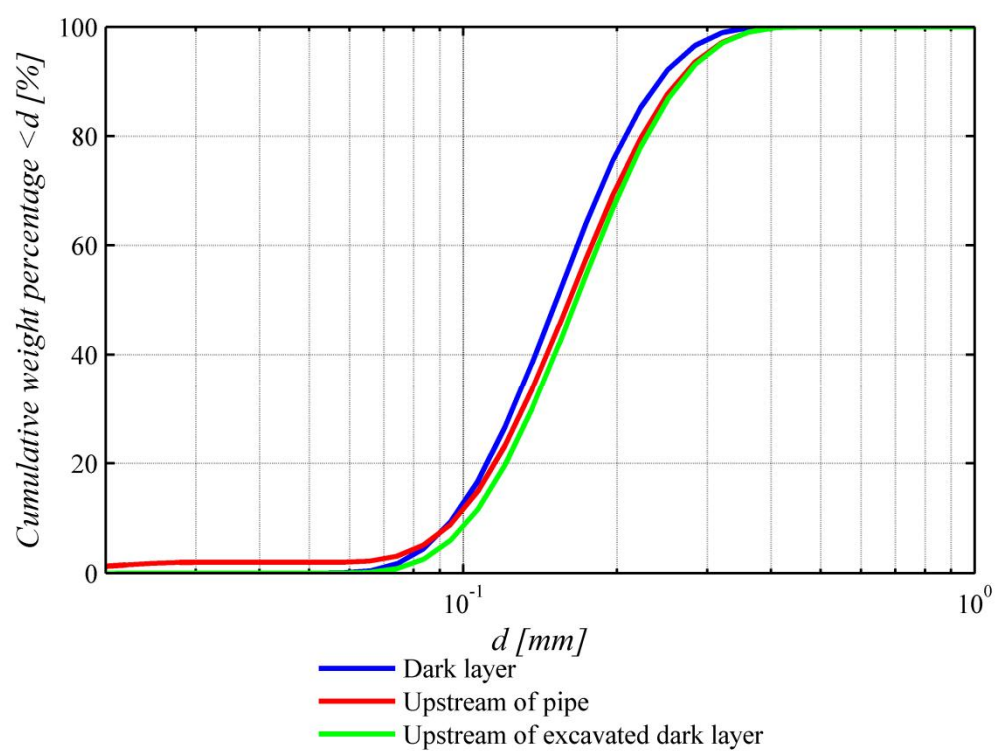


Figure 4.44. Grain size distribution obtained with laser diffractometry

The dark layer in which the pipe formed and the layer upstream of the dark layer (both upstream of the newly excavated zone and upstream of the pipe) were analysed in a Malvern laser diffraction particle size analyser. The grain size distributions can be found in Figure 4.44. It can be seen that the dark layer in which the pipe formed was indeed slightly finer than the layer upstream of the dark layer and the pipe. A difference in the mean particle size as small as 0.012 mm can result in a deviation in the pipe path.

4.11.4. SUMMARY

Two experiments were performed to determine the pipe dimensions in the equilibrium state. The laser data showed that pipe width and depth were larger in the coarser Enschede sand than in the finer Baskarp sand. In both sand types, pipe depth and width increased towards the exit hole, indicating erosion on the bottom of the pipe and the pipe walls. The pipe depth at the tip was 2.4 times the mean grain diameter for Enschede sand and 3.8 times the mean grain diameter for Baskarp sand.

In the experiment with Baskarp sand, the pipe path evolved to follow the layering pattern. Analysis of the grain size indicates that the pipe path can deviate when there is even a minimal difference in mean particle size (as little as 0.012 mm).

4.12. SUMMARY OF LABORATORY EXPERIMENTS

The laboratory work has contributed to the clarification of the process of piping and indicates the direction that should be taken for the development of prediction models.

Forward erosion can only occur when the top grains are not fixed and this means it is unlikely to occur in the field where a cohesive layer exerts a pressure on the sand bed. This process will therefore not be analysed further.

Small-scale experiments confirm that, depending on the type of exit configuration, the critical head can be determined by two processes: pipe initiation and pipe progression. In experiments with a large exit area, the pipe will initiate and progress to the upstream side without equilibrium. When the head is lowered after some pipe development, it emerges that the head required for progression is significantly smaller than the head required for initiation and this explains the observed lack of equilibrium in previous experiments. By contrast, in experiments with a small exit area, pipe initiation occurs at a relatively low head and so the required head for progression is not yet exceeded. This explains the observation of equilibrium in these experiments.

Now that this has been confirmed, the processes of pipe initiation and pipe progression can be modelled.

Experiments were performed to complement the existing database of experiments for pipe initiation and pipe progression. These consisted of small-scale experiments and medium-scale experiments investigating the effect of soil type and scale on critical head. The experiments showed that the critical head for pipe progression in uniform sands does not depend on the sand type. An increase in the uniformity coefficient leads to an increase in the critical head. The medium-scale experiments confirmed that the critical head is lower in larger-scale experiments.

Several experiments allowed for the analysis of pipe characteristics. The impact of the pipe on the groundwater flow was established in the visualisation experiments. Analysis

of the pipe dimensions under equilibrium conditions showed that the pipe width and depth increase towards the exit, indicating that its dimensions were determined by secondary erosion. The pipe depth converged to an initial value near the tip, and the pipe depth was 2.4 and 3.8 times the mean grain diameter in the two sand types tested. The pipe width at the tip was found to be approximately 26 and 30 times the mean grain diameter in the two sand types.

5. PIPE INITIATION

'It is the magnitude and distribution of seepage forces near the toe of water-impounding structures (particularly the discharge gradient at the toe) which determines the degree of safety against piping or underground erosion.'

Arthur Casagrande, referring to Terzaghi (1922)

5.1. INTRODUCTION

The models that predict critical gradient by including the presence of a pipe assume that, after initiation, the pipe does not get longer and that there is therefore 'equilibrium'. The gradient that allows the pipe to progress in the upstream direction is calculated accordingly. The implicit assumption is that the onset of pipe development, or 'initiation', requires a lower head drop than the 'progression' of the pipe.

However, this assumption is not valid for all experiments, as has been shown in the literature review and in the laboratory work in Chapter 4. In some experiments, equilibrium is observed after pipe formation and an increase in the head drop is needed for the pipe to lengthen (Müller-Kirchenbauer et al., 1993; Hanses, 1985; Miesel, 1978; Silvis, 1991, some of the experiments by Townsend et al., 1988, Pietrus, 1981, Van Beek et al., 2011 and the hole-type experiments described in Chapter 4). In these experiments, the presence of the pipe affects the continuation of pipe development. In other experiments, no equilibrium is observed: the pipe develops continuously to the upstream side without any further increase in head (small-scale experiments by Van Beek et al., 2011; experiments by De Wit, 1984; some of the experiments by Townsend et al., 1988, and Pietrus, 1981, and the plane-type experiments described in Chapter 4). Essentially, in the second type of experiment, the critical gradient (H_c/L) is determined by the initiation of the pipe rather than the progression of the pipe. Since there is no equilibrium during pipe development, it must be concluded that the initiation of the pipe in these experiments requires a larger head than the head required for the progression of the pipe (see also Section 4.6). The determination of the critical head by initiation or progression proves to be dependent on the type of exit (see Figure 3.9).

To maintain clarity, various notations have been used for the different heads and gradients in this chapter. The critical gradient (H_c/L) is defined as the average gradient

across the structure that leads to ongoing erosion. This critical gradient can be determined by two processes: initiation or progression. In all experiments, the pipe had to be initiated, and this event occurred at the initiation head (H_i) or average initiation gradient (H_i/L). In some experiments, pipe equilibrium was then observed, and the head needed to be raised until the pipe progressed in the upstream direction. The head required for pipe progression, assuming the presence of a short pipe, is referred to as H_p , and the corresponding average gradient for progression is H_p/L . In other experiments, no equilibrium was observed after the initiation of the pipe and the pipe progressed in the upstream direction without any further increase in the head. In these experiments the critical gradient was determined by the process of initiation and the progression gradient (H_p/L) remains in most cases unknown since the progression gradient had already been exceeded at the point of initiation.

The difference between initiation and progression has been confirmed in small-scale experiments described in Chapter 3, in which the head drops required for progression (H_p) and initiation (H_i) were studied separately. It is clear that the type of exit is one of the parameters that determines whether progression or initiation dominates the piping process and corresponding critical head.

Although initiation and progression are considered different steps in the process of internal erosion (Foster and Fell, 1999), this difference has not been acknowledged by the prediction models for backward erosion described here. Most models developed to predict the critical head for backward erosion piping relied on both experiments that were dominated by initiation (no equilibrium) and experiments that were dominated by progression (equilibrium) for calibration and validation, even though pipe initiation and pipe progression are different mechanisms (Schmertmann, 2000; Sellmeijer, 1988; Sellmeijer et al., 2011). An exception to this is the work by Richards and Reddy (2012), who performed experiments with the explicit aim of modelling piping initiation using a triaxial set-up. They found that exit seepage velocity was an important parameter for pipe initiation. However, it is proposed here that the local exit gradient causes the initiation of erosion, rather than the exit velocity. Furthermore, their approach is currently only applicable to the triaxial set-up, since the exit velocity near the toe of a water-retaining structure depends very much on the location and the exit configuration.

This chapter derives a prediction model for pipe initiation with different configurations. It puts forward suggestions to determine when initiation or progression is likely to be the dominant factor determining the magnitude of the critical head. This information is not only essential for experimental work studying backward erosion and the development of prediction models for backward erosion; it will also give the practical information required to decide whether it is likely that a sand boil indicates ongoing erosion that may result in failure with time.

5.2. PAST INITIATION EXPERIMENTS

Both initiation-dominated and progression-dominated experiments are suitable for the analysis of the initiation of piping since the initiation gradient (H_i/L) can be recorded in both types of experiment. However, the head at which the pipe is initiated (H_i) is not always recorded in progression-dominated experiments focusing exclusively on the critical gradient (H_c/L). As a result, the analysis here mainly includes experiments in which no equilibrium is observed after the initial sand transport, unless the initiation

gradient has been recorded. The experiments in which the critical head is determined by the process of initiation are typically small-scale experiments with a relatively large exit area, as described in Van Beek et al. (2013). New small-scale experiments were performed to supplement the work of De Wit (1984) and they are presented in Chapter 4. The characteristics of the sand types used in the experiments are listed in Appendix B.

Both sets of experiments by De Wit (1984) and Van Beek et al. (2011) were performed at different scales with different sand types and porosities. The observations reported by De Wit (1984) for plane-type and ditch-type experiments (characteristics summarised in Appendix A) are:

1. Expansion of the sand bed: at the toe of the clay layer the sand starts to expand, creating an elevated area with an estimated height of 1 mm and an estimated width of approximately 15-20 mm. This expansion is most clearly observed in experiments with fine sands and it is not seen in experiments with Coarse sand.
2. Small holes due to the local wash-out of grains near the toe of the embankment.
3. Small sand boils in which sand is lifted and deposited, no sand transport.
4. Increased boiling of sand in sand boils, with no sand transport.
5. A sand boil starts to deposit sand and grows in size. A crater is formed. The process continues until there is a breach.

This description indicates that the head at which the pipe reaches the upstream side (H_c) is equal to the head at which the pipe is initiated (H_i). In most experiments, the required head for sand boiling (4), H_b , is more or less equal to the head for sand transport (5). However, in some experiments sand boils occur at a much lower head drop (H_b) than the head at which sand transport takes place, indicating pipe initiation (H_i). This corresponds to the findings of Rice and Swainston-Fleshman (2013), who performed column experiments in which a sand sample was subjected to vertical flow. They observed sand boils at a lower hydraulic gradient than for total fluidisation in some, but not all, column experiments.

In the small-scale slope-type experiments reported by Van Beek et al. (2011), the pipe also developed in the upstream direction after initiation. In the medium-scale experiments, however, some erosion phenomena (pipe formation) were observed at a head that was lower than the critical head. These erosion phenomena involved the formation of pipes that did not start entirely at the downstream end. The head at which the first pipe formed was selected as the initiation head. For the analysis of the slope-type experiments, the slope angle and friction angle are required. The friction angle was measured for several sand types (Appendix B).

During the analysis of the slope-type experiments it emerged that the head loss caused by the upstream filter was considerable in experiments with medium-grained sands, comprising a large part of the total head applied to the filter. Since the filter head loss was not measured directly during these experiments but established using a correlation, the filter resistance was reassessed (Appendix C). Because the head loss across the sand sample was uncertain and data for the friction angle were limited, the analysis here is restricted to the Baskarp sand experiments.

The supplementary plane-type experiments were performed in the small-scale set-up described in Chapter 4. The critical head in this experiment was also found to be dominated by initiation, and so H_i equalled H_c .

Experiments by Pietrus (1981) and Townsend et al. (1988) were performed for a slope-type configuration with an artificially created pipe. Richard and Reddy (2012) used a triaxial set-up with a circular pipe as the exit. These experiments have not yet been included in this analysis of initiation because of the 3D exit configuration.

In summary, the plane- and ditch-type experiments by De Wit (1984), the small- and medium-scale slope-type experiments (Baskarp sand only) and the small-scale plane-type experiments described in Chapter 4 are used for the analysis. Appendix A includes an overview of all the experiments.

5.3. INITIATION HEAD ANALYSIS

Now that experiments have been selected in which the head required for initiation is known, these experiments can be compared to determine the effects of exit gradient, scale, sand-layer shape and sand characteristics. There will also be a discussion here of the relationship between the head required for sand boiling and the critical head in the experiments by De Wit (1984).

5.3.1. EFFECT OF EXIT CONFIGURATION ON INITIATION GRADIENT

Given the processes and experiments described in previous chapters, the exit configuration is already known to have a major impact on the initiation gradient. Miesel (1978) investigated how hole size affects the piping process and found that the head for sand fluidisation increased with exit-hole diameter. The small-scale experiments described in Chapter 3 show that the initiation head is larger for a slope-type configuration than for a hole-type configuration.

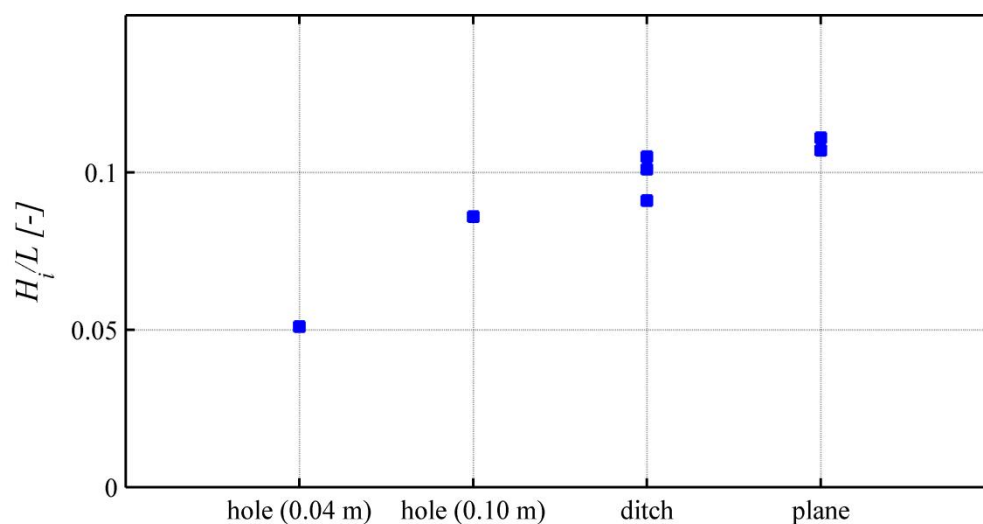


Figure 5.1. Effect of configuration on initiation gradient (experiments De Wit (1984))

De Wit (1984) performed experiments on Beach sand (medium-high density) in experimental set-ups with a hole-type exit (0.04 m and 0.1 m in diameter), plane-type exit and ditch-type exit (ditch width 0.05 m) while retaining other parameters like

seepage length (2.4 m) and sand layer thickness (1.5 m). The initiation gradients obtained in these experiments are presented in Figure 5.1. An increase in gradient can be observed with increasing exit flow area.

Pietrus (1981) created artificial pipes with varying diameters and lengths, and registered the head at which the pipe started to develop. Figure 5.2 shows that the initiation heads are generally larger for the pipes with a large diameter.

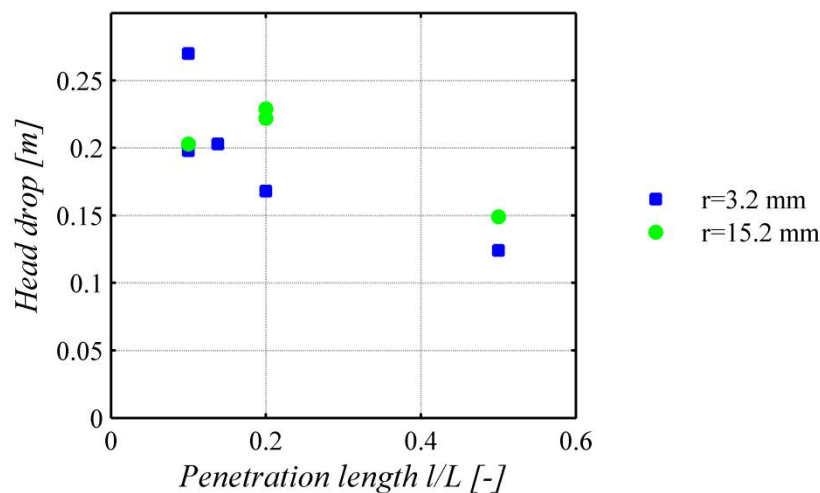


Figure 5.2. Initiation heads for artificial pipes with varying diameters and penetration lengths

It makes sense that the initiation of a pipe is highly dependent on the type of exit since flow lines will be more concentrated when the exit area is smaller. The gradient required for initiation will therefore be reached at a low critical head when the exit is small.

5.3.2. EFFECT OF SCALE ON INITIATION GRADIENT

The existence of scale effects can be shown by analysing experiments with a constant D/L ratio (thickness aquifer / seepage length) but with different dimensions. The role played by scale was investigated in the small- and medium-scale experiments by Van Beek et al. (2011) and in the plane-type experiments by De Wit (1984). Figure 5.3 shows the effect of scale on the initiation gradient in experiments on sand types with a medium-high relative density and constant D/L ratio. Scale effects were indeed observed: the gradient fell as the scale increased.

Assuming that the critical gradient is a function of L^x , the effect of length can be quantified for different experimental series by least square fitting. The wide scatter in the data affects the relation obtained: the scale effect for Coarse sand, for example, would be comparable to the scale effects in the other sand types if the two large values were neglected. The scale effects are considerably larger than would be expected on the basis of the Sellmeijer model (in which the scale effect is defined as $H_c / L \propto L^{-1/3}$), suggesting that the process of initiation involves a different scale effect than the process of progression.

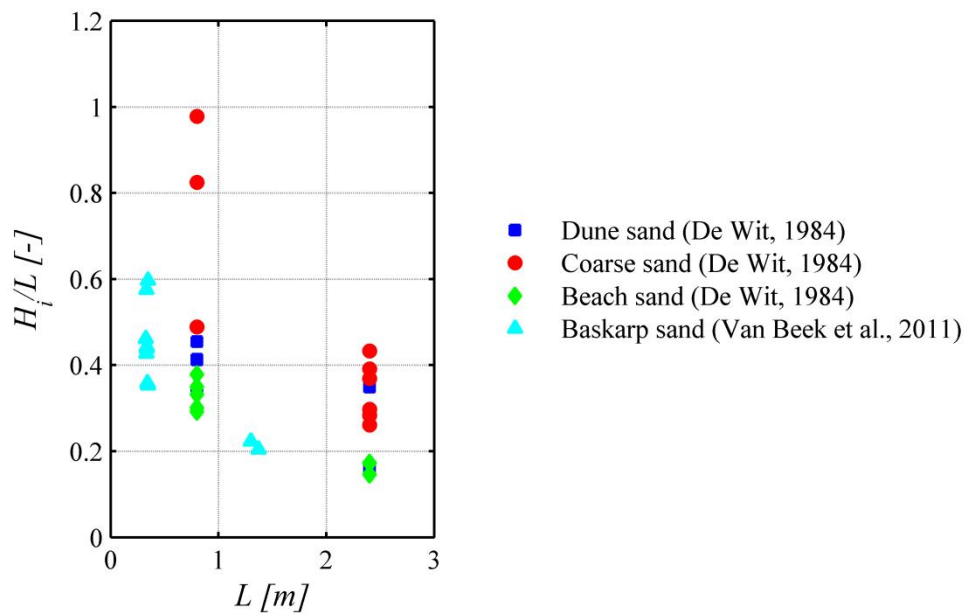


Figure 5.3. Effect of scale in experiments with a constant D/L ratio

Table 5.1. Effect of seepage length on initiation gradient expressed as the power of L

	Dune sand (area-type)	Coarse sand (area-type)	Beach sand (area-type)	Baskarp (slope-type)
X	-0.50	-0.72*	-0.64	-0.54

*Wide scatter in experimental data

5.3.3. EFFECT OF SAND LAYER SHAPE ON INITIATION GRADIENT

The role played by seepage length when the thickness of the sand layer remains constant was investigated in the experiments described by De Wit (1984). Figure 5.4 shows initiation gradients obtained in area-type experiments in which the seepage length was varied (medium-dense Beach sand, $D=1.5$ m). Despite the remarkable spread in the results for small seepage length, the required gradient for initiation proved to be quite constant.

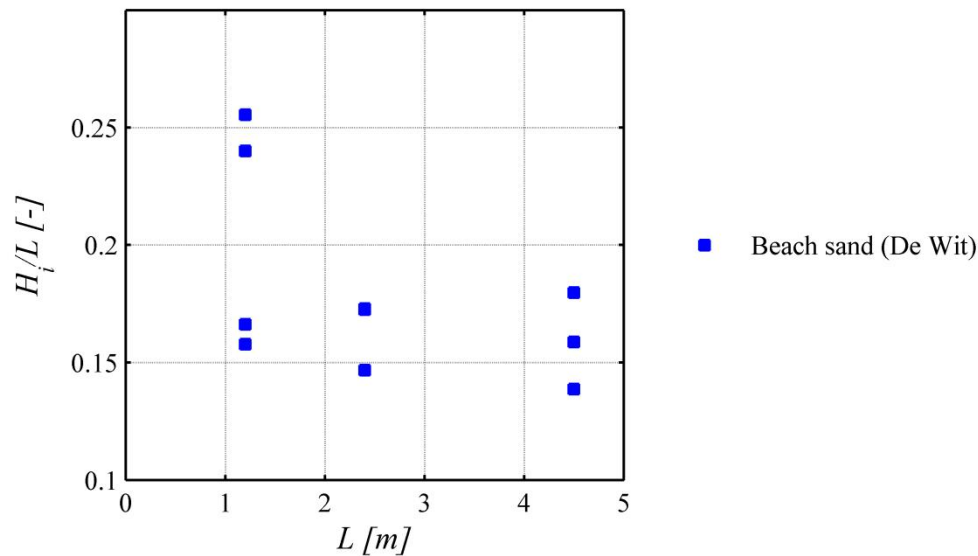


Figure 5.4. Effect of seepage length on initiation gradient (Beach sand, D=1.5 m)

5.3.4. EFFECT OF SAND CHARACTERISTICS ON INITIATION GRADIENT

Sand characteristics such as grain size, permeability, uniformity coefficient and porosity affect the initiation gradient. Figure 5.5 and Figure 5.6 show how grain size and porosity affect the initiation gradient.

It is remarkable that the small-scale slope-type experiments described by Van Beek et al. (2011) show a slight decrease in the initiation gradient with increasing grain size, whereas the other experiments show an increase with increasing grain size. It should be noted here that there is considerable scatter in the small-scale slope-type experiments.

Although the local gradient required for the fluidisation of sand is mainly determined by the porosity and the local flow pattern near the exit, which are independent of parameters such as permeability and grain size, grain size was found to have an effect. This could be linked to the size of the grains in relation to the size of the sand layer. Essentially, an increase in grain size should have the same effect as a decrease in scale. The positive effect of grain size on scale observed in most experimental series concurs with the observed increase of gradient with smaller scale (Figure 5.3).

It should be noted that, in slope-type experiments, the sand type can be expected to have a different effect because the local gradient required for grain motion in a sloping area depends on the friction angle and slope angle (as will be described in the following sections). Furthermore, in the small-scale slope-type experiments on medium-grained sands, the head loss at the upstream filter was obtained by correlation and was found to be considerable (Appendix C). A cautious approach to the interpretation of these experiments is therefore justified.

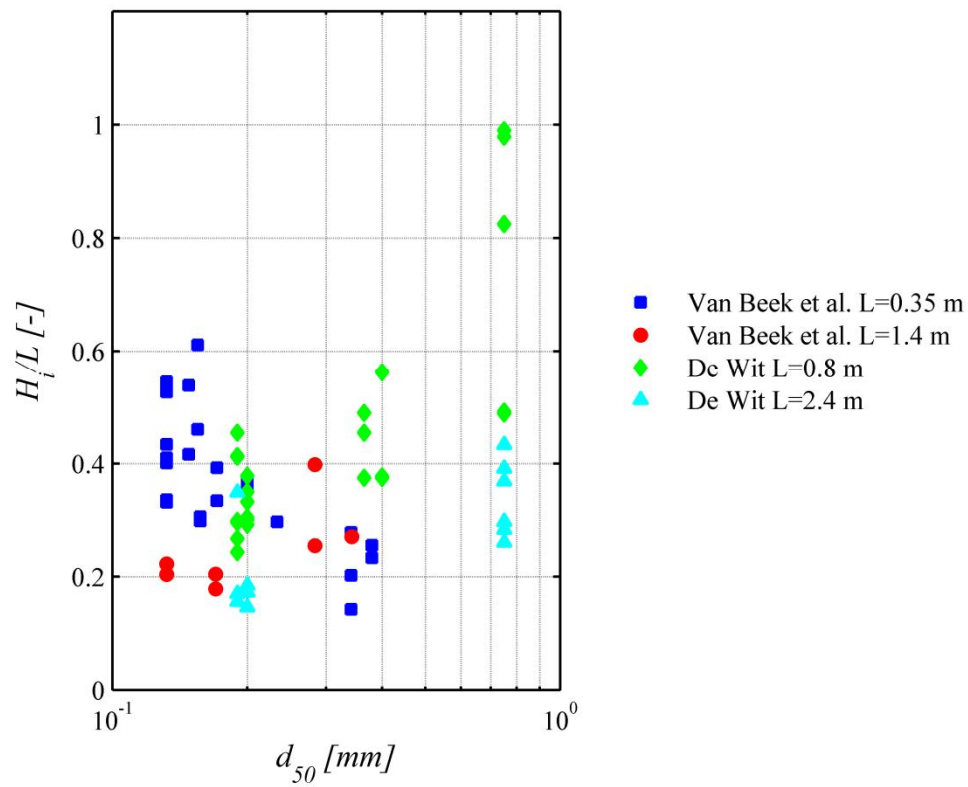


Figure 5.5. Effect of grain size on initiation gradient determined in slope-type experiments and plane-type experiments

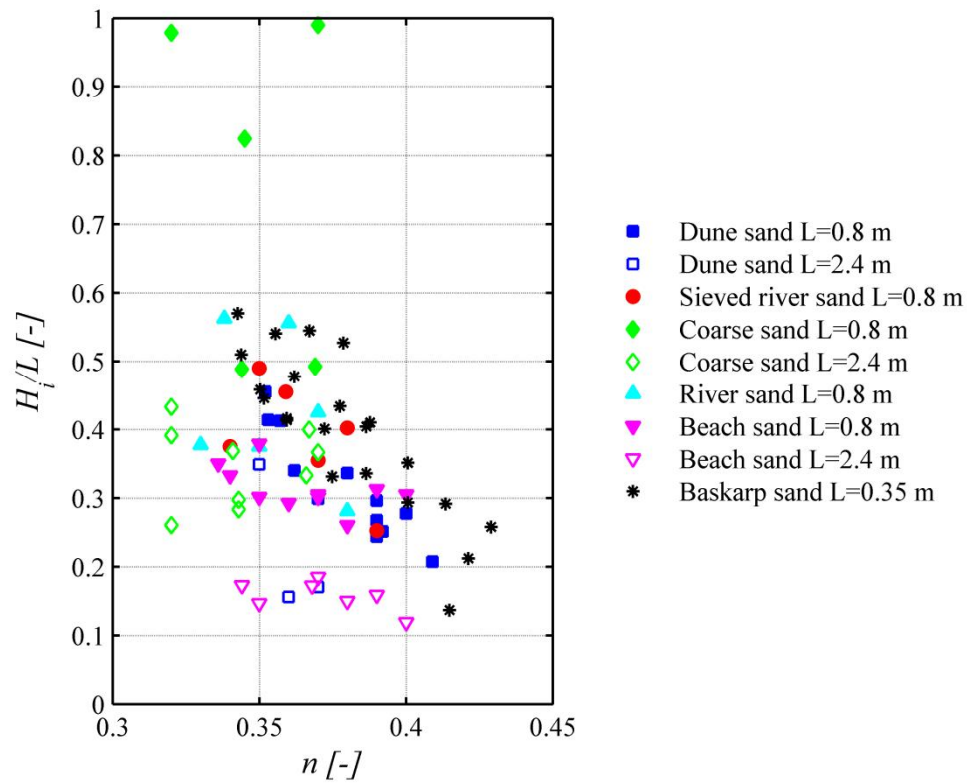


Figure 5.6. Effect of porosity on initiation gradient

As the head required for fluidisation is linked to porosity, the gradient required for initiation of pipe development is also likely to be affected by this parameter. A fall in the overall gradient is expected with increasing porosity. Both De Wit (1984) and Van Beek et al. (2011) investigated this parameter in area-type experiments and slope-type experiments respectively (Figure 5.6). The role played by porosity in slope-type experiments may be different than in the case of plane-type areas because the slope angle and friction angle, which determine the onset of grain movement on a slope, are also affected by the porosity of the sand sample. Although the gradient did fall with increasing porosity in most sand types, it is remarkable that the initiation gradient proved more sensitive to porosity in some sand types than in others.

5.3.5. RELATIONSHIP BETWEEN H_B AND H_C

In the experiments by De Wit (1984), sand boiling often precedes sand transport. The head for sand boiling (H_b) and the head for sand transport (H_c) were reported and the general description indicates that sand transport resulted in ongoing pipe development so that the critical head was found to be equal to the initiation head.

Theoretically, the fluidisation of the sand is a precondition for sand boiling. Sand boiling can therefore be expected to lead to sand deposition after only a small head increase. Although this is indeed the case in most experiments, H_b is very different from H_c in some cases.

Bearing in mind the fact that, when the experiments were performed, it was not realised that equilibrium occurs in some experiments and that, depending on the configuration or scale, equilibrium need not occur in other cases, it is possible that the experiments in which there was a large difference between H_b and H_c were progression-dominated rather than initiation-dominated. Detailed descriptions of experiments with the ditch-type exit (De Wit, 1982) show that this was the case in the larger-scale ditch-type experiments (model VII).

On average, the differences between H_b and H_c are larger for the experiments with coarse sand and the difference increases in line with increasing relative density in most sand types. In other configurations, such as the ditch-type configuration, the scale affects the difference: much larger differences are found in larger-scale experiments than in their small-scale equivalents.

5.4. MODEL DEVELOPMENT

5.4.1. THEORY OF PIPE INITIATION

On the basis of experiments and theory, Terzaghi (1922) noted that the magnitude and distribution of seepage forces near the toe of a water-retaining structure, and particularly the discharge gradient at the toe, determine whether piping or underground erosion will occur. The onset of particle movement requires the uplift of particles. The critical heave gradient (i_c) that causes the fluidisation of the granular material is based on the vertical equilibrium of the granular material, which depends in turn on the soil porosity (n), particle density (ρ_s) and water density (ρ_w):

$$i_c = -(1-n) \left(\frac{\rho_s - \rho_w}{\rho_w} \right) \quad 5.1$$

This criterion is considered to be valid for internally stable soils that move 'en masse' in the vertical direction as a result of a uniformly distributed upward flow.

Many column experiments have been performed to study this criterion. Experiments of this kind determine the average gradient across the soil sample in the column at which fluidisation occurs. Rice and Swainston-Fleshman (2013) observed three stages: movement, boiling and then total heave, noting that in some experiments the boiling phase was not seen. The experimentally observed average gradient for the first movement appeared to be close to the Terzaghi heave criterion, but both the first movement of particles and the boiling of sand led to an increase in the final critical heave gradient by approximately a factor of two due to the distortion of the sample, which resulted in non-uniform flow. In addition, the roughness of the test-device wall and the angularity of the grains appeared to lead to an increase in the critical heave gradient obtained experimentally. Here, it should be noted that the flow pattern at the micro-scale along the wall of the test set-up differs from the flow in a more realistic situation. However, soil angularity and 'wall' resistance may be relevant factors requiring further research.

Lower values for the critical heave gradient than those found using equation 5.1 have been observed in internally unstable suffusive soils (Skempton and Brogan, 1994) or for sloping surfaces. Van Rhee and Bezuijen (1992) investigated the erosion of grains on a sloping surface, subjected to a flow perpendicular to the surface, comparing continuum and particle approaches with experimental results. They concluded that a continuum approach for predicting erosion fits the experimental results for outward flow best. This also conforms with theory: if a single grain is lifted from the bed, the seepage forces on this grain immediately decrease and the grain falls back to the surface. To cause erosion, a group of particles needs to be uplifted. It is therefore more likely that erosion depends on the exit gradient exerted on a group of grains rather than on the exit velocity exerted on a single grain.

The equation for the critical gradient depends not only on the angle of the sloping surface (β) but also on the friction angle (ϕ):

$$i_c = -(1-n) \left(\frac{\rho_s - \rho_w}{\rho_w} \right) \frac{\sin(\phi - \beta)}{\sin(\phi)} \quad 5.2$$

Equations 5.1 and 5.2 will be used as the criteria for the initiation of piping in the subsequent analyses in this chapter.

5.4.2. EXIT GRADIENT ANALYSIS

Most experiments to investigate heave criteria are performed in columns: test set-ups with a unidirectional flow, where the average gradient in the soil sample H/L equals the exit gradient (here: i). In backward erosion experiments, however, the flow pattern is not unidirectional. Large flow differences are present near the structure toe on the downstream side. The average gradient H/L across the structure is therefore not equal to the local exit gradient i near the toe on the downstream side. Given an average

gradient across the structure (H/L), the exit gradient (i) can be calculated as a function of the distance from the toe using groundwater calculations for the specific geometry.

To determine the conditions at which a pipe is initiated, it is necessary to determine the relationship between the local exit gradient (i) near the toe of the structure and the overall average gradient (H/L). The exit gradient is largely dependent on the geometry of the outflow surface and on the shape and size of the sand layer. Several types of geometry are considered here – plane-, ditch- and slope-type (Figure 2.2) – which correspond to the geometries of experiments in the laboratory.

To calculate the exit gradient, analytical solutions are preferable to numerical solutions because they provide more accurate results close to the exit. Polubarinova-Kochina (1962) provides a solution for the exit gradient (i) at the surface downstream of the toe for a confined aquifer (below a dam) with a plane-type exit. Using this equation (5.3), the exit gradient i can be calculated for the plane-type experiments (Figure 1a), which, in essence, simulate the downstream half of the dam described in Polubarinova-Kochina (1962). In equation 5.3, the x -coordinate is defined as the distance from the upstream filter, the thickness of the sample is D , the head drop applied over the sand sample is H , the shortest distance from the upstream filter to the downstream plane is the seepage length L , and K is a complete elliptic integral of the first kind over m , as seen in equation 5.4.

$$i = \frac{H\pi}{2KD} \frac{\cosh\left(\frac{\pi L}{2D}\right)}{\sqrt{\sinh\left(\frac{\pi(L+x)}{2D}\right)\sinh\left(\frac{\pi(x-L)}{2D}\right)}} \quad 5.3$$

in which:

$$K = \int_0^{\frac{1}{2}\pi} \frac{d\varphi}{\sqrt{1-m\sin^2\varphi}} \quad m = \tanh^2\left(\frac{\pi L}{2D}\right) \quad 5.4$$

There are no standard solutions available for the flow in a ditch-type configuration. Using conformal mapping, the complex potential Ω ($\Omega = \Phi + i\Psi = k\varphi + i\Psi$, in which Φ is the ground water potential, k the permeability, φ the groundwater head and Ψ the stream function as a function of the complex coordinate z ($z = x + iy$)) can be obtained for this configuration (Figure 5.7). The geometry in the z -plane can be mapped onto the Ω -plane, where boundary AB is a line of constant potential (equal to 0) and line CC (with a constant potential) is situated at infinity on the right. Line DD is situated at infinity at the left and has no prescribed potential. The entire flow passes AB and CC, and it is equal to Q . Equation 5.5 fulfils this mapping. The sample thickness is defined as h and the width of the ditch is s (Figure 5.7).

$$\cosh^2\left(\frac{\pi \Omega}{2Q}\right) = \frac{\exp\left(\frac{\pi z}{h}\right) - 1}{\exp\left(\frac{\pi s}{h}\right) - 1} \quad 5.5$$

The complex velocity $\bar{w} = -k \frac{\partial \varphi}{\partial x} + ki \frac{\partial \varphi}{\partial y}$ is obtained by taking the derivative of equation 5.5 with respect to z :

$$-\frac{\bar{w}h}{Q} \cosh\left(\frac{\pi}{2} \frac{\Omega}{Q}\right) \sinh\left(\frac{\pi}{2} \frac{\Omega}{Q}\right) = \frac{\exp\left(\pi \frac{z}{h}\right)}{\exp\left(\pi \frac{s}{h}\right) - 1} \quad \frac{d\Omega}{dz} = -\bar{w} \quad 5.6$$

Rewriting and substituting the boundary condition for AB (complex component of z equals 0) results in equation 5.7, which gives the complex velocity for line AB.

$$\bar{w} = \frac{1}{h} \frac{-Q}{\sqrt{1 - \exp\left(\pi \frac{-x}{h}\right)} \sqrt{1 - \exp\left(\pi \frac{s-x}{h}\right)}} \quad 5.7$$

in which Q can be defined using equation 5.5 by filling in the upstream potential $k\phi_0$ at distance $L+s$, assuming that distance $x=L+s$ is large enough to make Q constant:

$$\cosh^2\left(\frac{\pi}{2} \frac{k\phi_0}{Q}\right) = \frac{\exp\left(\pi \frac{L+s}{h}\right) - 1}{\exp\left(\pi \frac{s}{h}\right) - 1} \quad 5.8$$

The exit gradient is then obtained by dividing the modulus of the velocity w by the permeability k :

$$i = \frac{|\bar{w}|}{k} = \frac{\pi H}{2h} \left[\sqrt{1 - \exp\left(\pi \frac{-x}{h}\right)} \sqrt{1 - \exp\left(\pi \frac{s-x}{h}\right)} \operatorname{arccosh} \sqrt{\frac{\exp\left(\pi \frac{L+s}{h}\right) - 1}{\exp\left(\pi \frac{s}{h}\right) - 1}} \right]^{-1} \quad 5.9$$

For larger values of s , the gradient i obtained with equation 5.9 converges to the value for i obtained with equation 5.3 for plane-type experiments.

The exit gradient i in the slope-type experiments was not determined analytically since the semi-permeable downstream filter rendered analytical analysis impossible. It should be noted that these experiments were not designed for initiation analysis. Given this, a numerical calculation was conducted using the 2D finite element model MSeep (GeoDelft, 2002). Numerical models can be refined to deliver output very near to the singularity, but this will always result in an averaged value for the exit gradient rather than an exact value. The numerical analysis was therefore combined with an exact solution that was likely to be valid near the singularity.

The exact solution for groundwater flow near a sloping exit is determined using conformal analysis. The conformal mapping scheme for this situation is shown in Figure 5.7 (bottom figures).

The complex potential as a function of a complex coordinate is:

$$\frac{\Omega}{kH} = \left(-\frac{z}{\lambda}\right)^{\frac{1}{2\alpha}} \quad \alpha = 1 - \frac{\beta}{\pi} \quad 5.10$$

in which λ represents a scaling parameter and β is the slope angle with the horizontal. The exit velocity can be obtained by taking the derivative of the complex potential with respect to z .

$$\frac{d\Omega}{dz} = -\bar{w}$$

$$\bar{w} = \frac{kH}{2\alpha\lambda} \left(-\frac{z}{\lambda} \right)^{\frac{1}{2\alpha}-1}$$

5.11

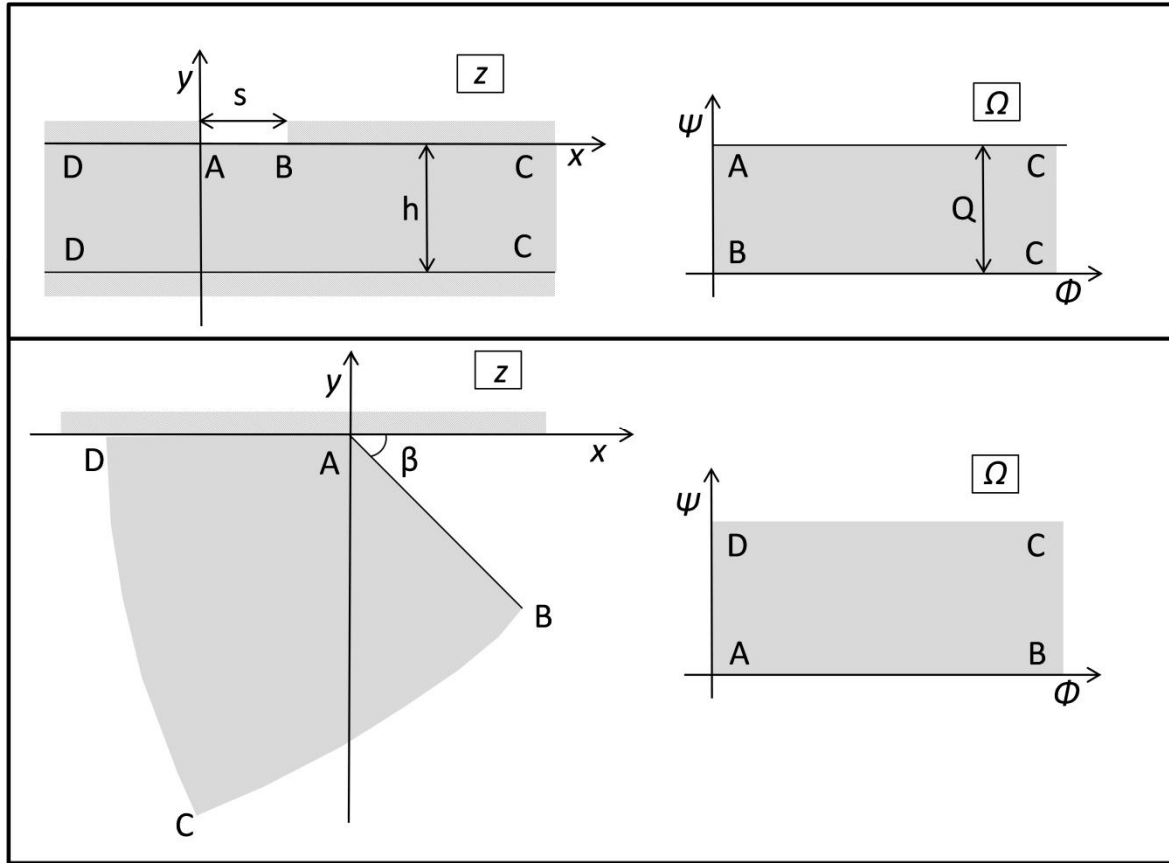


Figure 5.7. Conformal mapping schemes for a ditch (top) and a slope (bottom)

The absolute value of the exit velocity w is now expressed as a function of the distance along the slope, r , by replacing z ($z = re^{-i\beta\pi}$). As the modulus of the exponential of any imaginary number is equal to one, the absolute value of the exit gradient can be written as in equation 5.12, after dividing the modulus of the complex exit velocity by the permeability.

$$i = \frac{|\bar{w}|}{k} = \frac{H}{2\alpha\lambda} \left(\frac{r}{\lambda} \right)^{\frac{1}{2\alpha}-1} \quad 5.12$$

Since λ is a scale parameter, it is easy to conclude from equation 5.12 that the effect of scale (denoted by L or λ) on the average gradient (H/L) is defined by the inverse square root of L if $\alpha=1$, thus $\beta=0$ (see equation 5.10). As will be shown later, this effect is equal to the effect found in plane-type experiments.

Figure 5.8 shows an example of the flow net and exit gradient profile obtained with equations 5.10 and 5.12. Fitting the scaling parameter λ to the numerical results gives

the exit gradient profile near the singularity (Figure 5.8, right). It should be noted that the analytical solution is only valid when the sample can be regarded as a continuum.

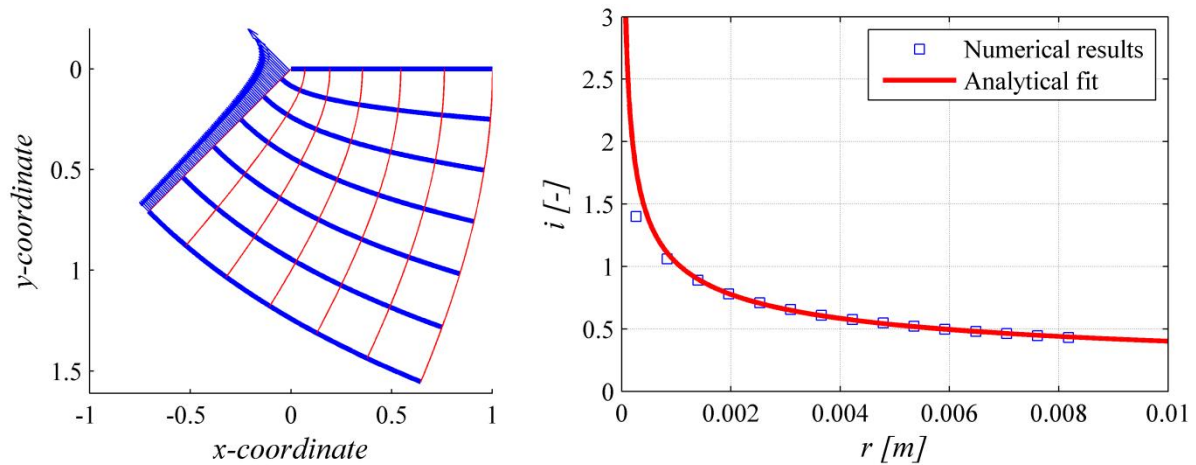


Figure 5.8. Flow net and corresponding numerically obtained exit gradients and analytical fit for experiment B19

5.4.3. EXPERIMENT ANALYSIS

The exit gradient analysis in the previous section allows for the calculation of the actual exit gradient in the experiments at the head at which a pipe was initiated.

Heave can only occur if a group of grains is subjected to a certain gradient. However, theoretically, the exit gradient increases to infinity when the toe of the embankment, which is a singular point, is approached. In reality, the flow will be controlled by the micro-scale processes around the grains. In the approach proposed here, it is assumed that the gradient across a group of grains will determine whether heave will take place. The actual size of this group is unknown. However, the size of the expansion area has been observed in experiments and is estimated to be 15-20 mm in width for fine sands (De Wit, 1984), which may be an indication of the distance across which the sand needs to be fluidised. The present study verified whether the initiation gradient H_i/L was indeed determined by local fluidisation near the toe of the simulated embankment. The equations in the previous section – which describe the relationship between exit gradient and head across the structure – were used for this purpose. By applying the initiation gradients H_i/L obtained from the experiments, the exit gradients (i) were calculated as a function of distance from the toe for the situation in which the pipe was initiated. Subsequently, the distance dx from the embankment toe was calculated at which the actual exit gradient i in the experiments equalled the critical heave gradient i_c (this concept is illustrated in Figure 5.9). This distance can be expressed as a number of grains in the lateral direction and will be denoted as the group size a .

It is argued here that the size of the group of grains that has to be uplifted to initiate a pipe is independent of the scale and configuration of the setup and grain size. To verify this assertion, the size of the group of grains to be uplifted is calculated in the following sections using the initiation gradients obtained from the available experiments. If the hypothesis is true, the calculated group size should be in the same range for all experiments, without variations depending on scale or grain size.

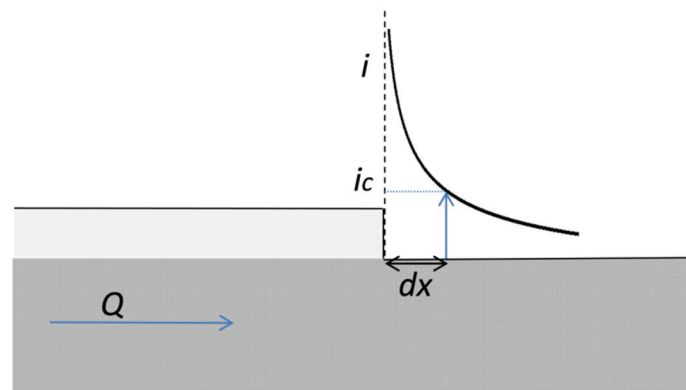


Figure 5.9. Conceptual model to determine the group size

Plane-type experiments

The theoretical critical heave gradient (i_c) was calculated for all available plane-type experiments (Appendix A) using equation 5.1. Using the geometry of the sand layer and the initiation gradient as observed in the experiments, the actual exit gradient profile along the surface was calculated as a function of the distance from the toe. The distance dx from the simulated embankment toe at which the critical heave gradient i_c equalled the exit gradient i was calculated for each experiment.

Using this approach, it is possible to explain scale effects, that is to say differences in initiation gradients H_i/L as a result of differences in the dimensions of the set-up. The obtained distances dx , which indicate the size of the group to be uplifted, were calculated for all available plane-type experiments with Beach sand to observe the effect of scale. The distance dx is expressed as the number of grains a in the lateral direction by:

$$dx = a \cdot d_{50} \quad 5.13$$

Figure 5.10 (left) shows that calculations of the typical group size a in Beach sand experiments result in values that are approximately 20-60 times the average grain diameter (or 4-12 mm), regardless of the dimensions of the experiment. This number is of the same order of magnitude as the size of the expansion area observed in these experiments. The wide scatter in the results is, in part, linked to experimental deviations, as can be seen in the experiments where $L=1.2$ m; these experiments were identical in all aspects but there was considerable scatter in the outcomes. Given the proposed theory that local fluidisation of the sand bed in a very small zone initiates piping, this seems reasonable. The experimental scatter in the initiation gradient H_i/L may have been caused by small variations in density and permeability, which have a large impact on the exit gradient near the toe of the simulated embankment. There is uncertainty about the homogeneity of the compaction and the degree of saturation for the experiments of De Wit (1984), and this may explain the scatter.

Although the analysis included experiments with different dimensions (L and D/L) and consequently variation in the initiation gradients H_i/L , the group size a was not found to be linked to these parameters. This analysis therefore shows that differences in the initiation gradient (H_i/L) as a result of the scale and shape of the sand sample can be explained by the relationship between the gradient across the structure H/L and exit

gradient i exerted on a small group of grains. The scale effects can be explained as follows: the linearity of the laminar groundwater flow in saturated conditions causes the flow velocity distribution to be linearly dependent on scale, but the size of the grains does not change with scale. Consequently, when considering the exit gradient for a group of grains in a large-scale experiment, this group of grains is closer to the toe of the embankment in relative terms than in a small-scale experiment. As the convergence of flow lines near the toe of the structure causes the exit gradient i there to rise (theoretically) to infinity (Figure 5.9), the exit gradient across this group is higher when the group of grains is situated closer to the structure toe. This is seen in Figure 5.9, which shows a group size dx as well as the corresponding exit gradient i . As the curve of the exit gradient in Figure 5.9 is independent of scale, a larger scale can be imagined in which the group size dx , which does not change with scale, is situated closer to the toe in relative terms and is therefore subjected to a higher exit gradient i .

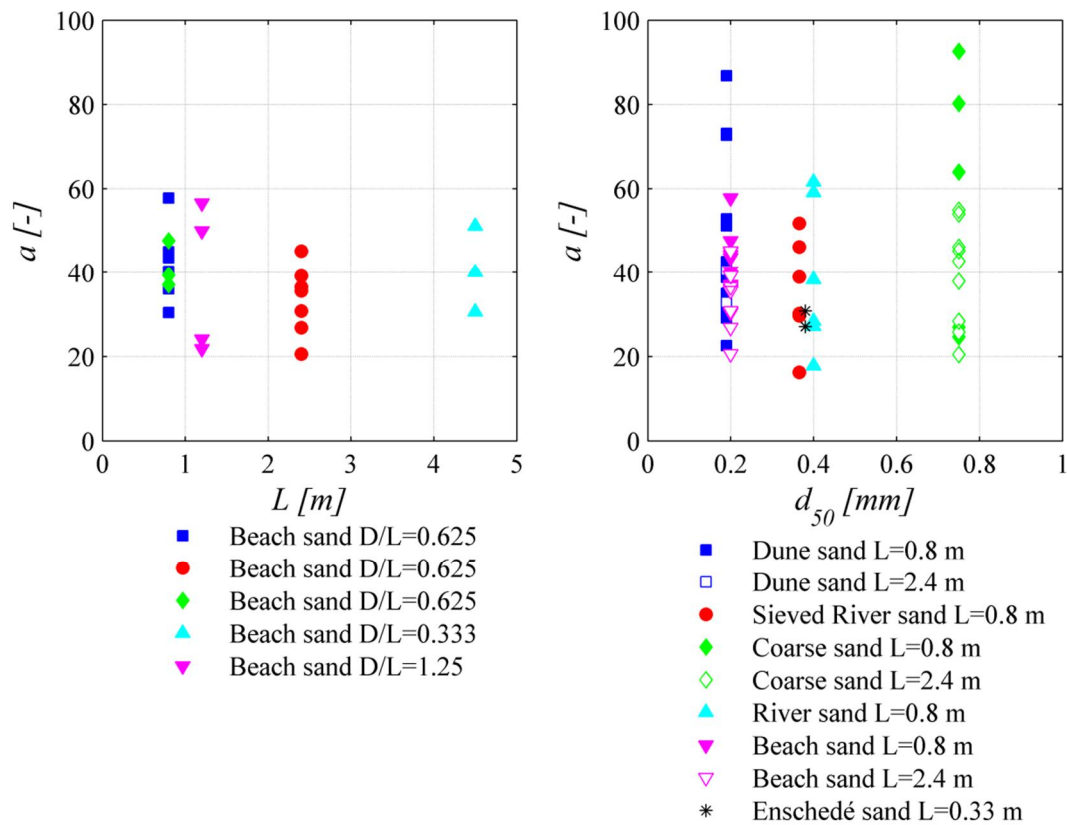


Figure 5.10. Calculated heave group size as function of seepage length and grain size (experiments by De Wit (1984) and additional small-scale experiments on Enschedé sand)

In large-scale experiments, therefore, the initiation gradient H_i/L is relatively low, since the group of grains to be fluidised is located close to the toe of the embankment in relative terms (and thus close to the singularity) by comparison with the overall dimensions of the set-up. In small-scale experiments the initiation gradient H_i/L is relatively high, because the group of grains is located further from the toe in relative terms.

The effect of grain size on the initiation gradient (Figure 5.10, right) can be analysed in a similar manner. If it is assumed that the size of the group of grains that will be uplifted, expressed as a number of grains, remains the same, the experiment with larger grains requires the exit gradient i to equal the critical heave gradient i_c at a larger distance from the toe, and this results in a higher overall gradient across the sand sample.

Figure 5.10, which shows the calculated group size for different sand types, validates the explanations given here. Figure 5.10 shows that the group of grains to be transported is independent of grain size or scale, and even shape (varying D/L ratio). The minimum group size appears to be approximately 20 grains. Until now, it has been assumed that a continuum approach is valid. Al Hattamleh et al. (2009) prove that the representative elementary volume (REV) radius for estimating the porosity of rounded sand is approximately 9-16 times the d_{50} . It can be expected that the REV radius for groundwater flow will be in the same range. The continuum approach is therefore likely to be valid for a range of 20 grains.

The effect of porosity on the critical head was investigated for several sand types. Figure 5.11 (left) shows that, due to the scatter of the initiation gradients obtained in experiments, the relationship between porosity and initiation gradient is not always clear. A clear trend was obtained in two experiment series – the experiments on Beach sand and Dune sand – with the main difference being the friction angle. The heave group size a for these experiments is presented in Figure 5.11 (right).

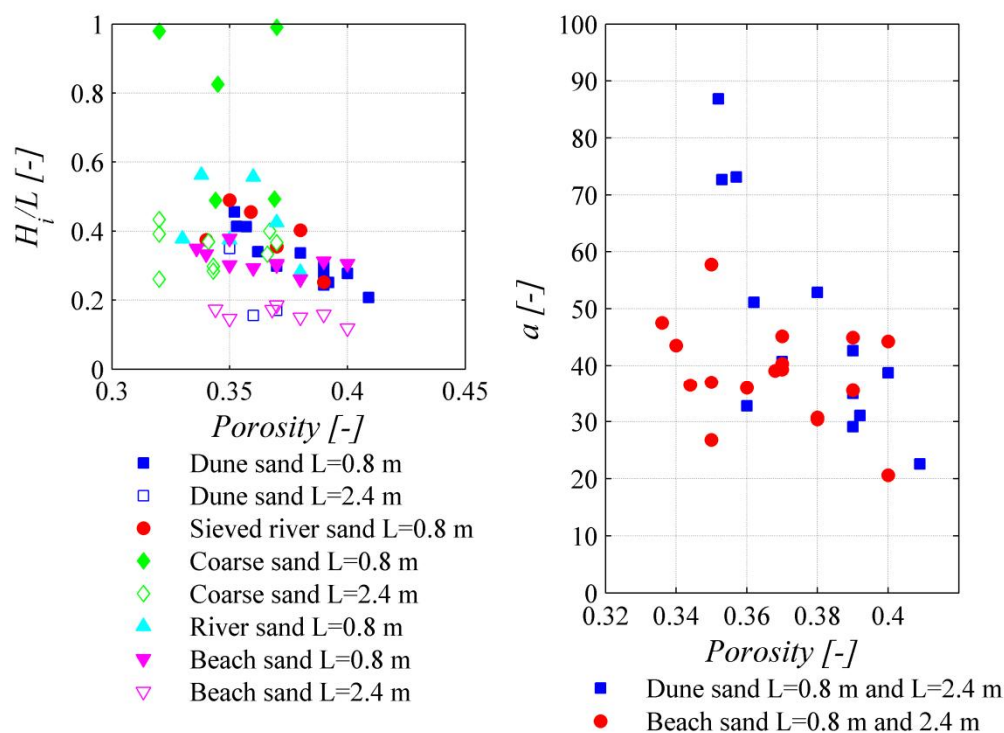


Figure 5.11. Effect of porosity on critical gradient and calculated heave group size for the experiments with Dune sand and Beach sand

It can be seen that the trend observed in Figure 5.11 – that is to say, the fall in the initiation gradient with increasing porosity – is not fully corrected by a change in the critical heave gradient i_c alone. The group size should be constant when the effect of porosity has been included correctly, but, particularly in the case of Dune sand, a fall in group size was observed as porosity increased. Large group sizes found in experiments on sand with low porosity indicate that the initiation gradient is larger than in the high-porosity samples. This behaviour could be explained by the inter-particle friction, which is not taken into account in the current approach. Rice and Swainston-Fleshman (2013) report that wall friction has a significant effect on the critical heave gradient: silicon-coated columns result in critical gradients that are approximately 1.5 times higher than in the case of smooth columns. Loezos et al. (2002) performed gas fluidisation in sand columns. They noted that wall friction is the main cause of pressure overshoot and that it increases with decreasing diameter of the column. In backward erosion experiments, where only part of the sample fluidises, the 'wall' consists of those sand particles that are not fluidised. Given that the area of fluidisation is very small, the friction at the interface of fluidised and non-fluidised sand could affect the fluidisation gradient. The 'wall friction' for fluidisation of a small local zone in a larger sand sample is therefore likely to depend on the friction angle of the sand and the interlocking of particles. The friction angles for Dune sand are higher than those for Beach sand. The difference in friction angle could be related to the grain roundness. A comparison of the particles of both sand types with grain roundness classification charts showed that Dune sand is slightly more angular than Beach sand. Another possible explanation for the difference in initiation gradients for the two sand types is the distortion of the sand sample, where it has expanded and loosened as a result of water pressure, a process that takes place in dense sand samples before the sand is fluidised. If the sand is loosened near the toe only, the total flow towards the exit will not increase. The increase of permeability in this loose zone near the toe will therefore result in a local fall in the exit gradient. As a result, the initiation gradient H_i/L needs to be increased before total fluidisation can occur near the toe. Although this may explain why group size a varies with porosity, it cannot explain the difference in the trend for porosity and group size for Beach sand and Dune sand, since the increase in permeability with porosity (which can be derived from the relationship between porosity and permeability using the values in Appendix A) is comparable for both types of sand. The cause of the difference between the trends therefore remains rather unclear. Experimental scatter or differences in wall friction, caused by differences in the friction angle or the interlocking of grains, remain as speculative explanations.

Ditch-type experiments

The available ditch-type experiments are listed in Appendix A. The effect of scale and porosity on the critical head have been investigated using Beach sand (De Wit, 1984). The exit gradient i at the surface of the ditch can be calculated using equation 5.9. Using the same approach described in the previous section for each experiment, the distance dx was determined at which the exit gradient i equalled the critical heave gradient i_c (calculated using equation 5.1).

In some experiments, it was found that the calculated exit gradient i exceeded the heave gradient i_c at every location in the ditch. In these experiments (mainly the larger-scale experiments and experiments with dense sand only) the difference between the

required head for sand boiling H_b and sand transport H_i was large. When applying the head for sand boiling H_b , instead of the head at which the first sand transport is observed H_i , the exit gradient was found to be slightly smaller across the width of the ditch, making it possible to determine the heave group size in most of the experiments.

Chapter 3 describes the effect of the configuration of the setup on the initiation and progression heads. Large-scale experiments and experiments with small exit areas are likely to be dominated by progression rather than by initiation. It is likely that the small exit area in these experiments resulted in a reduction of the sand boiling head. As the ditch width was the same in all ditch-type experiments, the exit area was small in relative terms in the large-scale experiments. It is possible that, although the general observations in the ditch-type experiments match the observations in plane-type experiments (De Wit, 1984), the required head for progression exceeded the head for pipe initiation, causing the critical head to be higher than might have been expected on the basis of initiation theory. Detailed descriptions of the ditch-type experiments (De Wit, 1982) do indeed show that an increase in the head is required after sand transport has occurred. The initiation head was approximately equal to the sand boiling head in these experiments and these observations therefore validate the approach described.

Despite the application of H_b , the value of the group size a is still large for the dense samples. Another possible explanation for the large initiation gradients in ditch-type experiments could be that the grains are locked in more tightly in the ditch-type experiments than in the plane-type experiments because of the concentration of flow lines towards the ditch (bridging). A third explanation is that the dense sand samples result in higher wall friction, a result of inter-particle friction and the interlocking of grains, leading to more resistance than would be expected on the basis of the critical heave gradient. Finally, the distortion of the sample due to loosening before fluidisation takes place is likely to reduce the exit gradient, as was the case in the plane-type experiments. However, expansion is likely to occur over a larger area in a ditch-type experiment, since the exit gradient is also high for the downstream side of the ditch, and so the effect on the exit gradient i differs from that in the plane-type experiments.

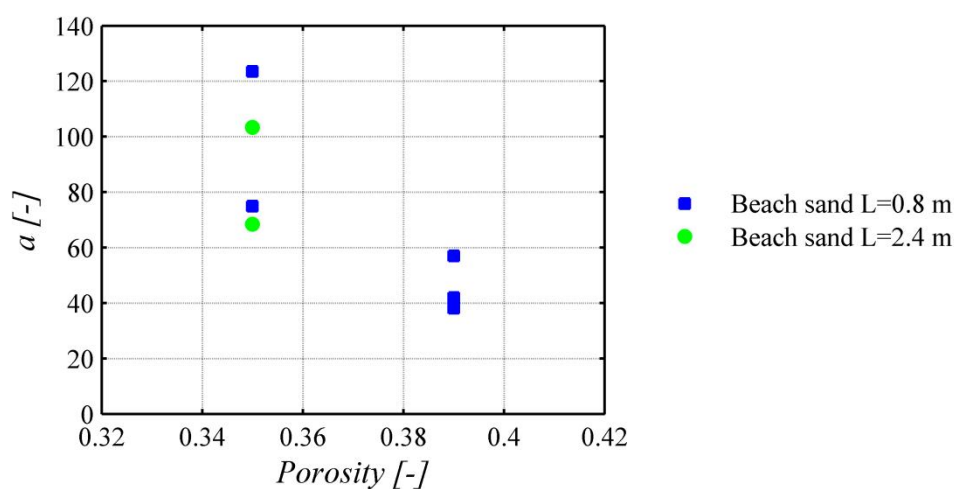


Figure 5.12. Calculated heave group size as function of porosity for Beach sand experiments with a ditch-type exit

Figure 5.12 shows the group sizes obtained using the sand boiling head H_b . Although only a few experiments are available, it is reasonable to conclude that the group sizes in experiments with loose sand are in the same range as in area-type experiments, but that there is more scatter. The calculated group heave size appears to be in the same range at different scales, suggesting that scale effects can be explained satisfactorily using this theory.

Slope-type experiments

Slope-type experiments were performed for different sand types, porosities and scales (small $L \approx 0.35$ m and medium $L \approx 1.40$ m). The experiments were not designed to study the initiation of piping. Furthermore, relevant parameters such as the slope angle and geometry were not determined accurately during the experiments. Nevertheless, the experiments were dominated by the process of initiation and pipe formation was seen to occur where the exit gradients were highest (Figure 5.8) near the top of the sand sample, as in the plane- and ditch-type experiments.

Table 5.2 lists the experiments with Baskarp sand. The critical heave gradient i_c was calculated using equation 5.2. The slope angle, which was determined using photographs of the experiments, has a major impact on the critical heave gradient i_c and this resulted in a wide margin of inaccuracy.

Table 5.2. Slope-type experiments (Van Beek et al., 2011, improved filter correction) and scaling parameter λ

Test no.	Sand type	L [m]	D [m]	β [deg]	n [-]	k [m/s]	i_c [-]	H_i [m]	H_c [m]	λ^* [m]
B19	Baskarp sand	0.340	0.100	28	0.386	1.5E-04	0.360	0.114	0.114	1.18
B23	Baskarp sand	0.338	0.100	28	0.343	5.9E-05	0.441	0.193	0.193	1.31
B24	Baskarp sand	0.338	0.100	27	0.344	6.8E-05	0.464	0.172	0.172	1.30
B28	Baskarp sand	0.335	0.100	22	0.421	2.7E-04	0.441	0.071	0.071	1.18
B35	Baskarp sand	0.335	0.100	23	0.386	1.3E-04	0.479	0.135	0.135	1.28
B36	Baskarp sand	0.334	0.100	24	0.388	1.1E-04	0.441	0.137	0.137	1.27
B40	Baskarp sand	0.332	0.100	22	0.352	5.3E-05	0.571	0.148	0.148	1.38
B41	Baskarp sand	0.334	0.100	23	0.350	7.3E-05	0.563	0.153	0.153	1.35
B54	Baskarp sand	0.330	0.100	25	0.367	7.4E-05	0.457	0.180	0.180	1.28
B55	Baskarp sand	0.325	0.100	21	0.377	8.8E-05	0.548	0.141	0.141	1.31
B57	Baskarp sand	0.330	0.100	23	0.372	8.8E-05	0.508	0.132	0.132	0.89
B58	Baskarp sand	0.345	0.100	21	0.379	1.0E-04	0.536	0.182	0.182	1.09
B61	Baskarp sand	0.345	0.100	24	0.375	9.9E-05	0.467	0.114	0.114	0.51
B82	Baskarp sand	0.336	0.100	26	0.359	5.9E-05	0.459	0.139	0.139	0.98
B83	Baskarp sand	0.334	0.100	24	0.359	6.0E-05	0.498	0.139	0.139	1.03
B84	Baskarp sand	0.334	0.100	25	0.401	9.7E-05	0.388	0.098	0.098	0.91
B85	Baskarp sand	0.336	0.100	27	0.401	7.7E-05	0.360	0.118	0.118	0.93
B86	Baskarp sand	0.336	0.100	27	0.414	1.0E-04	0.333	0.098	0.098	0.90

B87	Baskarp sand	0.336	0.100	27	0.415	1.8E-04	0.331	0.046	0.046	0.75
B101	Baskarp sand	0.310	0.100	19	0.408	1.0E-04	0.505	0.080	0.080	0.90
B103	Baskarp sand	0.320	0.100	20	0.438	1.6E-04	0.406	0.080	0.080	0.90
B105	Baskarp sand	0.335	0.100	28	0.362	7.6E-05	0.408	0.160	0.160	0.94
B107	Baskarp sand	0.333	0.100	28	0.355	6.1E-05	0.421	0.180	0.180	0.95
B121	Baskarp sand	0.335	0.100	22	0.426	1.8E-04	0.379	0.090	0.090	0.71
B122	Baskarp sand	0.335	0.100	21	0.430	1.6E-04	0.387	0.080	0.080	0.72
Bms1	Baskarp sand	1.370	0.400	25	0.392	1.2E-04	0.446	0.220	0.280	1.47
Bms2	Baskarp sand	1.450	0.400	25	0.405	1.4E-04	0.434	0.290	0.370	1.00
Bms7	Baskarp sand	1.300	0.400	25	0.386	1.5E-04	0.451	0.140	0.290	2.08
Bms8	Baskarp sand	1.330	0.400	25	0.405	2.6E-04	0.434	0.190	0.190	2.13

* Obtained by fitting the analytical solution to the numerical solution

Figure 5.13 shows the slope angle determined as a function of porosity for Baskarp sand. A very weak correlation was observed between slope angle and porosity, but there was considerable scatter. A correlation was expected as the slope was formed naturally after the removal of part of the sand sample. Theoretically, the slope angle should equal the angle of repose, which is related to the porosity. The scatter in slope angles was presumably caused by the difficulty of determining this angle using photographs. In the medium-scale experiments, the slope angle could not be determined using the pictures. The slope angle was estimated on the basis of the slope angles observed in the small-scale experiments, using a least square correlation with porosity. The slope angle variation for dense sand samples (22-28 degrees) results in a range for the critical heave gradient (i_c) of 0.58 to 0.42, which indicates the degree of inaccuracy that can also be expected when predicting the initiation gradient for this type of experiment.

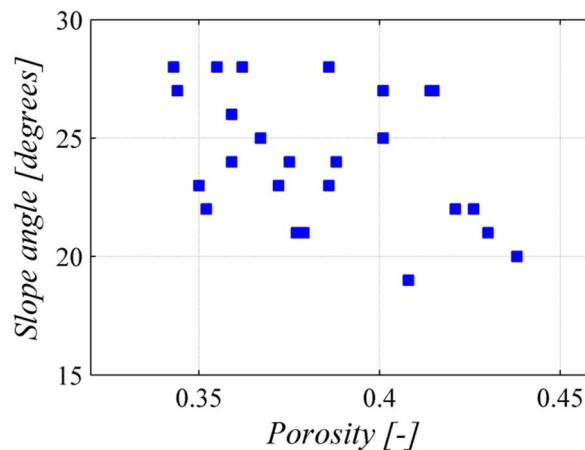


Figure 5.13. Observed slope angles as a function of porosity in small-scale Baskarp experiments

Using the initiation gradients in Table 5.2, and the numerical and analytical analysis of the exit gradient, the group size a was determined for each experiment. Figure 5.14 shows the group sizes obtained as a function of porosity. The scatter in experiments with this configuration was larger than in experiments with plane- and ditch-type

configurations. Local variations in density or poor saturation are unlikely to have caused the scatter since the slope-type experiments were prepared using the method proposed by Van der Poel and Schenkeveld (1998) described in Section 4.3, which ensures a well-saturated and homogeneous sample. The relatively short time interval used for the incremental steps in the head increase in the slope-type experiments could be another explanation for the scatter, but this is also considered to be unlikely. Although, in other types of internal erosion experiments, the time interval matters because the detachment of particles takes time and the gradual detachment of fines will alter the sample, the role of fine grain detachment will be negligible with the internally stable and uniform sands considered in this chapter. The process of backward erosion relies on the removal of groups of sand grains rather than the removal of fines from a matrix. The most likely causes of the scatter are therefore the variation in the slope angle, which was difficult to measure using photographs, or random irregularities at the interface of the sand and the acrylate cover.

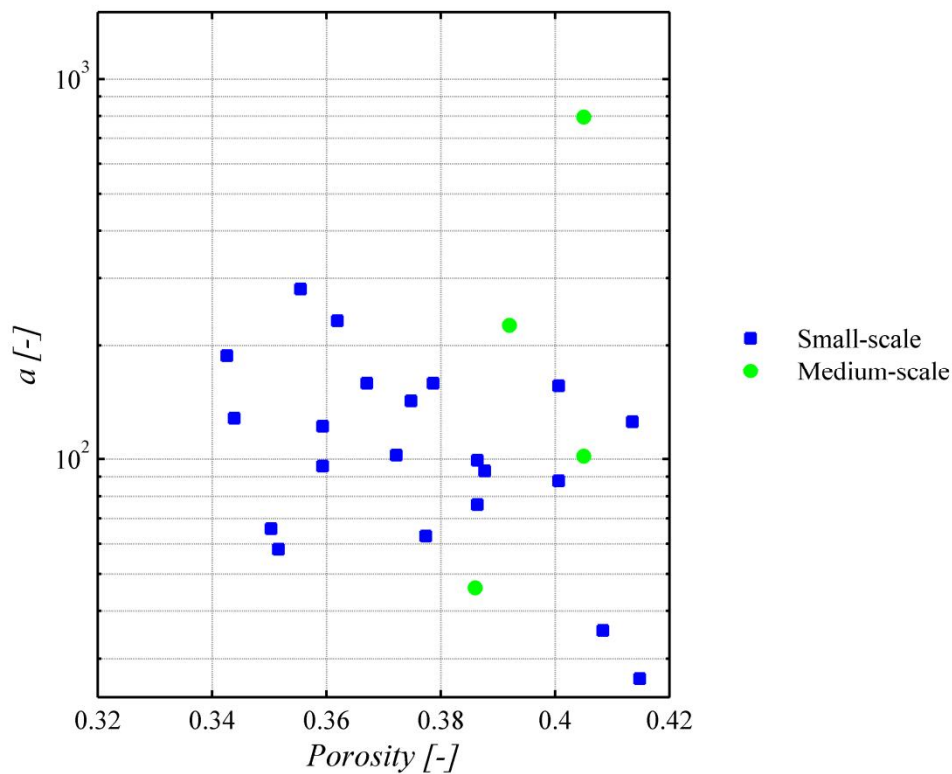


Figure 5.14. Calculated group sizes for small- and medium-scale slope-type experiments

Most of the medium-scale results are covered by the scatter for the small-scale results, although the initiation gradients (H_i/L) in medium-scale experiments are much lower than those in small-scale experiments. This indicates that the scale effect can be explained by the relationship between exit gradient i and H , as is stated in equation 5.11. The relationship between group size and porosity is similar to the relationships observed in the other configurations.

The wide scatter is presumably caused by the lack of accurate data for the slope angle and by the experimental scatter itself, which resulted from the differences in the slope

shape. Nevertheless, the range of group sizes obtained is not very different from group sizes obtained for the other configurations, which ranges from 24 to 232 in the small-scale experiments. In the Dune sand area-type experiments, the group size is still dependent on porosity, which could be explained by the inter-particle friction and interlocking of grains resulting in high wall friction, or by the loosening of the sand bed as a result of increasing water pressures. Despite the wide scatter and the unintended use of the experiments for pipe initiation analysis, the experiments seem to confirm the theory.

5.5. DISCUSSION

Equations for the relationship between the overall gradient (H/L) and the exit gradient (i) on the one hand, and the experimental initiation gradients (H_i/L) on the other, have been used here to determine the group size a across which the sand needs to be fluidised to cause pipe initiation. A minimum group size of approximately 20 grains was calculated for all experiments. This empirically obtained value allows for the prediction of a minimum value for the initiation head H_i across the structure that causes pipe initiation. Using the equations proposed in Section 5.4.2, in which the head drop across the structure H is related to the exit gradient i in different configurations, the initiation gradient H_i/L can be calculated as the head at which the exit gradient i equals the heave gradient i_c at a distance from the toe of 20 times the mean diameter of the sand ($x = 20 \cdot d_{50}$).

Table 5.3 shows the equations for the configurations with a plane-type exit and a ditch-type exit that predict the initiation gradient H_i/L . In the case of the slope-type exit, a numerical calculation is required to determine the parameter λ and therefore the equation is not presented here. However, once this parameter has been determined, the initiation gradient H_i/L can be determined in the same way by calculating the gradient H/L at which the exit gradient i equals the critical heave gradient i_c for a distance along the slope of 20 times the mean grain diameter ($r = |z| = 20 \cdot d_{50}$).

Table 5.3. Equations for prediction of initiation gradient for plane- and ditch-type configurations

Configuration	Equation
Plane-type exit	$\frac{H_i}{L} = i_c \frac{2K}{\pi} \frac{D}{L} \frac{\sqrt{\sinh\left(\frac{\pi(2L + 20 \cdot d_{50})}{2D}\right) \sinh\left(\frac{\pi(20 \cdot d_{50})}{2D}\right)}}{\cosh\left(\frac{\pi L}{2D}\right)}$ <p style="text-align: center;">in which:</p> $K = \int_0^{\frac{1}{2}\pi} \frac{d\varphi}{\sqrt{1 - m \sin^2 \varphi}} \quad m = \tanh^2\left(\frac{\pi}{2} \frac{L}{D}\right)$

Ditch-type exit	$\frac{H_i}{L} = -i_c \frac{2}{\pi} \frac{D}{L} \sqrt{1 - \exp\left(\pi \frac{20 \cdot d_{50} - s}{D}\right)} \sqrt{1 - \exp\left(\pi \frac{20 \cdot d_{50}}{D}\right)} \operatorname{arccosh} \sqrt{\frac{\exp\left(\pi \frac{L+s}{D}\right) - 1}{\exp\left(\pi \frac{s}{D}\right) - 1}}$
-----------------	--

The equations show that the scale (variation of L for constant D/L) and grain size affect the initiation gradient H_i/L . The initiation gradient was plotted as a function of the seepage length for the plane- and ditch-type configuration while all other parameters were kept constant (Figure 5.15). It emerged that, in both configurations, the initiation gradient changes scale in line with the inverse of the square root of L ($H_i/L \propto 1/\sqrt{L}$). Bezuijen and Steedman (2010) previously derived this scaling factor theoretically for a configuration with infinite depth.

Using the equations in Table 5.3 and the combined numerical/analytical approach described in Section 5.4.2 for the slope experiments, the initiation head H_i was calculated for all experiments evaluated in this paper (Figure 5.16). This model provides a good explanation of the differences in the initiation gradient associated with scale, configuration and grain size, as can be seen in Figure 5.16.

Figure 5.16 shows that the approach is conservative. This is because the group size for many experiments was found to be significantly larger than 20 grains. This is particularly the case with high-density sands, a finding which may be linked to inter-particle friction and interlocking, leading to the critical heave gradient i_c being larger than the values obtained with equations 5.1 and 5.2. Alternatively, it may be linked to the loosening of the bed and the resulting fall in the exit gradient. The difference in critical heave gradient for boiling and piping, as observed in some experiments and also by Rice and Swainston-Fleshman (2013), merits more detailed investigation.

The model not only explains variations in the initiation gradient H_i/L due to scaling; it also clarifies the process of backward erosion piping itself at different scales. Calculations with this model show that the initiation gradient H_i/L drops with the inverse of the square root of the seepage length $H_i/L \propto 1/\sqrt{L}$, assuming that other parameters, such as the grain size and ratio of thickness to length, remain constant. Progression of the pipe as predicted using the model of Sellmeijer (1988) is known to result in progression gradients that decrease with the inverse third-power root of the seepage length ($H_p/L \propto 1/\sqrt[3]{L}$). This explains why initiation is more likely to dominate in small-scale experiments and progression in large-scale experiments. To study the progression of the pipe in small-scale experiments (which will remain necessary because costs increase rapidly with the size of the setup), a different configuration should be used. For example, there should be a small circular exit hole in which the concentration of flow lines causes initiation to occur at a relatively low gradient with respect to the progression gradient (Van Beek et al., 2013). The understanding of the different processes and their scaling effects is essential to each experiment, regardless of the scale of the experiment.

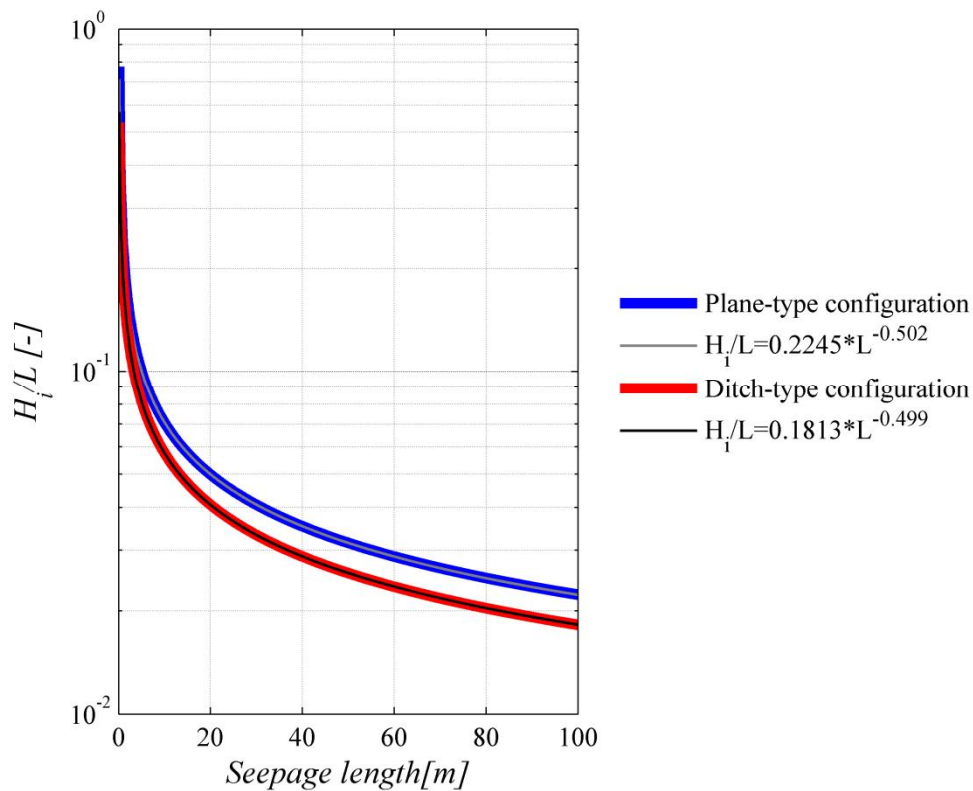


Figure 5.15. Illustration of the scale effects of the initiation gradient for plane- and ditch-type configurations, and their least square fits.

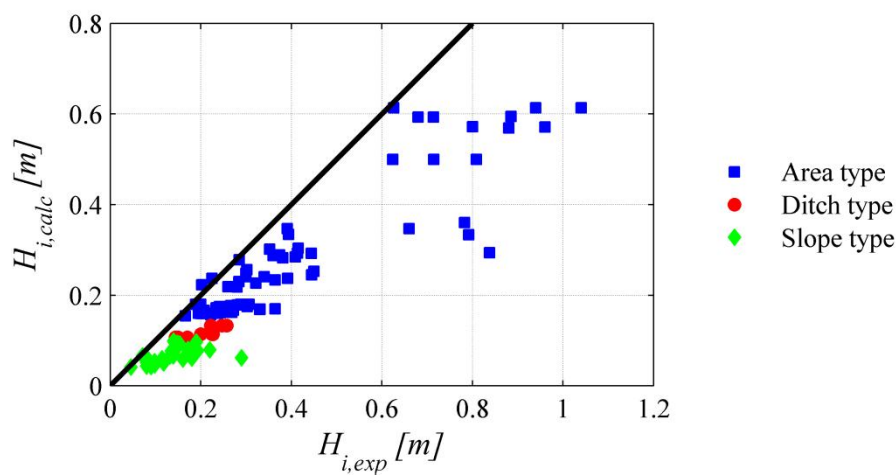


Figure 5.16. Experimentally obtained and calculated critical gradients

5.6. SUMMARY

Backward erosion is governed by two processes: pipe initiation and progression. As the mechanisms of the processes are different, which of the two processes determines the critical head leading to failure depends on scale and configuration. Observations in experiments illustrate that, in some experiments, the head at which the pipe initiates (H_i)

is equal to the critical head (H_c) at which the sample fails. In other experiments, after the initiation of the pipe, the head needs to be increased for the pipe to progress to the upstream side. The present study analysed experiments in which the initiation head equalled the critical head, or in which the initiation head was measured, to develop a model to predict pipe initiation.

The proposed model assumes the heave of a group of particles that causes the initiation of backward erosion. To validate this approach, relationships between the applied gradient H/L and the exit gradient i have been described and used to calculate the size of the group fluidised in each of the experiments. The group size obtained appears to be in the same range as in experiments with different scales, configurations and grain sizes, with a minimum of 20 times the mean grain diameter. Equations have been given for a conservative prediction of the initiation of piping for two configurations (listed in Table 5.3).

The understanding of the processes governing initiation and progression is essential for the further analysis of the topic. The understanding of the scaling effects of both mechanisms is required for the design of experimental work and an understanding of observations in the field.

The equations can be used to predict the initiation head H_i , but they are suitable for homogeneous samples only. Heterogeneity affecting the local flow pattern is likely to result in concentrated flows that will complicate the prediction of the initiation head. However, in the field, the approach could be useful for assessing the significance of a sand boil. A sand boil that emerges at a location where flow concentrates – such as an improperly closed borehole or at the end of a ditch that runs transverse to the embankment – is likely to initiate at a much lower head than the head required for progression. However, a sand boil that emerges in a sandy area is likely to initiate at a head close to the head for progression, and should be considered a more serious threat.

6. PIPE PROGRESSION

‘Die Primärerrosion gewährleistet die Fortentwicklung der Kanalspitze in Richtung des Oberwassers, während die Sekundärerrosion die Verbreiterung und Vertiefung des entstandenen Kanals herbeiführt.’

Ulrich Hanses

6.1. INTRODUCTION

In the field, pipe progression is more relevant for piping prediction than pipe initiation since the second mechanism is highly dependent on the exit conditions, which are often unknown in the field. Furthermore, the initiation of a pipe, as indicated by the presence of a sand boil in the field, does not necessarily lead to dike failure. In the Netherlands, sand boils are therefore tolerated. Some countries, such as the US, have adopted strict approaches in which sand boils are considered to be unacceptable. The probability of pipe progression can be estimated using a model that predicts the critical head, which, when exceeded, will lead to pipe progression. The Sellmeijer model is an example of a model of this kind (Sellmeijer, 1988). As described in Section 2.3.4, a validation of this model using small-, medium- and full-scale experiments resulted in the empirical adaptation of the model, mainly with respect to grain size (Sellmeijer et al., 2011).

However, the lack of a proper explanation for this entirely empirical adaptation is unsatisfactory and limits its practical use to sand types similar to those investigated. In addition, it is now known that, in small-scale configurations with a large exit area of the kind used for the validation of the model, the head required for pipe initiation (H_i) exceeds the head required for progression (H_p), causing the pipe to develop in the upstream direction without equilibrium in the pipe formation in the way assumed by the Sellmeijer model. It is therefore incorrect to use these experiments for the validation of the Sellmeijer model, since pipe initiation and progression are governed by different processes. The validation of the Sellmeijer models should be based solely on experiments in which the critical head is dominated by the process of progression.

The additional experiments performed for this dissertation (those presented in Chapter 3) allow for a new validation approach using experiments in which equilibrium in pipe formation has been observed. This validation, at the level of critical head, is

described in Section 6.4. The comparison of predicted and experimental critical heads does not explain any deviations between the model and the experiment. Such an explanation requires a more detailed investigation of the different components of the piping process. Figure 6.1 shows the relevant components: groundwater flow towards the pipe, flow through the pipe, erosion at the pipe tip (primary erosion) causing pipe lengthening, and erosion at the pipe walls (secondary erosion).

The pipe characteristics – the dimensions (width and depth) and hydraulic properties (indicated by pipe gradient and flow velocity), give relevant information for three of these four components. The empirical pipe characteristics are therefore discussed in Sections 6.5. The flow through the pipe is discussed in section 6.6. Sections 6.7, 6.8 and 6.9 then discuss the erosion mechanisms, starting with the relevance of both primary and secondary erosion and a description of both mechanisms based on the literature and experimental work. Section 6.10 contains a synthesis of the equations for pipe flow and particle equilibrium and comparison with the measurements allows for the validation of the hydraulic regime in the pipe and of assumptions about the erosion process (incipient motion). Finally, Section 6.11 discusses the results and puts forward suggestions for improvements to the model.

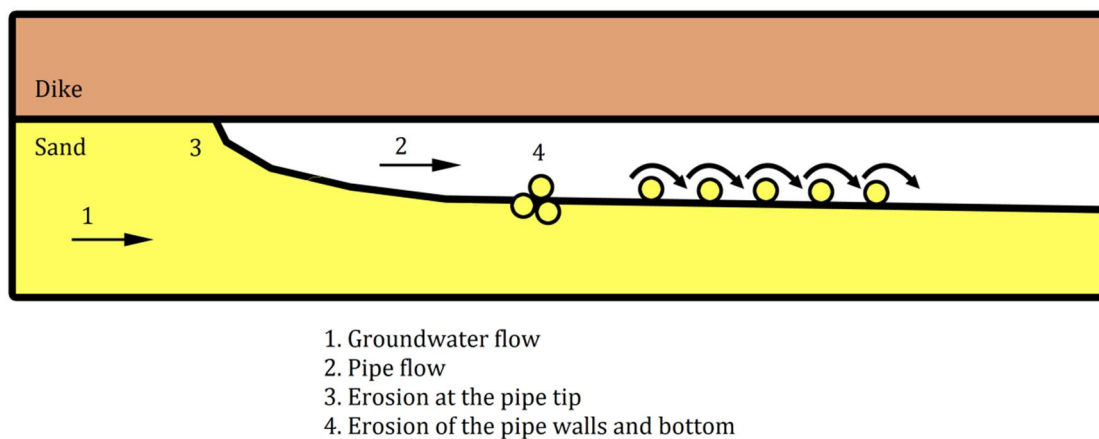


Figure 6.1. Illustration of the four components relevant for modelling pipe progression

6.2. AVAILABLE PROGRESSION EXPERIMENTS

Equilibrium in pipe development has been observed in experiments at a large scale and/or with a small exit area (Müller-Kirchenbauer, 1978; Hanses, 1985; Miesel, 1978; Silvis, 1991; Yao et al., 2007; Ding et al., 2007; full-scale experiments by Van Beek et al., 2011; and some of the experiments by Townsend et al., 1988 and Pietrus, 1981, and the additional experiments described in Chapter 3). In these experiments, a pipe is formed that comes to a halt in time in such a way that the head needs to be increased for the pipe to develop further. The hydraulic conditions in and around the pipe therefore determine its progress and the progression head. These experiments are suitable for the validation of the Sellmeijer model.

Silvis (1991) and Van Beek et al. (2011) described the available large-scale experiments, which are known to be well predicted by the Sellmeijer model (Sellmeijer, 2011; Weijers and Sellmeijer, 1993). The experiments in both of these studies were performed

with a 2D configuration, although the type of outlet was different: in the experiments by Silvis, the water exited towards a ditch; in the experiments by Van Beek et al. (2011), the water exited to a large area.

Experiments with a small exit area were conducted by Townsend et al. (1988), Pietrus (1981), Hanses (1985), Miesel (1978) and Yao et al. (2007). It should be noted that the scope of this dissertation is limited to experiments in single sand layers.

In the experiments by Townsend et al. (1988) and Pietrus (1981), an artificial pipe was created before starting the experiment. These experiments are therefore not suitable for progression analysis since the pipe dimensions do not match the natural pipe dimensions.

The experiments by Hanses (1985) and Miesel (1978) were performed in a 3D set-up, with water exiting to a circular hole in the cover layer. Hanses and Miesel simulated the presence of a thick soft soil layer by extending the exit point to the simulated surface using a vertical tube. The head loss originating from this vertical section was measured in the experiments by Hanses (1985), allowing for the head at which the pipe progressed to be corrected for this head loss.

Miesel (1978) investigated the effect of exit-hole diameter on the process and the critical head. The critical head was found to increase slightly with the increase in the exit-hole diameter (an increase of approximately 15 to 19 cm associated with an increase in the size of the exit hole from 2.5 to 13 cm). As the exit loss (the head loss resulting from flow through the vertical section of the exit hole) is not known for these experiments, the critical heads obtained by Miesel will not be analysed in greater detail here.

Hanses (1985) investigated the critical head and pipe hydraulics in both single- and multi-layer configurations at different scales. All experiments were performed on Sand A, the properties of which are described in Appendix B. Three of these experiments (26a, 53, 73) were performed specifically to determine the hydraulic gradient in the pipe. Accordingly, in the first phase of the experiment, the hydraulic head was raised until the critical pipe length was reached; in the second phase the hydraulic head was brought back to 0 and reapplied in steps to assess the head loss in the pipe.

The experiments by Yao et al. (2007) were conducted using a range of exit configurations. It should be noted that the uniformity coefficient of the sand type used was relatively high (3.5) by comparison with the other experiments.

The additional experiments for this dissertation were performed in a 3D hole-type configuration, as described in Chapter 3.

In summary, the experiments that are suitable for the validation of the Sellmeijer model are mainly large-scale experiments with a 2D configuration (these experiments are available from the literature) and small- and medium-scale experiments with a 3D configuration (these comprise the experiments described in the literature and the supplementary tests described in Chapter 4). These experiments will be used to validate the Sellmeijer model.

6.3. CRITICAL HEAD ANALYSIS

This section compares the results of the experiments in order to summarise the effects of exit configuration, grain size, uniformity coefficient, relative density, scale and sand layer shape on the critical gradient. A direct comparison of this kind is only feasible if just one parameter varies, and the comparison is therefore often limited to experiments with the same experimental set-up.

The effects of relative density and exit-hole size were discussed in Chapter 3 and it was concluded that the critical head is only slightly affected by the latter and moderately by the former. The effects of grain size (uniform sand), scale and sand layer shape (ratio of thickness to length) on critical gradient are discussed here, taking into account the results of all available experiments.

6.3.1. EFFECT OF EXIT CONFIGURATION ON CRITICAL GRADIENT

Yao et al. (2007) investigated the effect of exit configuration. Two medium-scale experiments, identical in all respects except for the exit, indicated that the critical gradient is considerably lower for a hole-type exit than for an area-type exit (0.214 and 0.278 respectively).

6.3.2. EFFECT OF GRAIN SIZE ON CRITICAL GRADIENT

The effect of grain size on critical gradient in uniform sands was investigated in small- and medium-scale experiments and in the IJkdijk experiments. To make it possible to observe trends, the vertical axis in Figure 6.2 was restricted to a critical gradient of 0.6, placing one outlier out of range. The medium-scale experiment showing that layering has a major impact has been removed from the selection.

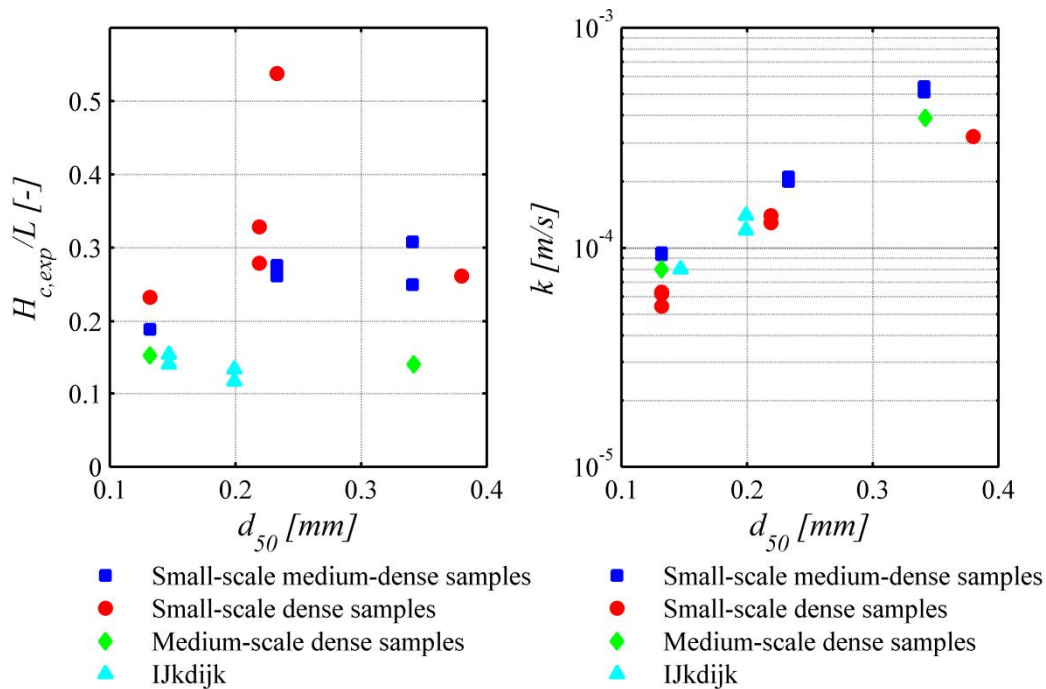


Figure 6.2. Effect of grain size on critical gradient, and the relationship between permeability and grain size (uniform sands only)

Figure 6.2 (left) shows the critical gradient as a function of grain size. In all configurations, grain size has a relatively minor effect. However, the trend linking grain size and critical gradient appears to become more negative as scale increases, being slightly positive for small-scale experiments and slightly negative for large-scale experiments. The change in trend is not related to the correlation of grain size and permeability, as is shown by Figure 6.2 (right-hand graph).

6.3.3. EFFECT OF UNIFORMITY COEFFICIENT ON CRITICAL GRADIENT

The effect of uniformity coefficient has been investigated in small-scale experiments by mixing different uniform fractions of sand and silt. The results are discussed in Section 4.7.3. Sand samples with a large uniformity coefficient result in critical gradients that are higher than those in the samples consisting of more uniform sand.

6.3.4. EFFECT OF RELATIVE DENSITY ON CRITICAL GRADIENT

The effect of relative density on the critical gradient was investigated in the small-scale experiments with Baskarp sand and Oostelijke Rivierenzand (Figure 6.2). It should be noted that the two outliers in the results of the small-scale experiments (one of which is out of range) were both obtained in dense samples (Figure 4.24), despite the fact that equal numbers of tests were available with medium-dense and dense samples. The effect of relative density proved to be quite large and it could – in part – be attributed to the change in permeability that accompanies a change in relative density and the change in friction angle, which is also likely to affect the bedding angle (see the description of the Sellmeijer model in Section 2.3.4).

6.3.5. EFFECT OF SCALE ON CRITICAL GRADIENT

The effect of scale on critical gradient can be determined by analysing the experiments performed using the same thickness-to-depth ratio. Hanses (1985) performed small- and medium-scale experiments that varied by a factor of 4 in all dimensions. The small- and medium-scale experiments performed with Baskarp sand (as described in Chapter 3) are also very suitable for determining the effect of scale. The characteristics of the Itterbeck 330 μm sand, when tested in medium-scale experiments, are comparable to those of Enschede sand tested in small-scale set-ups. The scale ratio between these small- and medium-scale experiments was 4.

The large-scale experiments described in section 2.2 also supplied valuable information about the critical gradient, but not all dimensions were scaled equally in these experiments. The depth in the Delta Flume experiments was constant. The configuration and D/L ratio of the IJkdijk experiments were different from the small- and medium-scale experiments. These experiments require a comparison with a prediction model.

Figure 6.3 shows the critical gradient of the selected experiments as a function of the seepage length. It should be noted here that, due to the constant D/L ratio, it was possible to plot the critical gradients as a function of the layer thickness without affecting the outcome of the analysis. The scale effect in the process of pipe initiation (Chapter 5) was calculated to be $H_i / L \propto L^{-1/2}$ and the scale effect in the Sellmeijer

model is $H_c / L \propto L^{-1/3}$. It is therefore likely that the critical gradient is related to the seepage length raised to the power of x . Assuming that the critical gradient is a function of L^x , the effect of length can be compared for different experiments:

$$\frac{(H_c / L)_{small}}{(H_c / L)_{medium}} = \left(\frac{L_{small}}{L_{medium}} \right)^x \quad 6.1$$

Table 5.1 shows the values of x for the three experimental series.

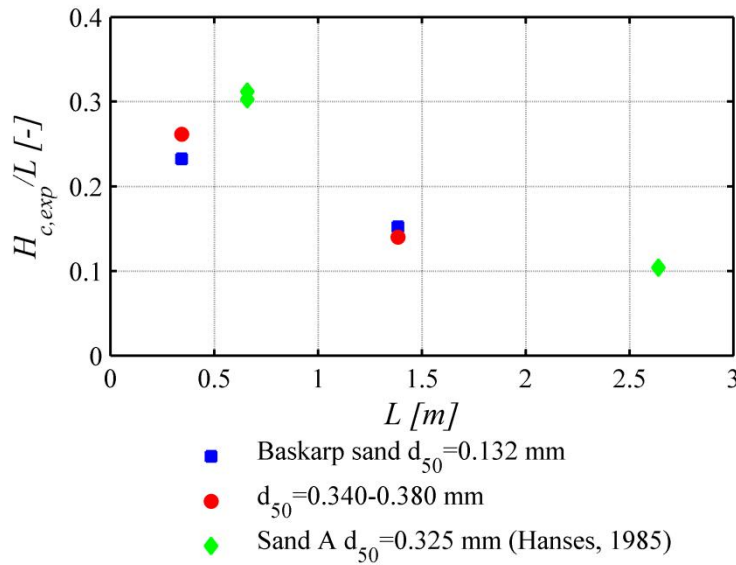


Figure 6.3. Effect of scale on critical gradient (D/L constant)

Table 6.1. Effect of the seepage length on critical gradient, expressed as the power of L

	Baskarp	Itterbeck 330 μm	Sand A (Hanses)
x	-0.30	-0.45	-0.74

Due to the different ratios of sand-bed thickness to seepage length, no direct quantitative comparison can be made between the results from Hanses (1985) and those from the new experiments presented in Chapter 3. However, a qualitative comparison allows for an assessment of the effect of scale.

An effect of scale was seen in all experimental series: critical gradient decreases with scale. The scale effect in the Baskarp sand experiments was close to the predicted scale effect in the Sellmeijer model ($H_c / L \propto L^{-1/3}$). It should be noted that the scale effect seems to have been strongest in the experiments by Hanses (1985). A possible explanation for this stronger scale effect is that the width of the box also affects the critical gradient: on the basis of numerical calculations of the flow towards the pipe, Vandenboer et al. (2014a) concluded that the width of the set-up in small-scale experiments should at least match the seepage length. An explanation of this observed effect could be the size of the pipe in relation to the width of the box. As the pipe dimensions remain more or less the same at different scales, a relatively narrow set-up may affect the critical gradient in larger-scale experiments less than in small-scale

experiments: at comparable pipe dimensions, the limited width restricts the flow towards the pipe more in a small box than in a large box.

Although the width and length were scaled proportionally by a factor of 4 in the experiments by Hanses, the small-scale set-up was very narrow (0.165 m). The limited width of the box could explain the relatively high gradient in the small-scale experiments that he conducted, and therefore a stronger scale effect than in larger experiments in which the width was adequate.

Another explanation could be that the exit hole in the experiments by Hanses (1985) was not scaled in line with the dimensions of the set-up. However, as it has been concluded previously that the hole size has a limited effect on the critical gradient, this is not likely to be the main cause of this discrepancy. The scale effect is also slightly more pronounced in Itterbeck 330 μm sand than in Baskarp sand. The variation could be within the margins of experimental error since a small variation in the critical gradient has a major effect on the calculated exponent, especially since only two data points are considered in each experimental series.

6.3.6. EFFECT OF SAND LAYER SHAPE ON CRITICAL GRADIENT

The effect of sand layer shape, or the ratio of sand layer thickness to seepage length, was investigated in different ways. Either the length was varied while retaining constant thickness (Silvis, 1991), or the thickness was varied while retaining approximately constant length (Hanses, 1985). The experiments by Silvis (1991) show that, given constant depth, the seepage length has little effect on the critical gradient. The experiments by Hanses (1985) indicate that the critical gradient is highly dependent on depth. In the light of these two experimental series, depth would appear to be an important parameter for the determination of the critical gradient.

The sand layer width varies in all experiments. Recent experiments performed at the University of Ghent (Vandenboer, 2014b) indicate that critical gradient declines with increasing width in small-scale experiments. The effect of width has not been investigated at larger scales. Large-scale experiments, like the Delta Flume experiments and IJkdijk experiments in which the width-to-depth and width-to-length ratios were very different, are predicted well by the 2D Sellmeijer model (Weijers and Sellmeijer, 1993; Sellmeijer et al., 2011). It can therefore be concluded that the width does not affect the critical gradient at larger scales, at least in 2D configurations. However, it could have a stronger effect in a 3D configuration than in a 2D configuration. Given that the pipe dimensions remain more or less the same, the effect of width can also be expected to decrease with increasing scale.

6.3.7. CONCLUSIONS

The analysis of critical gradients obtained in progression-dominated experiments results in the following conclusions:

- The exit configuration has a strong effect on the critical gradient.
- The effect of grain size (uniform sands) on critical gradient is limited, or counterbalanced by a change in permeability. The effect of grain size is not the same at all scales. A positive correlation of critical gradient with grain size was

found in small-scale experiments and the correlation in large-scale experiments was negative.

- All experiments indicate that there is a geometric scale effect: the critical gradient decreases with increasing scale. The critical gradient H_c/L decreased with L^x , where x was found to be -0.30, -0.45 and -0.74 for the three experimental series analysed. The high value of -0.74 was most likely caused by the limited width of the sand box.
- Depth appears to be an important parameter for the critical gradient.
- Width appears to affect the critical gradient in small-scale experiments, but not in large-scale 2D experiments. The relatively small pipe dimensions compared to the width of the box is the most likely cause here. The effect of width on critical gradient has not yet been investigated in large-scale 3D experiments but it is expected to be less marked at larger widths and scales, as long as only one pipe is present.

6.4. VALIDATION OF SELLMEIJER MODEL

The analysis of critical gradients is limited to experiments in which only one parameter was varied. It is therefore difficult to arrive at firm conclusions about the effect of parameters such as grain size, uniformity coefficient and relative density as these parameters cannot be varied independently. Using a model to compare actual critical gradients and predicted critical gradients could provide clearer insights. This section uses the Sellmeijer model to compare the critical gradients from experiments.

6.4.1. VALIDATION FOR 2D CONFIGURATION

The Sellmeijer model has been validated for large-scale 2D experiments. These 2D configurations are very similar to the 'standard dike geometry' and so the calculation rules described in Chapter 2 can be used instead of the model. It should be noted that the effect of KAS (grain angularity) is very small and that this parameter has been disregarded. The difference in the angularity of the tested sand types is also relatively small.

Figure 6.4 shows the results for the two experimental series. This figure compares the calculated critical gradients with the experimental gradients. To help with interpretation, the black and grey lines have been used to represent the 1:1 (calculated value equals the predicted value), 1:2 and 2:1 (calculated value is a factor 2 smaller or larger than the experimental value) lines. Differences in predicted values for the original and adjusted rules start when $d_{70} > 0.2$ mm. The figure shows that the adjusted rule works better for the experiments on coarse IJkdijk sand, and that the original rule is less safe.

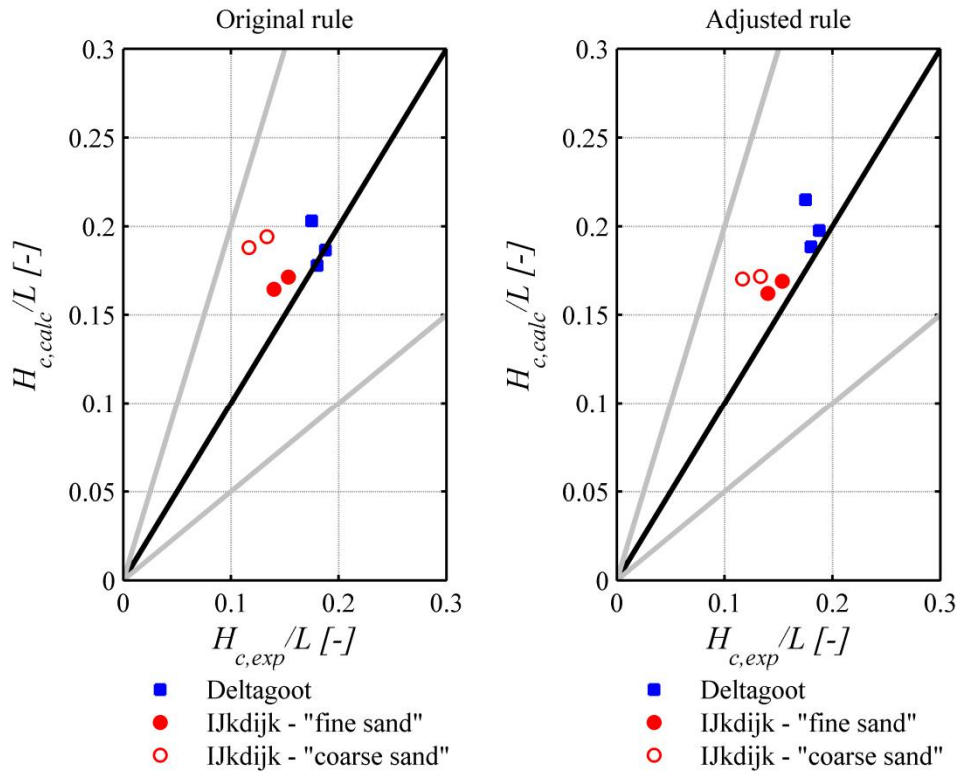


Figure 6.4. Experimental and calculated critical gradients for Delta Flume and IJkdijk experiments (the black and grey lines indicate no deviation (1:1) and a factor-two deviation (1:2, 2:1) respectively).

6.4.2. VALIDATION FOR 3D CONFIGURATION

As pipe formation is itself a 3D phenomenon (irrespective of whether the configuration is 2D or 3D), it has been assumed that the model could also be applied to 3D configurations, which are common in practice. Prior to the present study, this assumption had not been verified experimentally.

The calculation rule, which is suited for a standard dike geometry, was used to postdict the experiments described in the present study. As the rule is fitted to the results of the numerical model, the outcomes of the rule and the numerical calculation are the same for the standard dike geometry. When a configuration is used with an exit that deviates from the standard dike geometry, the difference between the outcomes of the model and the rule should be examined. The experiment was therefore numerically simulated in 2D, with the exit hole being represented by a gap of infinite length and width equal to the exit-hole diameter. It is not yet possible to assess the effect of a 3D configuration on critical gradient.

Figure 6.5 shows the expected effect of the exit-hole diameter on the calculated critical head for pipe progression using the 2D numerical Sellmeijer model for one of the experiments. As the effect of diameter on critical head is relatively small in the studied range, it is considered acceptable to use the rule rather than the 2D numerical model to postdict the experiments.

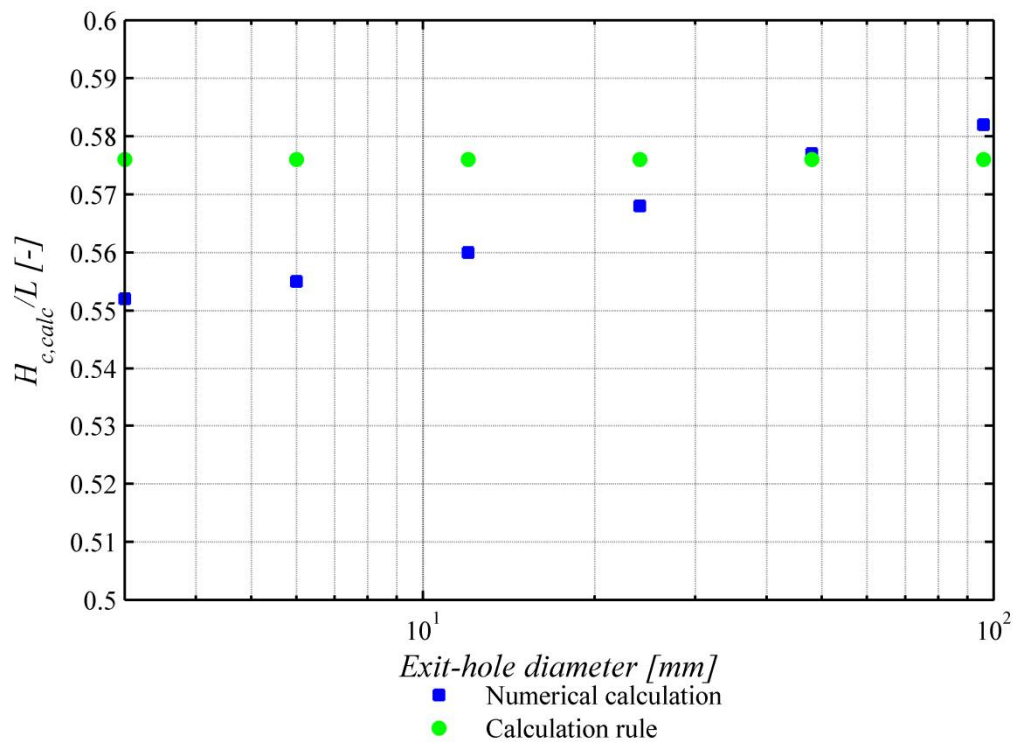


Figure 6.5. Calculated critical gradients for different exit-hole diameters comparing the outcome of the 2D numerical calculation and the calculation rule (using experiment B115 as an example)

Figure 6.6 shows both the experimental and calculated critical gradients for all experiments using the original and adjusted calculation rules. It is immediately clear that the calculated critical gradients are approximately twice as large as the experimentally obtained values. Apparently, the 3D configuration results in considerably lower critical gradients than a 2D configuration, for which the model has been validated. The 2D model cannot predict the 3D groundwater flow conditions, which apparently play a major role. Despite this, the comparison with the model is useful as a way of identifying the effect of other properties.

Figure 6.7 displays the results of those experiments in which the soil type and relative density were varied. The predicted critical gradients obtained with the original and adjusted rules were comparable in Baskarp sand experiments; variations were found mainly with coarser sands. The graphs show that the variation was more or less the same for all Baskarp experiments, indicating that the model accounts well for the effect of permeability and scale. The comparison of experiments with the Sellmeijer models did not establish a clear trend with respect to grain size. Again, the experiments on Sterksel sand and Oostelijke rivierenzand (high density only) are outliers for both models. The original rule performs better with Waalre sand and the adjusted rule performs better with the Itterbeck 330 μm sand and Enschede sand. The adjusted rule is more conservative than the original rule.

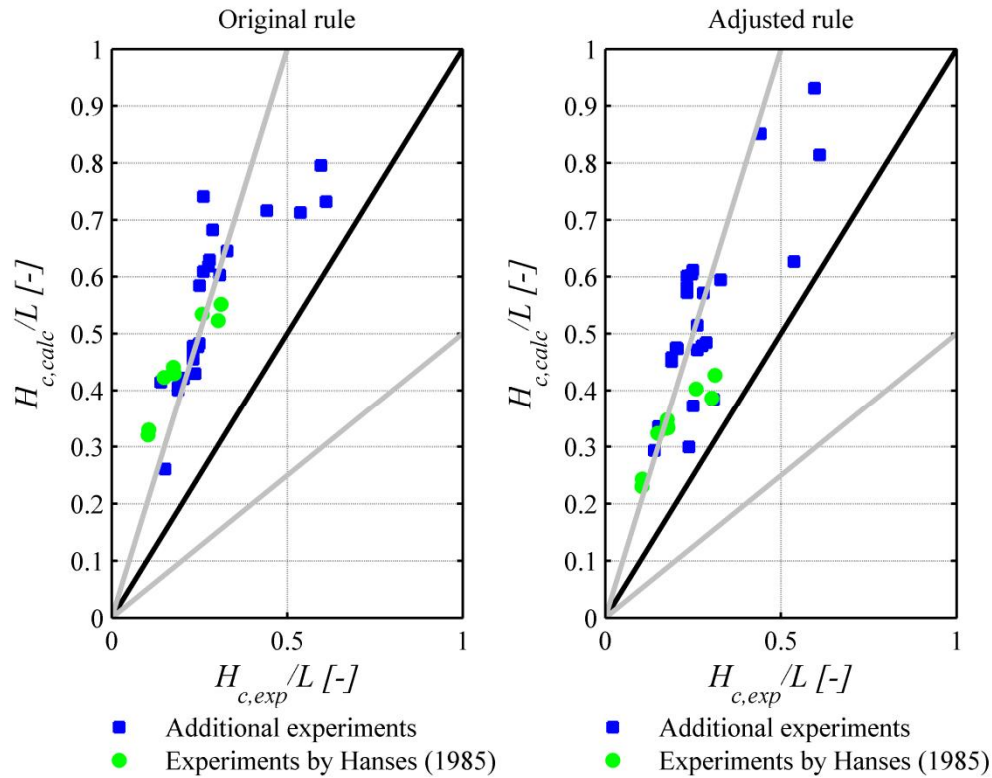


Figure 6.6. Experimental and calculated critical gradients for all available 3D experiments (the black and grey lines indicate no deviation (1:1) and deviation by a factor 2 (1:2, 2:1) respectively).

As in the experiments with Oostelijke rivierenzand and Sterksel sand, the experiments in which fines were added resulted in relatively high critical gradients by comparison with the uniform sands. The Sellmeijer model does not predict this improvement in strength accurately. It should be noted that the migration of fines might have affected the critical gradient.

Assuming that the 3D effect could be captured by a factor of 2, which seems reasonable given that the experiments with Baskarp sand are all very close to the 1:2 line in Figure 6.7, the deviation for the different sand types can be quantified. Table 6.2 gives the standard deviations for the different sand types calculated on the basis of the 1:2 line. The standard deviations are small for Baskarp sand and they are at their largest in the experiments where fines were observed in the exit cylinder, as in the case of mixtures 1 and 2, Sterksel sand and Oostelijke rivierenzand. The averages of the standard deviations for the original and adjusted Sellmeijer model are nearly the same: it is therefore concluded that the models perform comparably on average.

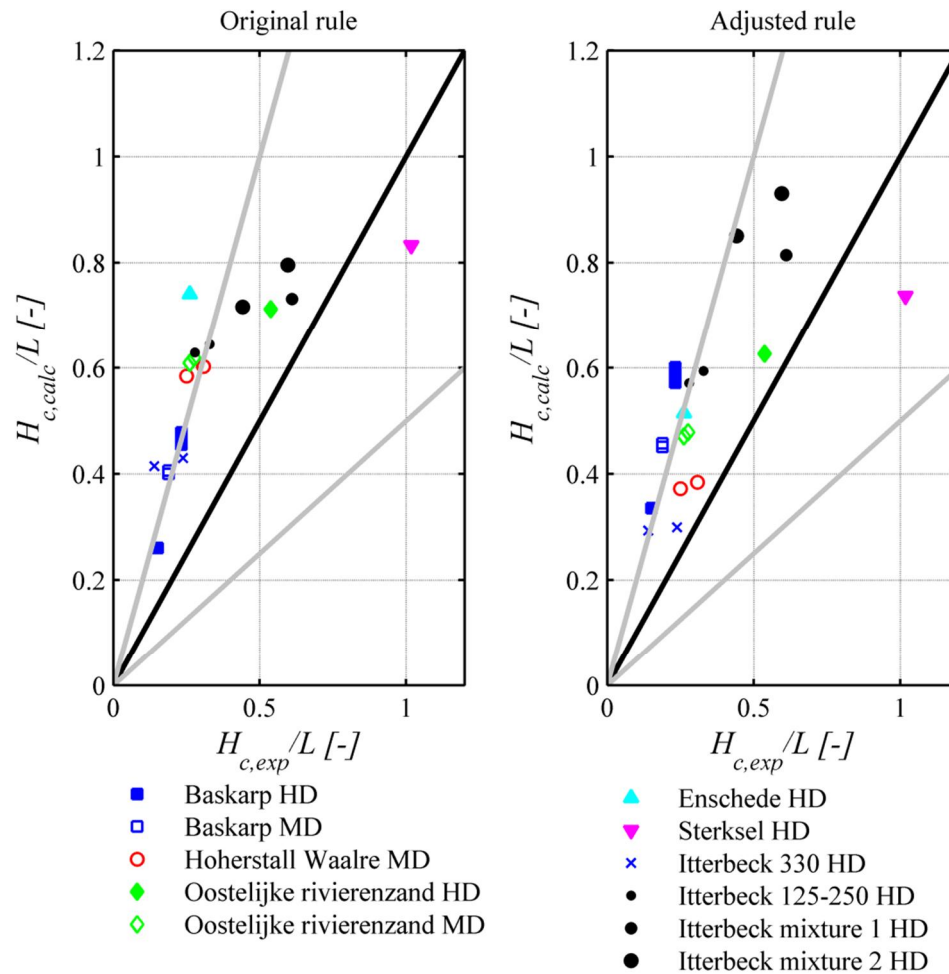


Figure 6.7. Experimental and calculated critical gradients for small- and medium-scale experiments investigating sand type and relative density (black and grey lines indicate no deviation (1:1) and factor of 2 deviation (1:2, 2:1) respectively; MD: medium density, HD: high density).

Table 6.2. Standard deviation for the different sand types, calculated relative to the 1:2 line.

Sand type	SD adjusted rule [-]	SD original rule [-]
Baskarp 1	0.048	0.010
Enschede sand	0.032	0.086
Hoherstall Waalre	0.094	0.030
Itterbeck 0.33 mm	0.063	0.050
Itterbeck 125–250	0.023	0.026
Itterbeck mixture 1*	0.203	0.245
Itterbeck mixture 2**	0.093	0.152
Oostelijke rivierenzand	0.132	0.109
Sterksel	0.649	0.601
All sand types	0.153	0.145

6.4.3. CONCLUSIONS

The comparison of critical gradients obtained experimentally with the gradients calculated with the Sellmeijer rules results in several insights: 2D configurations are well predicted using the Sellmeijer model and the adjusted model out performs the original model for the coarse IJkdijkzand.

However, in a 3D configuration, the deviation is approximately a factor of 2 for both small- and medium-scale experiments with fine uniform sands, indicating that the Sellmeijer model over-predicts the critical gradient in a 3D configuration. This suggests that the Sellmeijer models are not yet suitable for 3D situations. The effect of sand type remains speculative, with better performance using the original model in some experiments and better performance using the adjusted model in other experiments.

The effects of scale and model-size ratios are predicted quite well. However, the outliers indicate that certain processes or parameters that are currently not included in the model have a major impact on the critical head. A theoretical explanation for the effect of sand type cannot therefore be based on critical head alone: the processes driving pipe progression must also be studied.

6.5. EMPIRICAL PIPE CHARACTERISTICS

The experiments offer valuable information about the characteristics of the pipe in terms of dimensions and hydraulic conditions such as pipe gradient and water velocity. Parts of this section are cited from Van Beek et al. (2014c).

6.5.1. PIPE WIDTH

The pipe width was determined for the experiments described in Section 4.11, in which the pipe dimensions were measured using a laser. Furthermore, in the small- and medium-scale experiments on different soil types described in Sections 4.8 and 4.9, the width was also determined using the photographs of pipe formation. The pipes in equilibrium condition were drawn for the experiments by Hanses (1985) and so the width was determined for these experiments as well.

The laser scans revealed that the pipe width was larger in Enschede sand than in Baskarp sand. The pipe tip was found to be 26 and 30 times the mean grain diameter in Enschede and Baskarp sands respectively. Pipe width increased towards the exit hole.

The advantage of using photographs rather than the laser to determine pipe width is that more pipe lengths and more experiments can be analysed. The contours of the pipes in the available experiments were drawn manually for this purpose.

The depth of some of the pipes varied significantly over the cross-section, but remained limited to several millimetres (see also 6.5.2). The deeper preferential paths meander more and cover only a part of the total affected zone. Figure 6.8 shows an example of the severe meandering of preferential paths, as well as the contour of the piping zone in one of the medium-scale experiments. The pipes appear to widen downstream of the tip as a result of the scouring of the pipe walls, as shown by the curved contours of the pipe zone. As the contour indicates the extent to which the pipe widens and migrates, it has been decided to consider the whole affected zone as part of the pipe.

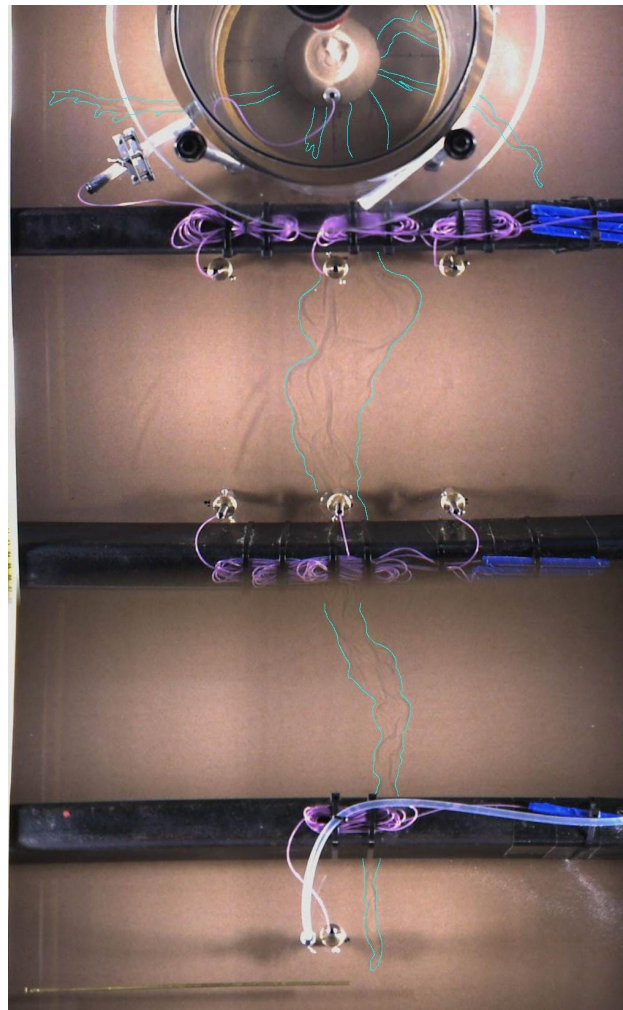


Figure 6.8. Example of meandering and preferential paths in experiment Bms19

The contours were drawn for four pipe lengths in the small-scale experiments at approximately $\frac{1}{4}$, $\frac{1}{3}$, $\frac{1}{2}$ and $\frac{3}{4}$ of the total seepage length. The width of the pipe varied along its length. Three values for the pipe width were determined on the basis of the contours. The tip width was defined as the width behind the tip at the point where it becomes approximately constant (about 1 cm behind the tip). The width of the tail was measured approximately 2 cm from the circular exit hole. The third value for the width was measured half way along the pipe. In all cases, the width was determined so that it reflects an average value at that point. The variation of the width along the length is not the only reason for scatter: in some experiments, the tip width was difficult to observe and this may also result in scatter. Figure 6.9 gives an example of the contours obtained for one of the small-scale experiments, showing the measured pipe width at three locations: tip, mid-point and tail for the pipe length at $\frac{3}{4}$ of the seepage length. The contours of the analysed experiments are presented in Appendix D.

Pipe contours are also available from the experiments by Hanses (1985) for pipes in equilibrium. Hanses (1985) analysed the pipe dimensions and concluded that the pipe width near the tip was constant in all experiments (performed with one sand type: sand A) at approximately 15–20 mm. However, analysis of the drawings of pipe formation in

these experiments showed that this is an overestimation of the pipe width at the tip. The tip width was defined here as the width of the pipe where it becomes more or less constant: approximately 1–2 cm behind the tip. The average tip width was found to be 13.7 mm in all available pipe drawings, which is about 42 times the average grain diameter.

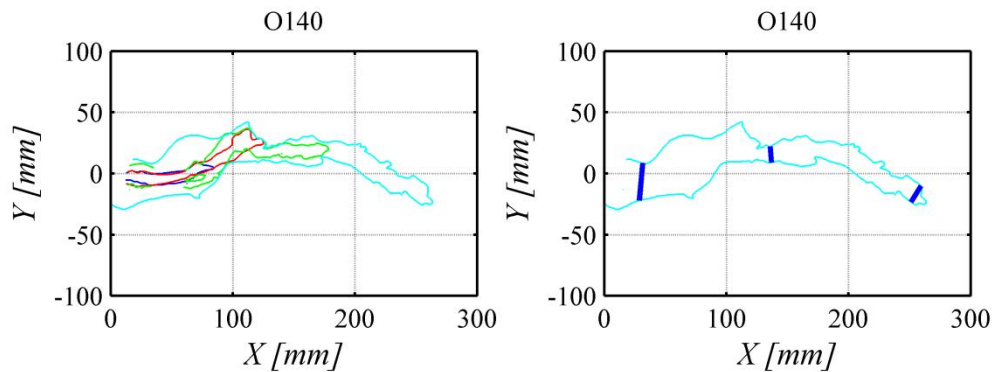


Figure 6.9. Example of pipe contours for different pipe lengths and width measurements at tip, mid-point and tail (experiment O140)

The pipe tip width was determined for all four lengths in the small-scale experiments and for several lengths in the medium-scale experiments. The pipe tip width is relatively constant when the pipe lengthens, but is often larger when the pipe length is $\frac{3}{4}$ of the seepage length than for the other analysed lengths (Figure 6.10). The critical pipe length may have been exceeded at this point so that the water pressures at the tip of the pipe are relatively large, causing a larger area to be involved in the erosion process.

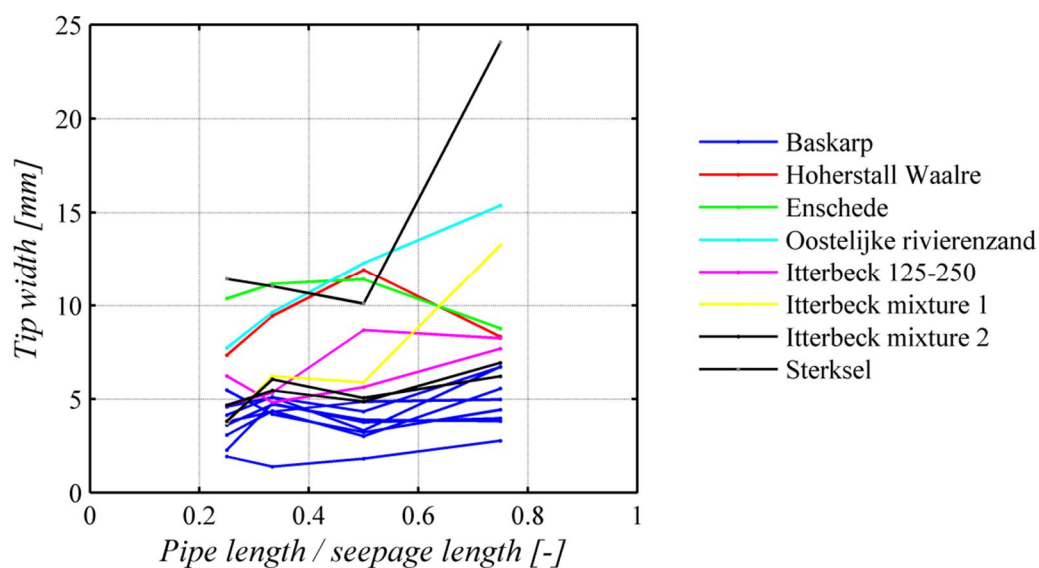


Figure 6.10. Tip width as a function of relative pipe length (measured at 0.25, 0.50 and 0.75) for all small-scale experiments

To reduce scatter, the pipe widths for pipe lengths of $\frac{1}{4}$, $\frac{1}{3}$ and $\frac{1}{2}$ of the seepage lengths were averaged. Figure 6.11 shows the average pipe widths as a function of d_{50} for all available experiments. Although the method used to estimate pipe widths was not exact, a relationship was observed between pipe width and grain size. The width of the tip of the pipe was found to be fairly constant for each soil type at approximately 30 grains in most of the small-scale experiments. No relation was found between exit-hole size and pipe width, or between relative density and pipe width. This confirms the conclusion by Hanses (1985) that there is no correlation between scale and the width of the pipe tip.

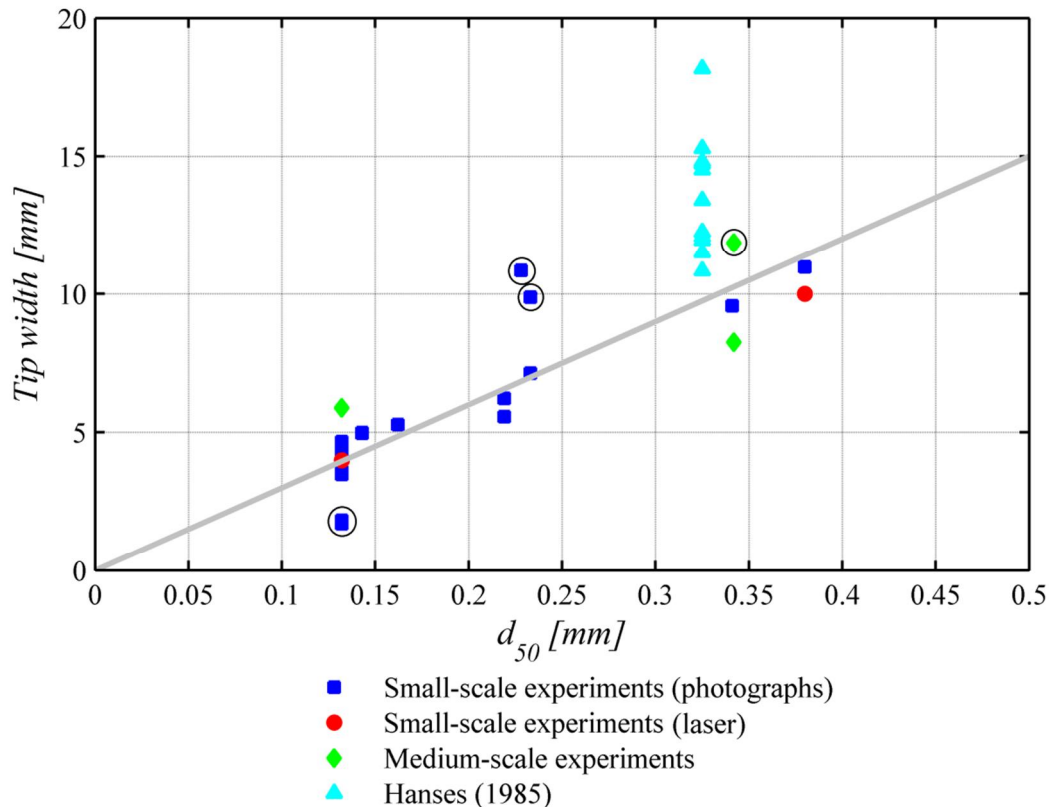


Figure 6.11. Average tip width as function of grain size: data points from experiments (the encircled data points are described in the text) and line showing the width of 30 times the mean grain size

The widths observed in some experiments were significantly different from those found in others (circled points in Figure 6.11): two experiments with Baskarp sand ($d_{50} = 0.132$ mm) surprisingly produced smaller tip widths than the other Baskarp sand experiments. This anomaly could not be explained in terms of critical head, relative density or exit-hole size. The two other striking points come from an experiment with Sterksel sand ($d_{50} = 0.228$ mm) and one of the experiments with Oostelijke rivierenzand ($d_{50} = 0.233$ mm). In the experiment on Sterksel sand, the critical head was very high and this may explain the relatively large width of the pipe. Furthermore, the velocity of pipe development was also relatively high in both of these experiments, possibly indicating the presence of a local resistance that needed to be overcome. Finally, the scatter in the tip width was quite large for the medium-scale experiments performed with Itterbeck 330 μm sand ($d_{50} = 0.342$ mm). This can be explained by the difference in critical head,

which was caused by the layering of the sand bed observed in one of the medium-scale experiments (described in Section 4.9.3).

The tip widths obtained from experiments by Hanses (1985) are all relatively large. A possible explanation is the difference in the cover. The cover in all the new experiments described in this chapter was coated on the inside with silicone to ensure a rough clay-like surface, while the cover in the experiments by Hanses was smooth. Another possible explanation for the relatively large tip widths is the angularity, which is not known for the sand used by Hanses. It should also be noted that, in the selected Hanses experiments, pipe drawings were only available for one pipe length.

Pipe widening resulting from secondary erosion was seen in all experiments. Water flow through the pipes, in combination with inflowing water from the soil into the pipe from the sides of the pipe, causes scour along the pipe walls, resulting in pipes that increase in size towards the downstream tail.

The pipe pattern downstream of the tip resembles a meandering river migrating laterally, with deposition in the shallow inner bend and erosion in the deeper outer section of the meander bend. The degree of meandering was more pronounced in the medium-scale experiments than in the small-scale experiments. This concurs with the finding of Hanses (1985) that pipes longer than 20–25 cm start to migrate laterally. Figure 6.12 shows the contours of one small-scale (B142) and one medium-scale (Bms19) experiment in Baskarp sand that demonstrate this clearly: although the width of the pipe tip is comparable for different pipe lengths, the width of the tail increases significantly as a result of pipe lengthening. It should be noted that the contours show the outer range of the eroded zone, with significant depth variations inside this zone.

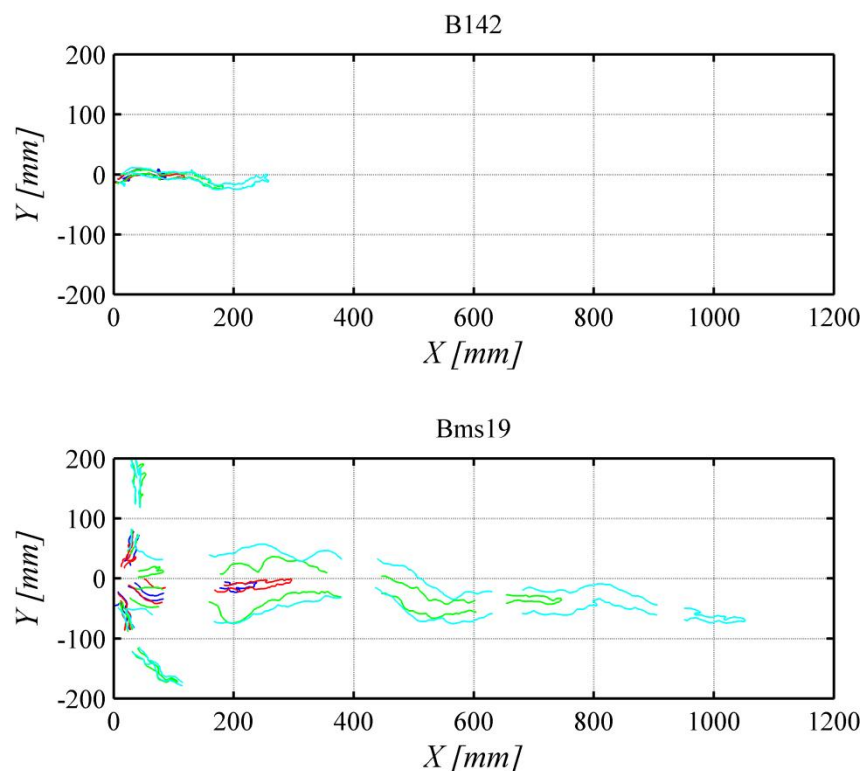


Figure 6.12. Pipe contours in a small-scale (B142) and a medium-scale (Bms19) experiment

The extent of widening is shown here as the ratio between the tail width and tip width. Figure 6.13 shows this ratio as a function of the distance between the tip and tail for all available data points. In some of the experiments, the tail width was not clear to see and so it could not be determined. These experiments have been excluded from Figure 6.13.

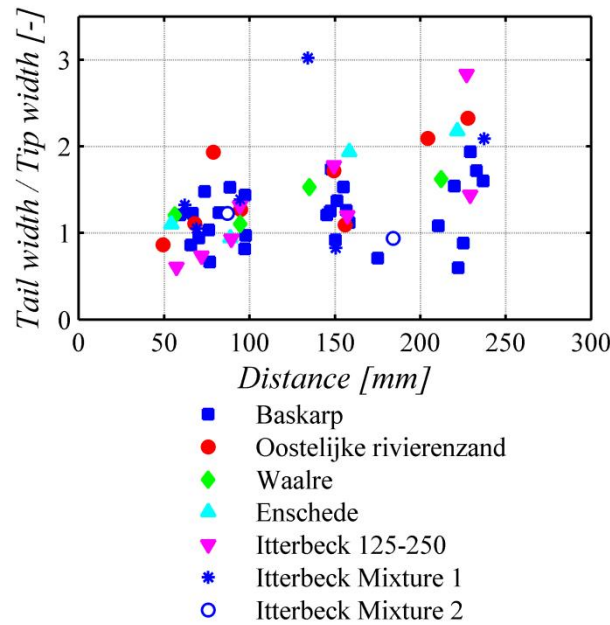


Figure 6.13. Ratio of tail width to tip width as function of distance between the tail and tip

In general, the ratio between the tail width and tip width remains constant, or increases slightly as the distance between the tip and tail increases. In some experiments, the ratio actually fell below 1, suggesting that the pipe is narrower at the tail than at the tip, which is unlikely. This finding can be explained by reference to the accuracy of the method for measuring width using photographs. Widening is expected, as the pipe conveys more water towards its tail (water will not only enter the pipe at its tip, but along the entire length). In the experiments where widening is limited, the erosion of the sand at the tip of the pipe determines the process.

Figure 6.13 shows there is more scatter at longer pipe lengths, probably due to the meandering described above. To investigate the correlation with sand type, the width difference from tip to tail was divided by the distance from tip to tail (Δx) and averaged for the pipe lengths of $\frac{1}{4}$, $\frac{1}{3}$ and $\frac{1}{2}$ of the total seepage length, which is an indication of the increase in width as a function of pipe length:

$$B = \frac{w_{tail} - w_{tip}}{\Delta x} \quad 6.2$$

The average of B for pipe lengths of $\frac{1}{4}$, $\frac{1}{3}$ and $\frac{1}{2}$ was plotted as a function of d_{50} (Figure 6.14) for all experiments. Figure 6.14 shows that width increases towards the tail at a rate of approximately 1–4 mm / 100 mm pipe in all sand types. There were two outliers: the experiments performed on Itterbeck Mixture 1 ($d_{50}=0.162$ mm) and Oostelijke

rivierenzand ($d_{50}=0.233$ mm). In both experiments, the critical head was found to be higher than in similar experiments.

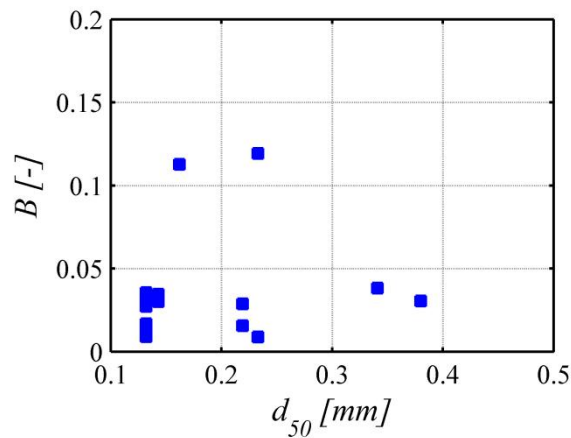


Figure 6.14. Average degree of widening as a function of grain size

The degree of widening increases with pipe length on average, but there is considerable scatter and, in a number of cases, the tail is actually not as wide as the tip. It should be noted that, at larger pipe lengths, the pipe was not in equilibrium and so the final shape of the pipe corresponding to the hydraulic load was probably not reached. More accurate results could be obtained by measuring the pipe width along its entire length.

As the degree of widening was comparable for all grain sizes considered and the pipe tip width increased with grain size, it can be concluded that pipes in sands with larger grain sizes are wider in general. The depth of the pipe may be related to its width and this possibility will be investigated in the next section.

6.5.2. PIPE DEPTH

Pipe depth was determined in a number of experiments conducted for the purposes of this dissertation and it is available from some experiments in the literature. In experiment E150, in which the pipe was observed through the transparent sides of the box, it was possible to determine pipe depth where the pipe developed along the wall. The pipe depth varied, with an observed maximum of 2.3 mm, which is approximately 6 times the mean grain size. No increase in pipe depth was observed in the sections where the pipe coincided with the wall. Laser equipment was used to determine the pipe dimensions in three experiments. In experiment I167 the pipe depth was measured at the end of the experiment when the pipe had reached the upstream side. Pipe depths of up to 3.5 mm were observed, which is approximately 24 times the mean grain size. The drawback to measuring pipe depth at the end of the experiment is that the pipe will already have deepened as a result of increased flow and will not be in an equilibrium condition.

Two supplementary experiments (B171 and E172) were therefore conducted in which the pipe depth was measured when the pipe was in an equilibrium condition. The pipe depth was found to increase towards the exit (Figure 4.40), starting at a depth of 2.4 times the mean grain diameter for Enschede sand and increasing to 4.5 times the mean

grain diameter near the tail. In Baskarp sand, the depth increased from 3.8 to 6.8 times the mean grain diameter. The increase in depth indicates that the pipe depth away from the tip is determined by secondary erosion.

Müller-Kirchenbauer and Van Beek et al. (2014b) studied pipe depth by evaluating the volume of sand that was ejected to the surface. They found that the average depth remained constant during lengthening. Van Beek et al. (2014b) calculated the average depth for an experiment on Oostelijke rivierenzand and found that it was approximately 2.6 mm, which is 11 times the mean grain diameter. Hanses (1985) estimated the pipe depth using plaster casts and photographs and found it to be approximately 1.5–2 mm, which is 5–6 times the mean diameter of the sand. Table 6.3 shows an overview of the available pipe depth estimates for pipes in equilibrium. The pipe depth varies along its length and along its width.

Table 6.3. Overview of pipe depths

Experiment	Sand type	d_{50} [mm]	Pipe depth [mm]		Pipe depth [no. of grains (d_{50})]	
			average	maximum	average	maximum
E150	Enschede	0.380		2.5*		6
O141	Oostelijke Rivierenzand	0.233	2.6		11	
Hanses experiments	Sand A	0.325	1–2		3–6	
B171	Baskarp sand	0.132	0.3–0.6	0.5–1.0	2.3–4.5	3.8–7.6
E172	Enschede sand	0.380	0.6–1.1	0.9–1.7	1.6–2.9	2.4–4.5

*maximum depth in observed section

It can be concluded that the pipe depth increases from the tail towards the exit. However, various researchers have found that the average pipe depth does not increase as a result of pipe lengthening and pipe depth did not increase linearly along the length of the pipe in experiment B171. It is curious that the average depth obtained with the laser was much smaller than the average depth obtained by measuring the crater volume. A possible explanation is the inclusion of the eroded volume underneath the hole. The absolute depth of the pipe was found to be larger in sand types with larger grains. However, the depth increase was not linearly related to grain size in the experiments considered and, in terms of the number of grains, the pipes in the fine sand were deepest.

In section 6.10.2 calculated pipe depths (based on critical shear stress and pipe gradient) will be compared with the measured depths in this section.

6.5.3. WIDTH-TO-DEPTH RATIO

The width-to-depth ratio can be determined for experiments B171 and E172, in which the pipe dimensions were determined using a laser. Figure 6.16 shows the width-to-maximum-depth ratio for both experiments and the width-to-average-depth ratio. The

average depth is determined by assuming that its shape resembles a sine. The relationship between maximum depth a_{\max} and average depth \bar{a} for a sine-shaped pipe is:

$$\bar{a} = \frac{2a_{\max}}{\pi} \quad 6.3$$

A sine proved to be a suitable approximation of the shape of a single pipe, which can be seen in two typical cross-sections obtained from experiments B171 and E172.

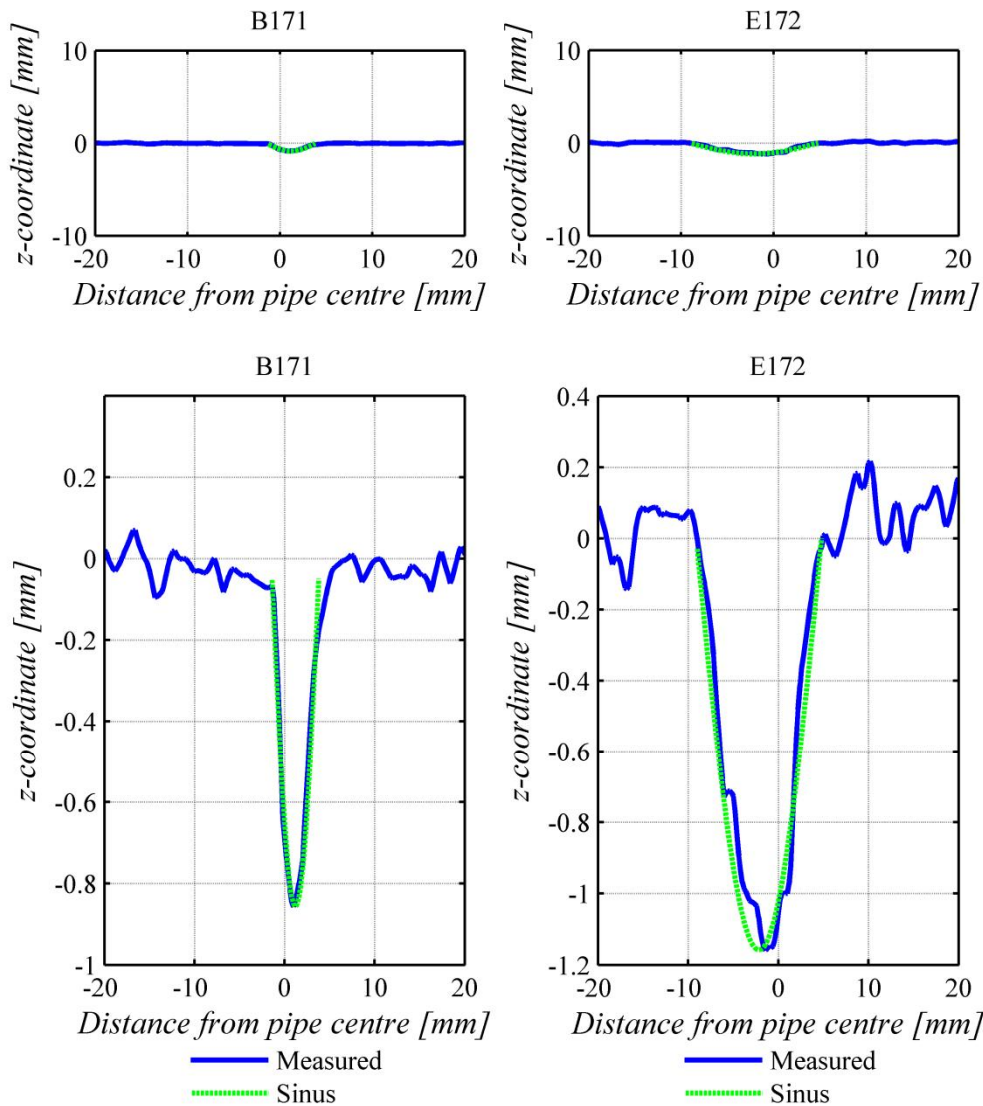


Figure 6.15. Examples of cross-sections in experiment B171 and E172 and a sine-shaped approximation of the pipe (top: true representation of pipe cross-section and bottom: scaled pipe cross-section)

The ratio of width to average depth varies considerably. This is expected because the width and, to a lesser extent, the depth also vary significantly along the pipe. The lower boundary of the width-to-depth ratio seems to be the most reliable basis for the

determination of the equilibrium ratio since the width will often be larger as a result of merging pipes or branches. This lower boundary of the ratio of width to average depth is approximately 7–8 in Baskarp sand, and 11–13 in Enschede sand.

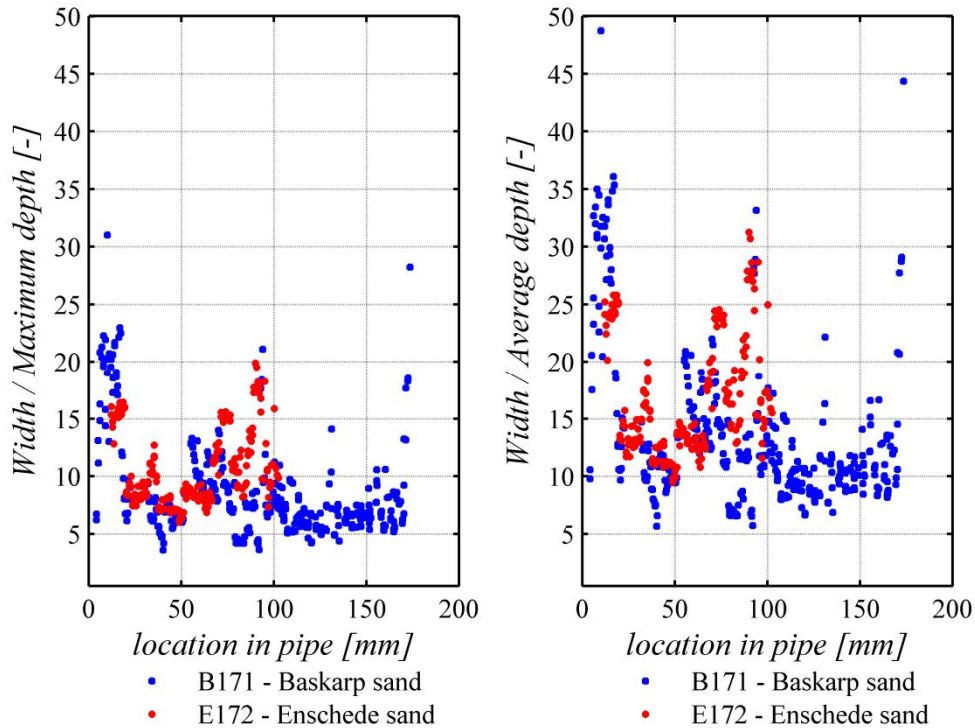


Figure 6.16. Width-to-depth ratios as a function of location in the pipe measured from the exit hole

6.5.4. PIPE GRADIENT

The pipe gradient was measured in a number of experiments. It is an important parameter since it determines the wall shear stress exerted by the water and it determines the hydraulic conditions in and around the pipe.

In the experiments, the pipe gradients were measured using riser tubes or pore pressure transducers in several locations on the top of the sand bed. Although there are only a few data points, these measurements show that the pressure drop in the pipe is linear over a large part of the pipe and that it drops significantly near the exit. The average gradient is calculated in a least squares regression analysis of the linear part of the pressure drop. The experiments in which the head drop was measured are the small-scale experiment E150, the medium-scale experiments Bms19 and Ims20, and selected experiments by Hanses (1985).

In the selected experiments by Hanses (1985), the hydraulic head in the pipe was measured at a pipe length that was expected to be close to the critical pipe length. At this length the head was brought back to 0 and then gradually reapplied such that the head distribution in the pipe could be measured using riser tubes. The measurements indicated a linear decrease in hydraulic head in the pipe until close to the exit. The pipe

gradient at the critical head was obtained by extrapolating the obtained pipe gradients at lower head drops.

In experiment E150, the pipe gradient was determined in a similar way for two pipe lengths, 0.175 m and 0.235 m. It should be noted that these pipe lengths are presumably larger than the critical pipe lengths, in other words when the pipes were not in an equilibrium condition. It is possible that the pipe width had not fully developed because erosion at the tip of the pipe was still ongoing. As a result, the gradient in the pipe may have been slightly larger than a fully eroded pipe in equilibrium.

Equilibrium was observed several times in the medium-scale experiments Bms19 and lms20 and the pipes developed in the path of the pore pressure transducers, allowing for the measurement of the hydraulic head in the pipes. The average pipe gradients at the equilibrium head (obtained by a linear least squares regression analysis of the hydraulic heads measured in the pipe) are listed for each of the experiments in Table 6.4.

Table 6.4. Average pipe gradients ($d\phi/dx$) and measured flow (Q_{exp}) for equilibrium conditions in various experiments

Experiment	Sand type	d_{50}	l	H	$d\phi/dx$	Q_{exp}
		[mm]	[m]	[m]	[-]	[m ³ /s]
26a	Sand A	0.325	0.250	0.130	0.089	3.98E-06
53	Sand A	0.325	0.165	0.214	0.092	2.01E-06
73	Sand A	0.325	0.615	0.298	0.060	1.32E-05
E150	Enschede	0.380	0.175	0.093	0.131	3.22E-07
E150	Enschede	0.380	0.235	0.079	0.119	1.45E-06
Bms19	Baskarp	0.132	0.440	0.149	0.096	2.16E-06
Bms19	Baskarp	0.132	0.480	0.159	0.093	2.35E-06
Bms19	Baskarp	0.132	0.520	0.170	0.095	2.58E-06
Bms19	Baskarp	0.132	0.690	0.179	0.088	2.95E-06
Bms19	Baskarp	0.132	0.940	0.187	0.089	3.31E-06
Bms19	Baskarp	0.132	1.135	0.203	0.108	3.81E-06
lms20	Itterbeck 330 μ m	0.283	0.647	0.175	0.059	1.14E-05
lms20	Itterbeck 330 μ m	0.283	0.742	0.162	0.038	1.17E-05
lms20	Itterbeck 330 μ m	0.283	1.197	0.170	0.065	1.54E-05

The effect of soil type on pipe gradient can be shown by comparing the medium-scale experiments (Figure 6.17, left-hand graph). The pipe gradient in Baskarp sand is considerably higher than the pipe gradient in Itterbeck sand, whereas the applied heads are comparable. Enschede sand, Itterbeck 330 μ m sand and Sand A are comparable, all being uniform medium-grained sands. However, the pipe gradients vary significantly. Differences in pipe gradient therefore result from differences in the hydraulic head, scale and configuration. Figure 6.17 (right-hand graph) shows the pipe gradient as a function of the total flow that exits the set-up through the hole. Obviously, the flow

through the pipe is linked to the overall head drop and the scale of the set-up. A relationship was observed between the pipe flow and pipe gradient. No correlation was found between the pipe gradient and pipe length. Apparently, the pipe gradient is not severely affected by the pipe length.

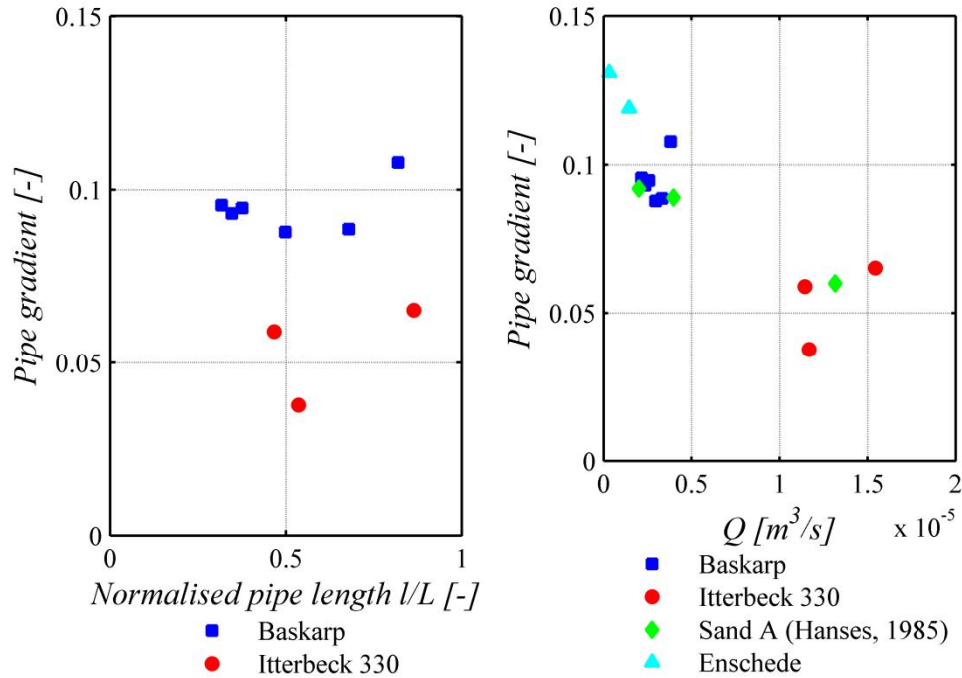


Figure 6.17. Pipe gradient as a function of (left) normalised pipe length (l/L) and (right) measured flow

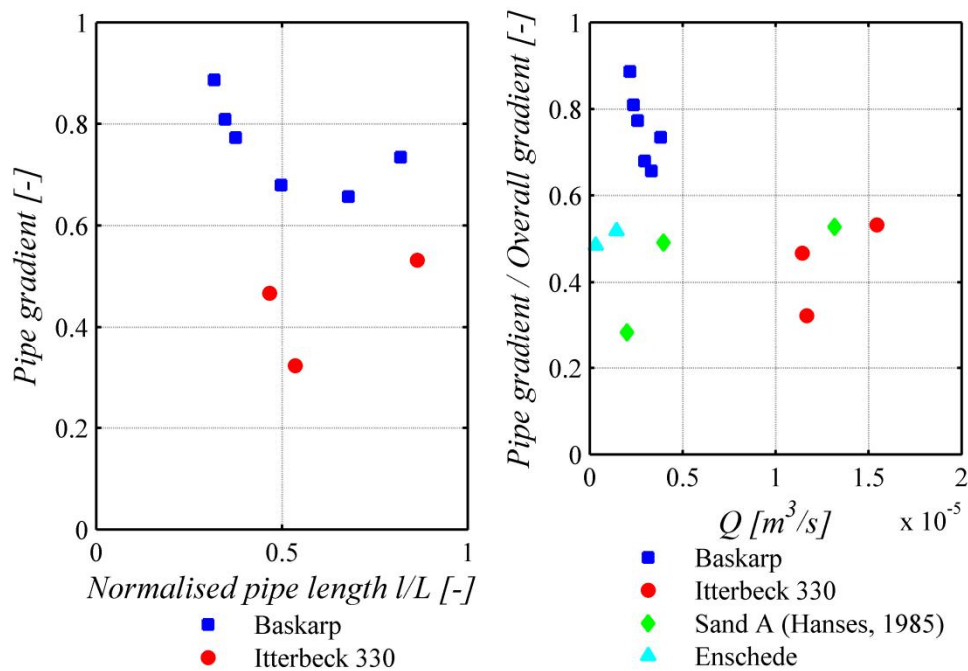


Figure 6.18. Relative pipe gradient as function of (left) normalised pipe length (l/L) and (right) measured flow

Naturally, the pipe gradient is lower than the overall gradient. Figure 6.18 shows the ratio of pipe gradient to overall gradient (relative pipe gradient) as a function of normalised pipe length and measured flow, representing the 'impact' of the pipe on the groundwater flow. In this figure it can be seen that, in the experiments on medium-grained sands, the relative pipe gradient was approximately 0.3 to 0.5, whereas the relative pipe gradient for Baskarp sand was approximately 0.8. This implies that the pipe in Baskarp sand has a much smaller effect on the flow pattern than the pipe in medium-grained sands.

In section 6.10.2 the pipe gradient will be combined with the critical shear stress to obtain the expected pipe depth.

6.5.5. PARTICLE AND FLOW VELOCITY

The water flow velocity is an important parameter for determining the hydraulic regime in the pipe. It was measured in experiment E150 by tracking particles in the video frames. The highest velocities are likely to be observed near the pipe tail, and when the pipe is approaching the upstream side. One of the movies showed the pipe section 3–8 cm from the exit hole at the point when the pipe length increased from 24 to 28 cm. The frame rate of the movie was 25 s^{-1} , which allowed for the tracking of particles with velocities up to approximately 1 m/s.

Major variations in particle velocity were observed. As noted already in Section 4.10.3, particles were taken up in the flow and sometimes re-deposited. This process was also observed during the tracking of particles. Figure 6.19 shows several examples of tracked particles. The particle velocity varied considerably in some cases, such as the particle observed from 374.07 minutes onwards: the particle slowed down and was deposited before being taken up by the flow fractions of a second later. This process of deposition and uptake in the flow was also clearly visible in the case of the particle tracked at 374.95 minutes. Other particles remained in the flow. The particle tracked at 374.65 minutes moved at a relatively high and constant speed through the middle of the pipe. The particle tracked at 374.72 minutes also moved at a fairly constant speed, although this was much slower than the particle at 374.65 minutes.

A total of 42 particles were tracked to establish a picture of the velocity differences. This large number was selected to ensure the inclusion of not only slower particles but also particles transported by the main flow in the pipe. To reduce the possibility of mistakes, the particles selected for the tracking process were those that were relatively easy to track. These particles were often, but not always, black particles. Only those particles that could be tracked in several subsequent images were selected. Figure 6.20 shows the velocity distribution for all tracked particles. Most velocities were less than 4 cm/s. The maximum velocity measured was 11.3 cm/s.

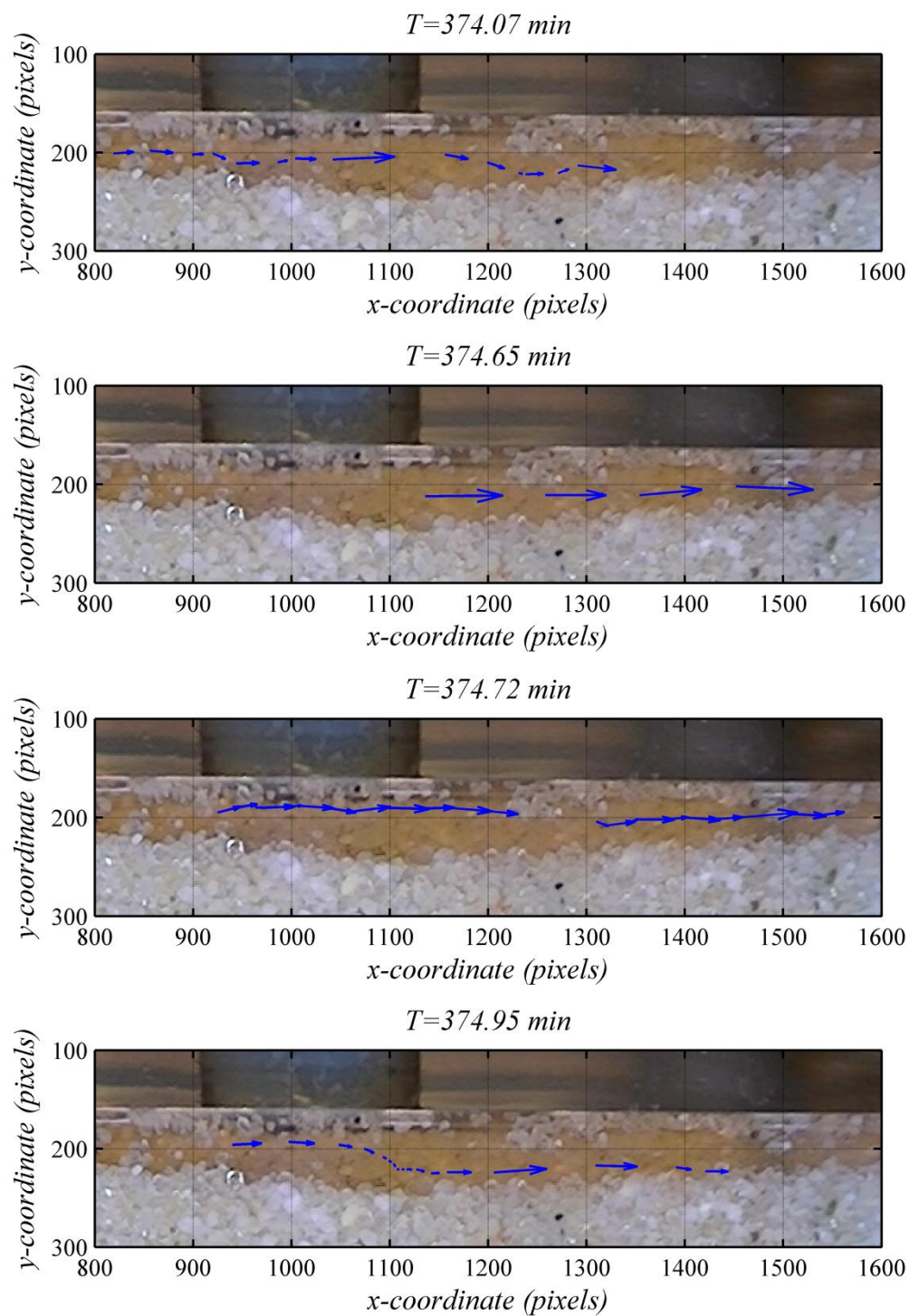


Figure 6.19. Particle tracking for different grains in the section 3–8 cm from the exit hole

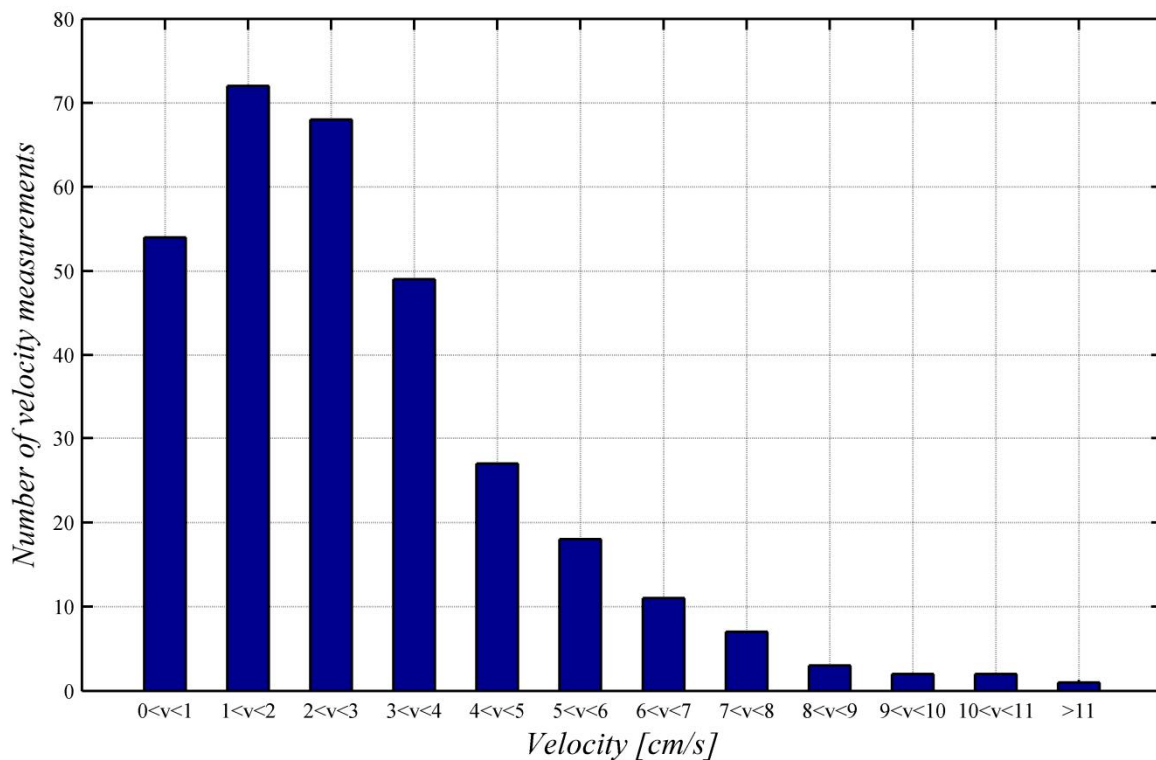


Figure 6.20. Velocity distribution for tracked particles in the section 3–8 cm from the exit hole (velocities in cm/s)

The flow velocity in the pipe is not constant: it reaches the maximum in the middle of the pipe and falls to zero towards the sides of the pipe. The average velocity is required to determine the hydraulic regime. Many of the particles will move slower than the average flow velocity, as they roll over the bottom or are deposited and taken up in the flow. Particles that move at a fairly constant speed are a good indication of the flow in the middle of the pipe. The particle tracked at 374.65 minutes moved at a velocity of 7 cm/s. Several more particles were tracked that moved at a fairly constant speed close to 7 cm/s. The average velocities of these particles were between 4.4 and 7.6 cm/s, with a standard deviation of 0.4–2.9 cm/s. Given that some of the measurements could be erroneous (the particle cannot always be clearly identified) and the fact that particles tend to move slower than the flow velocity, it is assumed here that the average flow velocity is between 5 and 9 cm/s. In section 6.10.2 this velocity will be compared to the calculated velocity based on equations for viscous flow through the pipe, limit-state equilibrium of particles and the experimentally obtained pipe gradient.

With an average sand permeability of $4.1\text{E-}4$ m/s and an average gradient of approximately 0.29, the average flow velocity in the sand sample is $1.2\text{E-}4$ m/s. This means that the flow velocity increases by a factor of nearly 600 from the sand sample to the pipe. Naturally, as the flow in the pipe is not restricted by the small size of the pores, the flow velocity will always be higher in the pipe than in the sample. However, the increase in velocity illustrates the contraction of flow lines towards the pipe.

6.5.6. CONCLUSIONS

The experiments made it possible to analyse pipe width and depth. The pipe width was assessed for all available experiments with a hole-type exit, mainly on the basis of photographs. The tip width was found to be approximately 30 times the grain diameter regardless of the particle size or scale. This constant width indicates the formation of a zone that needs to be fluidised. The width increases towards the downstream side. No relationship has been found between increasing pipe width and sand type.

The depth was determined in a variety of ways in the different experiments. The laser would appear to be the most accurate method. The pipe dimensions were measured in pipes in an equilibrium state in two different sand types using this method. It was found that depth increased towards the exit, indicating that particles in the pipe were in a limit-equilibrium state. The pipe depth ranged from 3.8–7.6 times the mean grain diameter in Baskarp sand and 2.4–4.5 times the mean grain diameter in Enschede sand. In these experiments, the pipe depth was not linearly related to the particle diameter. It should be kept in mind that there were only two experiments and so it was not possible to determine the experimental variation.

The width-to-depth ratio was approximately 7–8 for Baskarp sand and 12–13 for Enschede sand. The pipe in Baskarp sand was therefore relatively deep by comparison with the pipe in Enschede sand.

The hydraulic gradients in the pipe were measured in some of the experiments. The measurements suggested that the pipe affected groundwater flow more in Itterbeck 330 μm sand than in Baskarp sand. This concurs with the finding that pipe width increases with particle size. The impact of the pipe on the groundwater flow was not clearly affected by the scale or the shape of the sand box.

Particle velocity was determined in one of the visualisation experiments, in which a part of the pipe coincided with the side of the box. In the cases of the particles moving at a constant speed, the particle velocity more or less matched the water velocity. At a pipe length of 24–28 cm, the estimated average water velocity was approximately 5–9 cm/s.

6.6. PIPE FLOW

In the current Sellmeijer model, the pipe flow is relevant as it determines the flow forces on the grains and therefore determines the critical state equilibrium, assuming laminar flow in the pipe and infinite width. The relationship between flow rate, pipe depth and pipe gradient is derived from the Navier-Stokes equations for flow between parallel plates.

6.6.1. EFFECT OF PIPE SHAPE

The flow in the pipe depends on the pipe shape. The findings in Section 6.5.3 suggest that the pipe is sine-shaped, shallow and wide, with width and depth increasing towards the exit. The sides slope at an angle that is less than the friction angle.

Equations that relate the flow velocity to the dimensions of the pipe and the pressure drop in the pipe are not available for a configuration of this kind. Simplification is

therefore required. The typical shapes for which such equations are available are a circular pipe, rectangular duct and parallel plates (Figure 6.21).

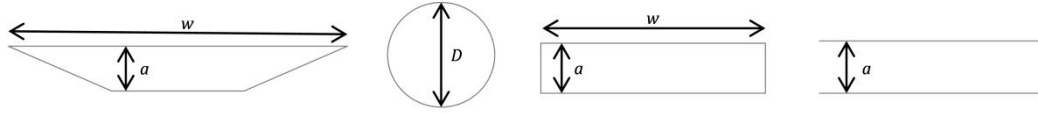


Figure 6.21. Pipe shapes: schematised erosion pipe, circular pipe, rectangular duct and infinitely wide pipe

Friction factors (f_F) for these channel shapes assuming laminar flow are available from Kakac et al. (1987). The friction factor links the pressure loss (Δp) in the pipe to the pipe dimensions and the average flow velocity in the pipe (\bar{v}):

$$f_F = \frac{\Delta p}{2l} \frac{D_h}{\rho_w \bar{v}^2} \quad 6.4$$

where D_h is the hydraulic diameter for non-circular shapes and l the pipe length. In the case of laminar flow, this friction factor is independent of the surface roughness (Smits, 2000). The friction factor for laminar flow depends on the Reynolds number:

$$\text{Re} = \frac{\rho_w \bar{v} D_h}{\mu} \quad 6.5$$

The hydraulic diameter for rectangular shapes is:

$$D_h = \frac{2aw}{(a+w)} \quad 6.6$$

which simplifies to $D_h = 2a$ for $w \gg a$.

In the case of circular pipe flow, the friction factor is:

$$f_F = \frac{16}{\text{Re}} \quad 6.7$$

Kandlikar et al. (2006), referring to Shah and London (1978), provided an equation for the Fanning friction factor for a rectangular channel with height a and width w :

$$f_F = \frac{24\beta}{\text{Re}} \quad 6.8$$

$$\beta = \left(1 - 1.3553 \frac{a}{w} + 1.9467 \left(\frac{a}{w} \right)^2 - 1.7012 \left(\frac{a}{w} \right)^3 + 0.9564 \left(\frac{a}{w} \right)^4 - 0.2537 \left(\frac{a}{w} \right)^5 \right) \quad 6.9$$

Equations 6.8 and 6.9 show that the friction factor for $w \gg a$ reduces to:

$$f_F = \frac{24}{\text{Re}} \quad 6.10$$

which concurs with the theoretical solution for parallel plates.

The pipe shape affects not only the flow but also the shear stress exerted on the pipe wall by the water flow. The wall shear stress is defined as:

$$\tau_w = \mu \left. \frac{\partial v}{\partial y} \right|_w \quad 6.11$$

and is related to the friction factor for laminar flow by:

$$f_F = \frac{\tau_w}{(1/2)\rho_w \bar{v}^2} \quad 6.12$$

The relationships between pipe flow, pipe dimensions and pipe pressure drop, and the wall stress following from these equations, are listed in Table 6.5.

Table 6.5. Pipe flow and wall shear stress

Circular pipe	Rectangular duct	Parallel plates
$\frac{dp}{dx} \pi D^4 = 128 Q \mu$ (6.13)	$\frac{dp}{dx} \frac{1}{\beta} \frac{(aw)^3}{(a+w)^2} = 12 Q \mu$ (6.14)	$\frac{dp}{dx} a^3 = 12 Q \mu^*$ (6.15)
$\tau_w = \frac{D}{4} \frac{dp}{dx}$ (6.16)	$\tau_w = \frac{1}{2} \left(\frac{aw}{w+a} \right) \frac{dp}{dx}$ (6.17)	$\tau_w = \frac{a}{2} \frac{dp}{dx}$ (6.18)

*Q is expressed here as volume per unit width per unit time, as opposed to Q in the other formulae, which is expressed as the volume per unit time.

Given the empirical findings in Section 6.5, a flat rectangular duct would seem to be the best representation of the pipe shape. When the width-to-depth ratio is high, the equations for a rectangular duct are similar to those for parallel plates. It can be easily seen that, when $w \gg a$, equation 6.14 reduces to:

$$\frac{dp}{dx} a^3 w = 12 Q \mu \quad 6.19$$

Figure 6.22 shows the relationship between flow and shear stress for a rectangular duct on the one hand and flow and shear stress for an infinitely wide rectangular duct ($F_{rd/pp}$) on the other (based on equations 6.14 to 6.18) as a function of a/w :

$$\frac{Q_{rd}}{Q_{pp}} = \frac{1}{\beta} \left(\frac{w}{a+w} \right)^2 \quad 6.20$$

$$\frac{\tau_{rd}}{\tau_{pp}} = \frac{1}{a/w + 1} \quad 6.21$$

This figure shows that the equations for parallel plates are a good approximation for very small depth-to-width ratios ($a/w=0.1$ results in a deviation of approximately 5%–10%) but that, as the ratios get higher, the equations for parallel plates overestimate the flow rate and shear stress by comparison with the more precise equations for rectangular ducts.

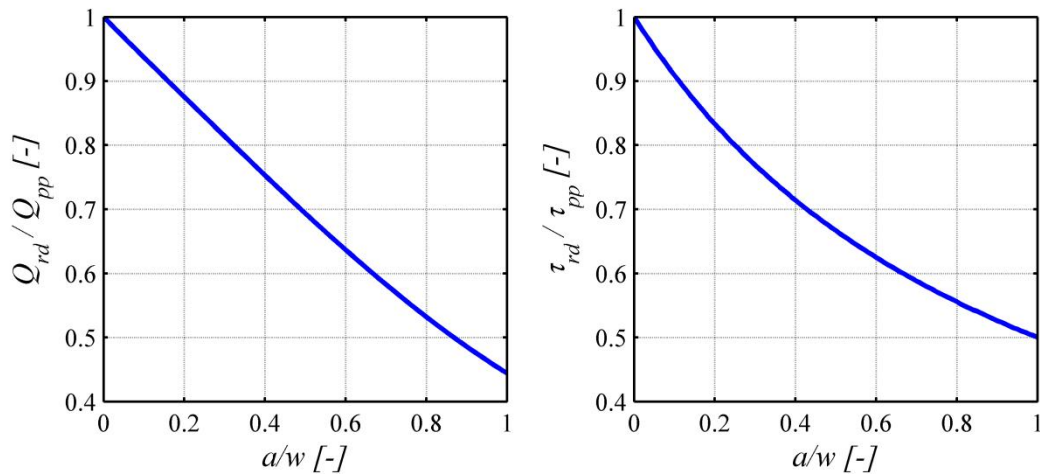


Figure 6.22. Ratio of flow and shear stress in a rectangular duct with respect to flow and shear stress between parallel plates, at different a/w ratios, showing the effect of width on the flow and shear stress

Table 6.5 shows that the equations for a circular pipe are very different from the equations for wide rectangular ducts and parallel plates. The wall shear stress is much lower for a circular pipe than for a wide rectangular pipe, assuming similar pipe depths ($D \cong a$) and pressure gradients in the pipe.

It can be concluded that the equations for flow through a rectangular duct will represent the pipe flow best. The equations can be simplified by assuming that width far exceeds depth, although this will result in a slight over-estimate of the flow. Even at the tip of the pipe, where the height-to-width ratio is highest, the ratio is 0.5 at most, even assuming a conservative ratio between width (approximately 30 grains) and depth (observed maximum 14 grains). In this extreme situation a 30% deviation in flow prediction can be expected. The main part of the pipe widens, as seen in the medium-scale experiments, while the increase of depth is limited and so the ratio falls. The simplified equation can therefore be considered appropriate.

6.6.2. HYDRAULIC REGIME

One of the assumptions relates to the hydraulic regime in the pipe. It is assumed that the flow is laminar, so that the equations in Table 6.5 are valid. The flow regime is determined by the ratio of inertial to viscous forces described by the Reynolds number:

$$Re = \frac{\rho_w \bar{v} D_h}{\mu} \quad 6.22$$

in which \bar{v} is the average flow velocity and D_h is the hydraulic diameter:

$$D_h = \frac{4A}{P} \quad 6.23$$

in which A is the cross-sectional surface and P the wetted perimeter.

The precise transition from laminar to transitional flow marked by the critical Reynolds number Re_c depends on many factors, including surface roughness, vibrations, noise and thermal disturbances. Below a Reynolds number of 2300 most of these

disturbances in the velocity field are suppressed and will not increase. If the disturbances are very small, turbulence may occur at a much higher value than the critical value (Smits, 2000).

The critical Reynolds number also depends on the type of configuration. Table 6.6 shows the critical Reynolds number for circular pipes, wide ducts and parallel plates. In the case of rectangular ducts, the critical Reynolds number depends on the width-to-height ratio. Chang et al. (2012) report experimental and theoretical values for the critical Reynolds number in relation to the width-to-height ratio that range from 1127 for a square duct to 2689 for a duct with $w \gg a$. These values are a good match with the critical Reynolds numbers for parallel plates.

Table 6.6. Critical Reynolds numbers for flow through circular tubes and flow through parallel plates

Circular pipes	Rectangular duct $w \gg a$	Parallel plates
$\text{Re} = \frac{\rho_w \bar{v} D}{\mu}$ $\text{Re}_c = 2300$ (Fox et al., 2009)	$\text{Re} = \frac{\rho_w \bar{v} 2a}{\mu}$ $\text{Re}_c = 2689$ (Chang et al., 2012)	$\text{Re} = \frac{\rho_w \bar{v} a}{\mu}$ $\text{Re}_c = 1400$ (Fox et al., 2009)

Given that the width-to-height ratio is generally quite high for erosion channels, for which the critical Reynolds numbers are in fair agreement with the critical Reynolds numbers for circular pipes, the latter provide a reasonable estimate of the critical Reynolds number and so the effect of shape on the critical Reynolds number does not require further investigation.

However, piping channels are not conventional channels: they are relatively small and have a rough wall consisting of grains which are relatively large by comparison with the size of the pipe. In Kandlikar and Grande's size classification (2003), the pipes are mini-channels ($3 \text{ mm} \geq D \geq 0.2 \text{ mm}$). Above a diameter of 3 mm, the pipes are classified as conventional channels.

Several researchers have reported that the critical Reynolds number in smooth channels is not affected by pipe dimensions (Kandlikar et al., 2006). However, the transition from the laminar to the turbulent region is affected by channel surface roughness. In the case of conventional channels, disturbances resulting from the roughness of the pipe channel are generally suppressed by the viscous forces. However, in smaller channels, large values of relative roughness are found more often because the roughness elements are relatively large with respect to the size of the channel. The critical Reynolds number is therefore likely to be lower for erosion channels than for conventional channels.

The ratio of roughness ε to channel diameter D_h defines the relative roughness. By analogy with Nikuradse's approach (1933), roughness is presented here in terms of grain diameter. As the pipe height is approximately 3–10 times the mean grain diameter, the relative roughness for piping channels (for which the hydraulic diameter is $2a$) is 0.17–0.05.

Kandlikar et al. (2006) describe the following criteria for critical Reynolds numbers in the ranges $(0 < \varepsilon / D_h \leq 0.08)$ and $(0.08 < \varepsilon / D_h \leq 0.15)$:

For $0 < \varepsilon / D_h \leq 0.08$:

$$\text{Re}_c = 2300 - \frac{(2300 - 800)}{0.08} \frac{\varepsilon}{D_h} \quad 6.24$$

For $0.08 < \varepsilon / D_h \leq 0.15$:

$$\text{Re}_c = 800 - 3270 \left(\frac{\varepsilon}{D_h} - 0.08 \right) \quad 6.25$$

Equation 6.25 also appears to function well for roughness numbers above 0.15: Brackbill and Kandlikar (2010) observed the transition at a Reynolds number of 200 at a relative roughness value of 0.276. Applying this model to piping channels with a relative roughness of 0.1–0.2 means that the critical Reynolds number will be approximately 408–735. These values have been investigated using circular pipes. No data are available for rectangular ducts. It has therefore been assumed here that critical Reynolds numbers for rectangular ducts are in the same range as for circular pipes.

Equation 6.25 for rectangular ducts where $w \gg a$ can be used to determine the Reynolds number for pipes encountered in backward erosion. Section 6.5.5 describes the velocity analysis for experiment E150: the estimated maximum average velocity based on particle tracking was 9 m/s. The maximum pipe depth measured in this area was 2.5 mm, but smaller depths were also observed. Assuming a temperature of approximately 20 degrees, both the critical and actual Reynolds numbers can be determined for different depths. Figure 6.23 shows that, at all depths considered, the flow in the pipe was laminar.

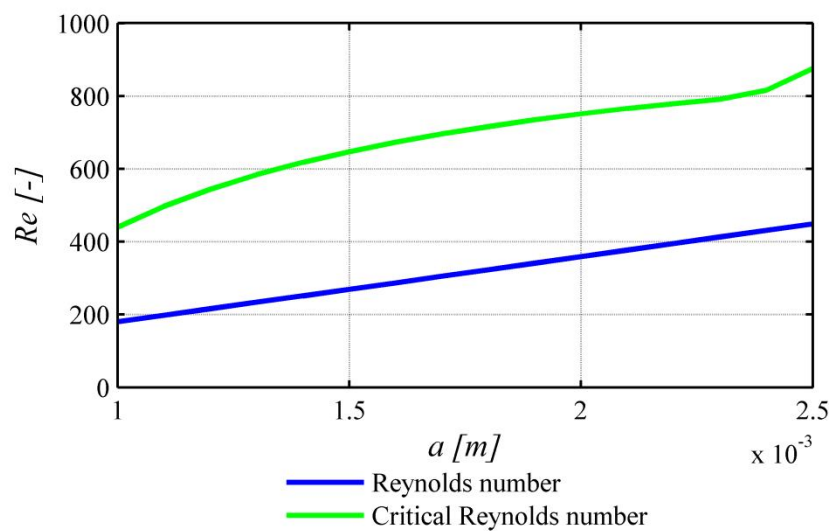


Figure 6.23. Actual and critical Reynolds numbers for different pipe depths

The question that remains is whether this conclusion can be extended to other sand types and scales. This would require determining the depth of the pipe and the flow velocity in situations that do not conform with experiment E150. Since no measurements are available of pipe depths and velocities at different scales, some assumptions will have to be made and information about pipe flow and critical shear stress will therefore be needed. This topic will therefore be covered in Section 6.10.

6.6.3. FLOW DEVELOPMENT

All the data presented are valid for fully developed flows only. As water enters along the entire length of the pipe, it is questionable whether flows will be fully developed. Near the tip of the pipe, this is unlikely to be the case; near the end of the pipe, the ratio of incoming flow to the pipe flow falls off and a fully developed flow is more likely. The entrance length, which is the length required for a Hagen-Poiseuille velocity profile to develop, is given by the following equation:

$$\frac{l_e}{D} = 0.05 \text{ Re} \quad 6.26$$

As the pipe depth is limited and the Reynolds number is relatively low, the assumption of fully developed flow in the middle of the pipe and at the tail is acceptable on the basis of this equation. However, the effect of roughness on the entrance length has not yet been investigated.

6.6.4. CONCLUSIONS

It is essential to include the flow through the pipe when modelling pipe progression. Equations are available in the literature that relate the pipe dimensions to both the flow through the pipe and the pressure gradient in the pipe in several configurations, such as a circular pipe, a rectangular duct, or parallel plates. Considering the large width-to-depth ratios observed in the experiments, a rectangular duct with width \gg depth seems to be the most appropriate configuration.

The hydraulic regime in the pipe depends on the relative roughness. A comparison of the critical Reynolds number and the actual Reynolds number from experiment E150 proved that, in this experiment, the flow through the pipe was laminar. At present, it is assumed that this will also be the case for pipes at other scales and other fine to medium-grained sands. This topic will be further elaborated in Section 6.10.

6.7. EROSION PROCESSES

The erosion mechanism that causes the pipe to lengthen and widen is the basis for the prediction of pipe progression and it is therefore essential to understand this mechanism properly. The analysis of the experiments presented in this chapter provides valuable information about the erosion mechanism that can serve as a basis for a new and more complete model.

Hanses (1985) distinguished between primary and secondary erosion. The first is defined as erosion at the tip of the pipe resulting in pipe lengthening, and the latter as the erosion of the walls of the pipe resulting in pipe widening or deepening.

The experiments show that both 'primary erosion' and 'secondary erosion' are important for the prediction of piping, as will be explained below.

A first indicator of the importance of primary erosion was found in the experiments in which the sand bed was layered (Ims18 and B171), resulting in pipe formation perpendicular to the direction of flow when a slightly coarser layer was encountered. The fact that such a small variation in grain size can stop lengthening is a strong indication that a resistance needs to be overcome near the tip of the pipe to facilitate pipe progression. In addition, the width of the pipe tip is independent of scale or pipe length. A possible explanation of this constant width is that the hydraulic load at the tip of the pipe needs to overcome the resistance for a certain group of grains. This corresponds to the findings of Hanses (1985) and Townsend et al. (1988), who observed the intermittent transport of groups of grains at the pipe tip. Another important finding is that the tip width of the pipe was found to increase with grain size and to be independent of scale: the width of the pipe tip was approximately 30 grains. This suggests that the area in which the sand resistance needs to be overcome is larger for sands with larger grain sizes; in other words, a larger zone needs to be brought into suspension. This concurs with the study of pipe initiation in Chapter 5, which showed that a group of at least 20 grains needs to be transported to initiate a pipe, irrespective of grain size and the scale of the set-up (Van Beek et al., 2014a). A relationship between particle size and pipe depth at the pipe tip has not been found, but this could be due to the fact that only two experiments have been performed.

If primary erosion indeed determines pipe lengthening, the relevance of secondary erosion becomes clear at once. Secondary erosion affects the hydraulic gradient in the pipe, which in turn determines the hydraulic conditions near the tip of the pipe. Indeed, secondary erosion was also observed in the experiments. In all experiments, the pipe width near the tail increased upon lengthening. Photographs and the measured pipe geometry in Figure 6.8 show the meandering of the pipe, resulting in scouring in the outer bend of the pipe. The scour results in the lateral widening and deepening of the pipe. Furthermore, a relationship was found between pipe gradient and flow, indicating that the pipe size adjusts to convey the amount of water transported through the pipe.

Both erosion mechanisms should therefore be taken into account to model the progression of the pipe correctly. This has not been done so far: Schmertmann (2000) neglected the effect of the pipe on the groundwater flow and Sellmeijer (1988, 2011) neglected the process of primary erosion. Hanses did take primary erosion into account, in combination with the gradient in the pipe obtained from experiments, but did not establish a model that was suitable for practice. The processes of primary and secondary erosion will be discussed in the following sections.

6.8. MODELLING PRIMARY EROSION

The modelling of primary erosion is required to determine pipe lengthening, especially in heterogeneous soils. Hanses (1985) was the first to describe the lengthening of the pipe by primary erosion. He observed that, despite the different geometries, the phenomenon of backward erosion at the tip was similar in all experiments. He concluded that the flow conditions must be such that the sand in front of the pipe is fluidised. To validate this hypothesis, he calculated the pore pressures at five locations near the pipe tip (at a distance of 2 cm in front of, below and besides the pipe),

assuming a fixed pipe width of 2 cm. The pressures calculated at these fixed locations were the same for different pipe lengths. The average calculated pressure gradients far exceeded the critical heave gradient. This can be attributed to the schematisation of the pipe. Hanses therefore concluded that the shape of the pipe tip is determined by fluidisation, with the pipe being deeper at the sides.

The continuous measurement of pore pressures using pore pressure gauges in the medium-scale experiments (Bms19 and Ims20) described in Section 4.9 made it possible to determine the local flow conditions required for pipe progression. In order to do so, photographs were selected in which the pipe was close to the pressure gauge. The location of the pipe tip was then determined in the photographs to show how the pipe tip moved over time. This made it possible to calculate changes in water pressure as a function of the distance from the pipe tip. It is hypothesised here that, as in the case of pipe initiation in an intact sand bed (Chapter 5), pipe development is driven by a given gradient exceeding a certain level in the sand upstream of the pipe. Using the measured pore pressures as a function of distance from the pipe, the gradient can be calculated for different distances from the pipe. This was done using 3 and 25 data points to reduce the effect of fluctuations in the measurements obtained from the pore pressure gauges associated with the limitations of the equipment.

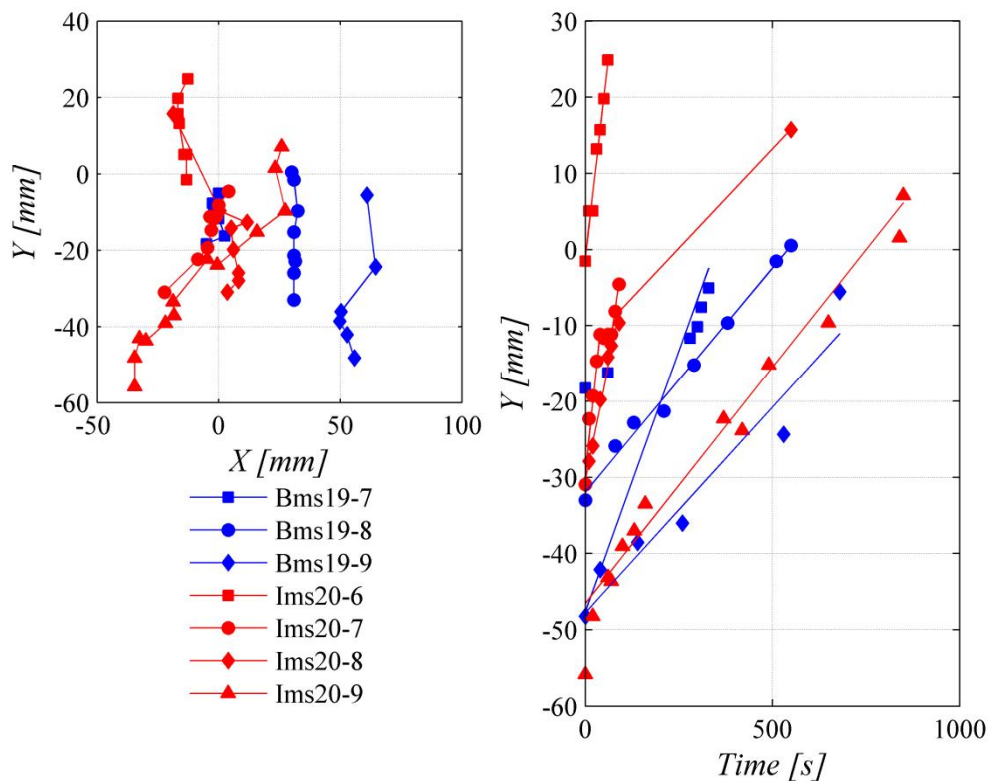


Figure 6.24. Development of the pipe tip near the pressure gauges, with the pressure gauges located in the origin of the graph (left-hand graph) and measured pipe development in time (right-hand graph), with markers indicating observations from photographs and the line the least square fit of time and location

The pressure gauges used for the analysis were numbers 6, 7, 8 and 9, which were located at 175, 385, 785 and 1085 mm from the exit hole respectively. Given the

seepage length of 1385 mm, the transducers were located at approximately 13, 28, 57 and 78% of the seepage length. It is not always possible to register pipe formation both before and after the transducer. Pressure gauges 6 and 7 were located close to the steel frame, which was placed on top of the acrylic plate in such a way that pipe formation either before or behind the gauge could not be observed. In some images, it was difficult to observe the pipe tip at all.

The pipe tip did not develop under all of the pore pressure gauges. Figure 6.24 shows the path of the pipe in relation to the pressure gauges in both experiments. The pipe tip does not follow a straight path. This complicated the determination of the time taken by a pipe to cover the distance between the gauges and the pipe tip. The relationship was determined by least square linear regression analysis of the distance in the x-direction and time, as shown in Figure 6.24. Although the y-direction of the pipe did vary considerably, the progression of the pipe in the direction of flow was fairly constant.

The pipe tip in the Baskarp sand experiment was located at quite a large distance from pressure gauges 8 and 9. It should be noted that the pipe may develop below the pressure gauges as a result of pipe lengthening and widening at a later stage. However, only the development of the tip is relevant for primary erosion.

Figure 6.25 and Figure 6.26 show the calculated gradients for experiments Bms19 and lms20 respectively. The fluctuation in gradient depends largely on the stability of the pressure transducers and absolute values are not reliable. Pressure gauges 6, 7 and 8 in experiment lms20 registered the pipe tip location as a sharp increase in the gradient of short duration. Pressure gauge 9 did not register any distinct peak. In experiment Bms19, a distinct peak was observed for gauge 7 only when the pipe tip was approximately 40 mm away from the pressure gauge. This shift could be related to the intermittent pattern of pipe development. This gauge registered pipe development only several centimetres in front of the gauge and it proved necessary to extrapolate pipe development beyond the gauge. If the pipe actually stopped developing before reaching the gauge, extrapolation may have led to an error in the location of the pipe tip.

The presence of a peak was found to be related to the lateral distance between the pipe tip and the gauge. Figure 6.24 shows that, in experiment Bms19, the pipe is near pressure gauge 7, but approximately 30 and 60 mm away from gauges 8 and 9. The pipe would therefore seem to be too far away to cause any change in the gradients measured by gauges 8 and 9.

In experiment lms20, the pipe tip formed relatively close to gauges 6, 7 and 8 but it was slightly further away (25 mm) from gauge 9. This corresponds to the observations of the gradient.

Apparently, the increase in gradient linked to the formation of the pipe tip occurs only in a very small zone around the pipe tip (< approximately 20 mm). The width of the tip should also be considered here: it is approximately 30 times d_{50} , or 4 mm for Baskarp sand and 10 mm for Itterbeck sand.

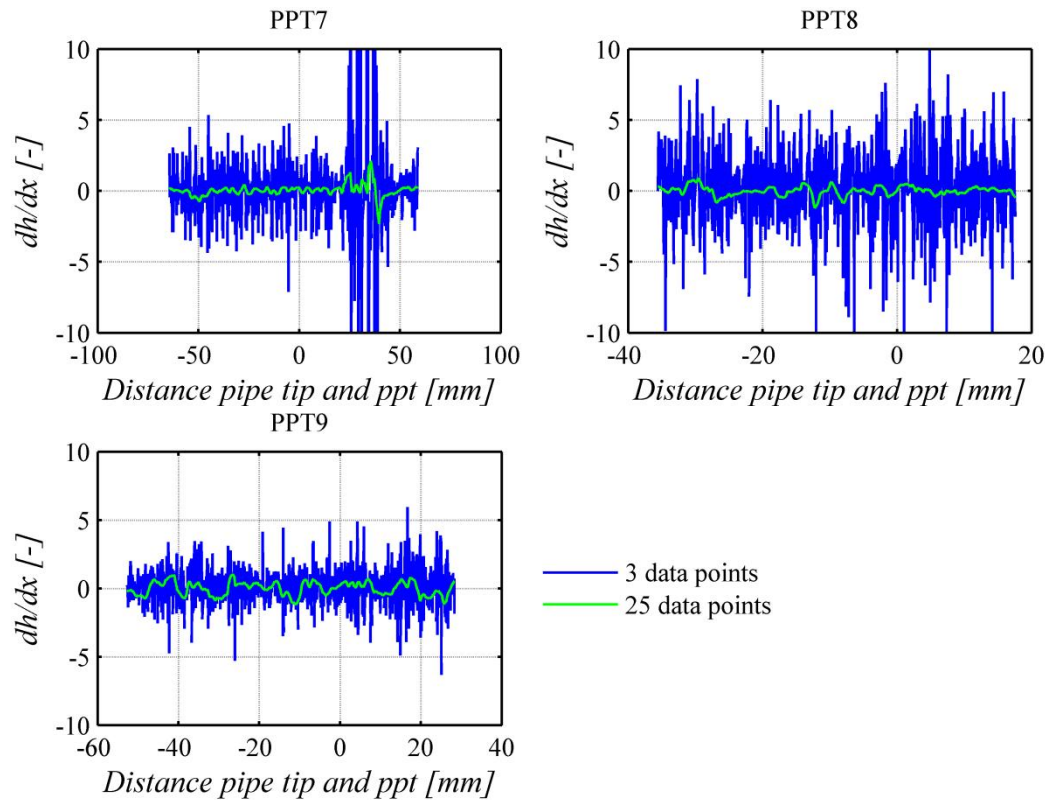


Figure 6.25. Calculated gradients as a function of distance between pipe tip and pressure gauge in experiment Bms19

The findings illustrate that the local increase in gradient causes the pipe to progress. An absolute value could not be obtained but it may be possible to derive it from numerical calculations. When analysing the flow around the tip, the same issues with singular behaviour will occur as were encountered with respect to the prediction of pipe initiation. It is possible that a similar approach involving the consideration of a group of grains to determine the gradient could resolve this difficulty and the constant width of the pipe tip suggests that this could be a suitable approach. Arching may cause the local critical gradient to be slightly higher than expected on the basis of the heave criterion, which concurs with the findings of Hanses (1985).

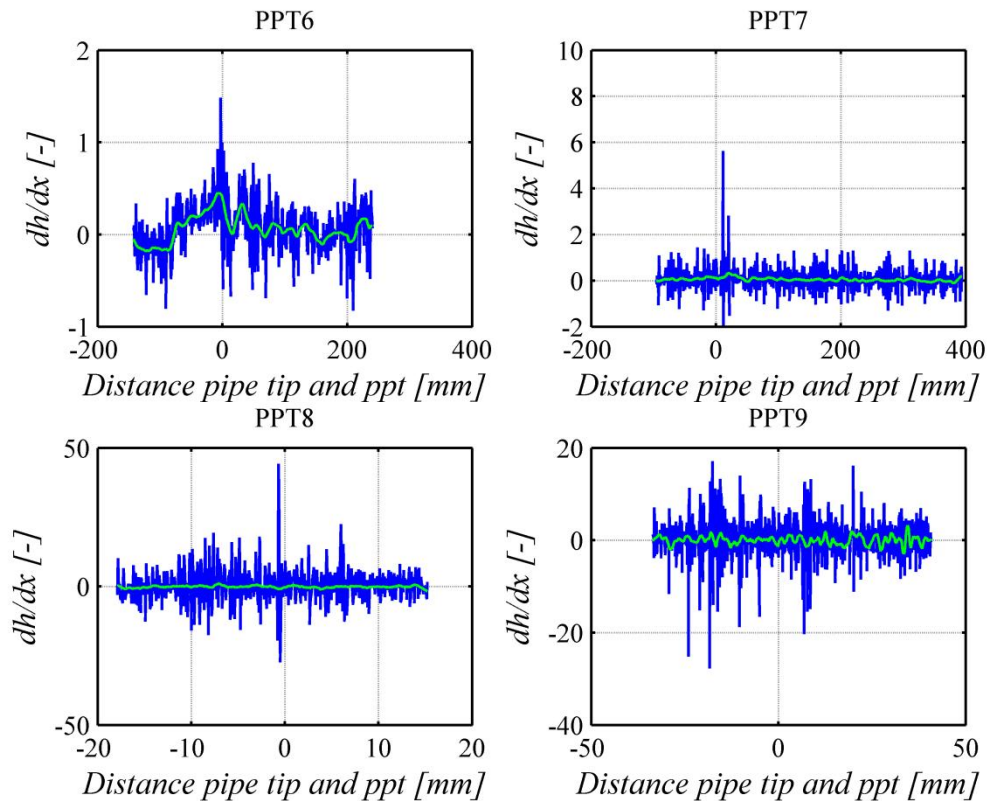


Figure 6.26. Calculated gradients as a function of the distance between pipe tip and pressure gauge in experiment lms20

6.9. MODELLING SECONDARY EROSION

The process of secondary erosion determines the shape of the pipe away from the tip, and thus the pipe gradient and its impact on the flow pattern in the sand body. It therefore indirectly affects primary erosion as well, making it essential for the prediction of backward erosion.

The erosion of particles under the action of horizontal flow is governed by the shear stress exerted by the water. Once this shear stress has exceeded a critical value – the critical shear stress (τ_c) – particles are transported.

Although this sounds like a well-defined concept, the determination of this threshold condition in experiments is fraught with difficulties. Even in uniform sediments, the surface bed consists of grains of various sizes, shapes and orientations, all of which affect the critical shear stress at which each grain will start to move. In addition, the shear stress that is exerted by the water is more or less constant in laminar flows but there is a considerable variation in the shear stresses exerted in turbulent flows and so not all grains will start to move at the same time. This process is even more complicated in non-uniform sediments. Clearly, the incipient motion of sediment is a stochastic phenomenon. It can therefore be difficult to determine the critical shear stress at which grains start to move. Some authors base incipience on observations of the bed load, whereas others use criteria based on visual observation. Kramer (1935) suggested the following stages:

- No sediment motion: all grains are motionless.

- Sparse sediment motion: only a few fine grains move, here and there.
- Mean sediment motion: sediment grains smaller than the median diameter move everywhere and the movement is too intense to count the number of grains that are moving in a given area.
- Strong sediment motion: all sizes of sediment move and the bed configuration changes progressively.

The spread in data observed in experimentally determined critical shear stresses could be a factor contributing to the subjectivity of the definition.

Erosion in piping channels differs in several respects from 'standard' erosion in the bed of a stream. There is a preferential tendency towards pipe widening, rather than deepening, that involves the erosion of particles along the sloping walls of the pipe. Water inflow through the walls and bottom of the pipe exert an extra force on the particles. Furthermore, the hydraulic regime in the small pipes can differ from that in a larger flume.

This section explains the forces relating to particle transport, the Shields curve and its applicability to piping channels, critical shear stresses for laminar flow and the effect of slope angle and water inflow on critical shear stress.

6.9.1. FORCES ON THE PARTICLES

As water flows over a channel bed, a frictional force is exerted on the rough surface represented by the bed of particles. Whether particles are eroded depends on the critical shear stress and therefore on the forces acting on the grain. Figure 6.27 shows the forces acting on the grain: the gravity force, the drag force and the lift force.

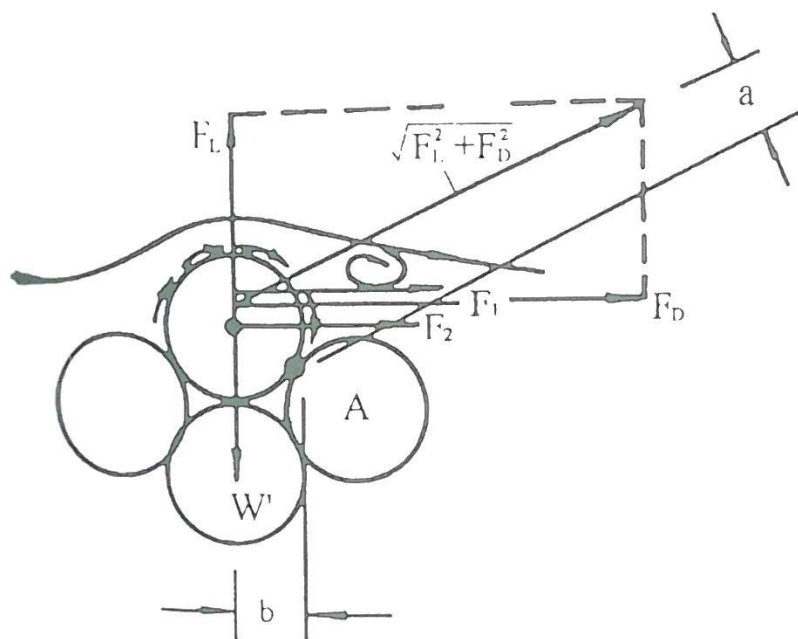


Figure 6.27. Drag and lift forces acting on particles resting on the bed surface (Chien and Wan, 1999)

The gravity force acts through the centre of the grain and is determined by its weight:

$$F_g = \frac{\pi}{6} \gamma_p' d^3 \quad 6.27$$

in which d is the mean grain size and γ_p' is the specific weight of the submerged particles.

The drag force exerted by the water flowing through the pipe depends on the flow velocity. If the flow around the grain is laminar, frictional forces determine the drag force. However, if the flow velocity increases, the flow lines separate in the form of a small wake, resulting in a pressure difference between the front and back surface of the grain. This happens when the grain Reynolds number is larger than 3.5 (Chien and Wan, 1999):

$$Re^* = \frac{\rho_w u^* d}{\mu} \quad 6.28$$

in which u^* is the shear velocity defined as:

$$u^* = \sqrt{\frac{\tau_w}{\rho_w}} \quad 6.29$$

It should be noted here that the value of 3.5 has been derived using flumes in which the flow is turbulent. The number might be related to the thickness of the laminar boundary layer in relation to the size of the grain. It is unlikely that wakes will form in fully laminar flow as a result of high grain Reynolds numbers (personal communication Van Rijn, 2014).

The frictional force (F_1 in Figure 6.27) does not act through the centre of the grain as only the upper part of the grain is exposed to the water flow. The force due to pressure differences between the front and back (F_2 in Figure 6.27) does act through the centre of the grain.

Lift forces are caused by the difference in horizontal flow velocity along the top of the grain and the velocity of the flowing water near the bed surface. In addition, water enters the pipe from the bottom and walls, adding an extra lift force.

The equilibrium of forces as proposed by Sellmeijer (1988) includes the drag force on the lines of White's approach (1940). It is derived from the shear stress that acts on a group of particles. This approach defines a packing coefficient η (also known as White's constant), which represents the ratio of the area of the grains over which the shear stress is divided to the total area considered:

$$\eta = \frac{nd^2}{A} \quad 6.30$$

in which n is the number of particles and A represents the unit area. In White's approach (1940), the packing coefficient is multiplied by an experimental coefficient α to account for the action of forces above the centre of gravity of the grain. In the approach by Sellmeijer (1988) the combined coefficient $\alpha\eta$ is represented as η and so the drag force on an average grain can be calculated as:

$$F_d = \tau_w \frac{d^2}{\eta} \quad 6.31$$

The packing coefficients, multiplied by a factor alpha, were found to be approximately 0.31 and 0.37 for the two sand types tested (in laminar flow) (White, 1940).

The lift forces were neglected in this approach. Initially, Sellmeijer (1988) included the force resulting from inflowing water from the porous medium into the pipe in his approach. The seepage force exerted by the water on a porous bed is:

$$F_s = \gamma_w \frac{\partial \phi}{\partial y}, \quad 6.32$$

taking into account the fact that the flow pattern near the surface is different from that inside the sand sample. Martin (1970) concludes that the seepage force acting on a grain on the bed of a stream is approximately 0.35–0.40 times the seepage force acting inside the sand sample. Martin (1970) also concludes that incipient motion is not measurably affected by an upward flow because the seepage gradient disappears when the particle is lifted. In 2006, Sellmeijer therefore reduced the four-force approach that took gravity, drag, vertical and hydraulic gradients into account into a two-force approach, that takes only drag and gravity into account.

On the basis of the equilibrium of forces, a semi-analytical formulation of the critical shear stress was defined as:

$$\tau_c = \eta \frac{\pi}{6} \gamma_p' d \tan \theta \quad 6.33$$

in which θ is the angle of repose or bedding angle, which was used as a calibration parameter in the Delta Flume experiments. The packing coefficient was set at a safe value of 0.25 based on the $\alpha\eta$ values derived from the experiments.

6.9.2. THE SHIELDS DIAGRAM

Shields (1936) proposed a different and more empirical approach to including the equilibrium of forces with the aim of determining the critical shear stress for incipient motion. This approach states that the drag force is a function of gravity and lift forces:

$$\frac{\tau_c}{\gamma_p' d} = f\left(\frac{\rho_w u^* d}{\mu}\right) \quad 6.34$$

In other words, the Shields parameter Ψ (the left-hand part of the equation) is solely a function of the particle Reynolds number. The critical Shields parameter, which reflects the incipience of motion, has been determined experimentally by various researchers for different regimes, resulting in the Shields diagram (Figure 6.28).

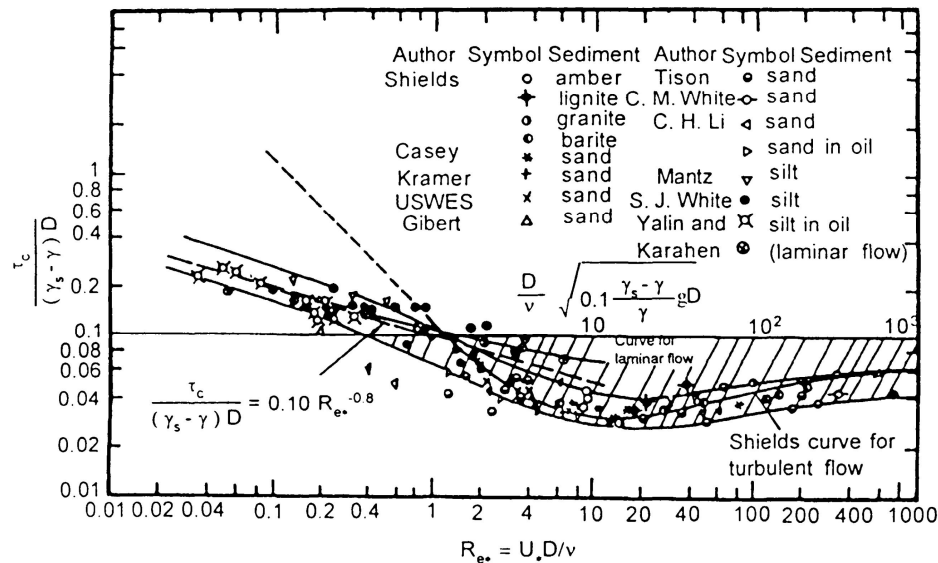


Figure 6.28. Condition for incipient motion for non-cohesive sediment (Shields curve and its modification) (Chien and Wan, 1999)

The Shields curve here is mainly intended for, and based on, experiments in flumes with turbulent flow. It can be broken down into three sections, which require explanation in order to clarify the applicability of the curve. The first part of the curve shows a more or less linear fall in the Shields parameter that results from an increase in the particle Reynolds number. This part of the curve reflects the laminar region, where particles are shielded from the turbulent flow by the laminar sub-layer, the region near the no-slip boundary where the velocities are relatively low, resulting in a laminar flow. The second section starts where the particle Reynolds number is approximately 10. Here, the curve reaches its lowest point and the thickness of the laminar sub-layer is approximately the grain diameter. In the third section, where the particle Reynolds numbers >10 , the Shields parameter increases as the weight of the grain becomes more important.

6.9.3. INCIPIENT MOTION IN LAMINAR FLOW

Section 6.6.2 consists of a discussion of the hydraulic regime in the pipe. Although it is still necessary to extrapolate the results, and so information about the critical shear stress and pipe depth is needed, the assumption of laminar flow appears to be reasonable on the basis of the experiments.

Several researchers have studied incipient motion in laminar flow. Generally, the Shields parameter has been determined in a flume with dimensions that far exceed those of the erosion channels. As the Reynolds number is linearly related to the water depth, the flow in the flume is generally turbulent when motion is incipient.

When the particles are relatively small by comparison with the thickness of the laminar sub-layer, the flow around the grain is laminar. Yalin and Karahan (1979), who performed experiments in fully laminar flows, state that the thickness of the laminar sub-layer does not affect incipient motion. The critical shear stress is the same in fully laminar flows and in turbulent flows with grains shielded by the laminar sub-layer. The results obtained in larger flumes, but with grains shielded in the laminar sub-layer, can therefore be used to predict the initiation of motion in fully laminar conditions, as is

assumed to be the case with piping channels. On the basis of experiments by Nikuradse (1933), White (1940) reports that, in turbulent flow, viscous forces around the grains dominate when the particle Reynolds number is less than 3.5 and so the flow around the grain can be considered to be laminar.

Experiments on incipient motion in laminar flow (due to the presence of a laminar sub-layer, a small water depth or the use of a viscous fluid) have been described in White (1940), Ward (1968), White (1970), Mantz (1977), Yalin and Karahan (1979), Govers (1987), Loiseleux et al. (2005) and Ouriemi et al. (2007). Table 6.7 presents an overview of these experiments.

Table 6.7. Overview of incipient motion for particles in laminar flow

Source	Material	Mean grain size [mm]	Medium
White (1940)	Sand	0.21 / 0.90	Oil
Ward (1968)	Sands / glass beads / taconite / plastics	0.240–2.29	Oil
White (1970)	Natural sands and silts / Plastics / Lead glass / Crushed silica	0.016–2.2	Water / Oil
Mantz (1977)	Natural grains / Crushed silica	0.015–0.066	Water
Yalin and Karahan (1979)	Sieved river sands	0.56–2.85	Glycerine / water mixture
Govers (1987)	Silt and Quartz sands	0.045–1.098	Water
Loiseleux et al. (2005)	Glass beads	0.110–0.220	Water
Ouriemi et al. (2007)	Polystyrene / PMMA / Glass spheres	0.132–0.538	Oil / water mixture

Figure 6.29 shows the experimental results in a Shields diagram (Shields parameter as a function of the particle Reynolds number). The experiments on plastics described in Ward (1968) have been removed from the selection since the particle density was only slightly higher than the water density. In most test series, the critical Shields parameter falls and there is a rise in the particle Reynolds number, except in the case of Ouriemi et al. (2007), who concluded that the critical Shields parameter is constant in the laminar regime ($\Psi_c = 0.12 \pm 0.03$).

Mantz (1977) presents a formulation for the critical Shields parameter derived for laminar flow around the grain (valid for particle Reynolds numbers of 0.03–1) on the basis of the experiments described by White (1970) and his additional experiments:

$$\Psi_c = 0.1 \text{Re}^{*-0.3} \quad 6.35$$

White's theoretical formulation (1940), as applied with a constant bedding angle ($\theta=37$ degrees) and the conservative coefficient $\eta=0.25$ commonly used in the Sellmeijer model, is also presented in the graph and can be written as:

$$\Psi_c = \eta \frac{\pi}{6} \tan \theta \quad 6.36$$

Figure 6.29 shows a considerable spread of data. White's experiments (1970) (performed with water) resulted in critical Shields parameters that were markedly lower than those from the other experiments. It is possible that the particle size in White's experiments (1970) started to approach the size of the laminar sub-layer and that the effect of turbulence therefore became apparent. Indeed, the particle Reynolds number approaches 3.5 in these experimental results and these values have therefore been disregarded. The critical Shields parameters found by Govers (1987) were relatively high by comparison with the other experiments. The reason for this remains unclear. The small water depths used by Govers (1987) and Loiseleux et al. (2005) may have resulted in slightly higher critical Shields parameters, although no effect of depth was observed with most sand types tested by Govers (1987).

Extrapolating the criterion selected by Mantz (1977) would underestimate the critical Shields parameter in the region of interest (0.1–0.5 mm) and the critical Shields parameter calibrated for the Sellmeijer model (0.1) is not conservative for larger particles. A new fit based on available experimental results will therefore be suggested.

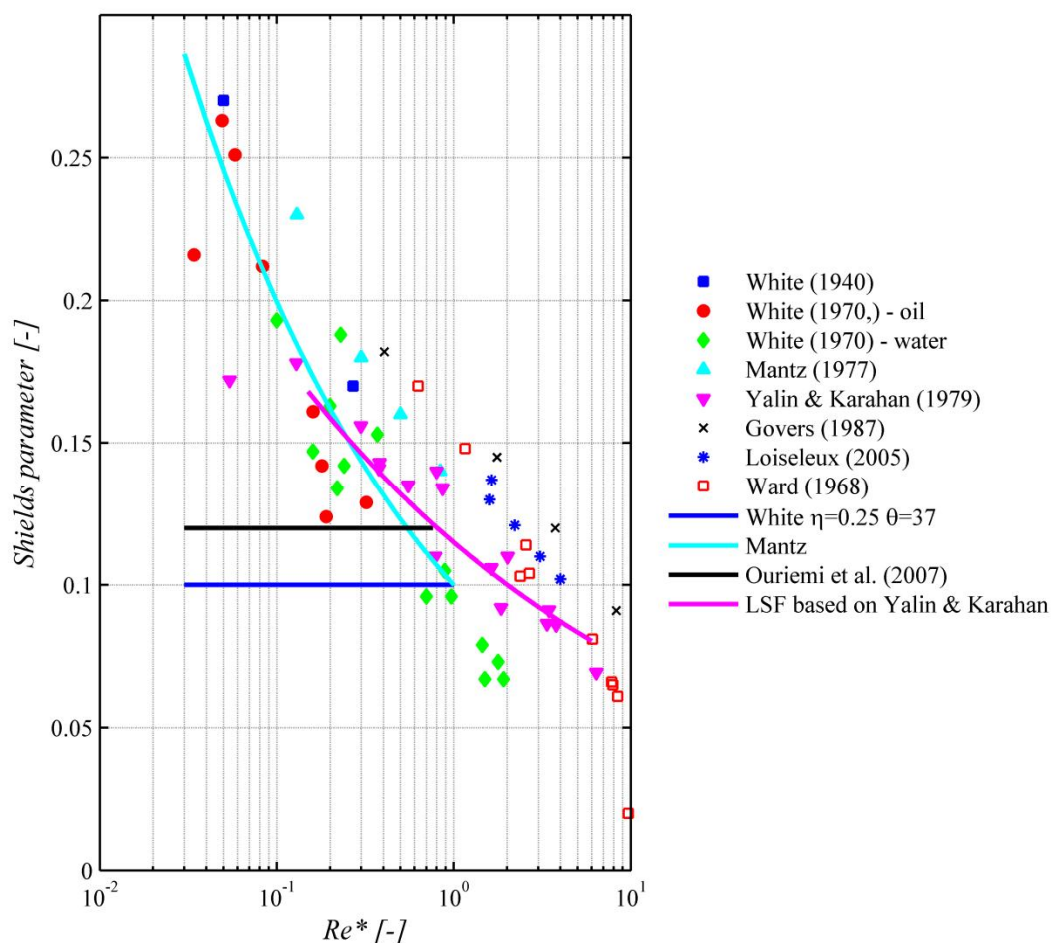


Figure 6.29. Shields parameter as a function of the particle Reynolds number showing experimental results for laminar flow, various fits and theoretical relations

The Shields diagram is useful for showing the effect of the hydraulic regime on the incipience of grain motion. However, it can be difficult to use since as the shear stress and particle diameter appear both in the particle Reynolds number and in the Shields parameter. The Shields parameter is therefore also often displayed as a function of the dimensionless particle number D^* to account for viscosity and particle density (see, among others, Cao et al., 2006):

$$D^* = d \left(\frac{\Delta g}{\nu^2} \right)^{\frac{1}{3}} \quad 6.37$$

Combining equation 6.37 and the definition of the Reynolds particle number (6.28) and critical Shields number (6.34) allows for the determination of D^* :

$$D^* = \left(\frac{\text{Re}^*}{\sqrt{\Psi_c}} \right)^{\frac{2}{3}} \quad 6.38$$

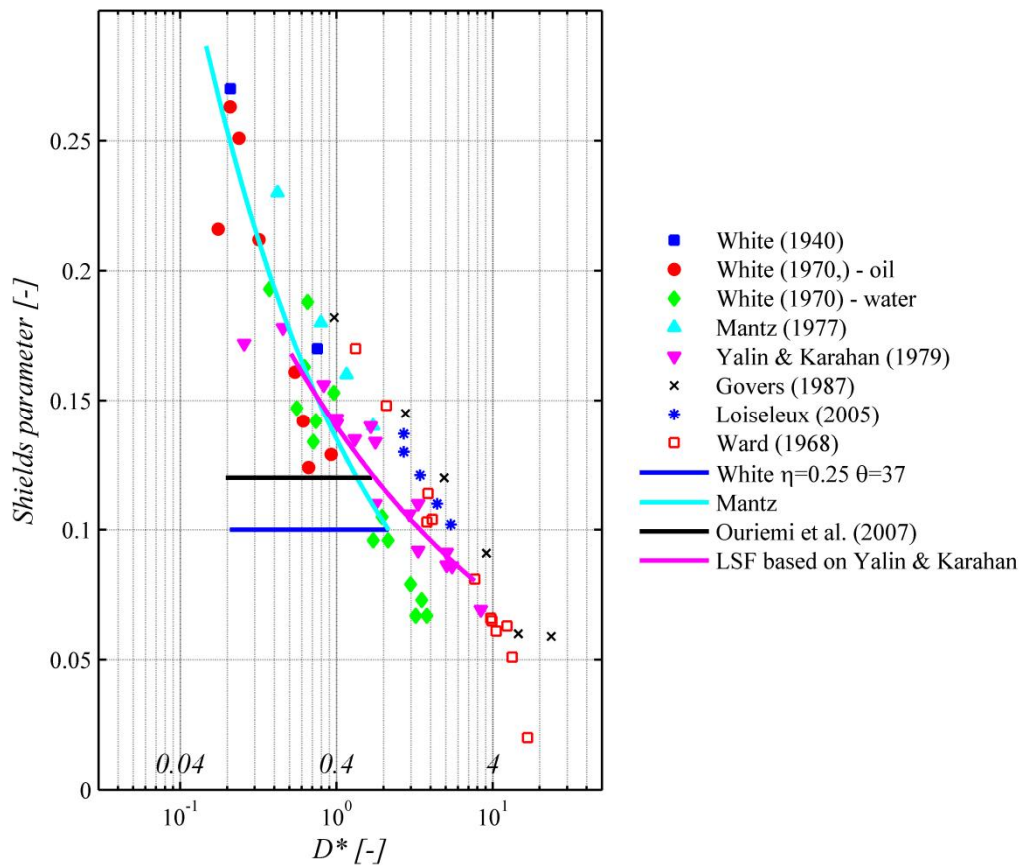


Figure 6.30. Shields parameter as a function of the dimensionless particle number showing experimental results for laminar flow. The second horizontal axis also shows the equivalent particle size in mm using a viscosity of $\nu=1.0\text{E}-6 \text{ m}^2/\text{s}$.

Figure 6.30 shows the dimensionless particle number D^* as a function of the critical Shields parameter. The relationship between the critical shear stress and a given particle size could be described as:

$$\tau_c = d\gamma_p' \left(-0.038 \ln \left(d \left(\frac{\Delta g}{\nu^2} \right)^{\frac{1}{3}} \right) + 0.1569 \right) \quad 6.39$$

This equation is still rather inconvenient because it requires the viscosity, even though viscosity is not a relevant parameter for the determination of the critical shear stress in laminar flow.

When considering laminar flow only, the most convenient approach is to express the critical shear stress as a function of the relevant parameters related to the equilibrium of the grain: the particle density and particle size. The equilibrium of forces in White (1940) describes this relationship (equation 6.33). In the Sellmeijer approach, the bedding angle (θ) in this equation is used as a constant, whereas it is actually a variable.

The available data for laminar flow will now be used to obtain an estimate of the bedding angle. Using a 'standard' set of parameters, such as $g=9.8$ m/s², $\Delta=1.65$, and $\nu=1.0E-6$ m²/s, the critical shear stress can be related to an equivalent grain size for conditions of constant density and viscosity (Figure 6.31, left-hand graph). Figure 6.31 (right-hand graph) shows the bedding angle (θ), which is calculated using equation 6.36. The parameter η chosen here is 0.30, which is consistent with the findings by White (1940). A deliberate decision has been made not to include a safety factor as yet.

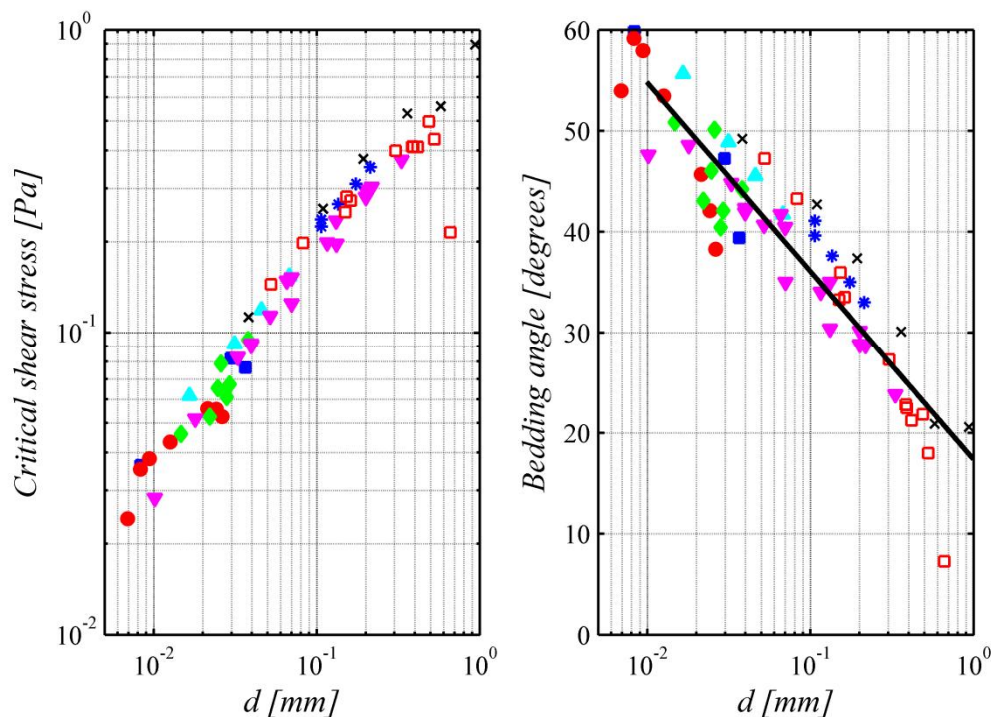


Figure 6.31. Critical shear stress (left-hand graph) and bedding angle (right-hand graph) plotted for various particle diameters (legend displayed in figure 6.26)

The least square fit obtained for the mean particle diameter (mm) and bedding angle (degrees), which is shown by the black line in Figure 6.31, is given by equation 6.40.

$$\theta = -8.125 \ln(d) - 38.777 \quad 6.40$$

The bedding angle appears to depend on the particle diameter: the bedding angle falls as the particle diameter increases. The reason is still unclear. Turbulence cannot explain this behaviour as the trend is the same in all test series, whether in water or in a viscous fluid. An analogy could be found in the behaviour of the angle of repose. Several researchers (Zhou et al., 2002; Carstensen and Chan, 1976) report that the angle of repose falls with increasing particle size, although the reason for this behaviour is not fully understood. The slope angle at which grains start to move along the slope has been determined for several sand types used in this research (Appendix B). No correlation was found between the slope angle and particle size.

Three approaches are now available: the equilibrium of forces by White, as applied in the original Sellmeijer model; the adjusted equilibrium of forces based on a multi-variate analysis of piping experiments, as applied in the adjusted Sellmeijer model; and a new approach, which complies with the Shields approach, based on the equilibrium of forces by White and calibrated using all available laminar-bed flow experiments.

The calibrated White approach is slightly unusual but it does have benefits that are relevant when predicting the critical shear stress in erosion channels. The approach is based on the equilibrium of forces on the particle and so it can also be applied to tilted beds or be adjusted to take forces due to inflowing water into account. Furthermore, the approach is very similar to the method that is currently applied in the Sellmeijer model, but it has a broader experimental basis.

Table 6.8. Three methods for determining the critical shear stress

Sellmeijer original	$\tau_c = \eta \frac{\pi}{6} \gamma'_p d_{70} \tan \theta \quad (6.41)$	where $\eta = 0.25$ and $\theta = 37$
Sellmeijer adjusted	$\tau_c = \eta \frac{\pi}{6} \gamma'_p d_{70} \tan \theta \left(\frac{d_{70,m}}{d_{70}} \right)^{0.6} \quad (6.42)$	where $\eta = 0.25$, $\theta = 37$ and $d_{70,m} = 0.208 \text{ mm}$
Calibrated White approach	$\tau_c = \eta \frac{\pi}{6} \gamma'_p d_{50} \tan \theta \quad (6.43)$	where $\eta = 0.30$ and $\theta = -8.125 \ln d_{50} - 38.777 \quad (6.44)$

Figure 6.32 shows the critical shear stresses for different particle diameters in the three approaches. It is clear to see that the results are comparable for small particles but that they differ for larger grain sizes. The graph explains why the original model results in unsafe critical gradients: the approach that was adopted, with a constant bedding angle of 37 degrees, results in overly high critical shear stresses for larger particles. The adjusted model is close to the Sellmeijer model with the calibrated White approach. The three methods will be compared in section 6.10 with the results of the piping experiments.

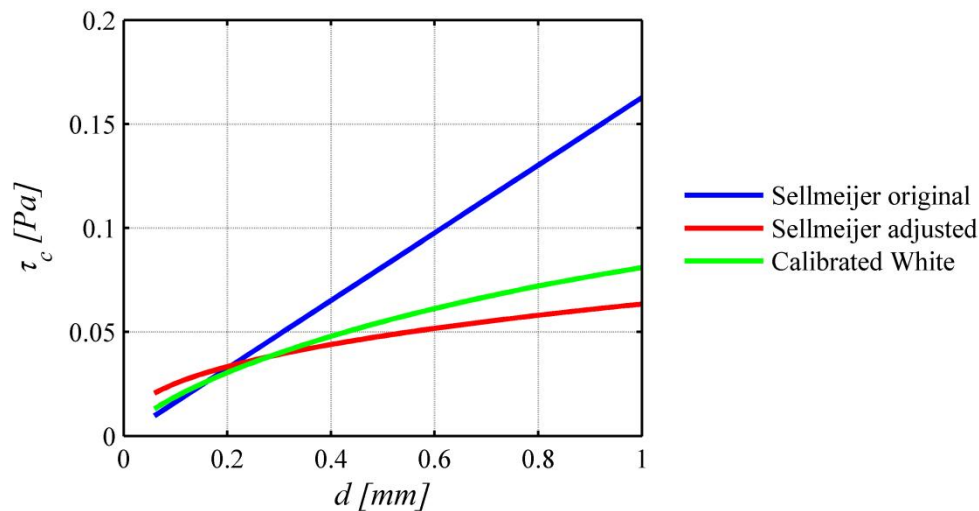


Figure 6.32. Comparison of critical shear stresses calculated with the three different models for various particle diameters

The representative diameter used for the analysis of incipient motion is generally d_{50} . Sellmeijer (1988) selected d_{70} on the assumption that incipient motion is not sufficient: larger particles need to be transported as well. This leads to the question of how incipient motion should be defined in laminar flow. There is a difference between laminar flow and turbulent flow because the latter involves a more gradual detachment of grains due to the fluctuations in the shear stress exerted. This has been confirmed by Govers (1987) and Yalin and Karahan (1979), who observed that the pattern of detachment and movement of grains in laminar flow differs from that in turbulent flow: once a grain has been detached, it keeps moving at a nearly constant velocity and brings other grains into motion by collision so that a 'grain carpet' is formed. The transition from a stable to an unstable bed proves to be sharper in laminar flows. This would indicate that the difference in the shear stress exerted between incipient motion and the motion of all grains is relatively small.

These observations apply to uniform sands in which the difference in size for d_{50} and d_{70} is also relatively small. No literature is available for incipient motion in laminar flow for sands with relatively large uniformity coefficients.

Another area requiring discussion is the use of the criterion for incipient motion. In the Sellmeijer model it is used as a limit-state equilibrium for erosion causing the deepening of the pipe. The pipe needs to deepen to progress. However, when the criterion for primary erosion is used to determine progress, the critical shear stress will be used to determine the corresponding hydraulic conditions in which the grains on the bottom of the pipe are in equilibrium. In that sense, it would be more appropriate to choose a criterion related to incipient motion represented by d_{50} .

Although the considerations stated here indicate that further research is required into the incipient motion of non-uniform sands in laminar flow, d_{50} would seem to be an appropriate representative diameter.

The packing coefficient η determines the distribution of shear stress across the particles. The relative density of the sand sample will therefore affect this parameter. The relationship between relative density and η requires further investigation.

6.9.4. EFFECT OF OUTWARD GRADIENT ON INCIPIENT MOTION

The effect of seepage on bed stability has been extensively studied. Lu et al. (2008) presented a summary of the findings and found numerous contradictions. All of the research has been performed in flumes with a turbulent flow. Lu et al. (2008) conclude that the effect of upward seepage on bed flow involves two processes. On the one hand, an additional upward force is added to the forces acting on the particle, causing the particle to be entrained more easily. On the other hand, vertical seepage affects the horizontal pipe flow near the boundary and therefore the shear stress exerted on the particle. Cheng and Chiew (1999) found that upward seepage reduces the critical shear velocity, most significantly when the sand bed is close to fluidization. The same researchers also looked at the change in the flow pattern due to upward seepage, finding that an increase in the upward flow velocity is accompanied by a fall in the shear velocity.

Incipient motion resulting from horizontal and upward flow was also investigated by De Graauw et al. (1983), who studied the flow through a filter parallel to a base layer and also looked at outward flow through a finer base layer and horizontal flow through the overlying filter layer. The vertical gradient in the base layer only affected the horizontal critical gradient, when the vertical gradients were relatively large (approximately >0.5).

Eventually, the balance of the lower exerted shear stress and the higher lift force will determine whether the particle will be removed more easily as a result of upward seepage. The correct inclusion of the effect of upward seepage on the entrainment of particles must therefore take the impact on the flow in the pipe into account.

For now it will be assumed that the net effect is negligible for the particles and the upward seepage considered. More research is required to determine the flow pattern in a rectangular duct with a permeable bottom.

6.9.5. EFFECT OF SLOPE ANGLE ON INCIPIENT MOTION

Seizilles et al. (2013) formulated an equilibrium of forces for the particles in a slope subjected to laminar flow along the slope, combining the angle of repose and the Shields parameter.

The forces acting on the grain are the friction force, the drag force, the normal force and the gravity force, as shown in Figure 6.33.

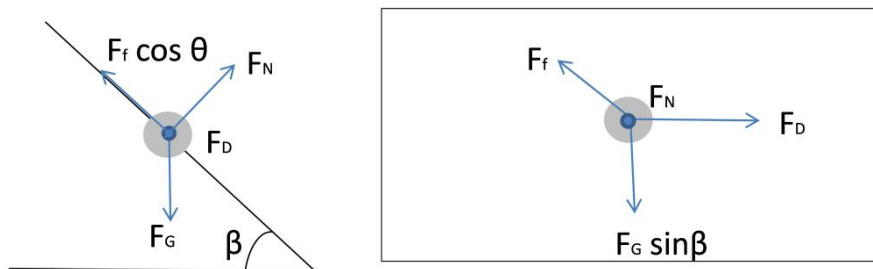


Figure 6.33. Equilibrium of forces on a particle on a slope subjected to a water flow perpendicular to the slope (left-hand figure: cross-section of slope; right-hand figure: forces in the plane of the slope)

A limit-state equilibrium is obtained when the maximum friction force equals the resultant of the drag force and the component of the gravity force in the slope plane (right-hand figure). Combining equation 6.27 and 6.31, and the friction coefficient for the equilibrium of the slope (μ):

$$\mu = \frac{F_f}{F_N} = \tan \beta_c \quad 6.45$$

in which β_c is the angle of repose, F_f the friction force and F_N the normal force. As in Seizilles et al. (2013), this results in the following equation:

$$\mu^2 \cos^2 \beta = \sin^2 \beta + \left(\frac{\tau}{\frac{\pi}{6} \eta \gamma'_p d} \right)^2 \quad 6.46$$

in which β is the slope angle. This equilibrium, combined with equations for the wall shear stress, resulted in a good simulation of the shape of the experimental open channel (Seizilles et al., 2013).

Although the flow in the experiments by Seizilles et al. (2013) is laminar, the pipe depth is different from what can be expected in backward erosion pipes. In the experiments by Seizilles, the maximum depth is approximately 1.5 cm and the mean grain diameter is 0.220 m, and so enough particles are present along the slope to allow for a continuum approach for the maximum slope angle. Erosion pipes can be as shallow as a few grains and the angle of repose can therefore be exceeded.

A difference between the configuration of Seizilles et al. (2013) and erosion pipes is the inflow of water towards the channel. Section 6.9.4 described how the effect of flow on the critical shear stress for a horizontal bed can be neglected. However, the inflow of the water does have an effect on the angle of repose, as has been described by Van Rhee and Bezuijen (1992). Equation 5.2 in Section 5.4.1 describes this effect.

The inflow of water from the sand body affects both the normal force and the friction force, as well as the velocity profile in the pipe. It is likely that the equilibrium of particles on a slope is affected more by the inflow of water than the equilibrium of particles in a horizontal bed. This is because the inflowing water directly counteracts the driving gravity force on the particles on the slope whereas the inflowing water lifts the particles in the bed but also reduces the drag force.

There will also be variations in the slope parallel to the pipe direction. No experimental data are available for laminar flow in a sloping set-up. Sellmeijer (1988) developed the limit-state equilibrium for sloping pipes:

$$\tau_c = \eta \frac{\pi}{6} \gamma'_p d_{70} \frac{\sin(\theta + \alpha)}{\cos(\theta)} \quad 6.47$$

in which α is the slope of the pipe. Recent experimental work with sloping sand beds indicates that this criterion works well (Van Essen et al., 2014).

6.9.6. CONCLUSIONS

Secondary erosion involves the erosion of particles along the pipe walls and pipe bottom. Due to the large width-to-depth ratio, the main concern when analysing secondary erosion is to determine the incipient motion on the bottom of the pipe.

The hydraulic regime determines the drag exerted on the particle. In laminar flow, or in a laminar sub-layer, the flow exerts a frictional drag on the particle. When particle Reynolds numbers are larger than 3.5, eddies are formed behind the particle and so a pressure difference over the particle controls the drag force. Piping channels are very small, and the flow in the pipe is presumably laminar, suppressing eddy formation.

Experiments determining the critical Shields parameter (indicating incipient motion) have been conducted in laminar flow conditions and in turbulent conditions with a smooth boundary where the particles are shielded by a laminar sub-layer. The regime is controlled by using a viscous fluid, a small particle size or a shallow depth. The experiments indicate that the approach adopted in the Sellmeijer model (which uses a constant Shields parameter of 0.10) results in an unsafe prediction of incipient motion for larger grain sizes ($>0.200\text{mm}$). In the case of laminar flow, a relationship between critical shear stress and particle diameter and density is more useful than a relationship including the Reynolds particle number. The bedding angle has therefore been calibrated on the basis of all available laminar flow experiments for incipient motion. The criterion obtained for critical shear stress is close to the criterion adopted in the adjusted Sellmeijer model but it has a sounder experimental basis.

It is not yet possible to determine the effect of the uniformity coefficient since no laminar flow experiments have been conducted with non-uniform sands. It was possible to include the effect of relative density by adjusting the packing coefficient η , but this area also requires further investigation.

The effect of the outward gradient was investigated for turbulent flow. The literature indicates that, when there is outward flow, incipient motion is favoured by the additional lift force, but also hindered by a fall in the drag force. For the time being, the effect of flow towards the pipe on the critical shear stress for horizontal beds has therefore been disregarded.

Due to the large width-to-depth ratio, the bottom makes up most of the pipe. However, the width of the pipe is also relevant for 3D calculations. The shape of the pipe can be determined using the limit-state equilibrium proposed by Seizilles et al. (2013), who included the angle of repose in the force equilibrium.

The final equation for limit-state equilibrium is:

$$\tau_c = \eta \frac{\pi}{6} \gamma_p' d_{70} \frac{\sin(\theta + \alpha)}{\cos(\theta)} \quad 6.47$$

in which

$$\theta = -8.125 \ln d - 38.777 \quad 6.44$$

The final equation for pipe shape is:

$$\mu^2 \cos^2 \beta = \sin^2 \beta + \left(\frac{\tau}{\frac{\pi}{6} \eta \gamma'_p d} \right)^2 \quad 6.46$$

in which

$$\mu = \tan \beta_c \quad 6.45$$

and

$$i = -(1-n) \left(\frac{\rho_s - \rho_w}{\rho_w} \right) \frac{\sin(\phi - \beta_c)}{\sin(\phi)} \quad 5.2$$

Finally, it should be noted that the Shields parameter indicates incipient motion. This corresponds to the transport of only a part of the sand sample. The entrainment of particles occurs gradually in the case of turbulent flow but the transition is more abrupt when the flow is laminar. This means that incipient motion reflects significant particle transport. At present, the choice of d_{50} as the representative grain size seems reasonable.

6.10. SYNTHESIS: VALIDATION AND EXTRAPOLATION

Now that information is available about the various erosion processes, the flow through the pipe, the pipe dimensions and pipe gradient, and related criteria, these can be combined to validate and extrapolate results. This section will start with a summary of the equations and observations that will be used for the synthesis, after which there will be an assessment of the assumptions about the regime and the range of validity.

6.10.1. BASIC ASSUMPTIONS

The basic assumptions and principles for the following sections will be:

- Primary and secondary erosion take place.
- Primary erosion results in a constant pipe tip width of approximately 30 grains.
- Secondary erosion results in pipe widening and pipe deepening.
- The observed pipe width is larger than the pipe depth. For a rectangular duct in which $w \gg a$, there are simplified equations for the relationship between flow velocity, pipe gradient and pipe dimensions and for the shear stress exerted by the water. These equations are summarised in Table 6.9.
- The flow in the pipe is laminar. Criteria for laminar flow in the pipe are listed in Table 6.10.
- The critical shear stress is determined using the 'calibrated White approach', which is valid for laminar flow around the grain.
- The shape of the pipe is determined by the limit-state equilibrium presented by Seizilles et al. (2013).

Table 6.9. Equations for laminar flow in rectangular ducts where $w \gg a$

Pipe flow	Wall shear stress	Reynolds number
$\frac{dp}{dx} a^3 w = 12Q\mu$ <p>where</p> $Q = \bar{v}wa \text{ and } \frac{dp}{dx} = \rho_w g \frac{d\phi}{dx}$	$\tau_w = \frac{a}{2} \frac{dp}{dx}$	$\text{Re} = \frac{\rho_w \bar{v} 2a}{\mu}$

Table 6.10. Criteria for laminar flow

Pipe $0 < \varepsilon / D \leq 0.08$	Pipe $0.08 < \varepsilon / D \leq 0.15$
$\text{Re}_c = 2300 - \frac{(2300 - 800)}{0.08} \frac{\varepsilon}{D}$	$\text{Re}_c = 800 - 3270 \left(\frac{\varepsilon}{D} - 0.08 \right)$

Table 6.11. Criterion for limit-state bed stability

Critical shear stress using calibrated White approach	Equations for pipe shape adapted after Seizilles et al. (2013)
$\tau_c = \eta \frac{\pi}{6} \gamma'_p d \frac{\sin(\theta + \alpha)}{\cos(\theta)}$ <p>where</p> $\theta = -8.125 \ln d - 38.777$	$\mu^2 \cos^2 \beta = \sin^2 \beta + \left(\frac{\tau_c}{\frac{\pi}{6} \eta \gamma'_p d} \right)^2$ <p>where</p> $\mu = \tan \beta_c$ $i = -(1-n) \left(\frac{\rho_s - \rho_w}{\rho_w} \right) \frac{\sin(\phi - \beta_c)}{\sin(\phi)}$

6.10.2. VALIDATION OF LIMIT-STATE EQUILIBRIUM - PIPE DEPTH

In this section, the available equations for critical shear stress and viscous flow are combined with the measured pipe gradient to calculate pipe depths. The resulting values are then compared with the measured depths. Limit-state equilibrium should be present in the pipes at all times, as was found in Section 4.11. This means that the wall shear stress in the pipe is equal to the critical shear stress. In pipes with a large width-to-depth ratio, the wall shear stress depends on the pipe depth and the pipe gradient only.

Since some experiments produced values for the pipe depth and others produced values for the pipe gradient, these experiments can be used to see if the equation for limit-state equilibrium is approximately correct. Table 6.12 shows the pipe depth calculated in the experiments for which the pipe gradient is available, assuming that the shear stress equals the critical shear stress. The table also shows the average pipe depth for experiments with similar sand types.

Table 6.12. Overview of calculated pipe depths based on critical shear stress and pipe gradient, and comparison with experimental depth measurements in similar experiments

experiment	d_{50} [mm]	$d\phi/dx$ [-]	τ_c [Pa]	calculated depth [mm]	calculated depth [no. of grains]	comparable experiment	measured average depth [no. of grains]
26a	0.325	0.089	0.412	0.95	2.9	exp. Hanses	3–6
53	0.325	0.092	0.412	0.91	2.8		
73	0.325	0.060	0.412	1.41	4.3		
E150	0.380	0.131	0.455	0.71	1.9	E172 / E150	1.6–2.9 / max 6
E150	0.380	0.119	0.455	0.78	2.1		
Bms19	0.132	0.096	0.225	0.48	3.6	B171	2.3–4.5
Bms19	0.132	0.093	0.225	0.49	3.7		
Bms19	0.132	0.095	0.225	0.48	3.7		
Bms19	0.132	0.088	0.225	0.52	4.0		
Bms19	0.132	0.089	0.225	0.52	3.9		
Bms19	0.132	0.108	0.225	0.42	3.2		
lms20	0.342	0.059	0.425	1.47	4.3	E172 / exp. Hanses	1.6–2.9 / 3–6
lms20	0.342	0.038	0.425	2.30	6.7		
lms20	0.342	0.065	0.425	1.33	3.9		

A pipe depth of 2.8–4.3 particles was calculated for the experiments by Hanses. This concurs with the general remark by Hanses that the pipe depth is approximately 3–6 particles.

The calculated pipe depth for experiment E150 was 1.9–2.1 particles, although a local maximum of 6 particles was observed. Given that the pipe depth increases towards the exit, that the pipe is not in full equilibrium (see Section 6.5.4) and that the average pipe depth is presumably lower, the measured and calculated depths correspond well. Experiment E172 is very similar to experiment E150 since the same sand type and seepage length were used. However, the analysed pipe lengths are different because the pipe length in experiment E150 was considerably longer than the pipe length in experiment E172. The pipe is expected to deepen slightly with increasing length. Bearing in mind that the pipe was not in full equilibrium in experiment E150 and so the calculated depth should be somewhat higher, and also bearing in mind the difference in pipe length, the values seem to be in fair agreement.

The scale of the set-up is likely to affect pipe depth significantly. It has been observed that pipes are a lot wider in medium-scale experiments than in small-scale experiments. Pipe depth is therefore expected to increase as well. In Baskarp sand, as tested in the medium-scale set-up in experiment Bms19, the calculated depth was 3.2–4.0 particles. The measured depth in experiment B171, which is a small-scale experiment, was 2.3–4.5 mm. Although these values are in the same range, the effect of scale on pipe depth is not clear enough as a basis for conclusions for this sand type.

Itterbeck 330 μm was also tested in the medium-scale set-up in experiment lms20. The calculated pipe depths ranged from 3.9–6.7 particles. Itterbeck 330 μm is similar to

Sand A (which was used in the experiments by Hanses) and to Enschede sand. The size of experiment Ims20 was closer to the experiments conducted by Hanses than to experiment E172. The depth observed by Hanses (3–6 particles) closely matches the calculated depth range for Ims20.

The water velocity was measured in experiment E150. Now that we have a calculated depth and the gradient for the pipe in this experiment, the corresponding average water velocity can be calculated using the equation for pipe flow with $w \gg a$, which can be written as:

$$\rho_w g \frac{d\phi}{dx} a^2 = 12\mu\bar{v} \quad 6.48$$

Using the pipe gradient at a pipe length of 0.235 m (0.119), a viscosity of $1\text{E}-3$ Pa s, and the corresponding calculated pipe depth of 0.78 mm results in an average velocity of 5.9 cm/s and a maximum velocity ($v_{\max} = \bar{v} \cdot 3/2$) of 8.9 cm/s. This is an excellent match with the measured values of 5–9 cm/s.

The conclusion is that the criterion for limit-state equilibrium results in an accurate way of determining pipe depth. The experimentally measured pipe depths are close to the calculated values. However, the data are not sufficient as a basis for the validation of the limit-state equilibrium for different soil types. Combining the limit-state equilibrium with the equation for pipe flow, the velocity in the pipe was calculated for experiment E150. The match with the velocity obtained in experiments is remarkably good.

6.10.3. VALIDATION OF LIMIT-STATE EQUILIBRIUM - PIPE SHAPE

The pipe shape is relevant for the modelling of the pipe in 3D calculations. The pipe shape can be determined using the limit-state criterion proposed by Seizilles et al. (2013) and the flow through the pipe. The theoretical pipe shape can be compared with the measured width-to-average-depth ratios in experiments B171 en E172.

Seizilles et al. (2013) investigated the shape of an open channel with a laminar flow. That procedure has been repeated here for closed pipes.

Combining the equation for wall stress (Equation 6.43) with the equilibrium of forces (Equation 6.46) results in:

$$\mu^2 \cos^2 \beta = \sin^2 \beta + \left(a \frac{d\phi}{dx} \frac{1}{C} \right)^2 \quad 6.49$$

in which

$$C = \frac{\gamma_p'}{\mu\gamma_w} \frac{\pi}{3} \eta d \tan \theta \quad 6.50$$

and β is the angle of repose.

It should be noted that the relationship between the coefficient of friction for slope stability and the bedding angle becomes apparent in equation 6.50.

Assuming that $\cos\phi$ is approximately equal to one, which is a valid assumption for shallow slopes, equation 6.49 can be rewritten as the following equation:

$$\left(\frac{d\phi/dx \cdot a}{C}\right)^2 + \left(\frac{\partial a}{\partial y}\right)^2 = \mu^2 \quad 6.51$$

in which y is the coordinate in the direction perpendicular to the pipe. Equation 6.51 shows that the solution for a horizontal bed ($\partial a / \partial y = 0$) returns an equation with the bedding angle whereas, at the top of the slope, when $a=0$, an equation with only the angle of repose is obtained.

A solution to this equation is:

$$y = \int \left(\sqrt{\mu^2 - \left(\frac{d\phi/dx \cdot a}{C} \right)^2} \right)^{-1} da = \frac{L}{d\phi/dx} \sin^{-1} \left(\frac{d\phi/dx \cdot a}{C\mu} \right) + c \quad 6.52$$

which can be rewritten as:

$$a = \frac{C\mu}{d\phi/dx} \sin \left(\frac{d\phi/dx \cdot y}{C} \right) \quad 6.53$$

Equation 6.53 can be used to derive several useful variables, such as the width, maximum depth, average depth and width-to-depth ratio:

$$w = \frac{\pi C}{d\phi/dy} \quad 6.54$$

$$a_{\max} = \frac{C\mu}{d\phi/dx} \quad 6.55$$

$$\bar{a} = \frac{2C\mu\pi}{d\phi/dx} \quad 6.56$$

$$\frac{w}{\bar{a}} = \frac{\pi^2}{2\mu} \quad 6.57$$

In this approach, the shape of the pipe, which is represented by the ratio of the width to the average depth, depends on the angle of repose only.

Width-to-depth ratios are available for experiment B171 (Baskarp sand) and E172 (Enschede sand). The angle of repose was measured in the column experiments described in Appendix B for different relative densities. Table 6.13 shows the angle of repose obtained from these experiments, as well as the theoretical and experimental width-to-depth ratios. The width-to-depth ratios obtained in the experiments significantly exceeded the theoretical values. This could be related to the inflow of water to the pipe, which was not yet taken into account. The inflow gradient required for a match between the theoretical width-to-depth ratios and the experimental values is 0.23–0.32 for Baskarp sand and 0.52–0.61 for Enschede sand. Considering that pipes in coarse sands have a larger impact on the groundwater flow, it seems reasonable that the inflow to the pipe in Enschede sand will be higher. Numerical calculations are required to validate the effect of inflowing water on the width-to-depth ratio.

Table 6.13. Comparison of experimental and theoretical width-to-depth ratios

	β_c [degrees]	$\frac{w}{\bar{a}}_{theory}$ [-]	$\frac{w}{\bar{a}}_{exp}$ [-]
B171	43.8	5.1	7–8
E172	42.8	5.3	11–13

It can be concluded that the approach by Seizilles et al. (2013) is appropriate for piping channels. However, the effect of the flow into the pipe needs to be taken into account.

6.10.4. VALIDATION OF LIMIT-STATE EQUILIBRIUM - CRITICAL HEAD

The limit-state equilibrium is the only criterion for pipe progression in the Sellmeijer model. Although there are several indications that primary erosion drives pipe progression, especially in heterogeneous sands, the Sellmeijer model functions well for homogeneous sands. The model produced accurate predictions of scale and shape effects, for example, even though the effect of sand type was still under investigation (see Section 6.4.2).

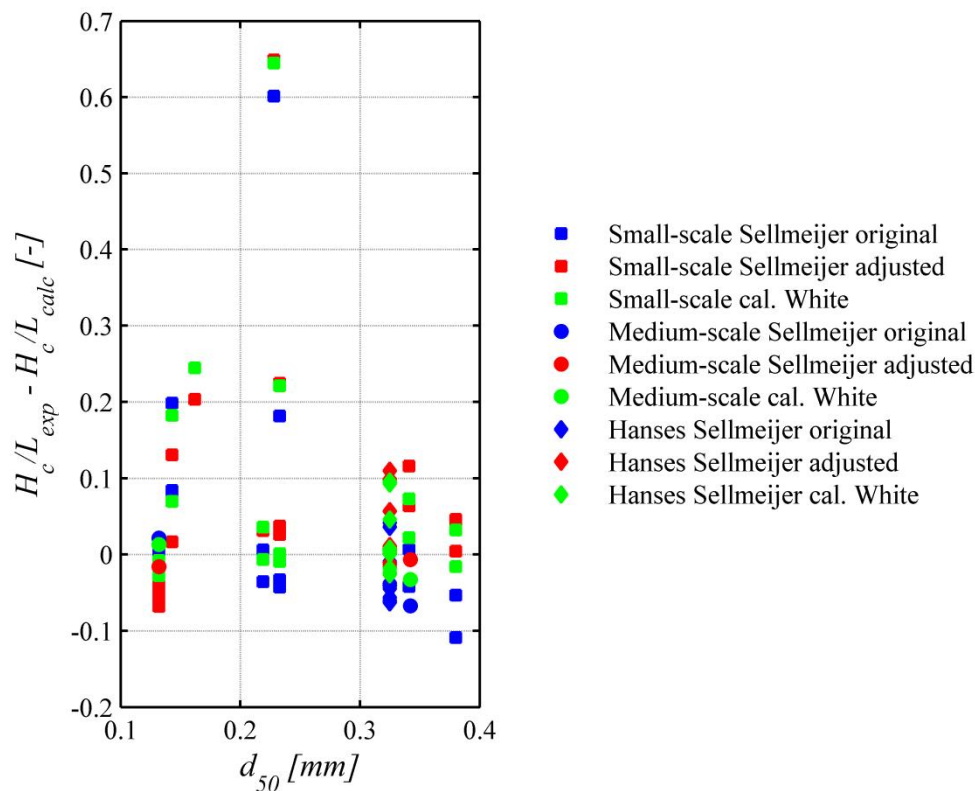


Figure 6.34. Difference between experimental and critical gradients for all hole-type experiments

Sellmeijer's rule shows that the critical gradient is linearly related to the critical shear stress for incipient motion. The original relationship for incipient motion in the Sellmeijer model can therefore be adapted in a straightforward way for another relationship. Once this had been done, the available experiments were compared with the results using the Sellmeijer model in combination with the calibrated White

approach, as well as the original or adjusted limit-state equilibrium. The calculated critical gradients were corrected by a factor of 2 to account for the 3D configuration. Figure 6.34 shows the difference between the experimental critical gradients and calculated critical gradients as a function of the mean grain diameter for all the hole-type experiments. Although the new equilibrium does not perform better for the outliers, the data points obtained with the calibrated White approach appear to be more concentrated along the line of zero difference than the other data points.

Figure 6.35 shows the results for the experiments with a 2D configuration. In general, the deviations in these large-scale experiments are much smaller than in the small- and medium-scale experiments with the 3D exit.

The trend for grain size and critical gradient is noteworthy. It was already concluded in Section 6.3.2 that the effect of grain size on critical gradient was not the same in each experimental series. This can be seen here as well: although the sand types used in the Delta Flume experiments and in the IJkdijk tests with 'coarser sand' are very similar, the resulting deviation is not the same. The two tests differ in terms of size, shape and configuration. Another noteworthy difference is the permeability of the sand, which was nearly three times as large in the IJkdijk tests as in the Delta Flume test.

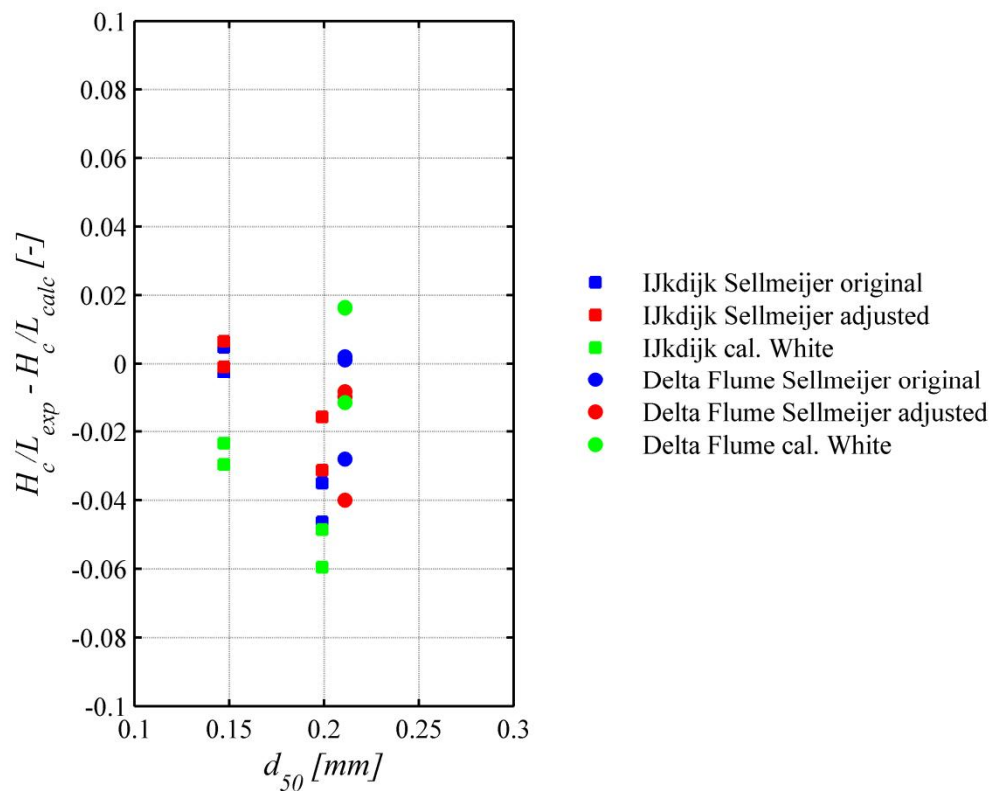


Figure 6.35. Difference between experimental and critical gradients in the 2D experiments

The reproducibility of the tests is good, indicating that experimental deviation is not a likely cause of the difference in the deviation between the Delta Flume experiments and IJkdijk experiments. There would seem to be another factor that has not yet been taken into account. The process of primary erosion, which has neglected until now, may affect the critical gradient.

6.10.5. VALIDATION OF HYDRAULIC REGIME IN THE PIPE

This section provides a validation of the assumption of laminar flow in the pipe. On the basis of the empirical data from experiment E150, it has been assumed until now that the flow is laminar. The extrapolation of this result to other sand types and scales requires an understanding of the erosion mechanism, the pipe dimensions and the pipe gradient.

Section 6.6.2 gave equations for the early transition from laminar to turbulent flow in pipes with an exceptionally rough surface. It will be assumed here that laminar flow in the pipe also implies laminar flow around the particle. It is irrelevant for the stability of the particle whether the particle is in a laminar sub-layer or in an entirely laminar flow. When the flow is laminar in the pipe, the frictional forces determine the drag. It is assumed that disturbances caused by the flow around the particle are suppressed.

The erosion processes and corresponding pipe depth are essential to determine the flow regime in the pipe and around the grain for other scales and sand types. The increase in width can be disregarded in this discussion since the pipe width does not affect the Reynolds number when $w \gg a$.

The experiments show that pipe depth is determined by the limit-state particle equilibrium. As a result, the shear stress in a pipe will be equal to the critical shear stress, which is defined here using the calibrated White approach described in Section 6.9.3. To determine the hydraulic regime, the actual and critical Reynolds numbers have been calculated for different sand types and pipe gradients. Combining the equations for wall shear stress, pipe flow and Reynolds number as defined in Table 6.9 and critical shear stress as defined in Table 6.11, the Reynolds number can be written as:

$$Re = \frac{4}{3} \frac{\rho_w}{\mu^2} \left(\frac{dp}{dx} \right)^{-2} \left(\eta \frac{\pi}{6} \gamma'_p d \tan \theta \right)^3 \quad 6.58$$

in which θ is a function of the grain diameter.

To determine the validity range for the assumptions of laminar flow, the Reynolds numbers obtained with this equation need to be compared with the critical Reynolds numbers defined in Table 6.10. The equation for the critical Reynolds number for laminar flow depends on the roughness of the pipe wall. The first step here will therefore be to determine the conditions in which the relative roughness is 0.08.

The relative roughness depends on the grain diameter and the pipe depth by $d/2a$. Combining the equation for wall shear stress and critical shear stress, the pipe depth can be written as:

$$a = \frac{\pi}{3} \frac{\eta \gamma'_p d \tan \theta}{dp/dx} \quad 6.59$$

The Reynolds numbers and critical Reynolds numbers are compared in Figure 6.36, where the ratio between the two is plotted as a function of particle size and pipe gradient. The contour for $Re/Re_c=1$ (the blue line) shows the transition from laminar to turbulent flow.

The contour plot depends on the criterion for the limit-state equilibrium. For the purposes of comparison, Figure 6.37 shows the contour plot using the criterion from the original Sellmeijer model. The area in which laminar flow is expected becomes much smaller when this criterion is used. Although Figure 6.36 is expected to conform more to reality, the lines should be seen as a rough indication rather than a precise boundary given the sensitivity to the critical shear stress equation.

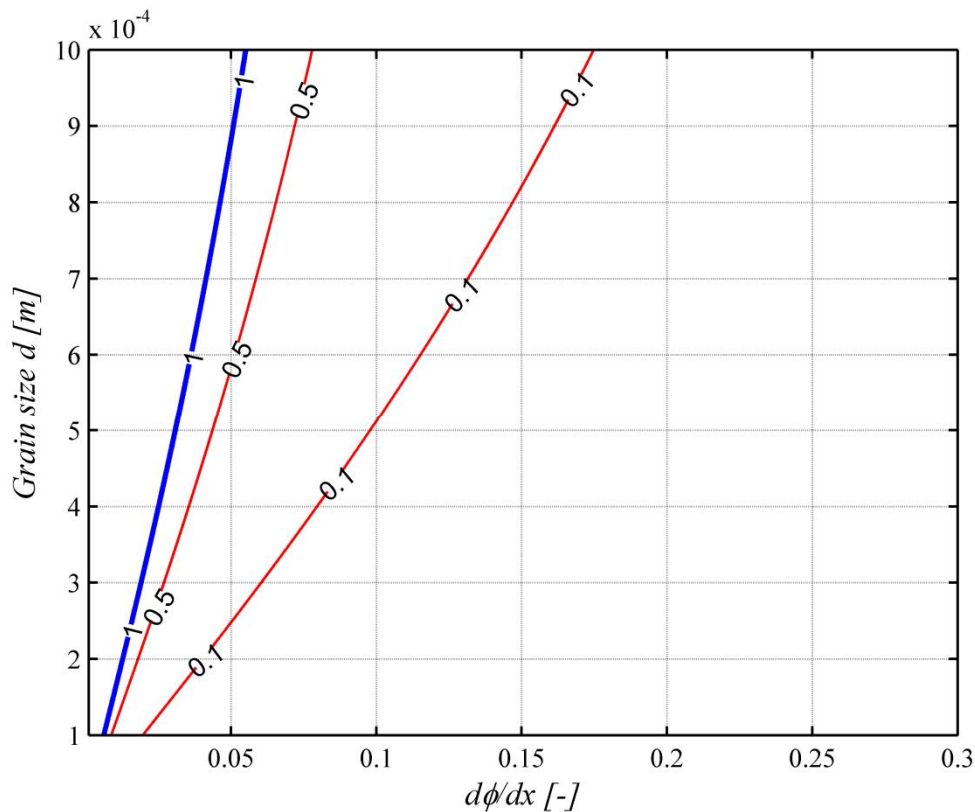


Figure 6.36 Contour plot of the ratio of the Reynolds number based on the calibrated White criterion to the critical Reynolds number. Contour line '1' outlines the area where the flow in the pipe is laminar.

Given that most experiments have pipe gradients of approximately 0.05–0.1, the assumption of laminar flow is valid for grain sizes up to approximately 1 mm in these experiments. However, it is known that the critical gradient falls with increasing scale and so the pipe gradient will be lower in the field. Still assuming limit-state equilibrium, a lower pipe gradient corresponds to a larger pipe depth and turbulence will therefore be more likely at larger scales.

In practice, average critical gradients as low as 0.023 ($L/H=44$) have been known to lead to numerous/large sand boils and critical locations have been found at gradients as low as 0.048 ($L/H=21$) (Ammerlaan, 2007).

The gradient in the pipe will always be lower than the average gradient. The ratio of the pipe gradient to the average gradient will depend on the sand type and on the configuration. In the experiments, ratios of pipe gradient to overall gradient have been determined in the range of 0.3–0.9. At low critical gradients (<0.05), or in the case of sand types with a relatively large grain size ($d_{50}>0.3$ mm), it is worthwhile to check

whether the assumption of laminar flow is still valid by investigating the expected pipe gradient using a numerical model.

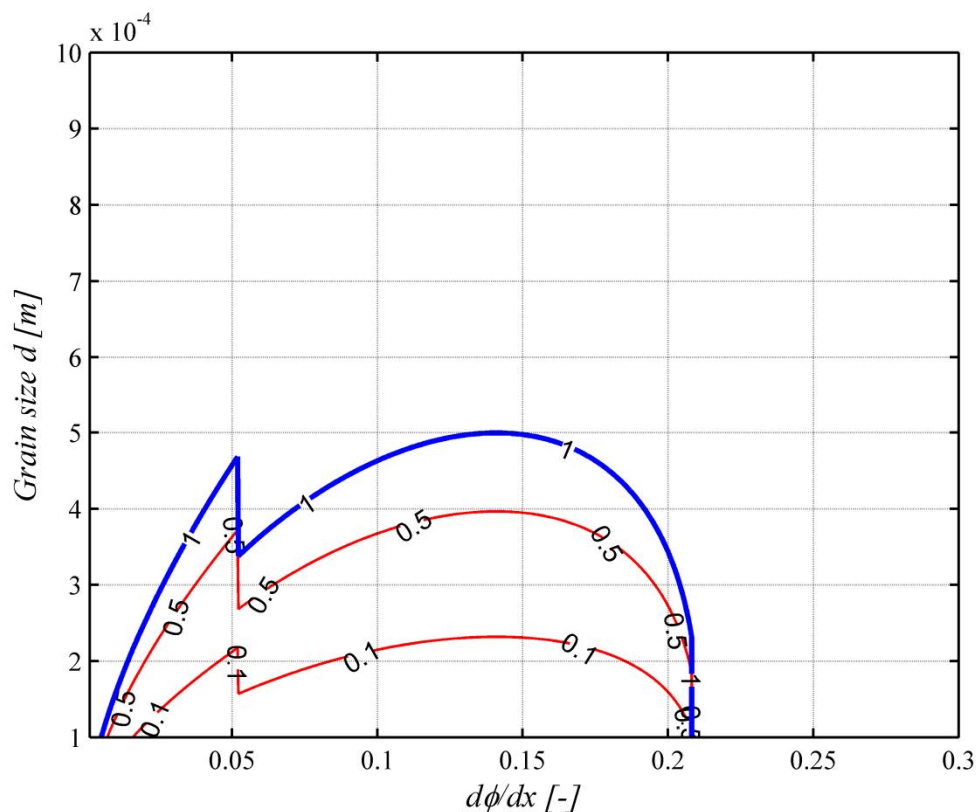


Figure 6.37 Contour plot of the ratio of the Reynolds number based on the limit-state equilibrium used in the original Sellmeijer model to the critical Reynolds number. The contour line '1' outlines the area where the flow in the pipe is laminar.

6.10.6. DISCUSSION AND CONCLUSIONS

The calculations indicate that the regime is laminar in most of the range considered (pipe gradient 0–0.3 and particle size 0.1–1 mm). When pipe gradients are very low, which is a possibility at large scales and when grains are large, the regime should be checked using a numerical calculation. The regime is highly dependent on the criterion for the limit-state equilibrium.

The observed pipe depth and shape are reasonably well explained by the limit-state equilibrium. However, it was not possible to properly determine the effect of soil type on the basis of the limit-state equilibrium and the observations in experiments. The experiments were therefore back-calculated using different criteria for limit-state equilibrium. This approach is not entirely reliable since it does not include primary erosion. The difference in the trends for the experimental critical gradient and grain size observed in the experimental series at different scales (Figure 6.2) cannot be explained by choosing a different criterion for limit-state equilibrium.

Given that the calibrated White approach is not based on any backward erosion experiment, it performs very well.

6.11. DISCUSSION

6.11.1. PRIMARY AND SECONDARY EROSION

Section 6.7 describes the evidence for the relevance of both primary and secondary erosion. It is essential to include both these processes to predict piping, especially in heterogeneous soils. This section will describe future developments and return to questions posed at the start of this dissertation.

Further research should focus on the establishment of a criterion that determines the onset of erosion near the pipe tip. The experiments will have to be simulated numerically for this purpose in order to determine the local gradients around the pipe tip that cause the pipe to progress. The loosening of grains in front of the pipe tip and arching may need to be taken into account when determining a criterion of this kind. The simulation of experiments with a layered sand sample is of particular interest since layering is commonly encountered in sand layers in the field and has been found to result in large critical gradients by comparison with homogeneous samples. Additional experiments with layered sand beds are recommended to confirm the observed effects.

Modelling of secondary erosion will be required to determine the gradient in the pipe, as shown in Figure 14. The pipe gradient is determined by the initial pipe size (width of approximately 30 grains) and by the subsequent erosion of the pipe walls and bottom. The literature describes criteria for incipient motion in laminar flow, which, in combination with equations for pipe flow and groundwater flow, could result in an estimate of the pipe gradient at which the grains are in a limit-state equilibrium.

The applicability of the criteria for incipient motion has been investigated. Although the data for non-uniform sand types are limited, the criterion for the initiation of motion results in a reasonable estimate of pipe depth. The inflow of water towards the pipe needs to be taken into account to predict the pipe shape correctly.

The combination of these two mechanisms will lead to a novel model that can take into account the effect of scale, sand properties and heterogeneity along the path of the pipe. It has the potential to explain the effect of coarse-grained 'barriers' on critical head, which is essential for the prediction of piping in practice. A model of this kind would also make possible the development of more practical rules for specific configurations.

6.11.2. MODELLING PRIMARY AND SECONDARY EROSION

It is likely that a group of grains at the tip of the pipe needs to be fluidised by a local critical hydraulic gradient (i_c) at the tip of the pipe. The tip of the pipe is a singular point and so, theoretically, the local gradients near the pipe tip will go to infinity. Although the continuum approach is not valid up to the pore scale, the gradient does increase towards the pipe tip. Figure 6.38 gives examples of potential distribution in 3D sand samples, including pipes with different impacts on the groundwater flow. The sharp decrease in potential near the pipe tip illustrates the concentration of flow lines. Upon approaching the tip, the gradient reaches a very high value and, at this point, the continuum approach is no longer valid.

A practical approach to deal with the singularity would involve considering the gradient across a group of grains, as when predicting pipe initiation (Van Beek et al., 2014a). The constant size of the pipe tip width (of approximately 30 times the mean grain diameter), as observed in the experiments, supports such an approach. For the pipe to progress, the local gradient i at some distance from the tip must exceed a critical value i_c . In the case of relatively large grains, the tip of the pipe is wider in absolute terms and it therefore requires fluidisation in a relatively large area in front of the pipe tip.

Whether the local gradient for fluidisation of the pipe tip is reached depends on the overall gradient, but also on the impact of the pipe on the ground water flow, in other words on the pipe gradient. The pipe gradient, in turn, depends on the initial pipe size (width of approximately 30 grains, depth of 2–4 grains) and the subsequent erosion (in other words, secondary erosion) of the pipe walls and bottom. The literature provides criteria for incipient motion in laminar flow that can be used to model secondary erosion, and therefore the limit-state equilibrium in the pipe (Section 6.9). The pipe gradient, limit-state equilibrium and pipe dimensions are related by the viscous flow equations and the groundwater flow towards the pipe. A limit-state particle equilibrium can be found for each applied head by combining these equations. Essentially, this was done in the Sellmeijer implementation in DGFlow (Van Esch et al., 2013). Primary erosion is not implemented entirely correctly in this model because progression is allowed until no equilibrium can be found in the element in front of the pipe. Basing progression on the equilibrium of particles in the bed of a stream is fundamentally incorrect but it does, in practice, produce useful values. This may be because the limit-state equilibrium also predicts an effect of grain size, as is expected for primary erosion.

6.11.3. EFFECT OF SAND TYPE ON PRIMARY AND SECONDARY EROSION

A combination of these mechanisms may explain why the critical gradient is not extensively affected by grain size (in uniform sands).

Given the rapid decrease in the local gradient i with distance from the pipe tip, as illustrated in Figure 6.38 by the slope of the potential, a relatively large overall gradient (H_c/L) is required to reach a critical value i_c for this local gradient. Taking primary erosion alone into account would therefore suggest that the critical head is larger for coarse sand types.

Although primary erosion determines the progression of the pipe, secondary erosion determines the boundary conditions required for this process to take place. Due to the larger size of the pipe and subsequent secondary erosion, the gradient in the pipe is relatively low for the coarser sand type, such that the local gradient in the sand upstream of the pipe and at the pipe tip is relatively high for a given hydraulic head. These two effects can counteract one another so that the net effect of grain size on critical head is limited. This is illustrated in Figure 6.38, which shows the examples of relatively fine and coarse sands at critical head. The figure is based on the 3D numerical simulations of the medium-scale experiments including a pipe (Van Beek et al., 2014b). The fine sand has a relatively large pipe gradient due to its limited size, whereas the gradient for the coarse sand is lower. The average and local gradients will therefore be higher in the sand layer upstream of the pipe for the coarser sand (in the example in Figure 6.38, the gradients upstream of the pipe were found to be up to 12% higher for the line representing coarse sand than for the line representing fine sand). This means

that, despite the fact that the average gradient (H/L) is the same for both sand types in this example, the local gradients in front of the pipe are higher for the coarse sand, which allows a larger area to be fluidised in front of the pipe.

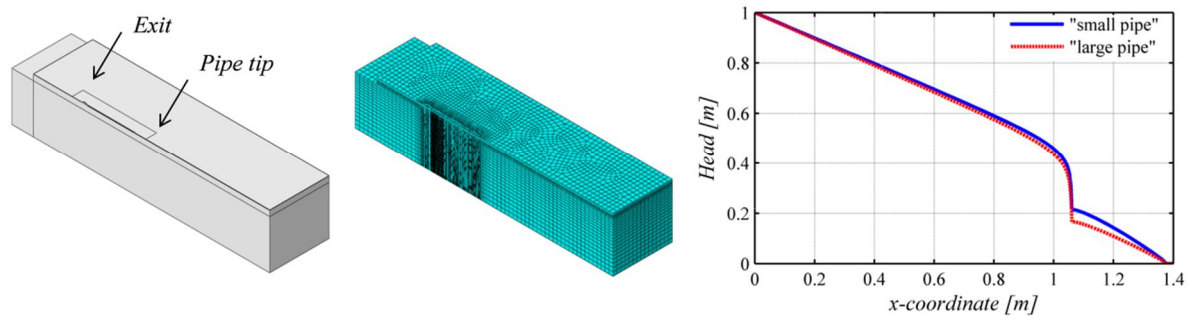


Figure 6.38. Configuration, mesh and potential distribution along the central axis of symmetrical 3D numerical simulations of the medium-scale experiments (Van Beek et al., 2014b). Pipes have been simulated by adding a permeable zone in the centre of the sand sample at 1.06 to 1.385 m from the upstream boundary. The permeability in the pipes differs for the blue line and the red line, which represent, respectively, a pipe with a smaller impact, as would be the case in a fine sand, and a pipe with a large impact, as would be the case in a coarse sand.

The effect of relative density on the critical gradient follows qualitatively from both primary and secondary erosion. Dense samples will be less permeable, reducing the flow in the pipe. This will lead to limited scour in the pipe and so the pipe gradient will be relatively high, requiring a relatively high overall head to cause primary erosion. In addition, the fluidisation of the pipe tip will require a relatively high gradient given the low porosity and dilatancy of the sand sample.

The uniform sand samples resulted in a lower critical gradient than those with added fines. Although non-uniform samples require additional research, the major impact on the critical gradient can be explained theoretically by reference to primary and secondary erosion. The main difference between uniform and non-uniform samples is their permeability, which decreases with increasing fines content. At equal overall gradients and comparable mean grain size, flow velocities in the pipe are higher in the uniform sample, resulting in more secondary erosion and consequently lower pipe gradients. Accordingly, the pipe will progress at a relatively lower head in the case of the uniform sample.

A large increase in strength resulting from the variation in grain size, as encountered in the layered sand sample in one of the medium-scale experiments, can be explained by reference to primary erosion. Layers with relatively coarse grains form a barrier since a larger zone needs to be fluidised in front of the pipe tip for the pipe to progress through these layers.

6.11.4. EFFECT OF SCALE ON PRIMARY AND SECONDARY EROSION

The effect of scale is a complex matter as it affects the mechanisms of primary and secondary erosion in different ways.

In the case of primary erosion, the scaling effect is comparable with that of pipe initiation. As the pipe tip will be the same size, regardless of scale, the local gradient will determine its progress. The modelling of pipe initiation shows that the critical initiation gradient decreases with the square root of the seepage length (assuming a constant D/L ratio).

However, when a pipe is present, the gradient upstream of the pipe depends not only on the groundwater flow, but also on the impact of the pipe on the groundwater flow. The gradient in the pipe will depend on the limit-state equilibrium driven by the flow towards the pipe and through the pipe. The critical gradient for the Sellmeijer model is known to depend on the cubic root of the seepage length. This is related to the criterion for the boundary condition of the pipe: a combination of the equation for particle equilibrium (Equation 6.41), the equation for flow through the pipe (Equation 6.15) and the equation for the shear stress on the particles (Equation 6.18). Equation 6.60 describes this boundary condition and indicates that the squared pipe gradient multiplied by the flow through the pipe is constant at every location in the pipe:

$$\left(\frac{d\phi}{dx}\right)^2 Q = c \quad 6.60$$

An increase in scale maintains the average gradient but also results in an equivalent increase in flow towards the pipe so that the condition is no longer fulfilled. As the pipe gradient and the flow towards the pipe depend linearly on the applied gradient, reducing the gradient by the cubic root of the scale factor results in a situation where the boundary condition is fulfilled again. In this situation the gradient upstream will decrease by the cubic root of the scale factor as well, even though, according to the scale rules of primary erosion, a decrease by the square root would have been sufficient to ensure the progression of the pipe.

Suppose now that we reduce the overall gradient by the square root: the gradient upstream of the pipe will be critical but the boundary condition for the pipe will not be fulfilled. The boundary condition can only be fulfilled if the pipe gradient is lowered and this will, in turn, affect the gradient upstream of the pipe in such a way that the overall gradient does not need to be reduced by as much as the square root of the scale factor. The expected scale effect will therefore be located between the scale effects of primary and secondary erosion. In any case, it is certain that there will be a fall in gradient with scale.

There are implications for the assumption of limit-state equilibrium at large scales: the critical gradient cannot be reduced infinitely and the pipe is formed at the tip with a depth of a few grains. The shear stress in the pipe must be high enough to transport the particles on the bottom of the pipe. As can be deduced from the equation for wall shear stress (Table 6.9), the shear stress is dependent only on the pipe depth and the pipe gradient. It should be kept in mind here that the pipe gradients can exceed the average applied gradient locally, for example near the exit. Once deepening has taken place, the pipe gradients required for limit-state equilibrium will be lower. It should also be noted that the initial pipe depth at the tip may be larger if the critical gradient at the pipe tip is

exceeded. Modelling can take these implications into account if more reliable data have been obtained about the initial pipe depth for different sand types and for different applied heads.

6.12. CONCLUSIONS

The total database of progression-dominated experiments, which consists of large-scale experiments or experiments with a hole-type exit, shows the impact of a range of parameters on the critical gradient. In uniform sand types, the critical gradient is independent of the mean particle size. The addition of fines or the presence of layering results in relatively strong samples. An increase in scale leads to a decrease in the critical gradient.

The critical heads obtained in the experiments, as well as those obtained from literature, were compared with the results of the Sellmeijer model (Sellmeijer et al., 2011), which was developed to predict the critical head for pipe progression. Although the adapted Sellmeijer model predicts critical gradients well for two-dimensional large-scale experiments with fine- to medium-grained sands, it has been found that 3D configurations with flow towards a single point result in significantly smaller critical gradients than those predicted by the model. Although, in practice, the exit type may not have such a strong effect as in the experiments due to the formation of multiple pipes and seepage through the blanket layer and towards the hinterland, as long as these mitigating effects cannot be quantified, the worst-case scenario of the development of a single pipe in a configuration similar to that in the laboratory should be taken into account. The model overestimates the critical head for both the small- and medium-scale experiments by a factor of approximately 2.

The comparison did not allow for a validation of the effect of the sand type on critical gradients. The adjusted model performed better for some experimental series, whereas the original model performed better for others. Given that the predictions for the IJkdijk using the original Sellmeijer model were unsafe, the adjusted model remains preferable for use in practice.

In order to find a possible explanation for the observed variations, the pipe width, depth and gradient were analysed in detail. The findings illustrate the importance of both primary and secondary erosion. Primary erosion, which is the erosion at the tip causing the lengthening of the pipe, determines pipe progress, as illustrated by one of the experiments in which the pipe developed perpendicularly to the flow direction when a slightly coarser layer was encountered. The finding that the width of the pipe tip increases linearly with grain size, and that it is approximately 30 times the mean grain diameter irrespective of scale or uniformity coefficient (within the studied range), supports the idea that a group of grains at the pipe tip needs to be fluidised for the pipe to progress. Secondary erosion is of importance as well: it determines the pipe gradient, which was found to be different for different sand types. The observation that flow through the pipe caused the pipe to widen towards its tail, causing lateral widening, is the main evidence underlying this conclusion, which is further supported by the relationship between flow and pipe gradient.

The elements required for modelling primary and secondary erosion were investigated. The flow through the pipe and the particle transport are relevant for secondary erosion. With a width-to-depth ratio of at least 7, the equation for rectangular ducts with $w \gg a$ is

most appropriate. The shape of the pipe can be reasonably well explained by the approach of Seizilles et al. (2013), who combined incipient motion with the angle of repose in an equilibrium of forces, although the inflow of water into the pipe needs to be taken into account. Incipient particle transport has been studied in laminar flow by various researchers. On the basis of these experiments, the bedding angle in White's equation has been calibrated so that it is dependent on particle size. However, a physical reason for this dependency could not be found.

The criterion for incipient particle transport appears to result in a reasonable estimate of depth in those experiments for which the pipe gradient is known. The Poiseuille equation for parallel plates provides a good estimate of the flow velocity. The validity range of the laminar regime is highly dependent on the criterion for incipient motion. Assuming the calibrated White method (see section 6.9.3) to be most appropriate, the regime is expected to be laminar for most situations considered, except at very low pipe gradients, and particularly in combination with large particles. Low pipe gradients may be found in large-scale situations. A precise boundary cannot yet be given because the relationship between overall gradient and pipe gradient depends on the configuration. The regime can be validated using numerical calculations in which the critical gradient is determined.

A novel model needs to be developed that takes primary and secondary erosion into account. The inclusion of primary erosion will have an impact on the effect of sand type and scale on the critical gradient and allow for the calculation of pipe progression in sand types with heterogeneity in the pipe path. The effect of scale on critical gradient in a model of this kind is expected to be slightly stronger than in the Sellmeijer model.

7. CONCLUSIONS

De weg is lang, maar onderweg is veel te zien.

Hans Sellmeijer

7.1. MAIN FINDINGS

The principal aim of this research has been to explain and predict the pipe-forming erosion processes in uniform sands. The mechanisms causing failure due to piping have therefore been analysed on the basis of past and new experiments.

Failure due to piping is known to occur as a sequence of processes. Uplift and cracking is followed by pipe initiation, causing the formation of a pipe in the sand layer and a sand boil at the surface. The pipe progresses to the upstream side, after which the pipe widens and deepens, followed by the settlement and failure of the dike.

One of the research questions is related to the process seen in loose sand samples in which the pipe developed in the direction of flow: the forward piping process. The field relevance of this process was questioned. The experiments described in this dissertation show that the forward mechanism is relevant only in situations where a minimal gap can be present above the sand, as in the case of a rigid structure overlying a sandy layer. The process cannot occur in dikes made of natural material.

The experiments available from the literature indicate that the backward erosion piping process depends on the type of configuration used. Typically, there is no equilibrium in pipe formation in small-scale experiments with a large exit. The flow through the intact sand sample that causes pipe initiation determines the critical head. Experiments have proven that the head required for pipe progression can be lower than the head for pipe initiation. In large-scale experiments, or in experiments with a small exit where the flow concentrates, pipe initiation takes place at a relatively low head, after which the pipe attains an equilibrium situation. Here, the flow towards and in the pipe determines pipe progression and the critical head.

The experiments in which no equilibrium was observed allowed for the development of a model for pipe initiation. The observed differences in critical gradient could be related to the fluidisation of sand very close to the exit, where the local gradients are high. Regardless of the type of sand or configuration, the size of the group of grains to be fluidised was at least 20 times the mean grain diameter. In order to develop this model,

the gradient at the exit was determined using an analytical calculation that could be used because the simulated experiments were homogeneous and two-dimensional. Numerical calculations can also be used for this purpose, but, since 20 times the grain diameter corresponds to a small distance in the order of 5 mm for sands, a very fine mesh will be needed. An alternative is to combine numerical calculations with an analytical solution that describes the flow behaviour near the singularity.

Experiments in which equilibrium was observed allowed for the analysis of pipe progression. Investigations of the pipe gradient, pipe width and pipe depth confirmed the findings by Hanses (1985) that pipe progression is determined by two mechanisms: primary erosion and secondary erosion. Primary erosion – in other words, the erosion at the pipe tip – results in the lengthening of the pipe. A peak of short duration in the hydraulic gradient near the pipe tip causes the breaking of the arch at the pipe tip. Other evidence pointing to the relevance of primary erosion are the width of the pipe tip, which was found to be linearly related to the mean grain size, and pipe development perpendicular to the flow upon encounter of a coarser layer. Secondary erosion controls the dimensions of the pipe downstream of the pipe tip and therefore the pipe gradient. This is shown by the increase in the pipe depth from tip to tail and the widening of the pipe. The pipe depth at the tip proves to be very shallow: 2 – 4 times the grain diameter in the two experiments in which it was determined. The width at the tip was found to be approximately 30 times the grain diameter and more or less constant for different lengths. The meandering bends and the relocation of the pipe are formed by scour, indicating that the water flow through the pipe is the main driver of erosion. The inflow of water from the sand bed into the pipe along its length could further aid the onset of motion of particles in the pipe and reduce the slope of the pipe. A combination of Poiseuille flow, flow towards the pipe and the criteria for incipient motion in laminar flow can be used to predict the pipe gradient. The pipe gradient proved to be considerably larger for a fine sand than for a medium-grained sand. This finding is related to the size of the pipe and the viscous flow in the pipe: the larger pipe in medium-grained sand can convey a much larger flow. Although the permeability of the medium-grained sand is larger than that of the fine sand, and also results in an increase in the flow, this does not compensate for the increase in the flow capacity of the pipe. The assumption of laminar flow in the pipe was confirmed in one of the small-scale experiments.

The pipe will therefore grow as a result of primary erosion, but this process is indirectly directed by secondary erosion and viscous flow through the pipe since the latter processes control the pipe gradient.

At present, the Sellmeijer model is the most advanced model available for predicting the occurrence of backward erosion piping. Recent research has shown that the original model over-predicts the critical gradient for sands other than fine sands. An empirical adaptation was made, for which there was still no theoretical explanation. On the basis of the current findings, it can be stated that the Sellmeijer model is theoretically incomplete since it includes only secondary erosion. Nevertheless, the adjusted model performs reasonably well in 2D configurations. In the 3D configurations considered here, in which the flow converges to one point, the model proved to be unsafe by a factor of 2. An evaluation of the influence of sand type on critical gradient in the 3D configuration failed to establish a preference for the adjusted or original Sellmeijer model. Some striking outliers were found, indicating that adding fines and layering in

the pipe path result in strengthening. Variation in grain sizes in the path of the pipe was found to result in critical gradients that were nearly twice the critical gradient observed in a homogeneous sample.

In experiments with the aim of investigating incipient motion in the bed of a laminar stream, the bedding angle was found to decrease in line with increasing mean grain diameter. However, in the Sellmeijer model, the bedding angle has been kept constant in calculations until the present at a value suitable for fine sands (mean particle size approximately 0.2 mm). A new criterion for incipient motion has therefore been proposed here that is based on available incipient motion experiments. The application of the new criterion to the Sellmeijer model gives results similar to the empirically adjusted Sellmeijer model. The inclusion of the correct bedding angle may therefore partly explain the discrepancy between the findings of the original Sellmeijer model and the outcomes of experiments with coarse sands.

A model that includes both primary and secondary erosion will allow for the investigation of backward erosion in heterogeneous soils. It is expected that including both types of erosion will lead to minor changes in predictions for homogeneous sand types as well. The scale effect is expected to be slightly more marked after the inclusion of primary erosion.

7.2. PRACTICAL IMPLICATIONS

The progression of the pipe is more relevant than pipe initiation for the prediction of backward erosion in practice. Pipe initiation cannot be predicted accurately because the initiation gradient is highly dependent on the local exit conditions, which are often unknown. The progression of the pipe is less dependent on the local exit conditions than the initiation of the pipe, as was already shown in the experiments by Miesel (1978). In the field, a safety factor to account for uncertainties in exit configuration would need to be very high. The use of this model for prediction purposes is therefore restricted to laboratory conditions, where the prediction of the relationship between pipe initiation and progression is essential.

The understanding of the relevant processes does generate an insight into the occurrence of sand boils, and helps with the assessment of the risk of pipe progression in the field. The occurrence of a sand boil in a sandy area is more likely to pose a risk than a sand boil in a location where the flow converges towards the surface because the head for pipe initiation in the first situation is relatively close to the critical head.

The prediction of pipe progression still requires further investigation. The present study shows that the adjusted Sellmeijer model functions reasonably well in 2D situations but is unsafe in situations where the flow converges to one point. In the field, the effect of 3D flow may be less pronounced than in the laboratory due to the occurrence of multiple parallel pipes and seepage through the layer covering the sand layer, which reduces the inflow towards the pipe. 3D analysis can also account for the geometry of the sand layers.

Furthermore, additional strength is expected in heterogeneous soils. The sedimentation of natural sand layers ensures that there is nearly always variation in the particle sizes.

In practice, the positive and negative effects described in this section should be taken into account when using the Sellmeijer model. In situations where the flow is

concentrated towards one point, it should be realised that the Sellmeijer model can overestimate the critical head for pipe progression by up to a factor of approximately 2. The sand type must also be considered because heterogeneous sand layers can be expected to be a lot stronger: assuming homogeneous sand is clearly a conservative approach. Furthermore, in areas where floods are not long-lasting, assuming steady-state conditions is also conservative. Finally, the Sellmeijer model should not be used outside the tested range described in Sellmeijer et al. (2011), because essential parts of the physical process (for example: primary erosion) are not included in the model.

7.3. RECOMMENDATIONS

The inclusion of primary and secondary erosion in a 3D transient groundwater model is an essential step for backward erosion prediction. A 3D model is necessary to understand the implications of 3D groundwater flow towards the exit. The inclusion of a criterion for primary erosion has proven to be necessary, especially for heterogeneous soils. A criterion for primary erosion could be developed by studying the local hydraulic conditions that cause the onset of pipe lengthening. The findings relating to the size of the pipe tip could help in the development of a criterion of this kind. The dimensions of the pipe are required to model the process in 3D. They can be estimated on the basis of secondary erosion. Although the literature provides information about incipient motion and width-to-depth ratios, the roles played by inflowing water, relative density and grading are not yet understood very well and they require further investigation.

Heterogeneity needs to be taken into account for the practical application of the model. A 2D approach with infinitely long homogeneous horizontal layers is a poor approximation of reality, especially when calculating very long seepage lengths. In 2D configurations, the approach currently adopted is conservative but it does not closely resemble reality. Practical guidelines are required to estimate the expected grain-size variation in the field and to take into account the approximate geometry of the sand channels.

REFERENCES

- Achmus, M. and Mansour, B.G.S. (2006). Considerations and model Tests on the Design of River Barrages with respect to Piping. 3rd International Conference on Scour and Erosion, Amsterdam, 1-3 November 2006.
- Al Hattamleh O. al, Razavi M. and Muhunthan B. (2009). Experimental determination of representative elementary volume of sands using X-ray computed tomography. *WIT Transactions on Engineering Sciences* 64: 145-153.
- Ammerlaan, P.R.M. (2007). *Levees and levee evaluation – The Dutch and US practice compared*. Msc. Thesis, TU Delft.
- Been, K. and Jefferies, M.G. (1985). A state parameter for sands. *Géotechnique* 35(2): 99-112.
- Bezuijen A. and Steedman R.S. (2010). Scaling of hydraulic processes, Proceedings 7th int. conf. on Physical Modeling in Geotechnics (Springman, Laue and Seward (eds), Taylor and Francis Group, London, UK.
- Bligh W.G. (1910). Dams Barrages and Weirs on Porous Foundations. *Engineering News* 64(26): 708-710.
- Bligh W.G. (1915). Submerged weirs founded on sand. In *Dams and Weirs*, p. 151-179. American Technical Society, Chicago.
- Brackbill T.P. and Kandlikar S.G. (2010). Application of lubrication theory and study of roughness pitch during laminar, transition and low Reynolds number turbulent flow at microscale. *Heat Transfer Eng.* 31 (8), 635- 645.
- Cao D. (1994). Countermeasures for seepage erosion of Yangtze River main dikes. *Yangtze River* 25(1): 25-30.
- Cao, Z. Pender G., Meng J. (2006). Explicit Formulation of the Shields Diagram for Incipient Motion of Sediment. *Journal of Hydraulic Engineering*, October: 1097-1099.
- Carstensen, J.T. and Chan P.C. (1976). Relation between Particle Size and Repose Angles of Powders. *Powder Technology*, 15:129-131.
- Chang, W., Pu-zhen G., Si-chao, T., Chao, X. (2012). Effect of aspect ratio on the laminar-to-turbulent transition in rectangular channel. *Annals of Nuclear Energy* 46: 90-96.
- Cheng, N.S. and Chiew Y.M. (1999). Incipient sediment motion with upward seepage. *Journal of Hydraulic Research*, 37(5): 665-681.
- Chevalier, C., Lindner A., Leroux, M., Clément, E. (2009). Morphodynamics during air injection into a confined granular suspension. *Journal of Non-Newtonian Fluid Mechanics*, 158: 63-72.
- Chien, N. and Wan Z. (1999). *Mechanics of Sediment Transport*. ASCE Press, Reston Virginia.
- Clibborn J. (1902). *Experiments on the passage of water through sand*. Technical Paper No. 97, Government of India.

- Davidenkoff, R. (1970). *Unterläufigkeit von Stauwerken*. Werner-Verlag GmbH, Düsseldorf.
- De Bruijn, H. and Knoeff, H. (2009). *SBW Piping: Hervalidatie Piping – HP5.4b Full-scale proeven (factual report proef 3)*. Deltares report 1200690-005-GEO-0005.
- De Graauw, A., Van der Meulen, T., Van der Does de Bye, M. (1983). *Design criteria for granular filters*. Report Delft Hydraulics Laboratory, Publication no. 287.
- De Wit, J.M. (1982). *Onderzoek zandmeevoerende wellen – Rapportage Proevenserie model VII en model VIII op fijn zand (slootmodel)*. Grondmechanica Delft report CO-220885/10.
- De Wit J.M. (1984) *Onderzoek zandmeevoerende wellen Rapportage Modelproeven*. Grondmechanica Delft report CO-220887/10.
- De Zwart, A.H. (2007). *Investigation of Clogging Processes in Unconsolidated Aquifers near Water Supply Wells*. Phd thesis, Delft, The Netherlands.
- Ding, L., Yao, Q., Sun D., Liu, C. (2007). Experimental studies on piping development in three-stratum dike foundations. *Water Resources and Hydropower Engineering*, 38(2): 19-22.
- Ding, L.Q, Yao, Q.L., Sun D.Y. (2008). Experimental studies on the seepage control effects of suspended cutoffs in dike foundations. 4th International Symposium on Flood Defence: Managing Flood Risk, Reliability and Vulnerability, Toronto, 6-8 May.
- El Shamy, U. and Aydin, F. (2008). Multi-Scale Modeling of Flood-Induced Piping in River Levees. *Journal of Geotechnical and Geoenvironmental Engineering*, ASCE, 134(9): 1385-1398.
- Flood - Data and statistics (n.d.). Retrieved from <http://www.preventionweb.net/english/hazards/statistics/?hid=62>).
- Foster M.A. and Fell R. (1999) *A Framework for Estimating the Probability of Failure of Embankment Dams by Piping Using Event Tree Methods*. The University of New South Wales: School of Civil and Environmental Engineering, Australia, UNICIV Report No. R377, Australia.
- Fox R.W., Pritchard, P.J., McDonald, A.T. (2009). *Introduction to Fluid Mechanics*. John Wiley & Sons, United States of America.
- Garde R.J. and Ranga Raju, K.G. (1985). *Mechanics of sediment transportation and alluvial stream problems*. Wiley Eastern, New Delhi, 589-595.
- GeoDelft (2002). MSeep User Manual, release 6.7, November 2002.
- Glynn, E. and Kuszmaul J. (2004). *Prediction of Piping Erosion along Middle Mississippi River Levees – An empirical model*. US Army Corps of Engineers, Report USACE ERDC/GSL TR-04-12.
- Govers, G. (1987). Initiation of motion in overland flow. *Sedimentology* 34: 1157:1164.
- Griffith, W. (1913). *The Stability of Weir Foundations on Sand and Soil subject to Hydrostatic Pressure*. 221(4004): 221-232.
- Hanses, U. (1985). *Zur Mechanik der Entwicklung von Erosionskanälen in geschichtetem Untergrund unter Stauanlagen*. Dissertation Grundbauinstitut der Technischen Universität Berlin, Germany.
- Harza, L.F. (1935). *Uplift and seepage under dams on sand*. ASCE Transactions, Paper No. 1920.
- ICOLD (2013). *Internal erosion of existing dams, levees and dikes, and their foundations – Volume 1: Internal erosion processes and engineering assessment*. Bulletin preprint 164. <http://icold-cigb.org/GB/Publications/bulletin.asp>.

- Johnsen, Ø, Chevalier, C., Lindner, A., Toussaint, R., Clément, E., Måløy, K.J., Flekkøy, Schmittbuhl, J. (2008). Decompaction and fluidization of a saturated and confined granular medium by injection of a viscous liquid or gas. *Physical review* 78: 051302.
- Kakac, S., Shah, R.K., Aung, W. (1987). *Handbook of Single-Phase Convective Heat Transfer*. John Wiley and Sons, Inc., New York, NY.
- Kandlikar, S.G., Grande, W.J. (2003). Evolution of microchannel flow passages—thermohydraulic performance and fabrication technology. *Heat Trans. Eng.* 24 (1): 3-17.
- Kandlikar, S.G., Garimella, S., Li, D., Colin, S., King, M.R. (2006). *Heat transfer and fluid flow in Minichannels and Microchannels*. Elsevier Ltd, Great Britain.
- Kanning, W. (2012). *The Weakest Link – Length Effects for Piping*. Phd thesis, Delft University of Technology, Delft, The Netherlands.
- Khilar, K.C., Fogler H.S., Gray, D.H. (1985). Model for Piping-Plugging in Earthen Structures. *Journal of Geotechnical Engineering* 111(7):833-847.
- Knoeff, H. (2008). *SBW Piping – Vooronderzoek kleine schaal laboratoriumproeven (A1. Literatuurstudie)*. Deltares report 433380-0011.
- Koelewijn, A., De Bruijn H., Van Beek, V. (2009). *SBW Piping: Hervalidatie Piping – HP5.4b Full-scale proeven (factual report proef 1)*. Deltares report 1200690-000-GEO-0023.
- Koenders, M.A. and Sellmeijer, J.B. (1991). Mathematical Model for Piping. *Journal of Geotechnical Engineering* 118(6): 943-946.
- Kramer, H. (1935). Sand mixtures and sand movement in fluvial models. *Transactions American Society of Civil Engineers* 100, 798–878.
- Lane, E. W. (1935). Security from under-seepage masonry dams on earth foundations. *Transactions American Society of Civil Engineers* 100(1): 929–966.
- Lee, K. L. and Seed, H. B. (1967). Drained strength characteristics of sands. *Journal of the Soil Mechanics and Foundations Division* 93(6): 117-141.
- Loezos, P.N., Costamagna, P., Sundaresan, S. (2002). The role of contact stresses and Wall friction on fluidization. *Chemical Engineering Science* 57: 5123-5141.
- Loiseleux, T., Gondret, P., Rabaud, M., Doppler D. (2005). Onset of erosion and avalanche for an inclined granular bed sheared by a continuous laminar flow. *Physics of fluids* 17(103304): 1-9.
- Lu, Y., Chiew, Y.M., Cheng, N.S. (2008). Review of seepage effects on turbulent open-channel flow and sediment entrainment. *Journal of Hydraulic Research* 46(4): 476-488.
- Mansur, C.I., Postol, G. and Salley, J.R. (2000). Performance of relief well systems along Mississippi river levees. *Journal of Geotechnical and Geoenvironmental Engineering* 126(8): 727-738.
- Mantz, P.A. (1977). Incipient Transport of Fine Grains and Flakes by Fluids – Extended Shields Diagram. *Journal of the Hydraulics Division, Proceedings of the American Society of Civil Engineers* 103(HY6): 601-615.
- Martin, C.S. (1970). Effect of a Porous Sand Bed on Incipient Sediment Motion. *Water Resources Research* 6(4): 1162:1174.
- Miesel, D. (1978). Rückschreitende Erosion unter bindiger Deckschicht. In *Baugrundtagung*. Deutschen Gesellschaft für Erd- und Grundbau e.V, Essen, p. 599-626.
- Ministerie van Verkeer en Waterstaat (2007). *Voorschrift Toetsen op Veiligheid Primaire Waterkeringen*.

- Moffat, R., Fannin, J., Garner S.J. (2011). Spatial and temporal progression of internal erosion in cohesionless soil. *Canadian Geotechnical Journal* 48(3): 399-412.
- Müller-Kirchenbauer, H. (1978). Zum Zeitlichen Verlauf der Rückschreitenden Erosion in Geschichtetem Untergrund unter Dämmen und Stauanlagen, *Beitrag zum Talsperrensposium*, München.
- Müller-Kirchenbauer, H., Rankl, M., Schlötzer C. (1993). Mechanism for regressive erosion beneath dams and barrages. In *Filters in Geotechnical and Hydraulic Engineering*, Brauns, Heibaum and Schuler (eds), 369-376, Balkema, Rotterdam.
- Munich Re (2013). Floods dominate natural catastrophe statistics in first half of 2013. Münchener Rückversicherungs-Gesellschaft, München.
<http://www.munichre.com/en/media-relations/publications/press-releases/2013/2013-07-09-press-release/index.html>.
- Nikuradse J. (1933). Laws of flow in rough pipes. Translation of Strömungsgesetze in rauhen Röhren. VDI-Forschungsheft 361. Beilage zu *Forschung auf dem Gebiete des Ingenieurwesens*, Ausgabe B Band 4.
- Ojha, C.S. and Singh, V.P. (2003). Determination of critical head in soil piping. *Journal of Hydraulic Engineering* 129(1): 511-518.
- Okajima K. and Tanaka, T. (2008). Evaluation of the downstream piping of weirs by model experiments and Elasto-Plastic FEM. Proceedings *4th International Conference on Scour and Erosion*, p. 460-467, <http://scour-and-erosion.baw.de/conferences/icse4/>.
- Okajima, K., Magara, N, Iida, T. (2010). Reexamination of Creep Theory in the Foundations of Weirs by Model Experiments and Elasto-Plastic FEM. In *Scour and Erosion*, Burns, Bhatia, Avila and Hunt (eds), 560-569, ASCE.
- Ouriemi, M., Aussillous, P, Medale, M. Peysson, Y., Guazzelli, E. (2007). Determination of the critical Shields number for particle erosion in laminar flow. *Physics of fluids* 19(061706): 1-4.
- Pietrus, T.J. (1981). *An experimental investigation of hydraulic piping in sand*. Master thesis, University of Florida, Dept. of Civil Engineering, USA.
- Polubarinova-Kochina P.Ya. (1962) *Theory of groundwater movement*. Princeton University Press. Princeton, USA.
- Rice, J. and Swainston-Fleshman, S.M. (2013). Laboratory Modeling of Critical Hydraulic Conditions for the Initiation of Piping. In *Proceedings Geo-Congress 2013: Stability and Performance of Slopes and Embankments III* (Meehan, Pradel, Pando and Labuz (eds)), ASCE, pp. 1044-1055.
- Richards, K.S. and Reddy K.R. (2012) Experimental investigation of initiation of backward erosion piping in soils. *Géotechnique* 62(10): 933-942.
- Rowe, P.J. (1962). The stress-dilatancy relation for static equilibrium of an assembly of particles in contact. Proc. Royal Society of London, Series A: 500-527.
- Sadrekarimi, A. and Olsen, S.M. (2011). Critical state friction angle of sands. *Géotechnique* 61(9): 771-783.
- Schmertmann, J.H. (1995). *Report on flume tests for piping and scour erosion of HL-2 sands*, IMC-Agrico.
- Schmertmann, J.H. (2000). The non-filter factor of safety against piping through sands. In *Judgment and innovation* (Silva and Kavazanjian (eds)), ASCE Geotechnical Special Publication 111: 65–132. Reston, USA.
- Schweckendiek T. (2014). *On Reducing Piping Uncertainties – A Bayesian Decision Approach*. Phd thesis, TU Delft, The Netherlands.

- Seizilles, G., Devauchelle, O., Lajeunesse, E., Métivier, F. (2013). Width of laminar laboratory rivers. *Physical Review E* 87(5): 052204.
- Sellmeijer, J.B. (2006). Numerical computation of seepage erosion below dams (piping). In *Proceedings Third International Conference on Scour and Erosion*, 596-601, CURNET, Gouda, The Netherlands.
- Sellmeijer, J.B. (1988). *On the mechanism of piping under impervious structures*. Doctoral dissertation, TU Delft, The Netherlands.
- Sellmeijer, J.B. (1995). *Heaving bij kunstwerken: Ontwerpmethodiek*. Report Grondmechanica Delft CO-356020/7.
- Sellmeijer, J.B., Calle, E.O.F., Sip, J.W. (1989). Influence of aquifer thickness on piping below dikes and dams. In *Proceedings of International symposium on analytical evaluation of dam related safety problems*, 357-366.
- Sellmeijer, J.B. and Koelewijn, A.R. (2007). Engineering Tools for Piping - Neural Networks Created using FEM. In: *Assessment of the Risk of Internal Erosion of Water Retaining Structures: Dams, Dykes and Levees - Intermediate Report of the European Working Group of ICOLD*. Berichte des Lehrstuhls und der Versuchsanstalt für Wasserbau und Wasserwirtschaft 114, Technische Universität München.
- Sellmeijer J.B., Lopéz de la Cruz J., Van Beek V.M., Knoeff J.G. (2011). Fine-tuning of the piping model through small-scale, medium-scale and IJkdijk experiments. *European Journal of Environmental and Civil Engineering* 15(8): 1139-1154.
- Shields, A. (1936). *Anwendung der Ähnlichkeitsmechanik und Turbulenzforschung auf die Geschiebebewegung*. Mitteilungen der Preußischen Versuchsanstalt für Wasserbau und Schiffbau, heft 26, Berlin.
- Silvis, F. (1991). *Verificatie Piping Model: Proeven in de Deltagoot*. Grondmechanica Delft, Delft, The Netherlands.
- Skempton, A.W. and Brogan J.M. (1994). Experiments on piping in sandy gravels. *Géotechnique* 44(3): 449-460.
- Smits, A.J. (2000). *A Physical Introduction to Fluid Mechanics*. John Wiley and Sons, New York.
- TAW (1999). *Technisch rapport Zandmeevoerende wellen*. Technische Adviescommissie voor de Waterkeringen, Delft, The Netherlands.
- Terzaghi K. (1922). Der Grundbruch an Stauwerken und seine Verhütung (The failure of dams by piping and its prevention), *Die Wasserkraft* 17: 445-449. Reprinted in Terzaghi K. (1960) *From theory to practice in soil mechanics*, Wiley, New York, pp. 114-118.
- Terzaghi K. and Peck R.B. (1967). *Soil Mechanics in Engineering Practice*. John Wiley and Sons, New York.
- Townsend, F.C.D., Bloomquist, D., Shiau, J.M., Martinez, R., Rubin H. (1988). *Evaluation of filter criteria and thickness for mitigating piping in sand*. University of Florida, Department of Civil Engineering, USA.
- USACE (1956). *Investigation of underseepage and its control – Lower Mississippi river Levees*. Technical memorandum No. 3-424, Volume 1, Waterways Experiment Station, Vicksburg, Mississippi.
- USACE (2000). *Design and Construction of Levees*. U.S. Army Corps of Engineers, Manual No. 1110-2-1913, Washington, DC.
- Van Beek, V.M., Koelewijn, A., Kruse, G., Sellmeijer, H., Barends, F. (2008). Piping phenomena in heterogeneous sands – experiments and simulations, *Proceedings of the 4th International Conference on Scour and Erosion*, p. 453-459, <http://scour-and-erosion.baw.de/conferences/icse4/>.

- Van Beek, V.M., Luijendijk, M.S., Knoeff, J.G., Barends, F.B.J. (2009a). Influence of relative density on the piping process – small-scale experiments. Int. Workshop Internal Erosion in Dams and Foundations, St. Petersburg, April 2009, 8 pp.
- Van Beek, V., De Bruijn, H., Knoeff, H. (2009b). *SBW Piping: Hervalidatie Piping - HP5.4b Full-scale proeven (factual report proef 2)*. Deltares rapport nr. 1200690-005-GEO-0005.
- Van Beek, V.M., Knoeff, J.G., Sellmeijer, J.B. (2011). Observations on the process of backward piping by underseepage in cohesionless soils in small-, medium- and full-scale experiments. *European Journal of Environmental and Civil Engineering* 15(8): 1115-1137.
- Van Beek, V.M., Bezuijen A., Schenkeveld F.M. (2012a). Piping in loose sands – the importance of geometrical fixation of grains. In *European conference on physical modelling in geotechnics Eurofuge* (Bezuijen, Lottum and Dijkstra (Eds.)), p. 1-10.
- Van Beek, V., Van Meerten, H., Nugroho, D. (2012b). *SBW Piping 5A: Model development for initiation of piping*. Deltares report 1206013-001-GEO-0003.
- Van Beek, V., Bezuijen, A., Sellmeijer, H. (2013). Backward Erosion Piping. In *Erosion in Geomechanics Applied to Dams and Levees* (Bonelli, S. (ed)), ISTE, London, UK, Wiley, Hoboken, USA, pp. 193-269.
- Van Beek, V.M., Bezuijen A., Sellmeijer, J.B., Barends F.B.J. (2014a). Initiation of backward erosion piping in uniform sands, *Géotechnique* 64(12): 927-941.
- Van Beek, V.M., Vandenboer K., Bezuijen, A. (2014b). Investigation of the backward erosion mechanism in small scale Experiments. *Physical Modelling in Geotechnics* (Gaudin & White (Eds)), 855-861, Taylor & Francis Group, London.
- Van Beek, V.M., Vandenboer, K., Bezuijen, A. (2014c). Influence of sand type on pipe development in small- and medium-scale experiments. In Cheng, Draper and An (Eds), *Scour and Erosion* (pp. 111-120). London: Taylor & Francis Group.
- Van Beek, V.M., Van Essen, H.M., Vandenboer, K., Bezuijen, A. (2015). Developments in modelling of backward erosion piping. *Géotechnique* 65(9): 740-754.
- Van Dam, P. and Beijersbergen, J.A. (1981). *Dijkdoorbraak Zalk – 8 januari 1926*. Report Centrum voor Onderzoek Waterkeringen S-80.056.
- Van den Ham, G.A. (2009). *SBW Piping Kunstwerken – KW9. Analyse kleine schaalproeven*. Deltares report 1200675-002-GEO-0001.
- Van der Poel, J.T. and Schenkeveld, F.M. (1998). A preparation technique for very homogeneous sand samples and CPT research. In *Proceedings of the International Conference Centrifuge* (Kimura and Kusakabe (eds)), 98: 149-154. Balkema, Rotterdam.
- Van der Zee, R.A. (2011). *Influence of sand characteristics on the piping process – research to the influence of grain size and other sand characteristics on the the critical head of piping*. MSc thesis, TU Delft.
- Van Esch, J.M., Sellmeijer, J.B., Stolle, D. (2013). Modeling transient groundwater flow and piping under dikes and dams. Proceedings COMGEO III, Krakow, Poland, International Centre for Computational Engineering.
- Van Essen, H.M., Kanning, W., Van Beek, V.M. (2014). *Research and Development of Flood Defense Assessment Tools for Piping in WTI 2017 - Report 12. Heterogeneity*. Deltares report 1207809-008-GEO-0003.
- Van Rhee, C. and Bezuijen, A. (1992). Influence of Seepage on Stability of Sandy Slope. *Journal of Geotechnical Engineering* 118(8): 1236-1240.

- Vandenboer, K., Van Beek, V., Bezuijen, A. (2014a). 3D finite element method (FEM) simulation of groundwater flow during backward erosion piping. *Front. Struct. Civ. Eng.* 8(2): 160 – 166.
- Vandenboer, K., Bezuijen, A., Van Beek, VM (2014b). 3D character of backward erosion piping: Small-scale experiments. In *Scour and Erosion* (Cheng, Draper and An (Eds)), Scour and Erosion, p. 81-86, Taylor & Francis Group, London.
- Verruijt, A. (1982). *Theory of Groundwater Flow*. 2nd ed, The Macmillan Press LTD, London.
- Vlasblom, A. (1977). Electrical density measurements. *LGM-mededelingen*, 18(2/3): 69-70.
- VNK (2014). Eindrapportage VNK – De veiligheid van Nederland in kaart. Publicatie Rijkswaterstaat Projectbureau VNK HB 2540621.
- Vrijling, J.K., Kok, M., Calle, E.O.F., Epema, W.G., Van der Meer, M.T., Van den Berg, P., Schweckendiek, T. (2010). *Piping - Realiteit of Rekenfout?* Technical report, Dutch Expertise Network on Flood Protection (ENW).
- Wan, R. and Guo, P. (1999). A Pressure and Density Dependent Dilatancy Model for Granular Materials. *Soils and Foundations* 39(6), 1-11.
- Ward, B.D. (1968). *Surface shear at incipient motion of uniform sands*. Phd thesis, University of Arizona.
- Weijers, J.B.A. and Sellmeijer, J.B. (1993). A new model to deal with the piping mechanism. In *Filters in Geotechnical and Hydraulic Engineering* (Brauns, Schuler and Heibbaum (eds)) 349-355, Balkema, Rotterdam, the Netherlands.
- White, C.M. (1940). The equilibrium of grains on the bed of a stream. *Proceedings Royal Society*, no. 174A, p. 322-338.
- White, S.J. (1970). Plane Bed Thresholds of Fine Grained Sediments. *Nature* 228(10): 152-153.
- Wong, Y.W. (1981). *Three dimensional finite element analysis of a quantitative piping theory*. MSc thesis, Department of Civil Engineering, University of Florida.
- Yalin, M.S. and Karahan, E. (1979). Inception of Sediment Transport. *Journal of the Hydraulics Division* 105(HY11): 1433-1443.
- Yao, Q. (2014). *Multi-size Experiments and Numerical Simulation for Backward Erosion Piping in Dike Foundations*. Phd thesis, China Institute of Water Resources and Hydropower Research.
- Yao, Q., Ding L., Sun, D., Liu, C., Zhang, Q. (2007). Experimental studies on piping in single- and two-stratum dike foundations. *Water Resources and Hydropower Engineering* 38(2): 13-18.
- Yao, Q., Xie, J., Sun, D., Zhao, J. (2009). *Data collection of dike breach cases of China*. Sino-Dutch Cooperation Project Report. China Institute of Water Resources and Hydropower Research.
- Zhou, Y.C., Xu, B.H., Yu, A.B., Zulli, P. (2002). An experimental and numerical study of the angle of repose of coarse spheres. *Powder Technology* 125: 45-54.

A. OVERVIEW OF PIPING EXPERIMENTS

This appendix presents an overview of the piping experiments used in this research, classifying them according to exit type. Most experiments had a vertical inlet, with the exception of the large-scale experiments performed at the IJkdijk location and in the Delta flume. The main characteristics of the experiments are stated in terms of sample dimensions, sand type, permeability, relative density and critical head. An indication is also given of whether the process is dominated by initiation or progression: in other words, whether or not equilibrium in pipe formation was observed. An overview of the sand characteristics can be found in Appendix B.

It should be noted that the list is not exhaustive: it presents only those experiments that are relevant for the purposes of validating models. The list contains both experiments that were performed specifically in the context of this study and experiments from the literature.

A.1. AREA-TYPE EXPERIMENTS

Area-type experiments have a large horizontal outflow area and they simulate dikes located immediately above a sandy aquifer where there is no downstream blanket layer. De Wit (1984) reported on a large experimental series with this exit type. In order to extend the available data set to include experiments looking at sand types with uniform medium-grained sands, additional area-type experiments were performed for this research. The experiments by De Wit and the additional experiments are shown in the schematisation in Figure A.1.

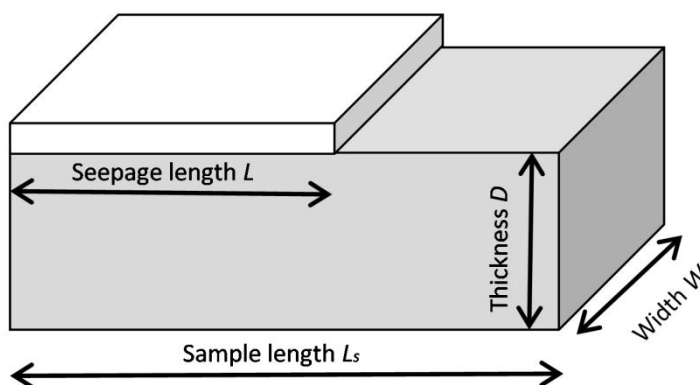


Figure A.1. Schematisation of area-type experiment

The characteristics of the area-type experiments by De Wit are presented in Table A.1. Two heads were measured in most experiments: the head at which the sand started boiling (H_b) and the 'critical head' (H_c), which is the head at which the pipe reached the upstream side. De Wit's description suggests that sand transport *generally* leads to ongoing pipe formation. It can therefore be concluded that most of the experiments were initiation-dominated: the critical head was the same as the initiation head (H_i). Table A.1 shows that the head for sand boiling in many experiments is also the same as the critical head.

Table A.1 presents the additional area-type experiments on Enschede sand. These experiments were initiation-dominated.

Table A.1. Overview of area-type experiments by De Wit (1984)

Test no.	Sand type	L [m]	L_s [m]	D [m]	W [m]	RD [-]	n [-]	k [m/s]	H_b [m]	H_i [m]	H_c [m]
220880-I-1	Dune sand	0.8	1.9	0.5	0.5	0.85	0.357	1.1E-04	-	0.330	0.330
220880-I-2	Dune sand	0.8	1.9	0.5	0.5	0.90	0.352	8.9E-05	-	0.364	0.364
220880-I-3	Dune sand	0.8	1.9	0.5	0.5	0.89	0.353	1.1E-04	0.331	0.331	0.331
220880-I-4	Dune sand	0.8	1.9	0.5	0.5	0.73	0.370	1.5E-04	0.239	0.239	0.239
220880-I-5	Dune sand	0.8	1.9	0.5	0.5	0.64	0.380	1.5E-04	-	0.269	0.269
220880-I-6	Dune sand	0.8	1.9	0.5	0.5	0.81	0.362	1.8E-04	-	0.272	0.272
220880-I-7	Dune sand	0.8	1.9	0.5	0.5	0.53	0.392	2.5E-04	-	0.201	0.201
220880-I-8	Dune sand	0.8	1.9	0.5	0.5	0.37	0.409	2.7E-04	-	0.166	0.166
220880-I-9	Dune sand	0.8	1.9	0.5	0.5	0.45	0.400	3.3E-04	-	0.222	0.222
220880-II-1	River sand	0.8	1.9	0.5	0.5	0.84	0.330	3.7E-04	0.243	0.302	0.302
220880-II-2	River sand	0.8	1.9	0.5	0.5	0.75	0.338	3.9E-04	0.366	0.450	0.450
220880-II-3	River sand	0.8	1.9	0.5	0.5	0.60	0.350	5.2E-04	0.251	0.300	0.300
220880-II-4	River sand	0.8	1.9	0.5	0.5	0.48	0.360	6.1E-04	0.391	0.445	0.445
220880-II-5	River sand	0.8	1.9	0.5	0.5	0.36	0.370	6.6E-04	0.254	0.340	0.340
220880-II-6	River sand	0.8	1.9	0.5	0.5	0.24	0.380	7.5E-04	0.225	0.225	0.225
220880-III-1	River sand 1A	0.8	1.9	0.5	0.5	0.72	0.340	3.7E-04	0.216	0.300	0.300
220880-III-2	River sand 1A	0.8	1.9	0.5	0.5	0.61	0.350	3.7E-04	0.285	0.392	0.392
220880-III-3	River sand 1A	0.8	1.9	0.5	0.5	0.51	0.359	3.8E-04	0.255	0.364	0.364
220880-III-4	River sand 1A	0.8	1.9	0.5	0.5	0.38	0.370	4.6E-04	0.284	0.284	0.284
220880-III-5	River sand 1A	0.8	1.9	0.5	0.5	0.27	0.380	5.3E-04	0.304	0.322	0.322
220880-III-6	River sand 1A	0.8	1.9	0.5	0.5	0.16	0.390	6.9E-04	0.202	0.202	0.202
220880-IV-1	Dune sand	2.4	5.75	1.5	0.5	0.92	0.350	1.4E-04	0.620	0.838	0.838
220880-IV-2	Dune sand	2.4	5.75	1.5	0.5	0.82	0.360	1.7E-04	0.374	0.374	0.374
220880-IV-3	Dune sand	2.4	5.75	1.5	0.5	0.73	0.370	1.9E-04	0.409	0.409	0.409
220880-V-1	Beach sand	0.8	1.9	0.5	0.5	0.91	0.340	1.6E-04	0.266	0.266	0.266
220880-V-2	Beach sand	0.8	1.9	0.5	0.5	0.83	0.350	1.9E-04	0.257	0.303	0.303
220880-V-3	Beach sand	0.8	1.9	0.5	0.5	0.74	0.360	2.1E-04	0.173	0.234	0.234
220880-V-4	Beach sand	0.8	1.9	0.5	0.5	0.66	0.370	2.6E-04	0.224	0.244	0.244
220880-V-5	Beach sand	0.8	1.9	0.5	0.5	0.57	0.380	2.4E-04	0.208	0.208	0.208
220880-V-6	Beach sand	0.8	1.9	0.5	0.5	0.49	0.390	2.9E-04	0.215	0.250	0.250
220880-V-7	Beach sand	0.8	1.9	0.5	0.5	0.40	0.400	3.4E-04	0.236	0.244	0.244
220880-VI-1	Beach sand	2.4	5.75	1.5	0.5	0.88	0.344	2.0E-04	0.415	0.415	0.415
220880-VI-2	Beach sand	2.4	5.75	1.5	0.5	0.83	0.350	1.9E-04	0.344	0.352	0.352
220880-VI-3	Beach sand	2.4	5.75	1.5	0.5	0.68	0.368	2.4E-04	0.414	0.414	0.414
220880-VI-4	Beach sand	2.4	5.75	1.5	0.5	0.66	0.370	2.3E-04	0.444	0.444	0.444
220880-VI-5	Beach sand	2.4	5.75	1.5	0.5	0.57	0.380	2.9E-04	0.351	0.360	0.360
220880-VI-6	Beach sand	2.4	5.75	1.5	0.5	0.49	0.390	3.0E-04	0.381	0.381	0.381
220880-VI-7	Beach sand	2.4	5.75	1.5	0.5	0.40	0.400	3.5E-04	0.285	0.285	0.285

220880-VII-1	Beach sand	0.8	1.9	0.5	0.5	0.95	0.336	1.4E-04	0.280	0.280	0.280
220880-VII-2	Beach sand	0.8	1.9	0.5	0.5	0.83	0.350	1.8E-04	0.241	0.241	0.241
220880-VII-3	Beach sand	0.8	1.9	0.5	0.5	0.66	0.370	2.2E-04	0.241	0.241	0.241
220881-40-1	Beach sand	4.5	5.75	1.5	0.5	0.81	0.360	2.2E-04	-	0.809	0.809
220881-40-2	Beach sand	4.5	5.75	1.5	0.5	0.71	0.360	2.1E-04	-	0.715	0.715
220881-40-3	Beach sand	4.5	5.75	1.5	0.5	0.62	0.360	2.1E-04	-	0.624	0.624
220881-40-4	Beach sand	1.2	5.75	1.5	0.5	0.74	0.360	2.1E-04	-	0.307	0.307
220881-40-5	Beach sand	1.2	5.75	1.5	0.5	0.74	0.360	2.1E-04	-	0.189	0.189
220881-40-6	Beach sand	1.2	5.75	1.5	0.5	0.74	0.360	2.1E-04	-	0.288	0.288
220881-40-7	Beach sand	1.2	5.75	1.5	0.5	0.74	0.360	2.1E-04	-	0.200	0.200
220883-35-1	Coarse sand	2.4	5.75	1.5	0.5	0.18	0.370	1.8E-03	0.760	0.880	0.880
220883-35-2	Coarse sand	2.4	5.75	1.5	0.5	0.20	0.367	1.5E-03	0.810	0.960	0.960
220883-35-3	Coarse sand	2.4	5.75	1.5	0.5	0.21	0.366	1.5E-03	0.630	0.800	0.800
220883-35-4	Coarse sand	2.4	5.75	1.5	0.5	0.35	0.343	1.1E-03	0.490	0.680	0.680
220883-35-5	Coarse sand	2.4	5.75	1.5	0.5	0.35	0.343	1.0E-03	0.660	0.714	0.714
220883-35-6	Coarse sand	2.4	5.75	1.5	0.5	0.36	0.341	1.0E-03	0.520	0.885	0.885
220883-35-7	Coarse sand	2.4	5.75	1.5	0.5	0.48	0.320	8.3E-04	0.610	0.626	0.626
220883-35-8	Coarse sand	2.4	5.75	1.5	0.5	0.48	0.320	7.5E-04	0.635	1.040	1.040
220883-35-9	Coarse sand	2.4	5.75	1.5	0.5	0.48	0.320	7.3E-04	0.675	0.940	0.940
220883-39-1	Dune sand	0.8	1.9	0.5	0.5	0.55	0.390	2.6E-04	0.237	0.237	0.237
220883-39-2	Dune sand	0.8	1.9	0.5	0.5	0.55	0.390	2.6E-04	0.195	0.195	0.195
220883-39-3	Dune sand	0.8	1.9	0.5	0.5	0.55	0.390	2.2E-04	0.172	0.214	0.214
220884-26-1	Coarse sand	0.8	1.9	0.5	0.5	0.19	0.369	1.6E-03	0.252	0.394	0.394
220884-26-2	Coarse sand	0.8	1.9	0.5	0.5	0.34	0.344	1.1E-03	0.353	0.391	0.391
220884-26-3	Coarse sand	0.8	1.9	0.5	0.5	0.48	0.320	8.9E-04	0.650	0.783	0.783
220884-26-4	Coarse sand	0.8	1.9	0.5	0.5	0.18	0.370	1.1E-03	0.374	0.792	0.792
220884-26-5	Coarse sand	0.8	1.9	0.5	0.5	0.33	0.345	8.0E-04	0.417	0.660	0.660

Table A.2: Overview of additional area-type experiments

Test no.	Sand type	L [m]	L_s [m]	D [m]	W [m]	RD [-]	n [-]	k [m/s]	H_b [m]	H_i [m]	H_c [m]
I-137	Enschede sand	0.33	0.48	0.1	0.3	0.98	0.322	3.1E-04	0.260	0.260	0.260
I-138	Enschede sand	0.33	0.48	0.1	0.3	0.97	0.323	2.8E-04	0.280	0.280	0.280

The IJkdijk experiments were also performed with a large outflow area. In these experiments, the sand sample was not rectangular and the water entered through the horizontal sand bed upstream of the dike (Figure A.2). Table A.3 shows the characteristics of the four tests.

The first signs of erosion in the IJkdijk experiments were ‘sand traces’: spots of local preferential path formation where fines whirled up from the bed. These were followed by sand boils, which did not continuously transport sand. A small crater often formed around these sand boils, indicating that some transport had taken place. The head at which this type of sand boil occurred was adopted as the initiation head. These values were obtained from the observations in the factual reports of the experiments (Koelewijn et al. 2009; Van Beek et al., 2009; De Bruijn and Knoeff, 2009).

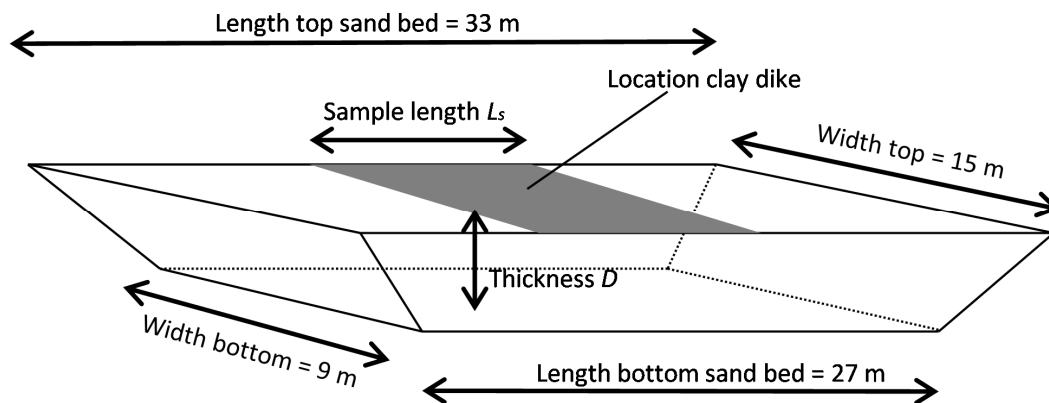


Figure A.2. Schematisation of IJkdijk experiment configuration with design dimensions (the actual dimensions were slightly different).

Table A.3: Overview of IJkdijk experiments

Test no.	Sand type	L [m]	L_s [m]	D [m]	W [m]	RD [-]	n [-]	k [m/s]	H_b [m]	H_i [m]	H_e [m]
IJkfs01	Fine IJkdijk sand	15	var	3	var	0,60	0,4	8,00E-05	0,92	0,92	2,30
IJkfs02	Coarse IJkdijk sand	15	var	2,85	var	0,75	0,37	1,40E-04	1,60	1,60	1,75
IJkfs03	Fine IJkdijk sand	15	var	3	var	0,60	0,4	8,00E-05	1,50*	1,50*	2,10
IJkfs04	Coarse IJkdijk sand	15	var	2,85	var	0,70	0,38	1,20E-04	n.a.	n.a.	2

* In this experiment the observation of possible sand boils might have been hindered by turbid water.

A.2. DITCH-TYPE EXPERIMENTS

Ditch-type experiments represent dikes on top of an aquifer with a blanket layer downstream, intersected by a ditch on the downstream side. This type of experiment has been performed by De Wit (1984) at small and medium scales, and at a larger scale in the Delta Flume (Silvis, 1991). The experiments by De Wit are shown in the schematisation in Figure A.3. The Delta Flume experiments were similar but the inflow area was horizontal.

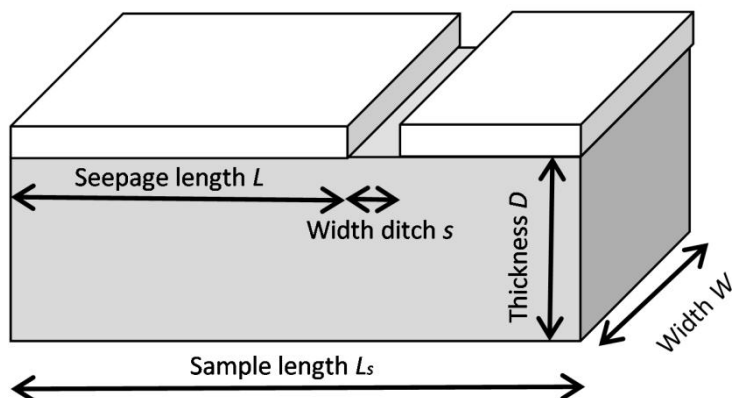


Figure A.3. Schematisation of ditch-type experiment

Two heads were recorded in the experiments: the head at which the sand started boiling (H_b) and the 'critical head' (H_c), which is the head at which the pipe reached the upstream side. The observations reported by De Wit (1984) for the ditch-type experiments matched those in the area-type experiment. At least some of the experiments were therefore dominated by initiation. However, the large difference between the head for sand boiling and the critical head, particularly in the large-scale experiments, suggests that an equilibrium in sand deposition is plausible. A report describing the ditch experiments in detail (De Wit, 1982) confirms that the head rose after sand transport was observed in the larger-scale experiments. The head for initiation was much lower than the head for progression in these experiments.

Table A.4 lists the characteristics of the ditch-type experiments conducted by De Wit (1984).

Table A.4. Overview of De Wit's ditch-type experiments (1984)

Test no.	Sand type	L [m]	L_s [m]	D [m]	W [m]	s [-]	RD [-]	n [-]	k [m/s]	H_b [m]	H_i [m]	H_c [m]
220885-10-1	Beach sand	0.9	1.9	0.5	0.5	0.05	0.49	0.39	n.a.	0.170	0.170	0.204
220885-10-2	Beach sand	0.9	1.9	0.5	0.5	0.05	0.83	0.35	n.a.	0.200	0.206	0.206
220885-10-3	Beach sand	0.9	1.9	0.5	0.5	0.05	0.49	0.39	n.a.	0.144	0.144	0.144
220885-10-4	Beach sand	0.9	1.9	0.5	0.5	0.05	0.83	0.35	n.a.	0.227	0.227	0.227
220885-10-5	Beach sand	0.9	1.9	0.5	0.5	0.05	0.49	0.39	n.a.	0.150	0.150	0.150
220885-10-6	Beach sand	0.9	1.9	0.5	0.5	0.05	0.83	0.35	n.a.	0.225	0.267	0.267
220885-10-1	Beach sand	2.7	5.75	1.5	0.5	0.05	0.83	0.35	n.a.	0.257	0.270	0.397
220885-10-2	Beach sand	2.7	5.75	1.5	0.5	0.05	0.83	0.35	n.a.	0.247	0.247	0.392
220885-10-3	Beach sand	2.7	5.75	1.5	0.5	0.05	0.83	0.35	n.a.	0.222	0.222	0.332

The critical heads in the DeltaFlume experiments were dominated by progression. Equilibrium in pipe formation was observed many times. Table A.5 presents these experiments. No record was made of the boiling or initiation heads. An indication of the initiation head was obtained by determining the head at which the first pipe was visible using the equilibrium graphs reported in Silvis (1991).

Table A.5. Overview of Delta Flume experiments by Silvis (1991)

Test no.	Sand type	L [m]	L_s [m]	D [m]	W [m]	s [m]	RD [-]	n [-]	k [m/s]	H_b [m]	H_i [m]	H_c [m]
T2	Marsdiepzand	9	>32.5	6	5	0.5	0.65	0.38	5.1E-05	n.a.	0.4*	1.05
T3	Marsdiepzand	12	>32.5	6	5	0.5	0.65	0.38	5.1E-05	n.a.	0.8*	1.69
T4	Marsdiepzand	6	>32.5	6	5	0.5	0.65	0.38	5.1E-05	n.a.	0.7*	2.16

*Derived from equilibrium graphs

A.3. HOLE-TYPE EXPERIMENTS

Hole-type experiments represent dikes on top of an aquifer with a blanket layer downstream that is locally punctured by a circular hole. Experiments with a hole-type configuration have been described in the literature and they have also been conducted by De Wit (1984) and Hanses (1985). Additional experiments were performed to investigate the effect of sand type at the small and medium scales. The schematisation in

Figure A.4 applies to all experiments except for the visualisation experiments, in which only half of the box is considered, as though it has been cut in half along the centre line.

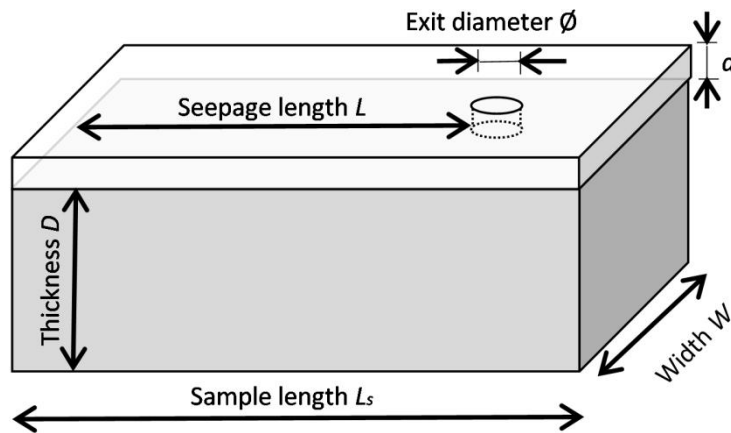


Figure A.4. Schematisation of hole-type experiment

The hole-type experiments performed by De Wit (1984) are presented in Table A.6. By contrast with the other experiments, water exited not only through the exit hole but also to the downstream side of the sand bed. A constant head was applied at the downstream side which was 0.145 m below the constant head in the exit hole.

The observations in the experiments with a hole diameter of 0.10 m were similar to those in the ditch- and area-type experiments. No equilibrium was found after sand boils appeared. It can therefore be concluded that the experiments were initiation-dominated and so the initiation head was the same as the critical head.

In the experiments with a hole diameter of 0.04 m, the exit gradually filled with sand as a result of increasing head. After some time, the level of the fluidised sand in the hole remained constant, indicating equilibrium. A head increase was required to increase the level of sand in the hole until the top was reached and sand flowed over the edge, after which continuous pipe formation took place. Given the significant vertical length of the hole (d), it is likely that the fluidised sand bed in the hole results in extra resistance. This extra resistance may have been one factor explaining the occurrence of equilibrium. The initiation head in these experiments is not known.

Table A.6. Overview of hole-type experiments conducted by De Wit (1984)

Test no.	Sand type	L [m]	L_s [m]	D [m]	W [m]	\emptyset [m]	d [m]	RD [-]	n [-]	k [m/s]	H_b [m]	H_i [m]	H_c [m]
220883-4-1	Strandzand	2.4	5.75	1.5	0.5	0.04	0.12	0.74	0.36	1.8E-04	0.258	-	0.470
220883-4-2	Strandzand	2.4	5.75	1.5	0.5	0.1	0.12	0.74	0.36	1.9E-04	0.352	0.456	0.456
220883-4-3	Strandzand	4.5	5.75	1.5	0.5	0.04	0.12	0.74	0.36	1.8E-04	0.492	-	0.862
220883-4-4	Strandzand	4.5	5.75	1.5	0.5	0.1	0.12	0.74	0.36	1.6E-04	0.679	0.780	0.780

Equilibrium was observed in all the experiments conducted by Hanses (1985). A selection of the experiments with one sand type is presented in Table A.7. The vertical length of the exit hole is relatively large in these experiments. The head loss originating

from this vertical section was measured during the experiments so that the head at which the pipe progressed could be corrected for this head loss. Three of these experiments (26a, 53, 73) were performed specifically to determine the hydraulic gradient in the pipe. Accordingly, in the first phase of the experiments, the hydraulic head was raised until the critical pipe length was reached; in the second phase, the hydraulic head was brought back to 0 and reapplied in steps to assess the head loss in the pipe.

Table A.7. Overview of hole-type experiments conducted by Hanses (1985)

Test no.	Sand type	L [m]	L_s [m]	D [m]	W [m]	\emptyset [mm]	d [m]	RD [-]	n [-]	k [m/s]	H_i [m]	H_c^* [m]
21	Sand A	0.7	0.96	0.2	0.2	6	0.24	1.00	0.41	4.0E-04	n.a.	0.126
22	Sand A	0.7	0.96	0.2	0.2	6	0.24	1.00	0.41	4.0E-04	n.a.	0.128
23	Sand A	0.7	0.96	0.2	0.2	6	0.24	1.02	0.40	3.9E-04	n.a.	0.127
24	Sand A	0.7	0.96	0.2	0.2	6	0.24	1.05	0.40	3.7E-04	n.a.	0.127
25	Sand A	0.7	0.96	0.2	0.2	6	0.24	1.00	0.41	4.0E-04	n.a.	0.126
26a	Sand A	0.7	0.96	0.2	0.2	6	0.24	0.96	0.41	4.2E-04	n.a.	0.107
51	Sand A	0.6	0.9	0.0	0.1	6	n.a.	0.99	0.41	4.0E-04	n.a.	0.206
52	Sand A	0.6	0.9	0.0	0.1	6	n.a.	0.87	0.42	4.7E-04	n.a.	0.200
53	Sand A	0.6	0.9	0.0	0.1	6	n.a.	0.92	0.41	4.4E-04	n.a.	0.170
71	Sand A	2.6	3.52	0.3	0.6	6	0.33	0.87	0.42	4.7E-04	n.a.	0.276
73	Sand A	2.6	3.52	0.3	0.6	6	0.33	0.80	0.43	5.1E-04	n.a.	0.275

* Critical heads corrected for exit loss

As it was found that the blanket layer caused a head loss, the additional experiments (presented in Table A.8) were designed with an exit hole with limited length. There was pipe formation followed by equilibrium in all the experiments, and so the critical heads in these experiments were dominated by pipe progression. In the visualisation experiment (E150) and the medium-scale experiments, it was not possible to measure the head losses near the exit. Despite the small vertical exit length, the exit losses were relatively large. The contraction of flow lines near the exit could explain part of the head loss. The critical heads listed in Table A.8 were not corrected for these exit losses. The initiation head is defined here as the head at which the first sand is moved from the exit hole and coincides with the head for sand boiling in the experiments by De Wit (1984).

Table A.8. Overview of additional hole-type experiments

Test no.	Sand type	L [m]	L_s [m]	D [m]	W [m]	\emptyset [mm]	d [mm]	RD [-]	n [-]	k [m/s]	H_i [m]	H_c^* [m]
B115	Baskarp 1	0.3	0.48	0.1	0.3	6	10	0.89	0.35	5.4E-05	n.a.	0.080
B118	Baskarp 1	0.3	0.48	0.1	0.3	6	10	0.89	0.35	6.3E-05	0.020	0.080
W130	Hoherstall Waalre	0.3	0.48	0.1	0.3	6	10	0.65	0.38	5.1E-04	0.020	0.106
W131	Hoherstall Waalre	0.3	0.48	0.1	0.3	6	10	0.65	0.38	5.4E-04	0.015	0.086
B132	Baskarp 1	0.3	0.48	0.1	0.3	6	10	0.65	0.38	9.3E-05	0.025	0.065
B133	Baskarp 1	0.3	0.48	0.1	0.3	6	10	0.65	0.38	9.5E-05	0.020	0.065
O140	Oostelijke	0.3	0.48	0.1	0.3	6	10	0.65	0.35	2.0E-04	0.030	0.095
O141	Oostelijke	0.3	0.48	0.1	0.3	6	10	0.65	0.35	2.1E-04	0.030	0.090
B142	Baskarp 1	0.3	0.48	0.1	0.3	6	10	0.91	0.35	6.2E-05	0.040	0.080
B143	Baskarp 1	0.3	0.48	0.1	0.3	12	10	0.91	0.35	5.5E-05	0.030	0.084
B144	Baskarp 1	0.3	0.48	0.1	0.3	12	10	0.91	0.35	5.3E-05	0.030	0.085
B145	Baskarp 1	0.3	0.48	0.1	0.3	12	10	0.65	0.38	8.0E-05	0.030	0.069
B146	Baskarp 1	0.3	0.48	0.1	0.3	12	10	0.65	0.38	8.0E-05	0.030	0.070
E150	Enschede sand	0.3	0.48	0.1	0.1	6*	10	1.00	0.32	4.1E-04	n.a.	0.099
O163	Oostelijke	0.3	0.48	0.1	0.3	6	10	0.94	0.32	1.3E-04	0.020	0.185

I164	Itterbeck 125-250	0.3	0.48	0.1	0.3	6	10	0.97	0.34	1.3E-04	0.020	0.113
I165	Itterbeck 125-250	0.3	0.48	0.1	0.3	6	10	0.93	0.35	1.4E-04	0.020	0.096
I166	Itterbeck mixture 1	0.3	0.48	0.1	0.3	6	10	1.00	0.33	4.6E-05	0.030	0.210
I167	Itterbeck mixture 2	0.3	0.48	0.1	0.3	6	10	0.93	0.32	3.7E-05	0.050	0.152
I168	Itterbeck mixture 2	0.3	0.48	0.1	0.3	6	10	0.89	0.33	2.7E-05	0.050	0.205
E169	Enschede sand	0.3	0.48	0.1	0.3	6	10	0.94	0.32	3.2E-04	0.020	0.090
S170	Sterksel	0.3	0.48	0.1	0.3	6	10	0.89	0.37	7.6E-05	0.050	0.350
B171	Baskarp 1	0.3	0.48	0.1	0.3	6	10	0.90	0.35	6.8E-5	0.040	0.079**
E172	Enschede sand	0.3	0.48	0.1	0.3	6	10	0.94	0.33	3.4E-4	0.020	0.085**
Ims18	Itterbeck 0.33 mm	1.3	1.91	0.4	0.8	20.5	20	0.87	0.35	3.5E-04	0.050	0.330
Bms1	Baskarp 2	1.3	1.91	0.4	0.8	20.5	20	0.94	0.37	8.0E-05	<0.05	0.210
Ims20	Itterbeck 0.33 mm	1.3	1.91	0.4	0.8	20.5	20	0.91	0.34	3.9E-04	<0.05	0.194

*semicircle

** equilibrium

A.4. SLOPE-TYPE EXPERIMENTS

The slope-type experiments (schematisation in Figure A.5) are not representative of a specific situation in the field. Assuming that the exit has little effect on pipe progression and the corresponding critical head, and can be accounted for using a numerical model, this exit type was selected for the purposes of validating the Sellmeijer model (Knoeff, 2008).

During the experiments conducted to validate the Sellmeijer model, it was not realised that, in some cases, pipe initiation requires a larger head than pipe progression and this was indeed seen in small-scale experiments with a slope-type exit. The critical gradients obtained in these experiments were therefore used to validate and calibrate the Sellmeijer model (Sellmeijer et al., 2011).

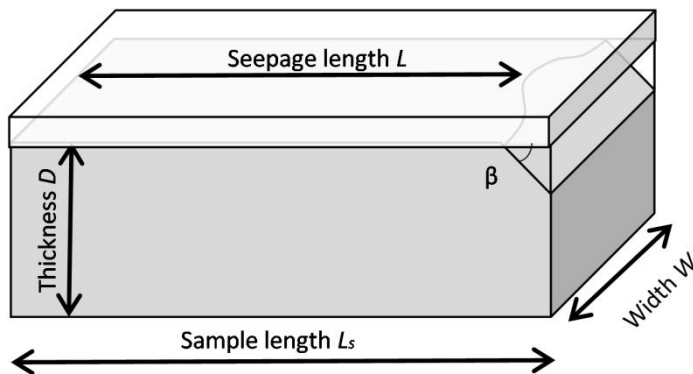


Figure A.5. Schematisation of slope-type experiment

Forward erosion was observed in some experiments, as shown in Table A.8. Most experiments in this list were described in Van Beek et al. (2011). Several additional experiments were performed to determine the relevance of forward erosion (B101, B103, B104, B121-B123) and to study the relationship between initiation and progression (B105 and B107).

The critical heads were corrected for the head loss originating from the upstream filter. In the earliest experiments (up to experiment S64), the upstream filter was semi-

permeable and no riser tubes were installed to measure filter resistance. The effect of this filter was therefore re-assessed in column experiments (described in Appendix C) as the head loss across this filter appeared to be quite large for relatively coarse sand samples. The upstream filter is partially closed at the sides of the filter, resulting in a concentrated flow through the middle (8 cm gap for older experiments, 20 cm gap for experiment 82 onwards).

Permeability was determined by simulating the experiment in MSeep using the head losses and the corresponding flow rates obtained from the experiments before pipe formation. As the head losses in the sand bed depend on the filter resistance, the permeability coefficients obtained were slightly different from the values reported in Van Beek et al. (2011). In the experiments in which riser tubes were installed, permeability was determined using the flow rate and the heads measured with the riser tubes.

The slope angle was estimated using photographs, assuming a linear slope from the top of the sand bed to the downstream filter. In the medium-scale experiments, this method produced very shallow slope angles. In the medium-scale experiments, the slope was not linear, becoming shallower in the direction of the downstream filter. In the medium-scale experiments with Baskarp sand, the slope angle near the top of the sand bed was estimated on the basis of the slope angles obtained in the small-scale experiments with Baskarp sand using a least squares correlation between slope angle and porosity. No correlation was available for the other medium-scale experiments.

Table A.8. Overview of slope-type experiments conducted by Van Beek et al. (2011)

Test no.	Sand type	L [m]	L_s [m]	D [m]	W [m]	β [degrees]	RD [-]	n [-]	k [m/s]	H_i [m]	H_c [m]	Note
B19	Baskarp	0.340	0.378	0.1	0.3	27.7	0.64	0.39	1.5E-04	0.114	0.114	
B22	Baskarp	0.340	0.379	0.1	0.3	27.0	0.67	0.38	1.5E-04	0.123	0.123	1
B23	Baskarp	0.338	0.376	0.1	0.3	28.0	0.98	0.34	5.9E-05	0.193	0.193	
B24	Baskarp	0.338	0.377	0.1	0.3	27.0	0.97	0.34	6.8E-05	0.172	0.172	
B25	Baskarp	0.338	0.376	0.1	0.3	27.5	0.31	0.43	4.8E-04	0.041	0.041	1
B26	Baskarp	0.338	0.373	0.1	0.3	29.5	0.35	0.42	1.0E-03	0.032	0.032	1
B27	Baskarp	0.334	0.375	0.1	0.3	25.9	0.34	0.43	5.4E-04	0.050	0.050	1
B28	Baskarp	0.335	0.385	0.1	0.3	21.8	0.37	0.42	2.7E-04	0.071	0.071	
B29	Baskarp	0.335	0.384	0.1	0.3	22.1	0.39	0.42	3.1E-04	0.062	0.062	1
B30	Baskarp	0.330	0.384	0.1	0.3	20.5	0.35	0.42	4.1E-04	0.037	0.037	1
D31	Dekzand Nunspeet	0.332	0.374	0.1	0.3	25.4	0.65	0.33	6.2E-05	0.179	0.179	
D32	Dekzand Nunspeet	0.332	0.375	0.1	0.3	24.9	0.65	0.33	8.3E-05	0.138	0.138	
D33	Dekzand Nunspeet	0.332	0.377	0.1	0.3	24.0	0.35	0.38	1.6E-04	0.084	0.084	1
D34	Dekzand Nunspeet	0.332	0.377	0.1	0.3	24.1	0.33	0.38	1.3E-04	0.072	0.072	1
B35	Baskarp	0.335	0.382	0.1	0.3	23.1	0.64	0.39	1.3E-04	0.135	0.135	
B36	Baskarp	0.334	0.378	0.1	0.3	24.4	0.63	0.39	1.1E-04	0.137	0.137	
D37	Dekzand Nunspeet	0.334	0.368	0.1	0.3	30.2	0.98	0.29	3.9E-05	0.265	0.265	
D38	Dekzand Nunspeet	0.335	0.381	0.1	0.3	23.7	0.92	0.30	5.9E-05	0.165	0.165	
D39	Dekzand Nunspeet	0.331	0.378	0.1	0.3	23.2	0.92	0.30	5.4E-05	0.139	0.139	
B40	Baskarp	0.332	0.381	0.1	0.3	22.2	0.91	0.35	5.3E-05	0.148	0.148	
B41	Baskarp	0.334	0.382	0.1	0.3	22.6	0.92	0.35	7.3E-05	0.153	0.153	
O42	Oostelijke rivierenzand	0.332	0.376	0.1	0.3	24.4	0.75	0.35	-	-	-	2
O43	Oostelijke rivierenzand	0.332	0.377	0.1	0.3	23.8	0.75	0.35	4.2E-04	0.099	0.099	
O44	Oostelijke rivierenzand	0.330	0.373	0.1	0.3	24.9	0.73	0.35	-	-	-	2
I45	Itterbeck Boxtel	0.332	0.375	0.1	0.3	24.9	0.72	0.36	8.8E-05	0.203	0.203	
I46	Itterbeck Boxtel	0.337	0.375	0.1	0.3	27.8	0.70	0.36	1.1E-04	0.155	0.155	
I47	Itterbeck Enschede	0.340	0.376	0.1	0.3	29.1	0.75	0.34	7.3E-04	0.087	0.087	
I48	Itterbeck Enschede	0.340	0.377	0.1	0.3	28.4	0.76	0.34	1.1E-03	0.079	0.079	
I49	Hoherstall Waalre	0.340	0.378	0.1	0.3	27.8	0.76	0.37	8.0E-04	0.069	0.069	
I50	Hoherstall Waalre	0.332	0.376	0.1	0.3	24.4	0.73	0.38	2.2E-03	0.047	0.047	

I51	Itterbeck Sandr	0.335	0.382	0.1	0.3	23.1	0.70	0.36	1.7E-04	0.112	0.112	
I52	Hoherstall Waalre	0.331	-	0.1	0.3	-	0.71	0.38	7.0E-04	0.092	0.092	
I53	Itterbeck Sandr	0.325	0.373	0.1	0.3	22.6	0.74	0.36	1.1E-04	0.128	0.128	
B54	Baskarp	0.330	0.372	0.1	0.3	25.5	0.79	0.37	7.4E-05	0.180	0.180	
B55	Baskarp	0.325	0.377	0.1	0.3	21.0	0.71	0.38	8.8E-05	0.141	0.141	
I56	Itterbeck Scheemda	0.335	0.389	0.1	0.3	20.3	0.69	0.40	1.3E-04	0.100	0.100	
B57	Baskarp	0.330	0.377	0.1	0.3	23.1	0.75	0.37	8.8E-05	0.132	0.132	
B58	Baskarp	0.345	0.396	0.1	0.3	21.4	0.70	0.38	1.0E-04	0.182	0.182	
B61	Baskarp	0.345	0.389	0.1	0.3	24.4	0.73	0.37	9.9E-05	0.114	0.114	
I62	Itterbeck Scheemda	0.325	0.392	0.1	0.3	16.6	0.63	0.41	2.0E-04	0.099	0.099	
S63	Hoherstall Sterksel	0.340	0.380	0.1	0.3	26.6	0.75	0.41	2.4E-04	0.125	0.125	
S64	Hoherstall Sterksel	0.335	0.379	0.1	0.3	24.4	0.75	0.41	1.7E-04	0.120	0.120	
B82	Baskarp	0.336	0.377	0.1	0.3	26.0	0.85	0.36	5.9E-05	0.139	0.139	
B83	Baskarp	0.334	0.378	0.1	0.3	24.4	0.85	0.36	6.0E-05	0.139	0.139	
B84	Baskarp	0.334	0.376	0.1	0.3	25.5	0.53	0.40	9.7E-05	0.098	0.098	
B85	Baskarp	0.336	0.376	0.1	0.3	26.6	0.53	0.40	7.7E-05	0.118	0.118	
B86	Baskarp	0.336	0.376	0.1	0.3	26.6	0.43	0.41	1.0E-04	0.098	0.098	
B87	Baskarp	0.336	0.376	0.1	0.3	26.6	0.42	0.41	1.8E-04	0.046	0.046	
B101	Baskarp	0.310	0.369	0.1	0.3	18.7	0.31	0.43	1.0E-04	0.080	0.080	
B103	Baskarp	0.320	0.374	0.1	0.3	20.4	0.09	0.46	1.6E-04	0.080	0.080	
B104	Baskarp	0.310	0.310	0.1	0.3	-	0.09	0.46	-	0.080	0.080	
B105	Baskarp	0.335	0.373	0.1	0.3	27.8	0.83	0.36	7.6E-05	0.160	0.160	
B106	Baskarp	0.335	0.373	0.1	0.3	27.8	0.74	0.37	1.4E-04	0.100	0.100	1
B107	Baskarp	0.333	0.371	0.1	0.3	27.8	0.88	0.36	6.1E-05	0.180	0.180	
B121	Baskarp	0.335	0.385	0.1	0.3	21.8	0.13	0.45	1.8E-04	0.090	0.090	
B122	Baskarp	0.335	0.386	0.1	0.3	21.4	0.12	0.45	1.6E-04	0.080	0.080	
B123	Baskarp	0.332	0.381	0.1	0.3	22.4	0.12	0.45	9.5E-05	0.050	0.050	1
B123b	Baskarp	0.332	0.381	0.1	0.3	22.4	0.12	0.45	9.5E-05	0.130	0.130	
Bms1	Baskarp	1.370	1.480	0.4	0.8	23.9	0.60	0.39	1.2E-04	0.280	0.280	
Bms2	Baskarp	1.450	1.501	0.4	0.8	23.4	0.50	0.40	1.4E-04	0.370	0.370	
Ims3	Itterbeck 125- 250 µm	1.455	1.572	0.4	0.8	9.7	0.64	0.39	2.0E-04	0.260	0.260	
Ims4	Itterbeck 125- 250 µm	1.455	1.586	0.4	0.8	8.7	0.51	0.40	3.7E-04	0.200	0.200	
Ims5	Itterbeck 125- 250 µm	1.415	1.522	0.4	0.8	10.6	0.75	0.38	2.2E-04	0.290	0.290	
Ims6	Itterbeck 125- 250 µm	1.465	1.586	0.4	0.8	9.4	0.30	0.43	-	0.160	0.160	1
Bms7	Baskarp	1.300	1.524	0.4	0.8	24.1	0.64	0.39	1.5E-04	0.290	0.290	
Bms8	Baskarp	1.330	1.546	0.4	0.8	23.4	0.50	0.40	2.6E-04	0.190	0.190	
IJkms9	Itterbeck 333 µm	1.460	1.560	0.4	0.8	11.3	0.50	0.40	2.3E-04	0.345	0.345	
IJkms1	Itterbeck 431 µm	1.430	1.530	0.4	0.8	11.3	0.47	0.41	1.6E-04	0.260	0.260	
Ims11	Itterbeck 333 µm	1.480	1.598	0.4	0.8	9.6	0.65	0.34	4.3E-04	0.590	0.590	
Ims12	Itterbeck 431 µm	1.440	1.533	0.4	0.8	12.1	0.65	0.32	4.0E-04	0.390	0.390	
Ims13	Coarse IJkdijk	1.450	1.592	0.4	0.8	8.0	0.55	0.35	4.6E-04	0.370	0.370	
Ims14	Fine IJkdijk	1.460	1.501	0.4	0.8	26.0	0.50	0.33	3.8E-04	0.480	0.480	

1. Forward erosion

2. Exceptionally high flow, unreliable

B. SAND CHARACTERISTICS

This appendix presents an overview of the sand characteristics in the experiments analysed in this research. The relevant experiments, which are summarised in Appendix A, are the experiments by De Wit (1984) and Hanses (1985), and experiments performed as part of the SBW programme (most of which were presented in Van Beek et al., 2011). The sand types used in the additional experiments, which are described in Chapter 3, are also listed here.

The characteristics are grain size (d_{10} , d_{50} , d_{70}), uniformity coefficient ($U=d_{60}/d_{10}$) and minimum and maximum porosity. The minimum and maximum porosities for the SBW and the additional experiments were obtained with the standard preparation method, which was also used for the preparation of sand samples in the piping experiments with a small column.

The development of a model for pipe initiation (Chapter 5) using the slope-type experiments required the friction angle (φ) for a low-stress situation. This angle was determined for a number of sand types by increasing the slope of a surface.

B.1. OVERVIEW OF SAND CHARACTERISTICS

Table B.1 provides an overview of the characteristics of the sand types used in the experiments. It should be noted that some sand types appear several times in the list, examples being Baskarp sand and Itterbeck sand 125-250 μm . In the case of these sands, different batches of the same sand type were used and this could result in different properties. All the experiments conducted with Baskarp sand were performed with Baskarp 1, except for the medium-scale hole-type experiments, which used Baskarp 2. The medium-scale slope-type experiments were performed with Itterbeck 125-250 μm 1 and the small-scale hole-type experiments were performed with Itterbeck 125-250 μm 2.

Table B.1: Overview of sand characteristics

Sand type	Reference	d_{50} [mm]	d_{70} [mm]	d_{60}/d_{10} [-]	n_{min} [-]	n_{max} [-]
Duinzand	De Wit (1984)	0.190	0.212	1.48	0.341	0.449
Beach sand	De Wit (1984)	0.200	0.220	1.33	0.330	0.447
River sand	De Wit (1984)	0.400	0.600	2.30	0.317	0.400
Sieved river sand (1A)	De Wit (1984)	0.365	0.480	2.10	0.315	0.404
Coarse sand	De Wit (1984)	0.750	1.390	3.85	0.235	0.400
Sand A	Hanses (1985)	0.325	0.355*	1.30	0.410	0.510
Marsdiep sand	Silvis (1991)	0.211	0.247	1.57	0.339	0.463
Itterbeck fraction 125-250 μm 1	Van Beek et al. (2011)	0.170	0.210	1.70	0.345	0.465
Itterbeck fraction 333 μm	Van Beek et al. (2011)	0.283	0.350	2.10	0.307	0.409

Itterbeck fraction 431 μm	Van Beek et al. (2011)	0.342	0.500	2.60	0.285	0.380
Itterbeck fraction 330 μm	Van Beek et al. (2011)	0.342	0.410	1.60	0.337	0.434
Itterbeck 125-250 μm 2	Van Essen et al. (2014)	0.219	0.278	1.71	0.345	0.465
Itterbeck mixture 1*	Van Essen et al. (2014)	0.162	0.223	2.43	0.333	0.450
Itterbeck mixture 2**	Van Essen et al. (2014)	0.143	0.203	3.17	0.319	0.440
Baskarp 1	Van Beek et al. (2011)	0.132	0.154	1.54	0.340	0.469
Baskarp 2	Van Essen et al. (2014)	0.132	0.152	1.50	0.367	0.477
Fine IJkdijk	Van Beek et al. (2011)	0.147	0.180	1.60	0.358	0.458
Coarse IJkdijk	Van Beek et al. (2011)	0.199	0.260	1.80	0.346	0.447
Enschede sand	Van Beek et al. (2011)	0.380	0.431	1.60	0.320	0.411
Dekzand Nunspeet	Van Beek et al. (2011)	0.148	0.192	2.60	0.284	0.428
Hoherstall Waalre	Van Beek et al. (2011)	0.341	0.400	1.58	0.350	0.450
Oostelijke rivierenzand	Van Beek et al. (2011)	0.233	0.307	2.06	0.322	0.423
Itterbeck Sterksel	Van Beek et al. (2011)	0.228	0.300	2.25	0.357	0.474
Itterbeck Scheemda	Van Beek et al. (2011)	0.157	0.175	1.30	0.372	0.473
Itterbeck Sandr	Van Beek et al. (2011)	0.171	0.195	1.50	0.331	0.441
Itterbeck Boxtel	Van Beek et al. (2011)	0.155	0.202	2.20	0.323	0.461

* estimated based on d_{60} and d_{10}

B.2. FRICTION ANGLES AT LOW STRESSES

The friction angle of a sand depends on the interparticle sliding friction between two adjacent surfaces, as determined by the particle roughness and by geometrical interference (or interlocking), which is mobilised when particles push against, climb over and damage adjacent particles (Sadrekarimi and Olsen, 2011). Although interparticle friction is independent of the stress level (Rowe, 1962; Lee and Seed, 1967; Terzaghi and Peck, 1967), geometrical interference is not (Been and Jefferies, 1985; Wan and Guo, 1999). In the case of pipe initiation, where the stresses are negligible, the friction angle needs to be determined in corresponding stress conditions.

The friction angle was determined using a simple experimental set-up in which the sloping angle of the sand surface in a column can be varied until the grains in the top of the sample start moving. This angle corresponds to the friction angle. Friction angles were determined for different porosities and sand types (Baskarp, Enschede sand, Waalre sand, Oostelijke rivierenzand).

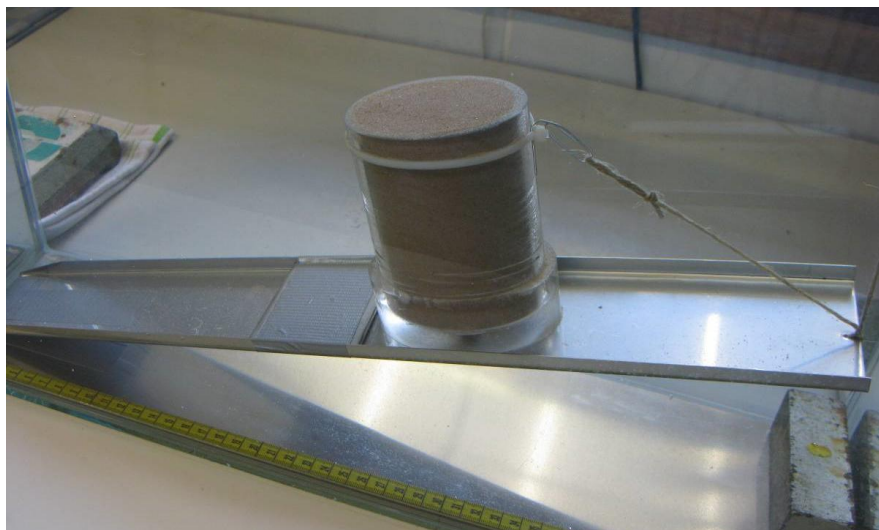


Figure B.1. Experimental set-up for determination of low-stress friction angles

The sample was prepared using the standard method described in Chapter 3. To ensure a homogeneous top sample with a density that corresponds to the density of the entire sample, the sample was made higher and the height could then be lowered by removing part of the column (Figure B.2). The column was placed on the aluminium plate, which was horizontal at the start of the test. The tank was filled with water so that the entire set-up was below the surface. The incline of the aluminium plate was gradually increased until grains start moving. The friction angle was defined as the angle at which groups of grains started moving. This angle was measured by hand and with a Lucas meter. The difference between the two measurements was less than 0.1 degrees.



Figure B.2. Sample preparation

The experiments were performed with Baskarp sand, Enschede sand, Oostelijke Rivierenzand and Waalre sand: the sands used in the slope-configuration experiments. Figure B.3 shows the friction angles obtained in all the experiments conducted as a function of porosity (the detailed results are presented in Van Beek et al., 2012b). The friction angles were interpolated using least-square linear regression to obtain the friction angles for porosities other than those measured.

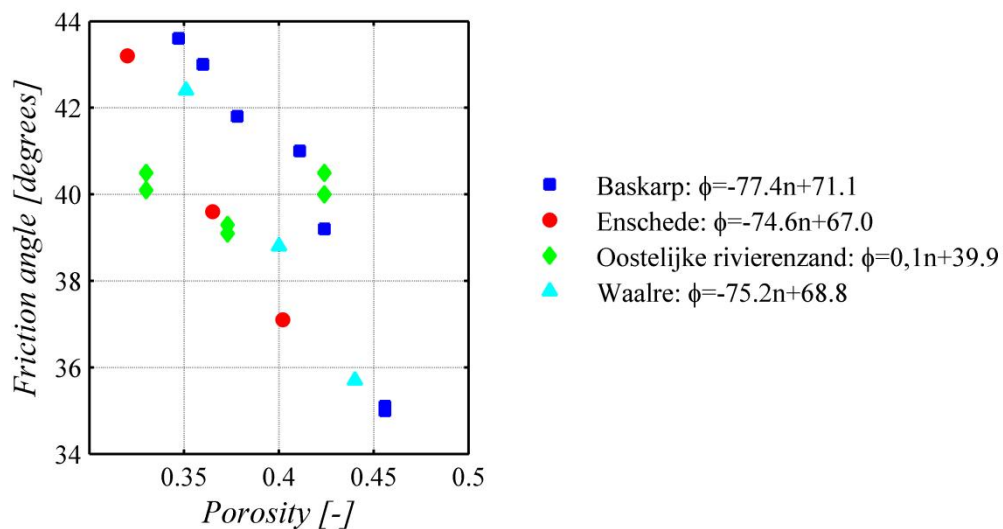


Figure B.3. Friction angle as a function of porosity: the legend shows the linear least-square regression fit.

C. FILTER RESISTANCE

This appendix presents the re-calculation of filter resistance in the slope-type experiments B19-S64 presented in Van Beek et al. (2011). The details of this calculation are described in Van Beek et al. (2012). In subsequent slope-type experiments, the head loss resulting from the filter was determined during the experiments using riser tubes and these measurements were used as the basis for the correction.

C.1. FILTER RESISTANCE

Geotextile resistance was determined for different sand types. A column experiment was conducted with the geotextile filter in combination with the perforated steel plates, as in the piping experiments.

The sample in the column was prepared using the standard method described in Chapter 3. The piezometric head was measured at different locations in the column (at 1, 5.1 and 10.1 cm from the lower filter). The height of the sand bed in the column was approximately 14 cm and it depended on the porosity. The flow was downwards. The experiments established the permittivity of the filter and the permeability of the sand as functions of porosity. The permittivity (ψ) and the permeability of the filter (k_f) are linked by $k_f = \psi t$, in which t is the thickness of the geotextile.

In all sand types, filter permittivity, permeability and sand permeability were determined at different porosities. The permeability of the sand was determined on the basis of the water-rise measurements in the top and bottom of the sample (1 cm and 10.1 cm away from the geotextile filter) and corrected for temperature (the results displayed are valid for a temperature of 20 degrees). The filter permittivity was determined using the water-head measurements at 1, 5.1 and 10.1 cm from the bottom of the filter. The filter permeability was determined at a geotextile thickness of 0.002 m. Figure C.1 and Figure C.2 show the results for porosity in relation to sand permeability, and sand permeability in relation to filter permittivity.

It can be seen in Figure C.2 that filter permittivity varies considerably depending on the porosity. In some sand types, filter resistance increases with porosity, whereas a decrease was seen in other types. Filter permittivity varies less in sand types with higher permeability.

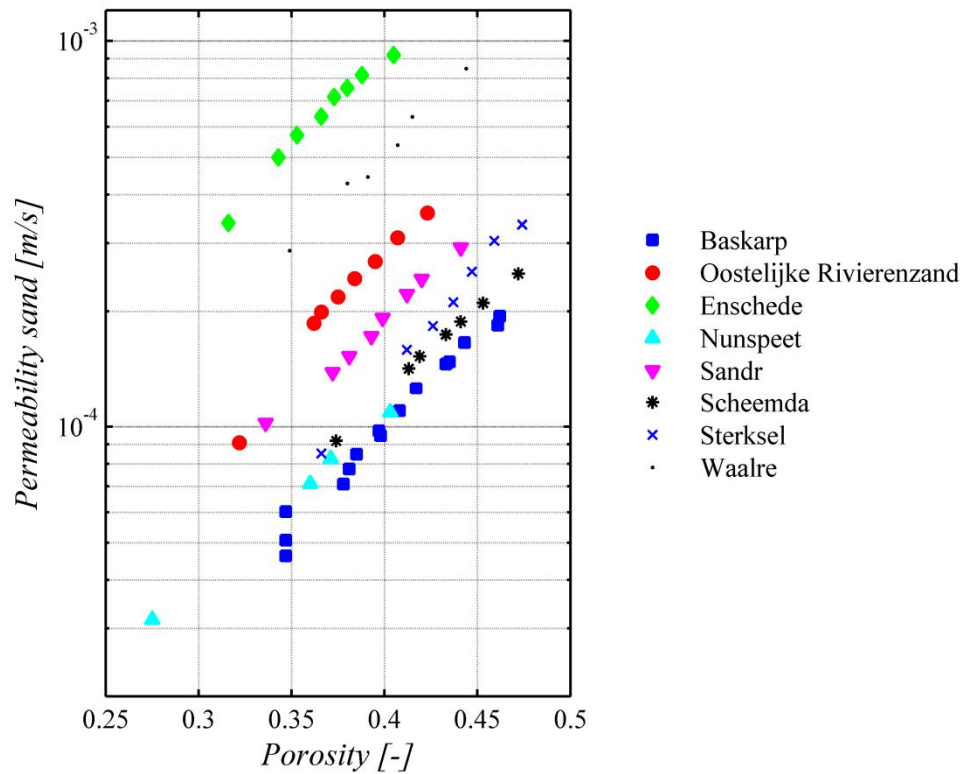


Figure C.1. Measured sand permeability as a function of porosity

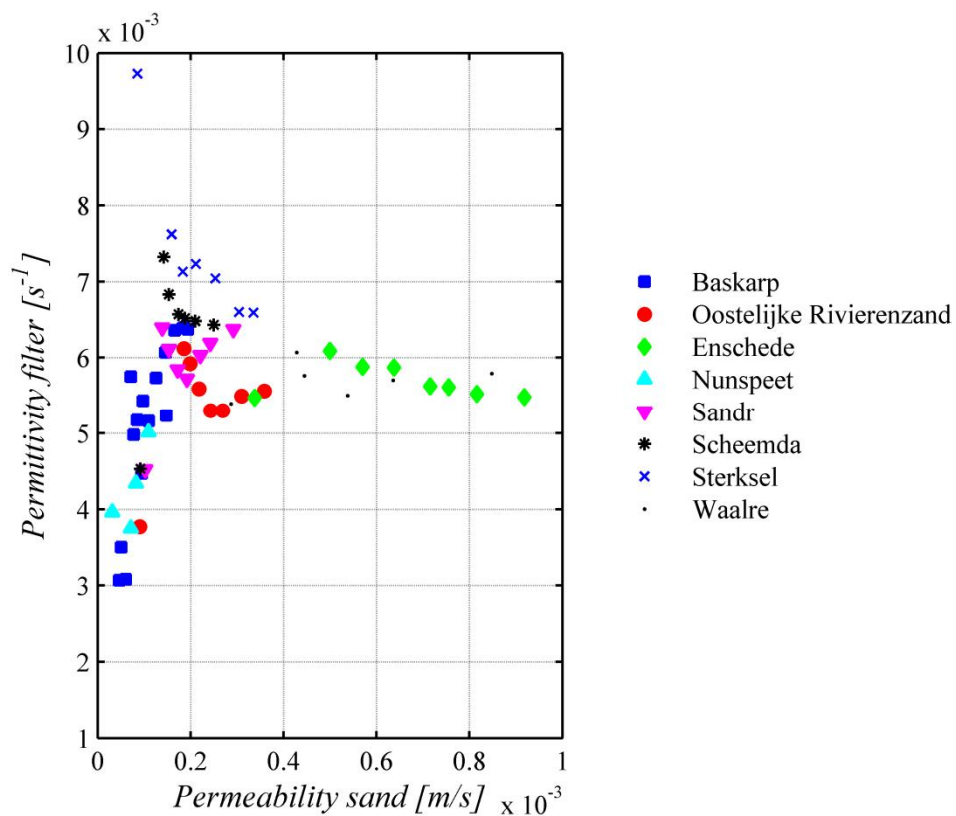


Figure C.2. Measured filter permittivity as a function of sand permeability

When the filter permittivities of the geotextile are relatively low, permittivity increases with increasing sand permeability. At higher permittivity values, this relationship is inversed. When the geotextile is in contact with less permeable sand, the permittivity of the geotextile may be determined by the permeability of the sand. In the case of coarser sand, the geotextile itself determines permittivity.

It can be concluded from the observed variation that it is difficult to determine filter permeability for sand types with relatively low permeabilities. In these sand types, the head drop across the filter is relatively small and this limits the accuracy of the method. In sand types with higher permeabilities, the head drop across the filter is relatively large and the filter permeability can be determined more accurately. In the piping experiments, the corrections were largest for the coarse sand types. The selected filter permittivity was therefore $5.5\text{E-}3 \text{ s}^{-1}$.

Using this value, it was possible to re-calculate the head drop in the sand for all small-scale piping experiments. In each experiment, the resistance of the upstream filter based on the measured flow through the sample was used to correct the total head. Using the new head across the sand bed, MSeep calculations were performed to determine the permeability of the sand (using the adapted filter resistance for the downstream filter).

Figure C.3 shows the adaptation of the experimental data. The adaptation was relatively small for most of the fine sands (with the exception of the low-density samples). The correction was more than a factor of 2 for the medium-coarse sands. The reliability of these data points is open to debate. The corrected critical heads are stated in Appendix A.

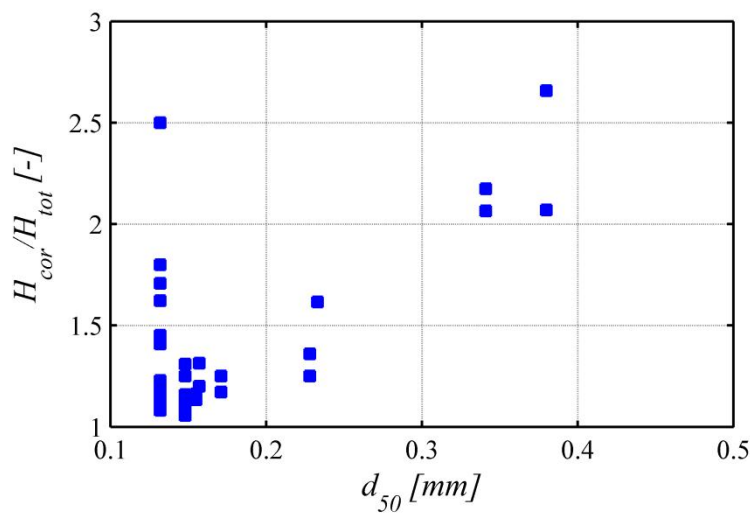


Figure C.3. Ratio of corrected critical head to uncorrected (total) applied head as a function of grain size

D. PIPE CONTOURS

The shapes and sizes of pipes were derived from photographs taken during the experiments. This appendix presents four contours for each of the hole-type experiments at pipe lengths that were approximately $\frac{1}{4}$, $\frac{1}{3}$, $\frac{1}{2}$ and $\frac{3}{4}$ of the seepage length.

D.1. SMALL-SCALE EXPERIMENTS

Appendix A.3 presents an overview of the small-scale experiments with a hole-type exit. The contours were drawn manually for these experiments: photographs were available covering the seepage lengths in all experiments with the exception of W130 and O141. It should be noted that the contour of the pipe was difficult to observe in some of the experiments. Turbid water in the exit cylinder, which was observed in some experiments, made it impossible to draw the contours in that area. Pipes initially tended to develop in all directions around the exit hole. Not all pipes were drawn because the focus was on the main pipe(s) developing in the upstream direction. Figures D.1. to D.18 show the pipe contours in a graph with the exit located at the origin.

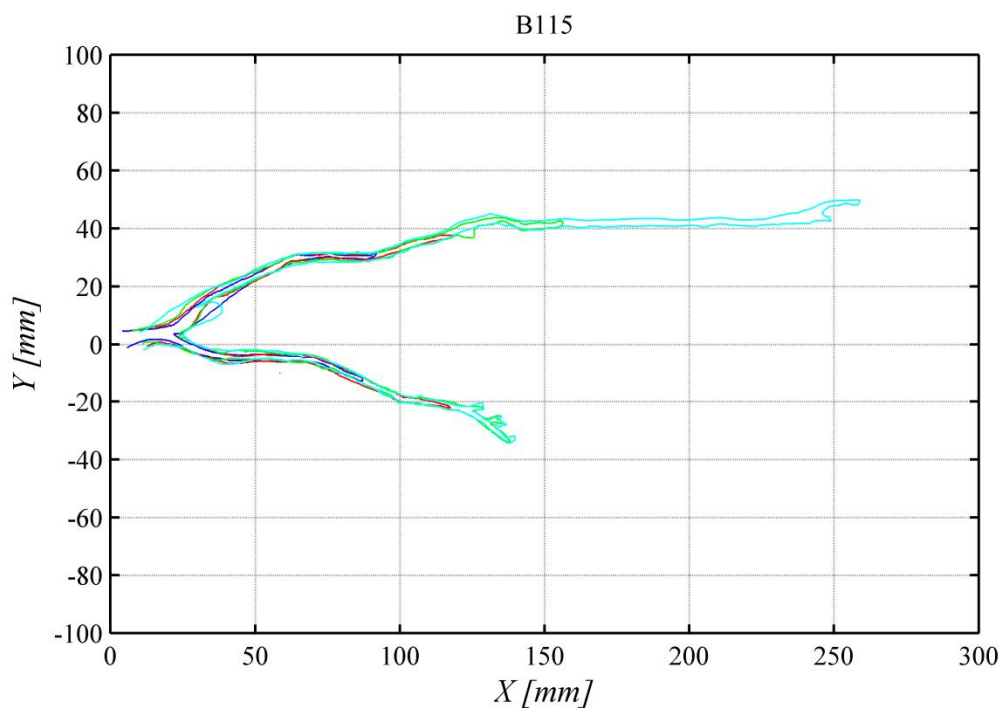


Figure D.1. Pipe contours in experiment B115

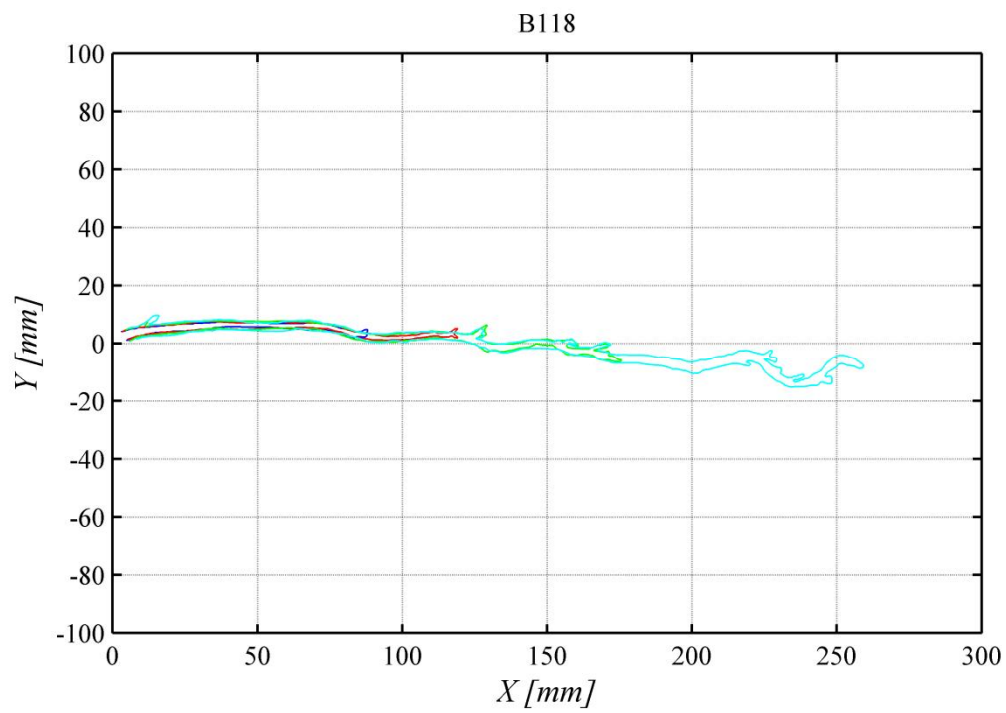


Figure D.2. Pipe contours in experiment B118

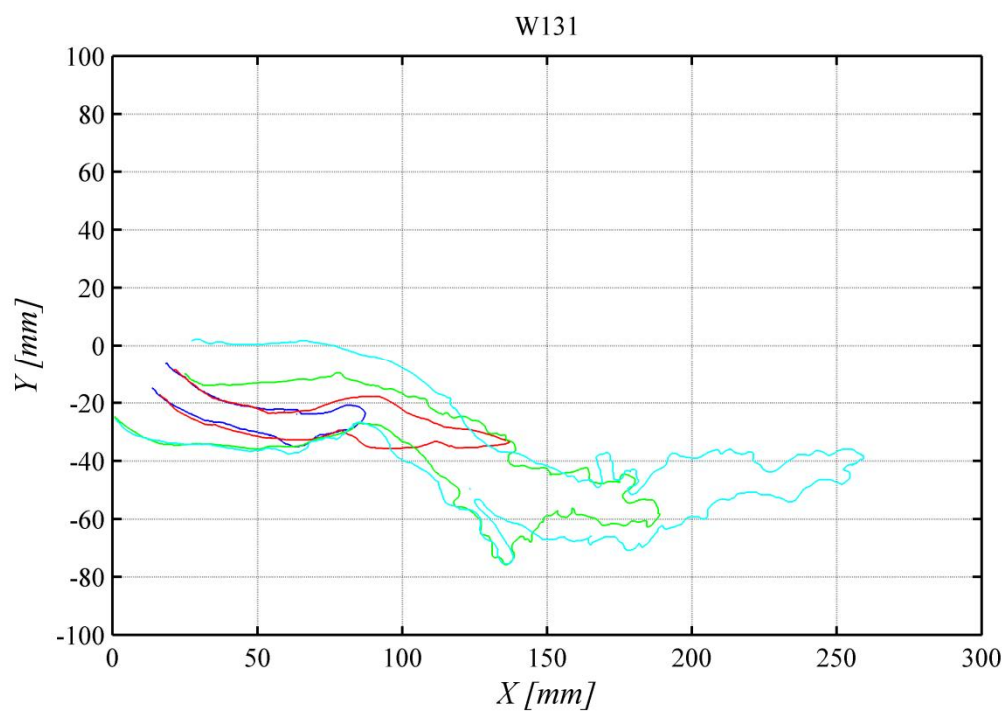


Figure D.3. Pipe contours in experiment W131

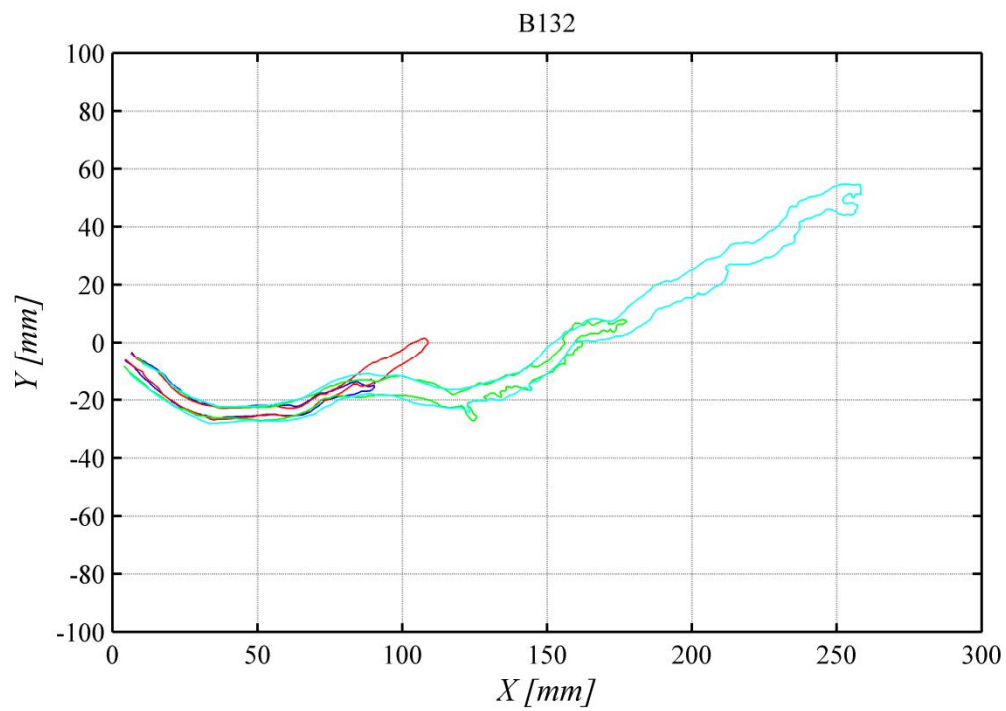


Figure D.4. Pipe contours in experiment B132

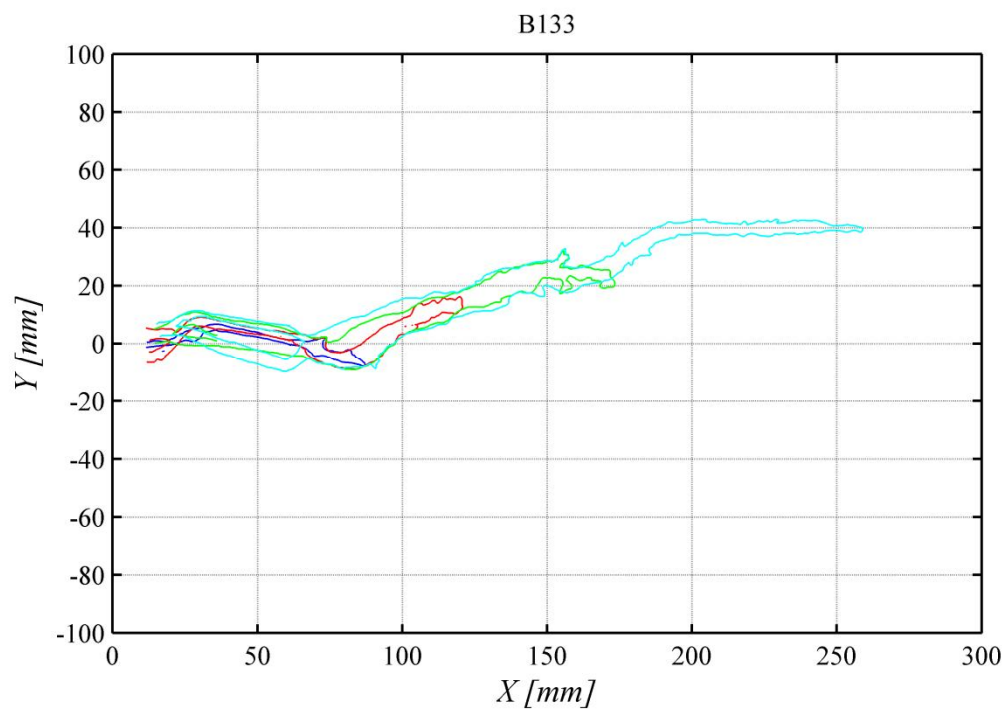


Figure D.5. Pipe contours in experiment B133

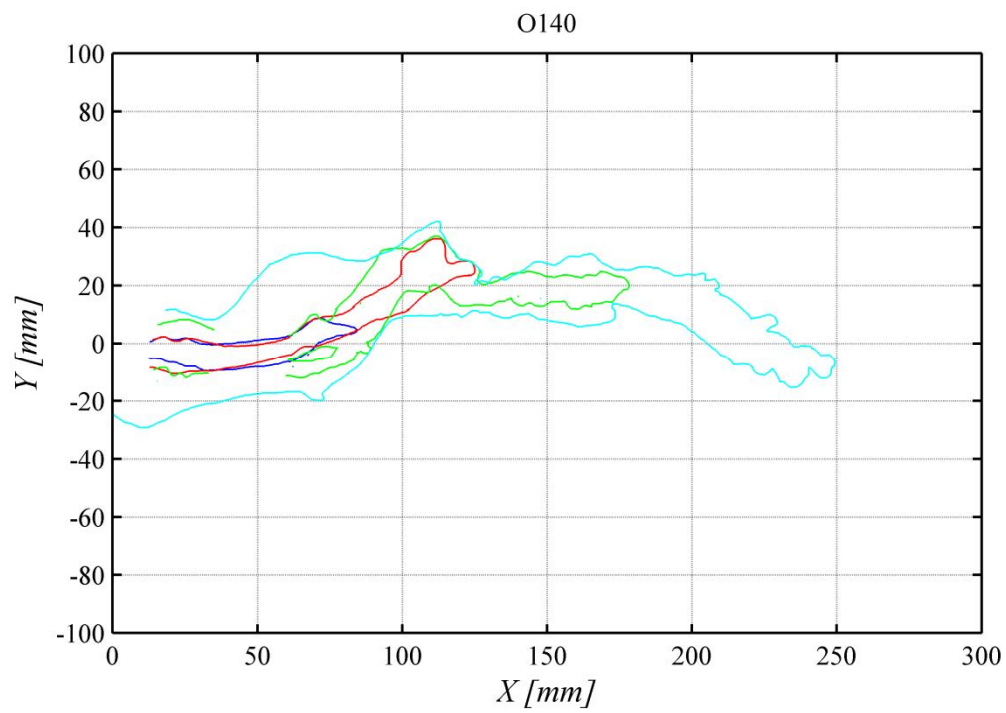


Figure D.6. Pipe contours in experiment O140

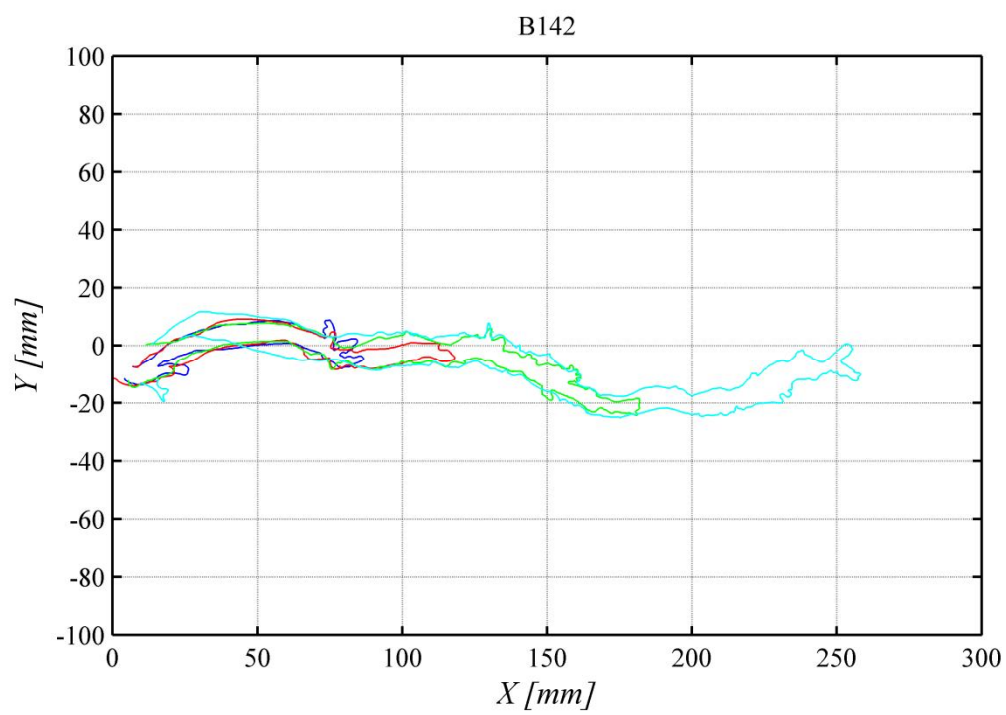


Figure D.7. Pipe contours in experiment B142

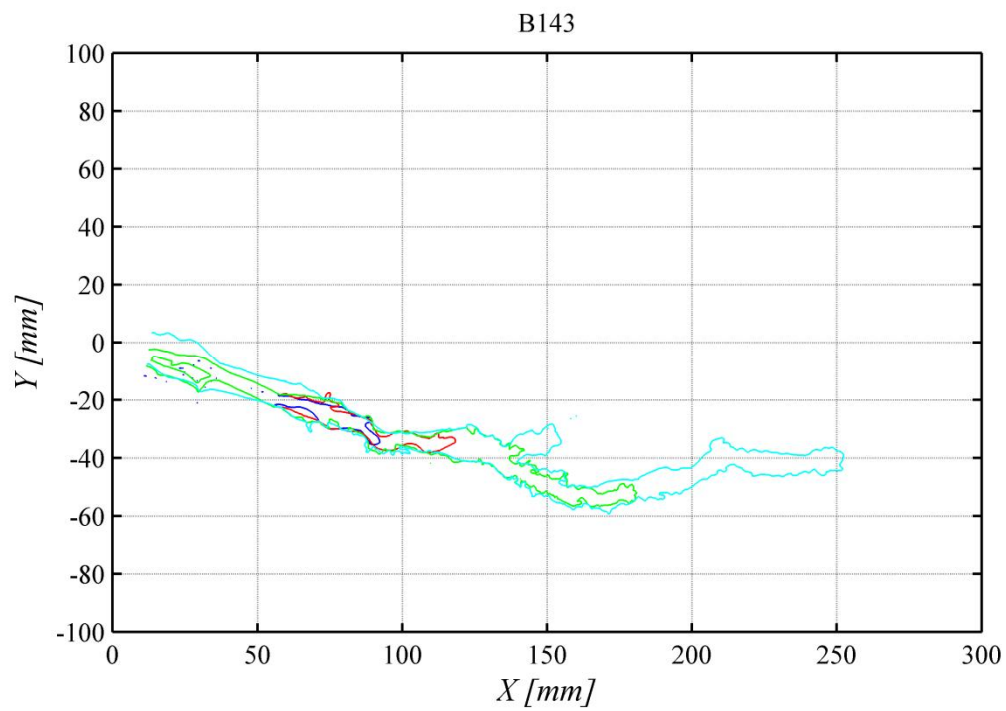


Figure D.8. Pipe contours in experiment B143

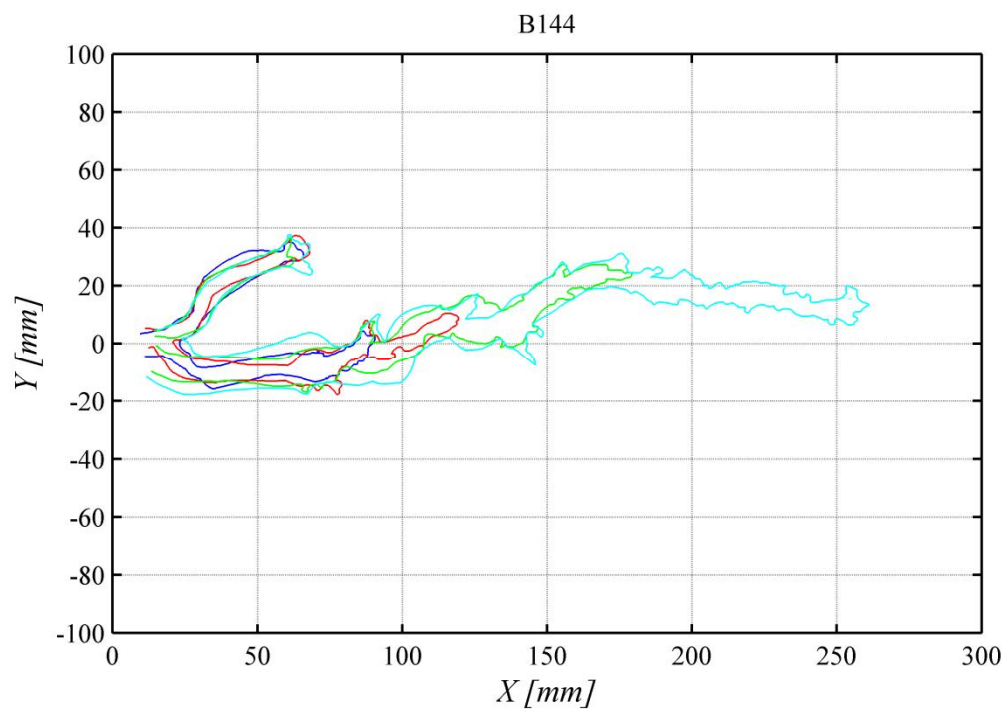


Figure D.9. Pipe contours in experiment B144

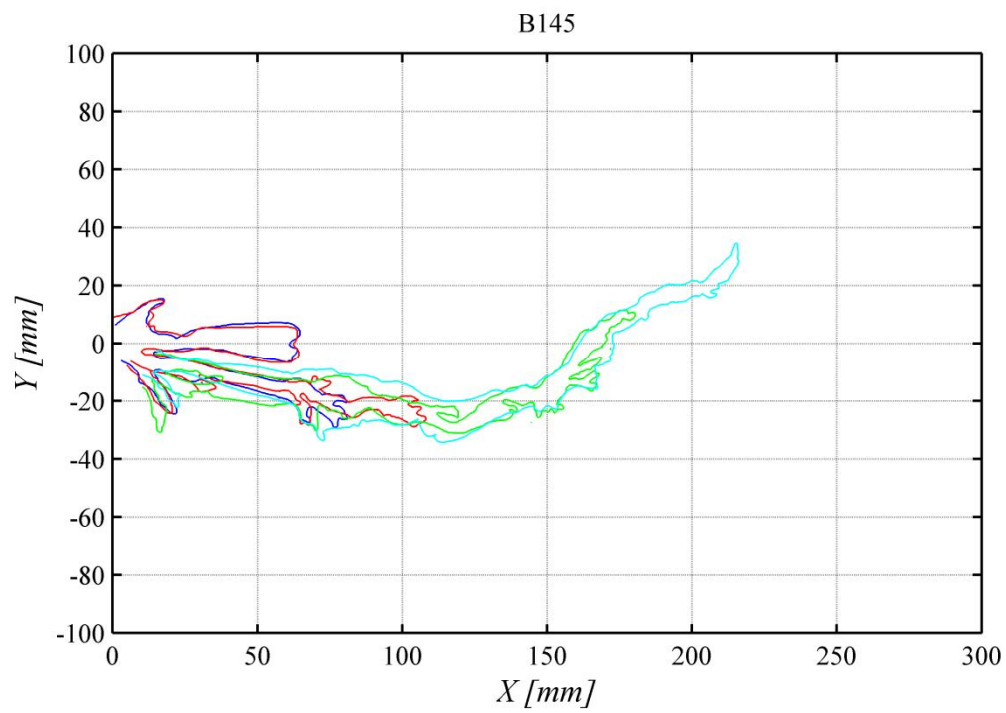


Figure D.10. Pipe contours in experiment B145

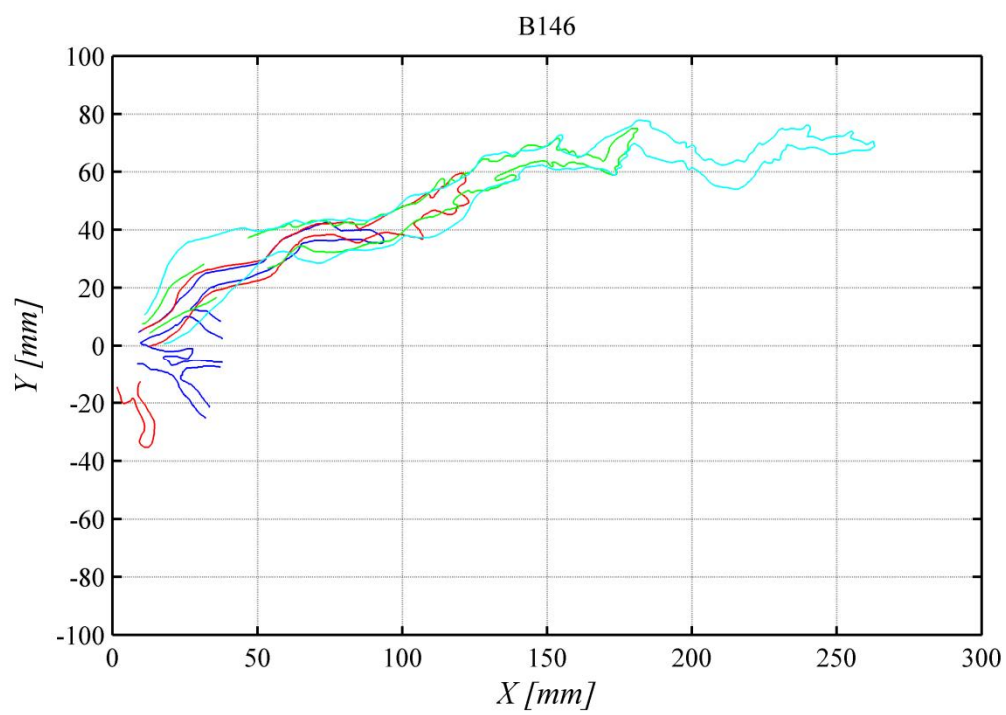


Figure D.11. Pipe contours in experiment B146

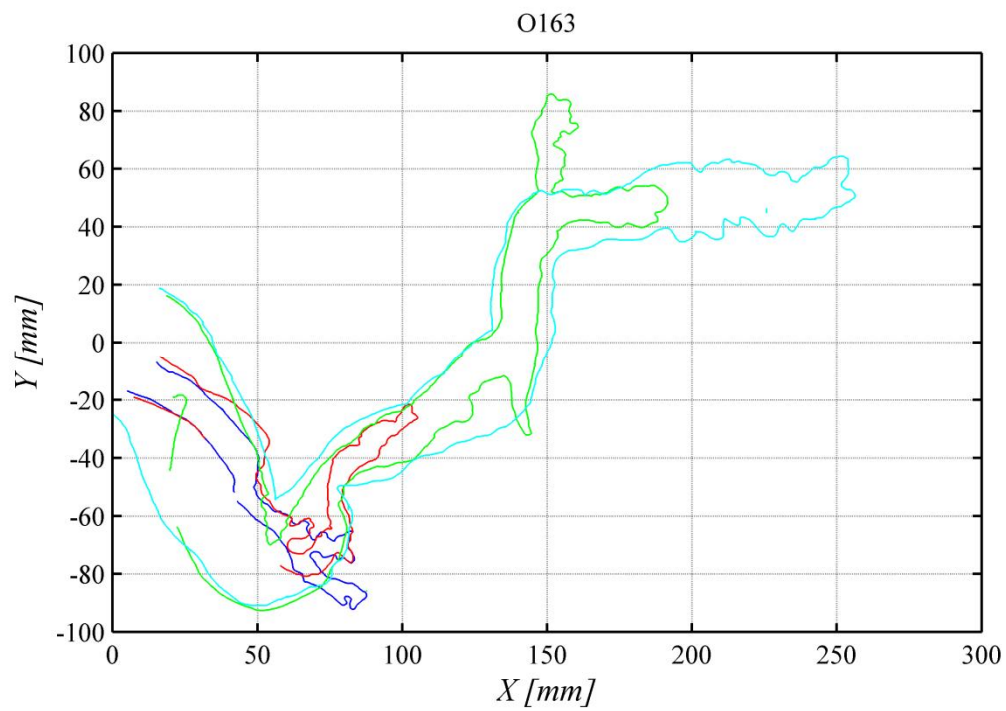


Figure D.12. Pipe contours in experiment O163

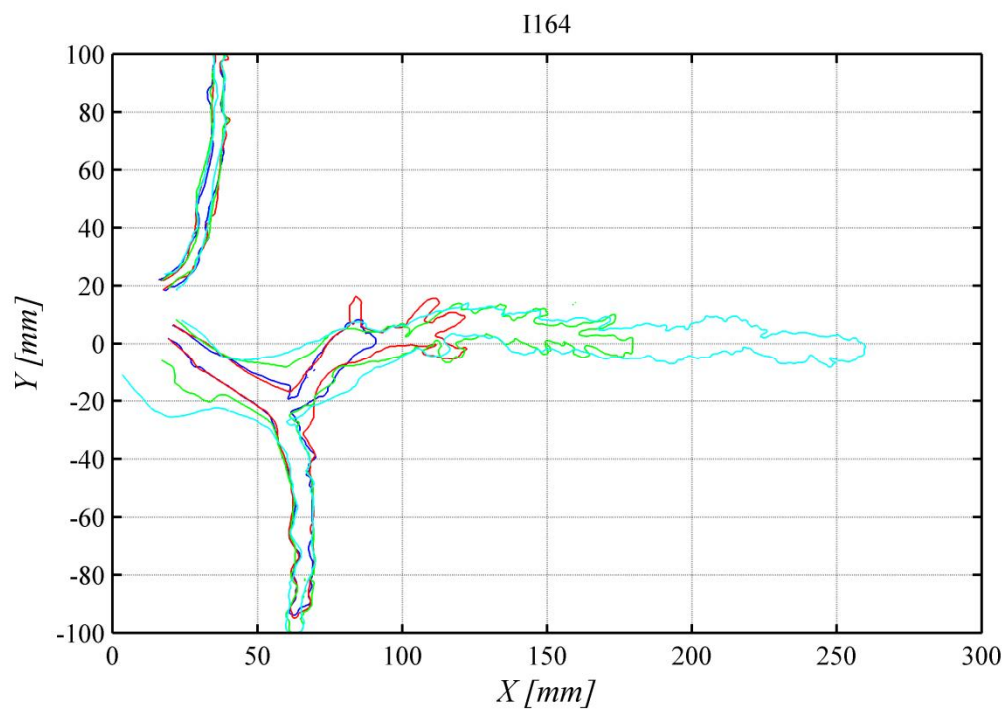


Figure D.13. Pipe contours in experiment I164

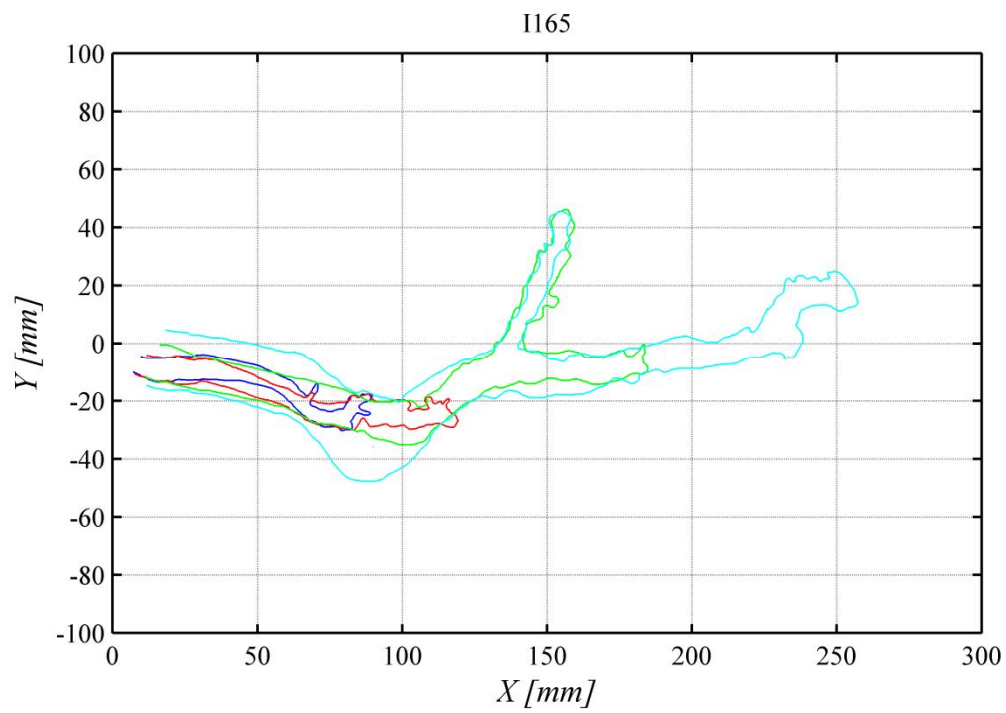


Figure D.14. Pipe contours in experiment I165

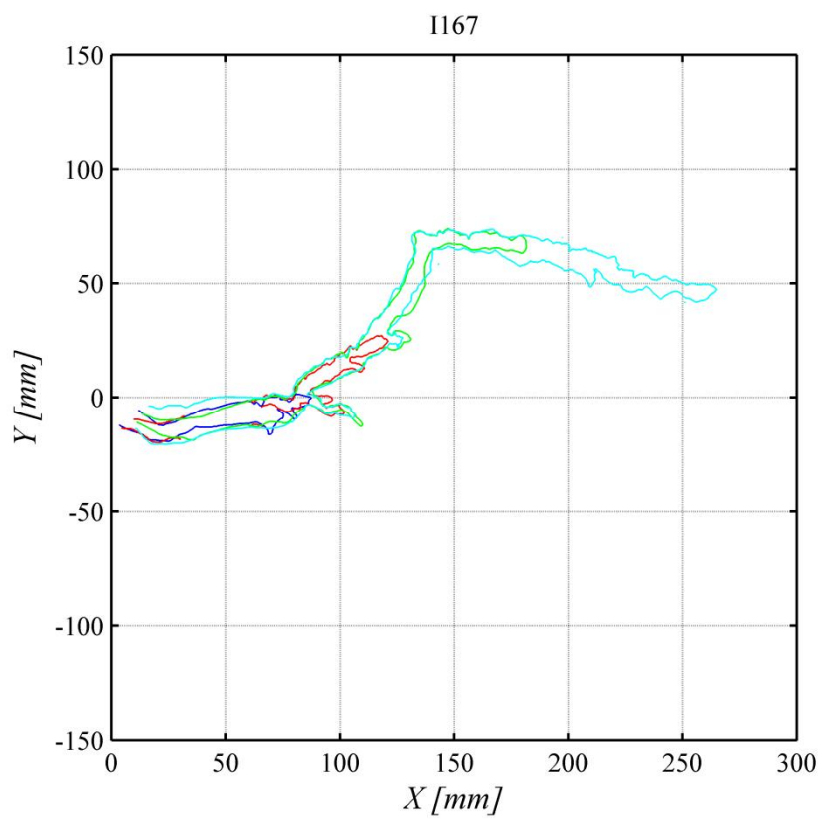


Figure D.15. Pipe contours in experiment I167

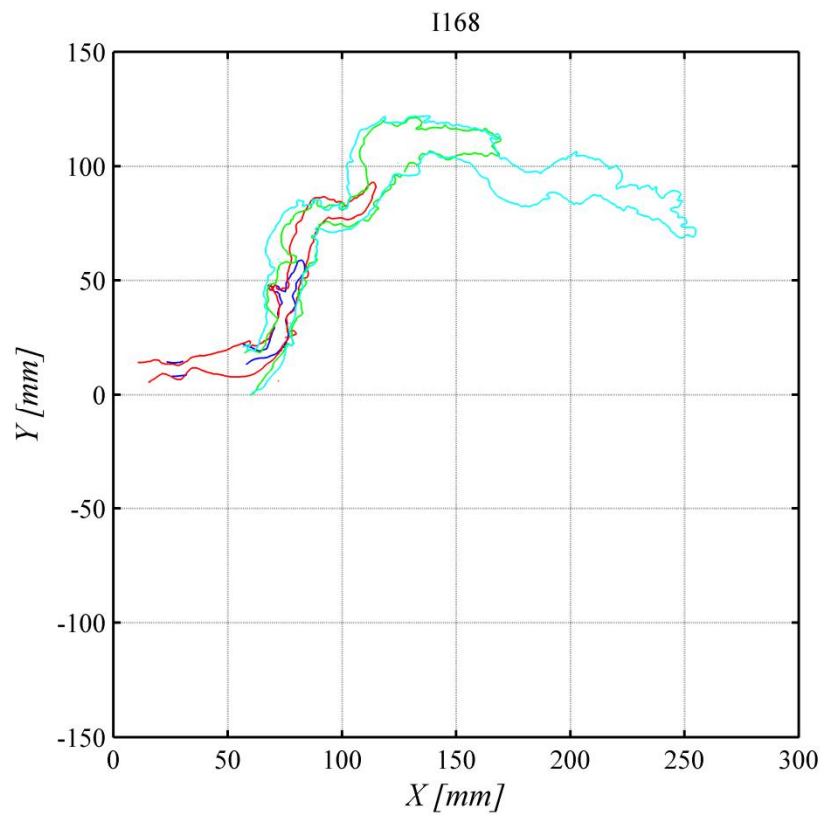


Figure D.16. Pipe contours in experiment I168

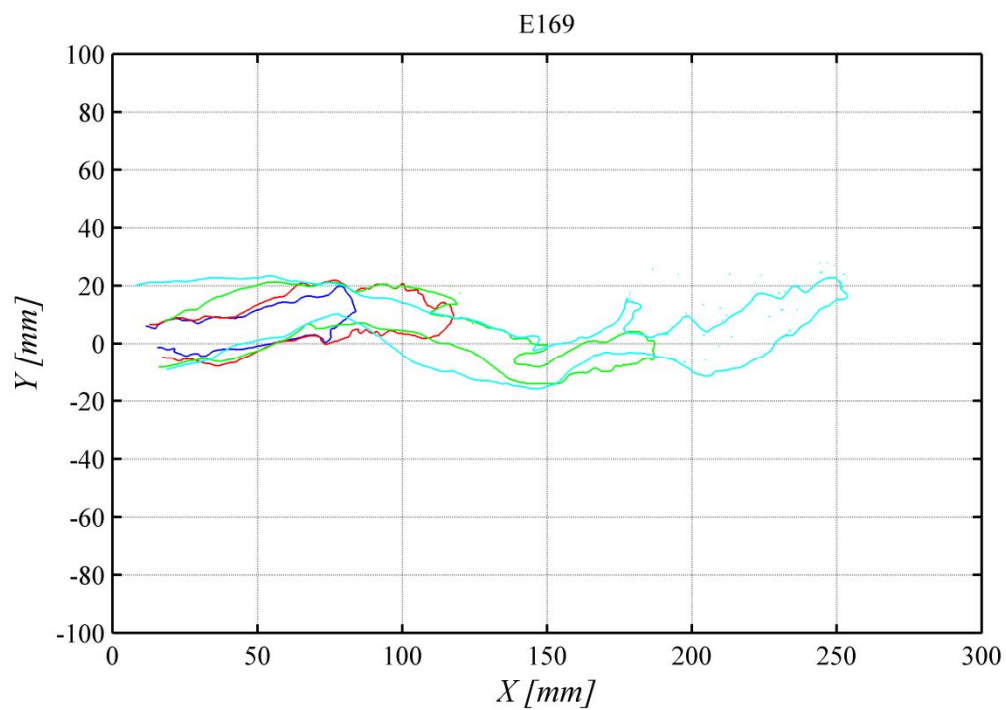


Figure D.17. Pipe contours in experiment E169

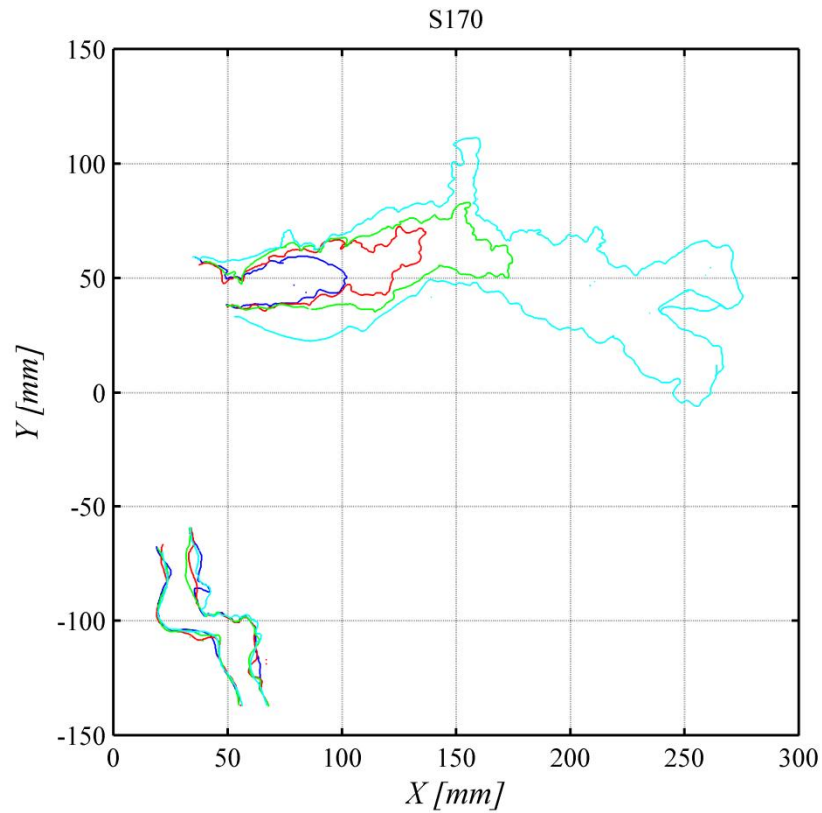


Figure D.18. Pipe contours in experiment S170

D.2. MEDIUM-SCALE EXPERIMENTS

The approach adopted for drawing pipe contours in the medium-scale experiments was similar to the approach adopted for the small-scale experiments. In the medium-scale experiments, the steel frame and the deposited sand near the exit made it impossible to produce a complete drawing.

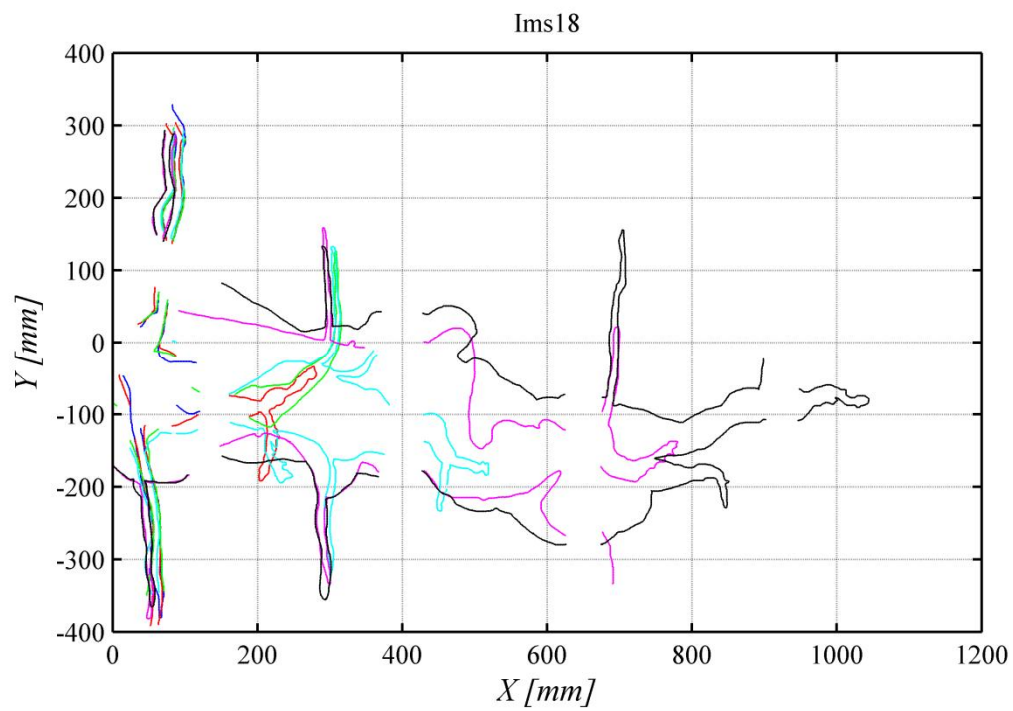


Figure D.19. Pipe contours in experiment Ims18

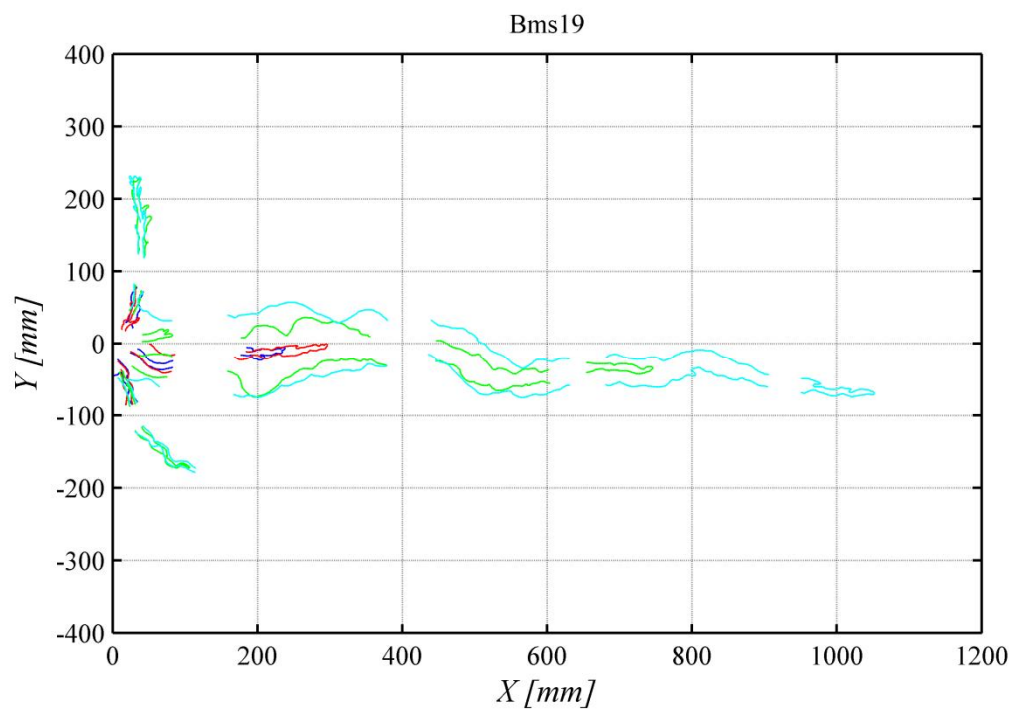


Figure D.20. Pipe contours in experiment Bms19

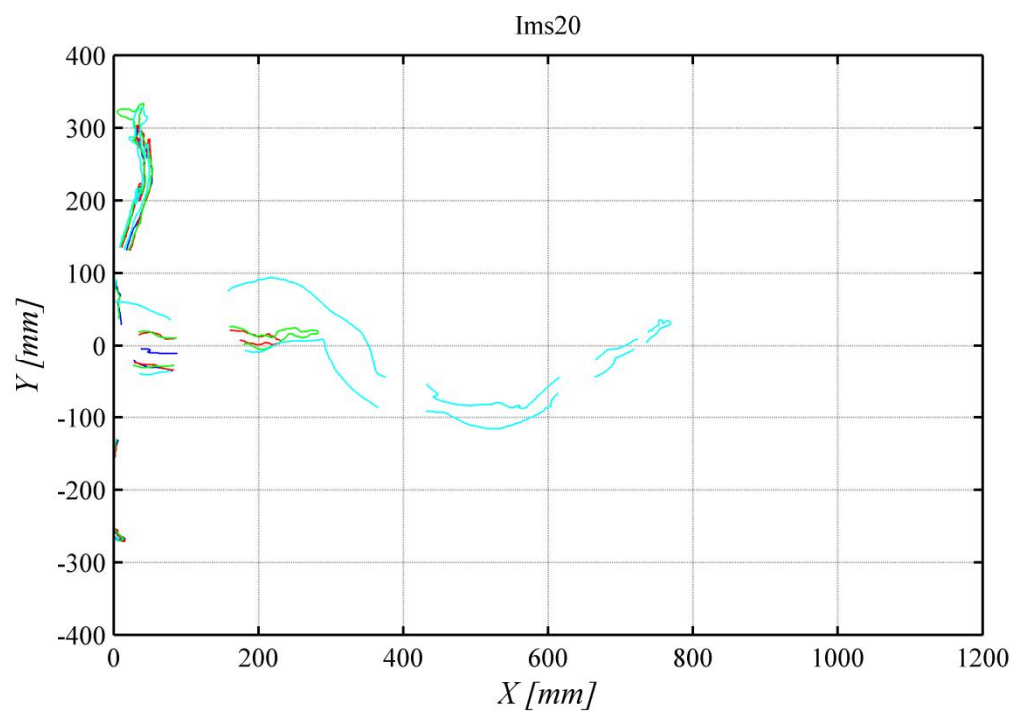


Figure D.21. Pipe contours in experiment Ims20

LIST OF SYMBOLS

a	size of the group of particles to be heaved expressed as number of particles / pipe depth / a constant related to the electrical resistance of the soil
A	cross-sectional surface or area
b	a constant related to the electrical resistance of the soil
B	degree of pipe broadening
C	coefficient of percolation in Bligh's rule
dx	absolute size of the group of particles to be heaved
d_x	grain diameter for which $x\%$ of the sample (by weight) is finer
d	penetration depth of cut-off wall
D	sand sample thickness / pipe diameter
D_h	hydraulic diameter pipe
D^*	dimensionless particle number
f_F	friction factor
F_d	drag force
F_g	gravity force
F_s	seepage force
F_f	friction force
F_N	normal force
F_G	geometrical shape factor
F_R	resistance factor
F_S	scale factor
g	gravitational acceleration
h	sand sample thickness / hydraulic head
H	head drop across the sand sample or embankment
H_c	critical head drop across the sand sample or embankment at which ongoing erosion occurs
H_i	minimum head drop across the sand sample or embankment at which the pipe is initiated

H_p	minimum head drop across the sand sample or embankment at which the pipe progresses, assuming the presence of a short pipe
H_b	minimum head drop across the sand sample or embankment at which sand boiling occurs
i	vertical exit gradient
i_c	critical heave gradient
k	permeability coefficient
K	complete elliptic integral over m
KAS	roundness of particles
l	pipe length
m	$\tanh^2(\pi / 2 \cdot L / D)$
L	length of seepage
n	porosity / number of particles
p	pressure
P	wetted perimeter
Q	(groundwater or pipe) flow
R	electrical resistance of the soil
Re	Reynolds number
Re^*	particle or grain Reynolds number
RD	relative density
s	width of the ditch
t	thickness geotextile
u^*	shear velocity
U	uniformity coefficient (d_{60}/d_{10})
v	exit or pipe velocity
\bar{v}	average pipe velocity
w	complex velocity / pipe width
W	sand sample width
x	x-coordinate
y	y-coordinate
z	complex coordinate
α	experimental coefficient in particle equilibrium by White / slope of the pipe
β	slope angle / empirical factor accounting for the shape of a rectangular duct
β_c	angle of repose

Δ	γ'_p / γ_w
ε	pipe roughness
γ_p	unit weight of particles
γ'_p	submerged unit weight of particles
γ_w	unit weight of water
η	White's constant
θ	bedding angle of sand
κ	intrinsic permeability
λ	scaling parameter
μ	dynamic viscosity / friction coefficient
ρ_g	specific electrical resistance of the soil
ρ_s	particle density
ρ_w	water density / specific electrical resistance of the pore water
τ	shear stress
τ_w	wall shear stress
φ	groundwater head
ϕ	friction angle
Φ	groundwater potential
ψ	permittivity
Ψ	stream function / Shields parameter
Ω	complex potential
\emptyset	exit hole diameter

subscripts

c	critical
$calc$	calculated
e	entrance
i	initiation
p	progression
m	mean value from selected small-scale experiments
max	maximum
exp	experimental
w	wall / water
rd	rectangular duct

pp parallel plates

LIST OF FIGURES

Figure 1.1 Overview of failure mechanisms (adapted after Ministerie van Verkeer en Waterstaat, 2007).....	2
Figure 1.2 Backward erosion leading to dike failure and breach.....	3
Figure 2.1. Different inlet types (vertical filter (<i>I</i>) and horizontal inlet (<i>II</i>)) and exit types (plane- (A), ditch- (B), hole- (C) and slope-type (D) exit); the slope- and hole-type exits can have either a filter or closed boundary at the downstream end.....	14
Figure 2.2. Three exit types: plane (a), ditch (b) and hole (c).....	15
Figure 2.3. Example of an embedded structure in combination with cut-offs (set-up used by Achmus and Mansour, 2006).....	15
Figure 2.4. Schematic of the set-up used at the University of Berlin.....	16
Figure 2.5. Effect of exit diameter on piping process (based on figure in Miesel (1978)).....	17
Figure 2.6. Schematic of UF flume (Schmertmann, 2000).....	19
Figure 2.7. Initiation and critical heads from the experiments by Pietrus (1981) using dowels with different penetration lengths and radii.....	20
Figure 2.8. Plane-type exit models Model I and II (De Wit, 1984).....	21
Figure 2.9. Critical gradients as a function of relative density for models I and II (plane-type exit).....	22
Figure 2.10. Critical gradients as a function of grain size for models I and II (plane-type exit).....	23
Figure 2.11. Schematic of the large-scale experiments (Silvis, 1991).....	23
Figure 2.12. Final pipe pattern in experiment T3 ($L=12$ m) registered at different head drops.....	24
Figure 2.13. Small-, medium- and full-scale experiments.....	25
Figure 2.14. Schematic for small- and medium-scale experiments.....	25
Figure 2.15. Schematic of full-scale experiments at the IJkdijk location.....	26
Figure 2.16. Pipe formation in laterally heterogeneous sands (fine downstream, coarse upstream).....	26
Figure 2.17. Pipe formation in laterally heterogeneous sands (fine sand with a band of coarse sand).....	26

Figure 2.18. Forward erosion as observed in one of the small-scale experiments (B30)	28
Figure 2.19. 'Mud fountain' after the completion of the widening phase in one of the large-scale experiments at the IJkdijk location	29
Figure 2.20. Observations from the 1950 flood in relation to the upward gradient through the confining layer at fifteen instrumented sites along the Lower Mississippi River (modified after USACE, 1956).....	33
Figure 2.21. Head distribution for models I and II	34
Figure 2.22. Pipe discretisation showing the calculated distribution of flux (Hanses, 1985).....	35
Figure 2.23. Potentials around the tip of the pipe for tests 21-25 with different pipe lengths (Hanses, 1985)	36
Figure 2.24. Comparison of real and simulated head distributions around the pipe and corresponding exit velocities in a cross-section of the pipe (b =pipe width) (Hanses, 1985).....	36
Figure 2.25. Dividing the sand layer into fragments (TAW, 1999).....	41
Figure 2.26. Simulation of particles under a dike at different water levels (El Shamy and Aydin, 2008).....	42
Figure 3.1. Saturated fields during the flood of 1993 in the Betuwe polder district; picture taken from a river dike (www.beeldbank.rws.nl , Rijkswaterstaat)	46
Figure 3.2. Sand boil, (left) without sand deposition, (right) with continuous sand deposition.....	47
Figure 3.3. Sand boil during high water period of 2011 (Herwijnen, Netherlands)	47
Figure 3.4. Failed dike in full-scale experiment (scenario 1)	49
Figure 3.5. Small holes observed in a full-scale experiment (Van Beek et al., 2011).....	50
Figure 3.6. Pipe development (pipe length) and applied head in test T3 with a total seepage length of 12 m (Silvis, 1991)	52
Figure 3.7. Photo of the tip of the pipe (a) and drawing showing pipe development over time in one of the tests (b) (modified after Hanses, 1985).....	53
Figure 3.8. Qualitative interpretation of expected scale effects for pipe initiation and progression in an arbitrary case	55
Figure 3.9. Relationship between the type of process, type of exit and seepage length ..	56
Figure 4.1. Schematic presentation of experimental work.....	58
Figure 4.2. Schematics showing experimental set-ups with slope-type (top), area-type (middle) and hole-type (bottom) exits.....	60
Figure 4.3. Schematisation of the water flow through the total set-up	61
Figure 4.4. Set-up with prepared sand bed area.....	62
Figure 4.5. Grain size distributions of the sands used in the experiments.....	63
Figure 4.6. Example of sand crater and sand in transport.....	65

Figure 4.7. Examples of pipe formation in two small-scale experiments (left: B118, right: I167), and in one of the medium-scale experiments (Bms19)	66
Figure 4.8. Applied head difference in time and as a function of pipe length	67
Figure 4.9. Measured flow as a function of time and measured flow normalised by the applied head as a function of pipe length (B133)	67
Figure 4.10. Permeability calculated using riser tubes h1 and h3 as a function of time and pipe length (B133)	68
Figure 4.11. Colour injected to indicate preferential paths (photos from experiments presented in Van Beek et al., 2009)	69
Figure 4.12. Pattern observed in Hele-Shaw cell for a grain fraction of 54% (Chevalier et al., 2009).....	70
Figure 4.13 Measurement of electrical resistance using eleven rows of 4 needles and measurement of total stress using two stress sensors TS1 and TS2	71
Figure 4.14. Column experiment to investigate the relationship between porosity and electrical resistance. The figure shows the locations of the copper needles.....	73
Figure 4.15. Relationship between calculated electrical density and porosity in column experiment for locations 1, 2 and 3	73
Figure 4.16. Effective stresses derived from stress sensors in test B101. The effective stress drops to 0 kPa when the pipe passes the stress sensors.	75
Figure 4.17. Total pressure development in time as a result of the compression of the strip between the cover and the sand box (the degree of compression is indicated as the distance in mm between the cover and the sand box)	76
Figure 4.18. Porosity derived from electrical resistance measurements in the cover of the set-up in test B122 (location A4-A8) at different steps of the compression of the strip between cover and sand box (legend indicates the distance in mm between the cover and the sand box).....	77
Figure 4.19. Pipes on the upstream side of the set-up, before (left) and after loading (right)	79
Figure 4.20. Equilibrium head as a function of normalised pipe length (pipe length divided by seepage length) for experiment B105 (slope-type experiment) and B118 (hole-type experiment).....	82
Figure 4.21. Pipe formation in experiment E137 (pipe contour drawn manually).....	84
Figure 4.22. Pipe and crater development in small-scale experiments W131 with Waalre sand (left; $d_{50}=0.341$ mm) and experiment B142 with Baskarp sand (right; $d_{50}=0.132$ mm). The pipe length was approximately half the seepage length in both experiments.	85
Figure 4.23. Influence of exit-hole diameter and relative density on critical gradient.....	86
Figure 4.24. Influence of grain size in uniform sand types (left) and uniformity coefficient (right) on critical gradients for medium-dense and dense samples.....	87
Figure 4.25. Pipe geometry in experiment I167.....	88

Figure 4.26. Cross-sections of the pipe at various distances from the upstream filter showing pipe width and depth.....	89
Figure 4.27. Pipe and crater formation in experiment Ims20 with Itterbeck 330 μm sand (left) and experiment Bms19 with Baskarp sand (right).....	91
Figure 4.28. Photographs showing the pipe patterns in a section of the medium-scale set-up: the pipe develops parallel to the direction of the stratification in experiment Ims18 (left); there is no preferential pipe path in experiment Ims20 (right). The flow is in the direction of the arrows.	92
Figure 4.29. Pipe formation in relation to pore pressure transducers in experiment Ims20 at pipe lengths of 0.647 m (left, downstream transducers) and 1.197 m (right, upstream transducers).	93
Figure 4.30. Normalised hydraulic head along the sand bed for different equilibrium pipe lengths in experiments Bms19 (left) and Ims20 (right).	94
Figure 4.31. Average pipe gradient as a function of normalised pipe length in experiments Bms19 and Ims20	94
Figure 4.32. 2D-set up (Van der Zee, 2011).....	95
Figure 4.33. Visualisation set-up.....	96
Figure 4.34. Pipe section at -2 to 4 cm from the exit hole when the pipe length was 60 mm (top photo, taken 135.5 minutes into the test, head drop 9 cm) and 97 mm (bottom photo, taken 200.67 minutes into the test, head drop 10 cm).....	98
Figure 4.35. Pipe section at 3 to 8 cm from the exit hole when the pipe length was 250 mm (top photo, taken 373.45 minutes into the test, head drop 8 cm) and 280 mm (bottom photo, taken 375.58 minutes into the test, head drop 8 cm)	98
Figure 4.36. Downstream part of developed pipe viewed from above 373.45 minutes into the test.....	99
Figure 4.37. Normalised head distribution for different pipe lengths.....	100
Figure 4.38. Laser data experiment B171	103
Figure 4.39. Laser data experiment E172	103
Figure 4.40. Maximum depth as a function of location in the pipe in the two experiments	104
Figure 4.41. Example of a pipe cross-section.....	105
Figure 4.42. Pipe width as a function of location in the pipe in the two experiments ...	105
Figure 4.43. Pipe formation in experiment B171 (after test and removal of acrylate plate)	106
Figure 4.44. Grain size distribution obtained with laser diffractometry.....	106
Figure 5.1. Effect of configuration on initiation gradient (experiments De Wit (1984))	112
Figure 5.2. Initiation heads for artificial pipes with varying diameters and penetration lengths.....	113
Figure 5.3. Effect of scale in experiments with a constant D/L ratio.....	114

Figure 5.4. Effect of seepage length on initiation gradient (Beach sand, $D=1.5$ m)	115
Figure 5.5. Effect of grain size on initiation gradient determined in slope-type experiments and plane-type experiments.....	116
Figure 5.6. Effect of porosity on initiation gradient	116
Figure 5.7. Conformal mapping schemes for a ditch (top) and a slope (bottom).....	121
Figure 5.8. Flow net and corresponding numerically obtained exit gradients and analytical fit for experiment B19	122
Figure 5.9. Conceptual model to determine the group size.....	123
Figure 5.10. Calculated heave group size as function of seepage length and grain size (experiments by De Wit (1984) and additional small-scale experiments on Enschede sand)	124
Figure 5.11. Effect of porosity on critical gradient and calculated heave group size for the experiments with Dune sand and Beach sand	125
Figure 5.12. Calculated heave group size as function of porosity for Beach sand experiments with a ditch-type exit	127
Figure 5.13. Observed slope angles as a function of porosity in small-scale Baskarp experiments.....	129
Figure 5.14. Calculated group sizes for small- and medium-scale slope-type experiments	130
Figure 5.15. Illustration of the scale effects of the initiation gradient for plane- and ditch-type configurations, and their least square fits.	133
Figure 5.16. Experimentally obtained and calculated critical gradients	133
Figure 6.1. Illustration of the four components relevant for modelling pipe progression	136
Figure 6.2. Effect of grain size on critical gradient, and the relationship between permeability and grain size (uniform sands only)	138
Figure 6.3. Effect of scale on critical gradient (D/L constant).....	140
Figure 6.4. Experimental and calculated critical gradients for Delta Flume and IJkdijk experiments (the black and grey lines indicate no deviation (1:1) and a factor-two deviation (1:2, 2:1) respectively).....	143
Figure 6.5. Calculated critical gradients for different exit-hole diameters comparing the outcome of the 2D numerical calculation and the calculation rule (using experiment B115 as an example)	144
Figure 6.6. Experimental and calculated critical gradients for all available 3D experiments (the black and grey lines indicate no deviation (1:1) and deviation by a factor 2 (1:2, 2:1) respectively).	145
Figure 6.7. Experimental and calculated critical gradients for small- and medium-scale experiments investigating sand type and relative density (black and grey lines indicate no deviation (1:1) and factor of 2 deviation (1:2, 2:1) respectively; MD: medium density, HD: high density).	146

Figure 6.8. Example of meandering and preferential paths in experiment Bms19.....	148
Figure 6.9. Example of pipe contours for different pipe lengths and width measurements at tip, mid-point and tail (experiment O140).....	149
Figure 6.10. Tip width as a function of relative pipe length (measured at 0.25, 0.50 and 0.75) for all small-scale experiments.....	149
Figure 6.11. Average tip width as function of grain size: data points from experiments (the encircled data points are described in the text) and line showing the width of 30 times the mean grain size.....	150
Figure 6.12. Pipe contours in a small-scale (B142) and a medium-scale (Bms19) experiment.....	151
Figure 6.13. Ratio of tail width to tip width as function of distance between the tail and tip.....	152
Figure 6.14. Average degree of widening as a function of grain size.....	153
Figure 6.15. Examples of cross-sections in experiment B171 and E172 and a sine-shaped approximation of the pipe (top: true representation of pipe cross-section and bottom: scaled pipe cross-section).....	155
Figure 6.16. Width-to-depth ratios as a function of location in the pipe measured from the exit hole.....	156
Figure 6.17. Pipe gradient as a function of (left) normalised pipe length (l/L) and (right) measured flow.....	158
Figure 6.18. Relative pipe gradient as function of (left) normalised pipe length (l/L) and (right) measured flow.....	158
Figure 6.19. Particle tracking for different grains in the section 3–8 cm from the exit hole.....	160
Figure 6.20. Velocity distribution for tracked particles in the section 3–8 cm from the exit hole (velocities in cm/s).....	161
Figure 6.21. Pipe shapes: schematised erosion pipe, circular pipe, rectangular duct and infinitely wide pipe.....	163
Figure 6.22. Ratio of flow and shear stress in a rectangular duct with respect to flow and shear stress between parallel plates, at different a/w ratios, showing the effect of width on the flow and shear stress.....	165
Figure 6.23. Actual and critical Reynolds numbers for different pipe depths.....	167
Figure 6.24. Development of the pipe tip near the pressure gauges, with the pressure gauges located in the origin of the graph (left-hand graph) and measured pipe development in time (right-hand graph), with markers indicating observations from photographs and the line the least square fit of time and location.....	170
Figure 6.25. Calculated gradients as a function of distance between pipe tip and pressure gauge in experiment Bms19.....	172
Figure 6.26. Calculated gradients as a function of the distance between pipe tip and pressure gauge in experiment lms20.....	173

Figure 6.27. Drag and lift forces acting on particles resting on the bed surface (Chien and Wan, 1999).....	174
Figure 6.28. Condition for incipient motion for non-cohesive sediment (Shields curve and its modification) (Chien and Wan, 1999).....	177
Figure 6.29. Shields parameter as a function of the particle Reynolds number showing experimental results for laminar flow, various fits and theoretical relations	179
Figure 6.30. Shields parameter as a function of the dimensionless particle number showing experimental results for laminar flow. The second horizontal axis also shows the equivalent particle size in mm using a viscosity of $\nu=1.0\text{E}-6 \text{ m}^2/\text{s}$	180
Figure 6.31. Critical shear stress (left-hand graph) and bedding angle (right-hand graph) plotted for various particle diameters (legend displayed in figure 6.26)	181
Figure 6.32. Comparison of critical shear stresses calculated with the three different models for various particle diameters	183
Figure 6.33. Equilibrium of forces on a particle on a slope subjected to a water flow perpendicular to the slope (left-hand figure: cross-section of slope; right-hand figure: forces in the plane of the slope).....	184
Figure 6.34. Difference between experimental and critical gradients for all hole-type experiments.....	192
Figure 6.35. Difference between experimental and critical gradients in the 2D experiments.....	193
Figure 6.36 Contour plot of the ratio of the Reynolds number based on the calibrated White criterion to the critical Reynolds number. Contour line '1' outlines the area where the flow in the pipe is laminar.	195
Figure 6.37 Contour plot of the ratio of the Reynolds number based on the limit-state equilibrium used in the original Sellmeijer model to the critical Reynolds number. The contour line '1' outlines the area where the flow in the pipe is laminar.	196
Figure 6.38. Configuration, mesh and potential distribution along the central axis of symmetrical 3D numerical simulations of the medium-scale experiments (Van Beek et al., 2014b). Pipes have been simulated by adding a permeable zone in the centre of the sand sample at 1.06 to 1.385 m from the upstream boundary. The permeability in the pipes differs for the blue line and the red line, which represent, respectively, a pipe with a smaller impact, as would be the case in a fine sand, and a pipe with a large impact, as would be the case in a coarse sand.	199

LIST OF TABLES

Table 2.1 Overview of research on backward erosion piping (horizontal piping path) ..	12
Table 2.2. Overview of experiments containing a separate engineering structure or a partly vertical seepage path	13
Table 4.1. Sand characteristics	63
Table 4.2. Experimental programme.....	71
Table 4.3. Test characteristics in first part (Experiments B101, B103 and B104)	74
Table 4.4. Test characteristics in second part (experiments B121 and B122)	76
Table 4.5. Test characteristics for test B123, first phase.....	78
Table 4.6. Test characteristics for test B123, second phase.....	79
Table 4.7. Critical pipe gradients at different pipe lengths	100
Table 4.8. Comparison of similar experiments.....	102
Table 5.1. Effect of seepage length on initiation gradient expressed as the power of L	114
Table 5.2. Slope-type experiments (Van Beek et al., 2011, improved filter correction) and scaling parameter λ	128
Table 5.3. Equations for prediction of initiation gradient for plane- and ditch-type configurations.....	131
Table 6.1. Effect of the seepage length on critical gradient, expressed as the power of L	140
Table 6.2. Standard deviation for the different sand types, calculated relative to the 1:2 line.....	146
Table 6.3. Overview of pipe depths.....	154
Table 6.4. Average pipe gradients ($d\phi/dx$) and measured flow (Q_{exp}) for equilibrium conditions in various experiments.....	157
Table 6.5. Pipe flow and wall shear stress.....	164
Table 6.6. Critical Reynolds numbers for flow through circular tubes and flow through parallel plates	166
Table 6.7. Overview of incipient motion for particles in laminar flow	178
Table 6.8. Three methods for determining the critical shear stress	182
Table 6.9. Equations for laminar flow in rectangular ducts where $w \gg a$	188

Table 6.10. Criteria for laminar flow	188
Table 6.11. Criterion for limit-state bed stability.....	188
Table 6.12. Overview of calculated pipe depths based on critical shear stress and pipe gradient, and comparison with experimental depth measurements in similar experiments.....	189
Table 6.13. Comparison of experimental and theoretical width-to-depth ratios.....	191

LIST OF PUBLICATIONS

The following publications are related to the subject of this dissertation:

PUBLICATIONS IN PEER-REVIEWED JOURNALS / BOOK CHAPTERS

- Van Beek, V.M., Van Essen, H.M., Vandenboer, K., Bezuijen, A. (2015). Developments in modelling of backward erosion piping. *Géotechnique* 65(9): 740-754.
- Van Beek, V.M., Bezuijen A., Sellmeijer, J.B., Barends F.B.J. (2014). Initiation of backward erosion piping in uniform sands, *Géotechnique* 64(12): 927-941.
- Vandenboer, K., Van Beek, V., Bezuijen, A. (2014). 3D finite element method (FEM) simulation of groundwater flow during backward erosion piping. *Front. Struct. Civ. Eng.* 8(2): 160 – 166.
- Van Beek, V., Bezuijen, A., Sellmeijer, H. (2013). Backward Erosion Piping. In *Erosion in Geomechanics Applied to Dams and Levees* (Bonelli, S. (ed)), ISTE, London, UK, Wiley, Hoboken, USA, pp. 193-269.
- Sellmeijer J.B., Lopéz de la Cruz J., Van Beek V.M., Knoeff J.G. (2011). Fine-tuning of the piping model through small-scale, medium-scale and IJkdijk experiments. *European Journal of Environmental and Civil Engineering* 15(8): 1139-1154.
- Van Beek, V.M., Knoeff, J.G., Sellmeijer, J.B. (2011). Observations on the process of backward piping by underseepage in cohesionless soils in small-, medium- and full-scale experiments. *European Journal of Environmental and Civil Engineering* 15(8): 1115-1137.

CONFERENCE PAPERS

- Koelewijn, A.R., De Vries, G., Van Lottum, H., Förster, U., Van Beek, V.M., Bezuijen, A. (2014). Full scale testing of piping prevention measures: three tests at the IJkdijk. In Gaudin and White (Eds), *Physical modeling in Geotechnics* (pp. 891-897). London: Taylor & Francis Group.
- Van Beek, V.M., Vandenboer K., Bezuijen, A. (2014). Investigation of the backward erosion mechanism in small scale Experiments. *Physical Modelling in Geotechnics* (Gaudin & White (Eds)), 855-861, Taylor & Francis Group, London.
- Van Beek, V.M., Vandenboer, K., Bezuijen, A. (2014). Influence of sand type on pipe development in small- and medium-scale experiments. In Cheng, Draper and An (Eds), *Scour and Erosion* (pp. 111-120). London: Taylor & Francis Group.
- Vandenboer, K., Bezuijen, A., Van Beek, V.M. (2014). 3D character of backward erosion piping: Small-scale experiments. In Cheng, Draper & An (Eds), *Scour and Erosion* (pp. 81-86). London: Taylor & Francis Group.

- Vandenboer, K., Bezuijen, A., Van Beek, V.M. (2014). 3D character of backward erosion piping: Small-scale experiments. In L Cheng, S Draper & H An (Eds.), *Scour and Erosion* (pp. 81-86). London: Taylor & Francis Group.
- Van Beek, V.M., Yao, Q.L., Van, M.A. (2013). Backward erosion piping model verification using cases in China and the Netherlands, *Proceedings of the 7th int. conference on Case Histories in Geotechnical Engineering* (pp. 1-7).
- Vandenboer, K., Van Beek, V., Bezuijen, A. (2013). 3D FEM Simulation of groundwater flow during backward erosion piping. In YJ Cui, F Emeriault, F Cuira, S Ghabezloo, JM Pereira, M Reboul, H Ravel & AM Tang (Eds.), *Advances in Soil Mechanics and Geotechnical Engineering, Volume 2" Proceedings of the 5th International Young Geotechnical Engineers' Conference* (pp. 301-304), IOS Press.
- Yao, Q., Van Beek, V., Van, M., Ding, L. (2013). Backward Piping in Multi-layer Dike Foundations: Experiments. In W Zhaoyin, J Hun-Wei Lee, G Jizhang & C Shuyou (Eds.), *Proceedings of the 35th IAHR World Congress* (pp. 10650-10659). Tsinghua University Press, Beijing
- Bezuijen, A., Van Beek, V.M., Van den Ham, G.A., Zwanenburg, C. (2012). Overview geotechnical model tests on dike safety at Deltares. In Bezuijen, Lottum and Dijkstra (Eds.), *European conference on physical modelling in geotechnics Eurofuge* (pp. 1-10).
- Van Beek, V.M., Bezuijen A., Schenkeveld F.M. (2012). Piping in loose sands – the importance of geometrical fixation of grains. In *European conference on physical modelling in geotechnics Eurofuge* (Bezuijen, Lottum and Dijkstra (Eds.)), p. 1-10.
- Van Beek V., Yao, Q., Van M., Barends F. (2012). Validation of Sellmeijer's model for backward piping under dikes on multiple sand layers. *Proceedings of the 6th International Conference on Scour and Erosion*, (pp. 543-550).
- Van Beek, V.M., Rietdijk, J., Luijendijk, M.S., Barends, F.B.J. (2011). Influence of vertical loading on underseepage piping in uniform sand. In *Internal erosion in embankment dams and their foundations*, proceedings of the institute of water structures, FCE, BUT, Brno - Fry, Riha, Julinek (eds.), vol. 13, pp. 233-234.
- Van Beek, V.M., Knoeff, J.G., Rietdijk, J., Sellmeijer, J.B., Lopez De La Cruz, J. (2010). Influence of sand characteristics and scale on the piping process – experiments and multivariate analysis. In *Physical Modelling in Geotechnics* – Springman, Laue and Sowards (eds), Taylor and Francis Group, London, pp. 1221-1226.
- Van Beek, V.M., Bezuijen, A., Zwanenburg, C. (2010). Centrifuge experiments on scaling effects and levee stability. In *Physical Modelling in Geotechnics* – Springman, Laue and Sowards (eds), Taylor and Francis Group, London, pp. 183-189.
- Van Beek, V.M., De Bruijn, H.T.J., Knoeff, J.G., Bezuijen, A., Förster, U. (2010). Levee failure due to piping: a full-scale experiment. In *Scour and Erosion: Proceedings of the Fifth International Conference on Scour and Erosion* – Burns, Bhatia, Avila and Hunts (eds), ASCE Geotechnical Special Publication no. 20, pp. 283-292.
- Knoeff, J.G., Van Beek, V.M., Förster, U. (2010). Observations of piping on the IJkdijk testdike in the Netherlands. Annual meeting of European Working Group on Internal Erosion, Granada.
- Van Beek, V.M., Luijendijk, M.S., Knoeff, J.G., Barends, F.B.J. (2009). Influence of relative density on the piping process – small-scale experiments. *Int. Workshop Internal Erosion in Dams and Foundations*, St. Petersburg, April 2009, 8 pp.
- Van Beek, V.M., Knoeff, J.G., De Bruijn, H.T.J. (2009). Influence of sand characteristics on the piping process – small-scale experiments. *Int. Workshop Internal Erosion in Dams and Foundations*, St. Petersburg, April 2009, 8 pp.

- Van Beek, V.M., Koelewijn, A.R., Kruse, G.A.M., Sellmeijer, J.B. (2008). Speculations on the process of piping in laterally heterogeneous sands. 19th European Young Geotechnical Engineers Conference, Győr, Hungary, Széchenyi István Egyetem, eds András Mahler, Péter Scharle, & Róbert Szepesházi, pp. 71-78.
- Van Beek, V.M., Koelewijn, A., Kruse, G., Sellmeijer, H., Barends, F. (2008). Piping phenomena in heterogeneous sands – experiments and simulations, Proceedings of the *4th International Conference on Scour and Erosion*, p. 453-459, <http://scour-and-erosion.baw.de/conferences/icse4/>.

OTHER PUBLICATIONS

- Bezuijen, A., Van Beek, V., Schenkeveld, F. (2012). Doorlatendheid geotextielen in zand. *Geotechniek* 16(2), 58-59.
- Van Beek, Vera, Knoeff, Han, Schweckendiek, Timo (2011). Piping: Over 100 years of experience – From empiricism towards reliability-based design. In *A feeling for soil and water – A tribute to prof. Frans Barends*, Deltares Select Series 07/2011, Deltares, Delft.
- Van Beek, V.M., Koelewijn, A.R., Kruse, G.A.M., Sellmeijer, J.B. (2009). Piping in een heterogeen zandpakket – kijkproeven en simulaties. *Geotechniek* vol. 13 no. 1, pp. 36-38.

CURRICULUM VITAE



Vera van Beek was born on 31 Augustus 1981 in Roelofarendsveen (Alkemade), the Netherlands. She finished her secondary education at the Aquino College in Leiden in 1999 and went to Delft University of Technology in the same year to study Applied Earth Sciences. She obtained her MSc in Engineering Geology in 2005 with the thesis: 'Injection of oxygen-rich water as an arsenic remediation technique: visualization experiments'.

After graduating, she started her career at GeoDelft, which later became part of Deltares. In the initial years she was involved in the development of BioSealing, a method for sealing subsurface leaks. In addition, she worked on a range of projects relating to soil mechanics and dike technology that contributed to her experience with physical modelling (both 1-g and n-g).

She turned to research in the field of backward erosion piping in 2008. In the years that followed, she worked on the validation of the Sellmeijer model by performing small- (1-g and n-g), medium and large-scale experiments and she contributed to the adjustment of the Sellmeijer rule. Vera completed this doctorate at Deltares and Delft University of Technology.

Vera and her partner Tino Rodewijk have two sons: James, who was born in 2010 and Noah, who was born in 2013.

Backward erosion piping is an internal erosion mechanism that poses a threat to dikes, dams and levees with sandy foundations. Shallow pipes are formed in the direction opposite to the flow underneath water-retaining structures as a result of the gradual removal of sandy material by the action of water. This dissertation describes the pipe-forming erosion processes in uniform sands, distinguishing between processes involving the initiation and the progression of the pipe. Field experiments, laboratory experiments, groundwater flow calculations and equations describing the mechanisms involved allowed for the development and reassessment of backward erosion piping prediction models.